Pathological changes in the cerebellum of spinocerebellar ataxia type 6 (SCA6): disease progression and selective vulnerability

Tsz Chui Sophia Leung
Department of Biology, McGill University, Montreal

January 2024

A thesis submitted to McGill University in partial fulfillment of the requirements of the degree of Doctor of Philosophy

Table of contents

LIST OF ABBREVIATIONS

4-AP	4-Aminopyridine
7,8-DHF	7,8-Dihydroxyflavone
8-OHdG	8-dihydro-2'-deoxyguanosine
Δψm	Mitochondria membrane potential
ACN	Acetonitrile
ARSACS	Autosomal-recessive spastic ataxia of Charlevoix-Saguenay
ASO	Antisense oligonucleotides
ATP	Adenosine triphosphate
BDNF	Brain-derived neurotrophic factor
BSA	Bovine serum albumin
Ca^{2+}	Calcium ion
CHS	Chédiak-Higashi syndrome
CRF	Corticotropin-releasing factor
CS	Christianson syndrome
CV	Coefficient of variation
DEGs	Differentially expressed genes
EAAT4	Excitatory amino acid transporter 4
ESI	Electrospray ionization
ETC	Electron transport chain
FCCP	Carbonyl cyanide-p-trifluoromethoxyphenylhydrazone
FDR	False discovery rate
GO	gene ontology
IQR	Interquartile range
LC/MS	Liquid chromatography–mass spectrometry
MitoVit-E	Mitochondria-targeting vitamin E
MRI	magnetic resonance imaging
mRNA	Messenger RNA
NPC1	Niemann-Pick disease type C1
Padj	Adjusted P value
PB	Phosphate buffer

PBS	Phosphate-buffered saline
PCA	Principal component analysis
PF-PC	Parallel fiber to Purkinje cell
PMI	Post-mortem intervals
RIN	RNA integrity number
RNA-seq	RNA sequencing
RNAi	RNA interference
ROS	Reactive oxygen species
SCA6	Spinocerebellar ataxia type 6
SCAs	Spinocerebellar ataxias
TEM	Transmission electron microscopy
TMRE	Tetramethylrhodamine, Ethyl Ester, Perchlorate
TrkB	Tropomyosin receptor kinase B
WT	Wildtype
Z+	Zebrin expressing
Z-	Zebrin non-expressing

LIST OF FIGURES AND TABLE

ABSTRACT

Spinocerebellar ataxia type 6 (SCA6) is a rare neurodegenerative disease that is currently incurable. Understanding of the cellular dysregulations that underlie disease progression and selective neuronal vulnerability will provide insights for therapeutics development. SCA6 is a mid-life onset disease clinically characterized by ataxia - motor incoordination - and neurodegeneration largely restricted to the cerebellum. Using a mouse model of SCA6 that recapitulates many features of the human disease, I investigated the transcriptional changes using RNA sequencing, and discovered reduced expression of mitochondrial genes. I then explored the cellular consequences of reduced gene expression and found that mitochondria damage progressively worsens, which contributes to SCA6 disease progression. I first showed that soon after disease onset, mitochondria in SCA6 Purkinje cells, the principal neuron of the cerebellum, had reduced energy production capacity. This was followed by an accumulation of cellular oxidative stress and progressive morphological damages to mitochondria during mid-disease stage, suggesting extensive disruption to Purkinje cell normal functioning. This was exacerbated by impairment in mitophagy later in the disease, reducing the cell's capacity to remove damaged mitochondria. To determine if these findings were relevant to the human disease, I also examined human post-mortem cerebellar tissues from SCA6 patients, and detected metabolic signatures that were consistent with mitochondrial damage. These findings suggest that mitochondrial dysfunction likely contributes to SCA6 progression and could be a target for therapeutic intervention, especially for patients diagnosed later in the disease. One unanswered question, nonetheless, was that why some Purkinje cells are vulnerable and eventually degenerate but the other persist in SCA6. Answering this question may provide valuable insights into the intrinsic resilience mechanisms of the cerebellum, mechanisms that may be exploited to enhance resilience in the vulnerable cell population. I first identified the population of vulnerable cells in SCA6 and found that they were Purkinje cells in the anterior zone, in contrast to the resilient cells in the nodular zone. I recorded the spontaneous firing properties of Purkinje cells as a measure of their functional output, and discovered that only cells in the anterior zone had reduced firing frequency and regularity, while the cells in the nodular zone fired indistinguishably from wildtype control. In other neurodegenerative diseases, such pattern of vulnerability has been correlated with the molecular marker zebrin; yet I discovered that SCA6 Purkinje cell vulnerability does not correlate with zebrin in neither anterior nor nodular zones. To identify molecular differences between these two populations of Purkinje cells that may give rise to selective

vulnerability, I performed bulk RNA sequencing on anterior cerebellum and posterior cerebellum separately. Surprisingly, most of the transcriptional changes in SCA6 take place in the posterior cerebellum, indicating that cells undergo molecular reprogramming that may confer resilience. These changes are mostly synaptic, and one of the most significantly altered gene ontology term was *parallel fiber to Purkinje cell synapse*. These results indicate that there may be circuit-level changes in response to SCA6 disease insult in the posterior cerebellum. Further investigation is needed to investigate if these changes in the posterior cerebellum are compensatory measures for the impairment in the anterior cerebellum. Taken together, the findings in this thesis identify mitochondrial damage as a key dysfunction contributing to disease progression in SCA6, as well as highlight posterior transcriptional changes that suggest compensatory mechanisms may protect posterior cerebellum from later damage, thereby revealing novel insights into disease mechanisms of SCA6.

RESUMÉ

L'ataxie spinocérébelleuse de type 6 (SCA6) est une maladie neurodégénérative rare qui est actuellement incurable. La compréhension des dysrégulations cellulaires qui sous-tendent la progression de la maladie et la vulnérabilité neuronale sélective fournira des informations pour le développement de thérapeutiques. La SCA6 est une maladie débutant à la mi-vie caractérisée cliniquement par une ataxie - incoordination motrice - et une neurodégénérescence largement limitée au cervelet. En utilisant un modèle murin de la SCA6 qui reproduit de nombreuses caractéristiques de la maladie chez l'humain, j'ai étudié les changements transcriptionnels en utilisant le séquençage de l'ARN, et j'ai découvert une réduction de l'expression des gènes mitochondriaux. J'ai ensuite exploré les conséquences cellulaires de la réduction de l'expression des gènes et j'ai trouvé que les dommages mitochondriaux s'aggravent progressivement, ce qui contribue à la progression de la maladie. J'ai d'abord montré qu'après l'apparition de la SCA6, les mitochondries dans les cellules de Purkinje , le neurone principal du cervelet, avaient une capacité de production d'énergie réduite. Cela a été suivi par une accumulation de stress oxydatif cellulaire et des dommages morphologiques progressifs aux mitochondries pendant le stage intermédiaire de la maladie, suggérant une perturbation importante du fonctionnement normal des cellules de Purkinje. Cela a été exacerbé par une altération de la mitophagie plus la maladie progresse, réduisant la capacité de la cellule à éliminer les mitochondries endommagées. Pour déterminer si ces découvertes étaient pertinentes pour la maladie chez l'humain, j'ai également examiné les tissus cérébelleux post mortem humains de patients atteints de SCA6, et j'ai détecté des signatures métaboliques qui étaient cohérentes avec les dommages mitochondriaux. Ces résultats suggèrent que les dysfonctionnements mitochondriaux contribuent probablement à la progression de la SCA6 et pourraient être une cible pour l'intervention thérapeutique, en particulier pour les patients diagnostiqués à un stage plus avancé de la maladie. Cependant, une question était restée sans réponse : pourquoi certaines cellules de Purkinje sont vulnérables et dégénèrent éventuellement tandis que d'autres persistent dans la SCA6? La réponse à cette question pourrait fournir des informations précieuses sur les mécanismes de résilience intrinsèques du cervelet, des mécanismes qui pourraient être exploités pour renforcer la résilience dans la population de cellules vulnérables. J'ai d'abord identifié la population de cellules vulnérables dans la SCA6 et j'ai trouvé qu'elles étaient des cellules de Purkinje dans la zone antérieure, en contraste avec les cellules résilientes dans la zone nodulaire. J'ai enregistré les propriétés de décharge spontanée des cellules de Purkinje

comme mesure de leur sortie fonctionnelle, et j'ai découvert que seules les cellules de la zone antérieure avaient une fréquence de décharge réduite et une régularité, alors que les cellules de la zone nodulaire déchargeaient de manière indiscernable en comparaison avec le contrôle de type sauvage. Dans d'autres maladies neurodégénératives, ce type de vulnérabilité a été corrélé avec le marqueur moléculaire zébrine, pourtant, j'ai découvert que la vulnérabilité des cellules de Purkinje de la SCA6 ne n'est pas corrélée à la zébrine dans les zones antérieure ou nodulaire. Pour identifier les différences moléculaires entre ces deux populations de cellules de Purkinje qui pourraient donner lieu à une vulnérabilité sélective, j'ai effectué un séquençage global de l'ARN du cervelet antérieur et du cervelet postérieur séparément. Étonnamment, la plupart des changements transcriptionnels dans la SCA6 ont lieu dans le cervelet postérieur, indiquant que les cellules subissent une reprogrammation moléculaire qui pourrait conférer de la résilience. Ces changements sont principalement synaptiques, et l'un des termes d'ontologie de gènes les plus significativement modifiés était *la synapse de la fiber parallèle à la cellule de Purkinje*. Ces résultats indiquent qu'il peut y avoir des changements au niveau du circuit en réponse aux dommages de la maladie SCA6 dans le cervelet postérieur. Des recherches supplémentaires sont nécessaires pour déterminer si ces changements dans le cervelet postérieur sont des mesures compensatoires pour la détérioration dans le cervelet antérieur. Prises ensemble, les conclusions de cette thèse identifient les dommages mitochondriaux comme une dysfonction clé contribuant à la progression de la SCA6, et mettent en évidence des changements transcriptionnels postérieurs qui suggèrent que des mécanismes compensatoires pourraient protéger le cervelet postérieur de dommages ultérieurs, révélant ainsi de nouvelles perspectives sur les mécanismes de la maladie.

ACKNOWLEDGEMENTS

I am grateful for current and past members of the Watt lab for creating a supportive environment that made my years in the lab enjoyable. I am especially thankful to Dr. Anna Cook, whose boundless curiosity and strong work ethic has been my inspiration during the five years we worked together on SCA6. To Dr. Brenda Toscano Márquez, thank you for trusting me in many of our collaborations and for sharing my fear for a certain organelle. To Eviatar Fields, thank you for your mental support and generous help through many little bumps along the way. To Dr. Kim Gruver, Dr. Daneck Lang-Ouellete, Bruna Soares de Souza, Ben Rogers and Rana Abdelhalim, thank you for the many times you bounced ideas with me during the many presentations and mid-experiments chit chats that has helped shape my project.

I am beyond grateful for my supervisor Dr. Alanna Watt. Thank you for your unwavering support during my years in the lab, from editing my every scholarship application to strategizing my graduate school career with me. You always have my best interest in mind, which is the biggest factor that makes graduate school gratifying for me. You are a role model to me in ways much more than a productive, rigorous scientist.

I must also thank my supervisory committee members. To Dr. Anne McKinney, thank you for always being uplifting and supportive. Every discussion with you always ends with new, exciting ideas. To Dr. Rosemary Bagot, thank you for lending me your expertise in bioinformatics whenever we meet to discuss my project. Your encouragement empowered me and instilled in me a sense of confidence to explore new avenue of research.

The work in this thesis would not have been possible without the professional animal management from Comparative Medicine and Animal Resources Centre (CMARC), especially the meticulous care from Dr. Tanya Koch and Dr. Behrad Sartip, who kept our animal colonies in good shape. Some of the techniques employed in my thesis were enabled by helpful staff from various core facilities at McGill. I am grateful to Jeannie Mui, Johanne Ouellette, Dr. Kelly Sears from the Facility for Electron Microscopy Research (FEMR) for preparing high quality samples and offering imaging training for my electron microscopy experiments. Special thanks to Dr. Joel Ryan and other members of the Advanced BioImaging Facility (ABIF). Without their effort in upkeeping microscopes and professional knowledge in confocal microscopy, I could not have generated beautiful images in this thesis. The staff at Metabolomics Innovation Resource (MIR),

especially Dr. Daina Avizonis, Luc Choinière, Cian Monnin and Mariana Russo, helped set up and run the LC-MS experiments which would otherwise be challenging to me.

I would also like to thank all the undergraduate members of the lab who also became coauthors on the two manuscripts in this thesis, Ru Yi Louisa Shen, Namrata Rana, Alexandra Bernstein, Daniel Phillips, Lois Lau, Chanelle Lawson Lartego and Maya Nachman. Thank you for being patient with me as I learnt how to supervise and manage projects. Without you, I would not have such rich data sets for my manuscripts. I am also grateful for Lois Lau, Genavieve Maloney, Anika Holur and Zoe Dubin for helping with genotyping and various housekeeping tasks that ensured my experiments would run smoothly. Special thanks to Élyse Zadigue-Dubé for editing my French abstract.

I am incredibility thankful for the supportive environment in the Department of Biology. I am especially grateful for members of the Reyes Lab, Brouhard Lab, Hekimi Lab and Moon Lab for lending me their equipment. Administrative staff in the department, especially Ancil Gittens, Drenusha Myha, Carole Smith, Susan Gabe, Patricia Lianos and Caroline Leblond, helped me in countless little ways that I could focus on my research.

I would like to express my deepest gratitude towards my family and friends. You stood by me through thick and thin. I will forever be indebted to you.

CONTRIBUTIONS TO ORIGINAL KNOWLEDGE

In this thesis, I explored factors that contribute to SCA6 disease progression and selective vulnerability of Purkinje cells of the cerebellum. I discovered -

In chapter 3:

- Damage in Purkinje cell mitochondria is one of the contributing factors of SCA6 disease progression in a mouse model of SCA6
- In the mouse model, reduction in mitochondrial gene expression level at disease onset precedes mitochondria dysfunction and morphological changes at early disease stage, which are followed by an accumulation of oxidative damage later in disease
- In the mouse model, impaired mitophagy at later disease stage limits cells' ability to remove damaged mitochondria, leading to progressive morphological changes to mitochondria
- In post-mortem human tissues from SCA6 patients, there are metabolic signatures consistent with damaged mitochondria, demonstrating relevance of animal study findings to the human disease

In chapter 4:

- Consistent with previous findings in human patients, Purkinje cell loss is most prominent in the anterior vermis of the cerebellum in a mouse model of SCA6, while Purkinje cells in the nodular lobe remain.
- Purkinje cells in the anterior vermis display firing deficits at ataxia onset, long before degeneration in the mouse model; while Purkinje cells in the nodular that later survive showed normal firing
- Zebrin immunopositive Purkinje cells in the anterior lobe are not more resilient to cell death in SCA6 mouse model as in the case of some animal models of neurodegenerative diseases
- Between lobule I-VI (anterior) and lobule VII-X (posterior) in SCA6 mice, gene expression landscape of the posterior cerebellum undergoes more extensive change, suggesting potential neuroprotective mechanisms brought about by transcription reprograming
- In SCA6 mice, there is an expended transcriptional heterogeneity between the anterior and posterior cerebellum: genes that do not show anterior-to-posterior expression difference in WT show regional enrichment in SCA6

CONTRIBUTION OF AUTHORS

For all chapters in this thesis, I designed and conducted experiments, analyzed, interpreted, and illustrated data.

Chapter 3

I designed and conducted all experiments, in whole or in part. I analyzed, interpreted, and illustrated data for all figures. Experimental design, result interpretation and manuscript writing were done in collaboration with my supervisor Dr. Alanna Watt. Contribution from co-authors and others are as below:

- E.F. contributed to the experiment conceptualization for Fig. 6;
- N.R. ran part of the experiments for Fig. 4 and Supp. Fig. 3, and analyzed data for Fig. 4, 5, Supp. Fig. 3 and Supp. Fig. 4
- R.L.L.S. and A.B. analyzed data for Fig. 5 and Supp. Fig. 4
- A.A.C. assisted with experiment for Fig. 2 and edited the manuscript
- D.E.P. analyzed data for Supp. Fig. 5e
- RNA sequencing run related to Fig. 1-2 was performed by Genome Quebec
- LC-MS/MS run related to Fig. 7 was performed by Rosalind and Morris Goodman Cancer Research Centre Metabolomics Core Facility

Chapter 4

I designed and conducted all experiments, in whole or in part. I analyzed, interpreted, and illustrated data for all figures. Experimental design, result interpretation and manuscript writing were done in collaboration with my supervisor Dr. Alanna Watt. Contribution from co-authors are as below:

- L. L. and M.N. analyzed data for Fig. 1
- C. L. L. analyzed data for Fig. 3
- RNA sequencing run related to Fig. 4-5 was performed by Genome Quebec

CHAPTER 1: INTRODUCTION

The research in this thesis has a specific objective of discovering new treatment targets for a rare disease and a broad goal of expanding knowledge of the cerebellum.

Spinocerebellar ataxia type 6 (SCA6) is a rare neurodegenerative disease characterized by mid-life onset of ataxia and late cerebellar degeneration. Because the pathology is largely restricted to the cerebellum, it is considered a pure cerebellar SCA subtype. There is currently no cure nor treatments to delay onset or halt progression for SCA6. Studying the pathophysiology of SCA6 presents the opportunity to discover novel therapeutic targets that may lead to better patient outcome and to reveal lines of defense in disease that are important to keep the cerebellum healthy. With these goals in mind, I studied SCA6 in two research directions: (1) what contributes to the worsening of disease in SCA6; (2) which part of the cerebellum is preferentially attacked by SCA6 and what factors make them specifically vulnerable. My study has led to two first-author manuscripts that have become two chapters in this thesis. In chapter 3, a published manuscript in *Acta Neuropatholoogica,* I showed that accumulation of unhealthy mitochondria is a contributing factor of SCA6 disease progression. In chapter 4, a manuscript ready for submission, I discovered that the anterior zone in cerebellum is specifically susceptible to SCA6 disease insult while the nodular zone is spared, and these responses are accompanied by differential transcriptional reprogramming that leads to synaptic changes.

The findings in this thesis support that mitochondria-targeting treatment may slow down SCA6 disease progression. Furthermore, the molecular differences between vulnerable and resilient regions in SCA6 shed light on the capacity of the cerebellum to compensate for regional deficits, augmenting the body of literature around spinocerebellar ataxias and selective vulnerability in the cerebellum.

CHAPTER 2: LITERATURE REVIEW

2.1 SCA6 etiology

In 1997, Zhuchenko and colleagues first determined the expansion of a track of CAG repeat in the gene *CACNA1A* to be the genetic cause of SCA6 (Zhuchenko et al. 1997). This discovery inspired subsequent research on the molecular mechanism of disease and enabled accurate clinical diagnosis through genetic testing. Since then, the ataxia field has seen 20-30 reports of SCA6 research publications every year.

The human gene *CACNA1A* encodes the α1A subunit of the P/Q type voltage gated calcium channel, and a transcription factor α1ACT (Fig 1). *CACNA1A* produces several isoforms of the P/Q channel by means of alternative splicing. The alternative splice site between exon 46 and 47 generates the isoform MPI containing the CAG repeat track and the isoform MPc that lacks exon 47 and thus also lacks the CAG repeats (Tsunemi et al. 2002). These two isoforms account for 60% and 40%, respectively, of the P/Q channel transcripts in the cerebellum (Unno et al. 2012). There is a third isoform, MPII, that carries different c-terminal sequence than MPI due to a frameshift but only accounts for less than 0.1% of the total transcript (Tsunemi et al. 2002). For the transcription factor α1ACT, it was discovered by Du and colleagues that it is generated by translation of only the c-terminal of the full length α1A mRNA, through an internal ribosomal entry site, and therefore contains the CAG repeats.

In unaffected individuals, there is a track of CAG in exon 47 of *CACNA1A* that is 18 or less repeats long. A heterozygous 19-repeats-long CAG expansion may or may not cause the disease, while at 20 repeats or longer it is considered to be pathogenic (Zoghbi 1997). CAG encodes glutamine. Therefore, CAG repeat expansion causes an elongated polyglutamine tract in the protein products of *CACNA1A*. Thus, at first, SCA6 was considered as (1) an ion channel disease, and/or (2) a polyglutamine disease. However, in 2006 when Kordasiewicz and colleagues described that *CACNA1A* produces another gene product, a transcription factor, that led to another hypothesis of SCA6 pathogenesis: (3) a transcription dysregulation disease (Kordasiewicz et al. 2006).

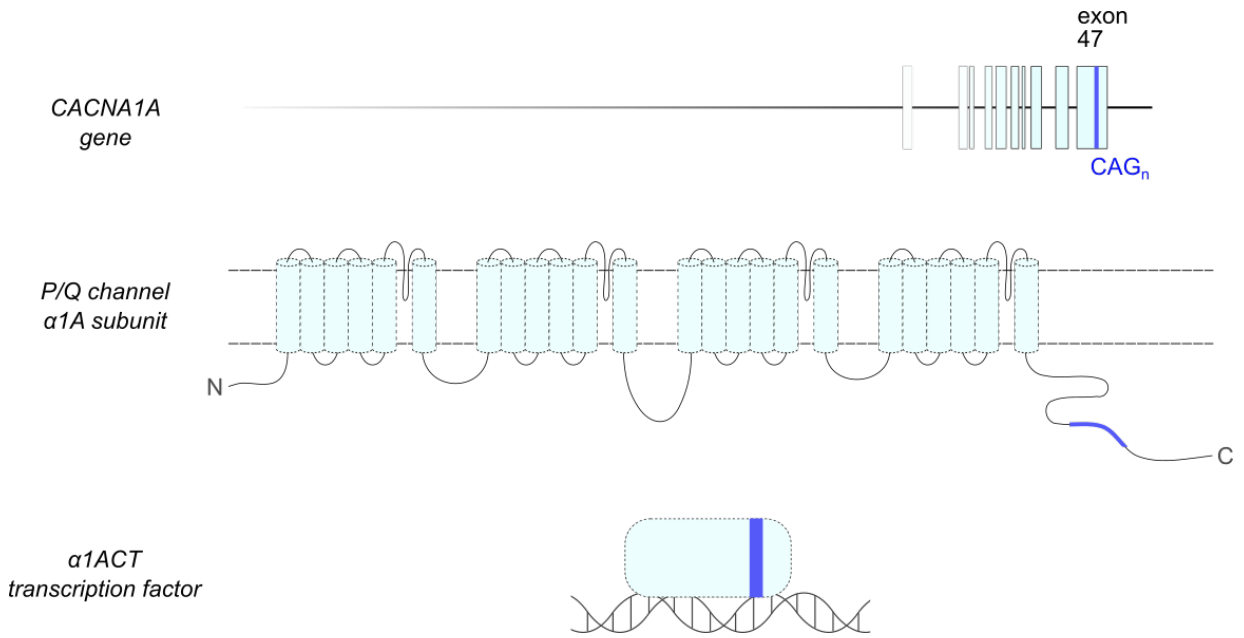

Figure 1 – CAG repeat expansion in *CACNA1A* exon 47 results in polyglutamine track expansion in the two gene products: α1A subunit of the P/Q type voltage gated calcium channel and α1ACT transcription factor. In the P/Q channel, the polyglutamine track is in the c-terminal intracellular portion.

2.2 SCA6 is progressive

SCA6 is a mid-life onset disease. In polyglutamine diseases, age of disease onset correlates with CAG repeat length – the longer the repeats, the earlier symptoms appear (Lieberman, Shakkottai, and Albin 2019). SCA6 is unique in that the pathological repeat length threshold (20 CAGs) falls in the normal range of other polyglutamine diseases. Indeed, the average age of onset of SCA6 patients is 53 years, more than a decade later than that in other polyglutamine SCAs (SCA1: 38 years, SCA2: 36 years, and SCA3: 40) (Tezenas du Montcel et al. 2014). The old age of onset makes it important to consider the interaction of aging with disease development. The most common early sign of SCA6 is episodic unsteadiness in gait. As the disease progresses, patients will eventually present with constant ataxia, tremor, dysarthria, and in some cases visual problems like nystagmus and diplopia (Solodkin and Gomez 2012; Perlman 1993; Ueno et al. 2017).

Atrophy of the cerebellum, especially in the cerebellar vermis, is a prevalent feature of SCA6 (Solodkin and Gomez 2012). In fact, SCA6 pathology is largely restricted to the cerebellum,

therefore, it is usually regarded as a purely cerebellar disease. SCA6 symptoms are shared with many other hereditary ataxias, making accurate diagnosis challenging. Also given the rareness of the disease, SCA6 patients are often not correctly diagnosed until later in the disease stage, delaying interventions (Perlman 1993). SCA6 is progressive, but progression is slow such that patients' lifespan is generally not shortened (Casey and Gomez 1993). Because SCA6 currently has no cure, affected individuals thus live with the disease for decades (Diallo et al. 2018). Therefore, it is particularly important to understand pathological changes during disease progression so to develop effective treatments for this disease stage.

2.3 SCA6 Interventions: current and emerging

There is currently no cure or prevention for SCA6, and treatments are symptomatic (Solodkin and Gomez 2012; Fujioka, Sundal, and Wszolek 2013). Rehabilitative therapy is the mainstay in SCA6 symptom management. Physical therapy, occupational therapy and at-home balance exercises all showed improvements in motor functions (Miyai et al. 2012; Keller and Bastian 2014). However, these therapies may become inaccessible later during disease when ataxia becomes severe.

Pharmacological treatment options include acetazolamide, which Yabe and colleagues discovered in their open-label trial in 2001, that mitigates ataxia but does not halt progression of the disease (Yabe et al. 2001). Another clinical pilot trial on gabapentin showed variable efficacy in alleviating symptoms (Nakamura et al. 2009). The molecule tandospirone was tested on many spinocerebellar degeneration diseases including SCA6 and showed some promise on helping motor functions (Takei et al. 2010). The most recent clinical trial tested rovatirelin but showed only slight effects on improving ataxia (Nishizawa et al. 2020). This highlights the urgency of discovering new, effective drugs for SCA6. Research from previous members of the lab has identified two molecules that mitigate ataxia in animal model of SCA6: 4-Aminopyridine (4-AP) and 7,8-Dihydroxyflavone (7,8-DHF) (Jayabal et al. 2016; Cook et al. 2022). Further research is required to determine if they are effective in patients.

An emerging avenue for genetic diseases such as SCA6 is gene therapy, by means of RNA interference (RNAi) or antisense oligonucleotides (ASO). Tsou and colleagues (2011) explored RNAi in SCA6 and was able to silence the CAG-repeat-encoding isoform of P/Q channel using miRNA-like delivery system in cell culture (Tsou et al. 2011). Another research group, Pastor and

colleagues, was able to reduce expression of one of the gene products of *Cacna1a*, α1ACT, using miRNA, and exert protective effect on Purkinje cell loss and dendritic thinning in a hyperacute SCA6 mouse model (Pastor et al. 2018). Gene therapy offers great promises in treating genetic diseases. However, numerous challenges such as choosing the right dosage, route of administration, controlling cell/tissue specificity and managing adverse effects need to be overcome before gene therapy becomes clinically available to patients. Further elucidation of molecular mechanisms of disease remains an important step in aiding development of effective treatments.

2.4 SCA6 molecular pathology: current views

2.4.1 Is SCA6 a channelopathy?

This hypothesis has been explored by many research groups since the mapping of the SCA6 gene to a gene encoding the P/Q calcium channel subunit. The CAG-repeat expansion mutation is at the last exon of *CACNA1A*, which corresponds to the C-terminus cytoplasmic domain of the transmembrane channel (Figure 1). *CACNA1A* produces a full-length transcript of 9.8kb, which then undergoes splicing to generate many isoforms of the pore-forming subunit of P/Q channel, out of which only some contain the expanded glutamine track. The C-terminus domain of the P/Q calcium channel, like other calcium channels, was shown to interact with calmodulin in a Ca^{2+} dependent manner, thereby allowing P/Q channel to quickly recover from voltage dependent inactivation (Lee et al. 1999). An interruption by the polyglutamine tract may have structural consequences for the protein and in turn alter its interaction with calmodulin or directly affect the pore formation, resulting in interruption to calcium current.

Two independent *in vitro* studies presented evidence in support of changes in channel inactivation properties caused by polyglutamine expansion. In one study, Matsuyama and colleagues (1999) have found that recombinant P/Q channel expressed in baby hamster kidney cell, carrying 30 or 40 polyglutamine repeats, both led to an 8mV hyperpolarizing shift in the inactivation (Matsuyama et al. 1999). This finding was confirmed by Toru and colleagues (2000), who demonstrated similar 6mV and 11mV hyperpolarizing shifts in inactivation of the P/Q channel, when the channel carrying 24 and 28 polyglutamine repeats respectively was expressed in human embryonic kidney cells (Toru et al. 2000). The shift in inactivation as shown in these two studies were thought to

reduce the available Ca^{2+} channel population, decrease Ca^{2+} influx, and eventually, directly or indirectly cause Purkinje cell death.

However, these findings was contradicted by results in a study conducted by Piedras-Rentería and colleagues, where they demonstrated P/Q channel harbouring 23, 27 and 72 CAG repeats to have normal channel kinetics when expressed with β1 and α2δ subunits in human embryonic kidney 293 cells (Piedras-Renteria et al. 2001). A later study by Chen and Piedras-Rentería (2007) even showed that there is a 6mV depolarising shift in inactivation when expressed with β4 and β2a subunits instead, opposite to previous findings (Chen and Piedras-Renteria 2007).

So far studies of the mutated P/Q channel property had been performed in non-neuronal cell culture system. Later studies in knock-in animal models have provided insights to how the mutated P/Q channel behaves in Purkinje cells, which argues against the channelopathy hypothesis. Saegusa and colleagues (2006) generated a knock-in mouse model that expressed the P/Q channel with 28 CAG repeats. Patch clamp recording of disassociated Purkinje cells revealed unaltered voltage dependence of inactivation and current density (Saegusa et al. 2007). In another study by Watase and colleagues (2008), three knock-in mouse models were generated which expressed the P/Q channel with 14, 30 and 84 CAG repeats respectively (Watase et al. 2008). Whole cell patch clamp of disassociated Purkinje cells revealed reduced current density over a wide range of voltages, irrespective of the repeat length. However, consistent with Saegusa and colleagues' finding, the voltage dependence of inactivation was unaltered. Taken together, there is no conclusive evidence as to whether CAG repeat expansion mutation lead to defective P/Q channels.

However, mutated P/Q channel is still likely to play a direct role in the pathogenesis of SCA6 by means other than altered channel function, such as altered expression level. P/Q channel is normally expressed throughout the cerebellum (Westenbroek et al. 1995). Watase and colleagues found that expression of mutated P/Q channel was diminished in SCA6 Purkinje cells compared to the level of normal P/Q channel in wildtype, which could explain the reduced current density (Watase et al. 2008). When P/Q channel expression was ablated specifically in Purkinje cells, animals developed cerebellar ataxia around P12 and later progressive Purkinje cell degeneration around P30 (Todorov et al. 2012). This suggest that P/Q channel is indispensable to Purkinje cells and cerebellum normal functioning, and its altered expression level could be one of the causes of pathological changes in SCA6.

2.4.2 Is SCA6 a polyglutamine disorder?

Out of the nine polyglutamine diseases characterized to date, SCA6 is the most atypical one based on several features. The nine polyglutamine diseases include Huntington's Disease, spinal bulbar muscular atrophy, dentatorubral-pallidoluysian atrophy, SCA1, 2, 3, 6, 7 and 17 (Shao and Diamond 2007). A hallmark of these diseases is nuclear, and at times accompanied by cytoplasmic, inclusion in affected cell types (Shao and Diamond 2007). These inclusions were thought to form due to polyglutamine tract induced conformation change (Minakawa and Nagai 2021). SCA6 is an exception in that mostly cytoplasmic inclusions have been observed (Ishiguro et al. 2010), and very rarely in the nucleus (Ishikawa et al. 2001). One possible explanation is that unlike in other polyglutamine diseases where the mutated genes encode cytoplasmic or nuclear located proteins, SCA6 gene *CACNA1A* encodes a transmembrane protein (Giunti et al. 2015). Another feature that distinguishes SCA6 from the others is that the pathogenic range of CAG repeats for SCA6 ($\geq$ 20 CAGs) falls within the normal range of the other polyglutamine diseases (< 30 CAGs) (Bunting, Hamilton, and Tabrizi 2022). These raised the possibility that the mechanism that gives rise to SCA6 is different from that underlying other polyglutamine diseases.

Emerging therapeutic avenues for polyglutamine diseases focus on reducing RNA transcript by antisense oligonucleotides, stabilizing protein confirmation, inhibiting aggregates formation and stimulating aggregates removal. It is worth considering if these strategies would have the same efficacy in SCA6 as in other polyglutamine diseases, given the many distinct features of SCA6 mentioned.

2.4.3 Is SCA6 a transcription dysregulation disease?

The suspicion that SCA6 is potentially a transcription dysregulation disease was first inspired by the potential Ca^{2+} dysregulation. Intracellular Ca^{2+} is an important signalling molecule and is known to regulate directly and indirectly the transcription of many genes. On top, Du and colleagues has shown that the C-terminal of *Cacna1a* acts directly as a transcription factor, potentially targeting many genes (Du et al. 2013). A follow up study later showed by blocking only the expression of the C-terminal portion of *CACNA1A* but sparing the P/Q channel portion, prevented development of ataxia in mice (Pastor et al. 2018). Therefore, it is likely that the mutation causes a disruption in transcription programming, which then disrupts the molecular homeostasis and eventually compromises the cell's defense against insults like ion disequilibrium

and oxidative stress. This hypothesis was relatively new and under-explored when I started my PhD. One research group conducted a transcriptomic study on one of the SCA6 mouse models at early disease stage where mice showed mild ataxia but no Purkinje cell loss. They found over 500 differentially expressed genes in SCA6, which were related to g-protein coupled receptor binding and inflammation (Aikawa et al. 2015). In this thesis, I explored this hypothesis in Chapter 3 and 4, and found extensive changes in transcription landscape in SCA6 mouse model cerebellum.

2.4.4 A multifactorial view of SCA6 molecular pathology

Despite the many evidence put forth regarding SCA6 pathology, it remains difficult to resolve the primary cause of the disease. It is likely that, like in other neurodegenerative diseases, the pathogenesis of SCA6 is a complex one that involves the accumulations of impairments in cellular, circuitry and tissue level. With the goal of developing effective treatments in mind, it is imperative to consider all fronts of SCA6 pathology, whether they can be targeted, how and when they should be targeted, and if such intervention could eventually lead to better patient outcome. Cook and colleagues has shown that BDNF-TrkB signalling was impaired in SCA6 mice at disease onset, and both exercises and small molecule activating TrkB, when administered before disease onset, could restore BDNF-TrkB signalling back to wildtype level, rescuing motor incoordination and Purkinje cell firing deficits (Cook et al. 2022). The difference was that effectiveness of exercise diminished when animals developed ataxia, which prevented them from exercising enough; while the small molecule remained effective (Cook et al. 2022). However, if the small molecule treatment commenced after disease onset, it could no longer rescues motor or firing deficits (Cook et al. 2022). This study highlights that molecular mechanisms that contribute to disease in early stage may not be an appropriate target for treatments of later disease stage.

SCA6 is a slow progressive disease that is often diagnosed post-onset, as aforementioned. Delineating pathological changes during disease progression is thus important for eventual therapeutics developments for treating middle disease stage patients. In this thesis, I explored this front in Chapter 3.

2.5 SCA6 animal models

To correlate pathological changes in cellular, circuitry and tissue level to motor coordination, several SCA6 animal models were generated over the years. They are summarized in Table 1.

The first SCA6 mouse model was generated by Saegusa and colleagues in 2007. The mouse model carried 28 CAG repeats in the knocked-in full-length human *CACNA1A* at the endogenous *Cacna1a* locus. Mice homozygous for the transgene presented with severe ataxia but died early at 3 weeks of age. Heterozygous mice, however, do not present with ataxic phenotype even at 12 months of age, the last timepoint tested.

Three other mouse models for SCA6 were then generated in the following year by Watase and colleagues (Watase et al. 2008). They carried 14, 30 and 84 CAG repeats in the humanized exon 46/47 sequences, respectively. The humanized sequences contained splicing acceptors that could lead to transcription of different isoforms of the gene products. This construct not only allows for production of the naturally occurring isoforms, it also allows these animals to survive until old age, making investigation of cellular and motor dysfunctions possible. Among these three models, only mice carrying 84 CAG repeats demonstrated motor deficits at 7 months, and later it was discovered to have late Purkinje cell degeneration at 24 months (Jayabal et al. 2015).

The most recent mouse model generated was an hyperexpanded mouse model generated by Unno and colleagues (Unno et al. 2012). This mouse harbors 118 CAG/CAA repeats and was designed to express only the CAG-containing isoform. They showed motor incoordination at 6 weeks of age and Purkinje cells degeneration at 10 weeks.

Table 1 – SCA6 animal models

Model name	CAG repeat length	Transgene species	Locus of transgene	Phenotype	Reference
HL28ki(+)/HL28ki(+)	28/28	Full length human *CACNA1A*	Endogenous *Cacna1a* locus	Severe ataxia and lethal at 3 weeks	(Saegusa et al. 2007)
+/HL28ki(+)	0/28			No motor phenotype tested at 12mo	
$SCA6^{14Q/14Q}$	14/14	Exon 46/47 splice sites and exon 47 CAG repeats from human *CACNA1A*		Undistinguishable from WT control at 20 months	(Watase et al. 2008)
$SCA6^{30Q/30Q}$	30/30				
$SCA6^{84Q/84Q}$	84/84			7 months / Rotarod	(Watase et al. 2008; Jayabal et al. 2015)
$MPI^{118Q/118Q}$	118/118	Exon 46/47 mutated splice sites and exon 47 CAG repeats from human *CACNA1A*		6 weeks / Rotarod 10 weeks / Purkinje cell loss	(Unno et al. 2012)

In this thesis, all animal experiments were conducted in the $SCA6^{84Q/84Q}$ model. This model offers a number of advantages over the others in faithfully recapitulating the human disease. First, in this mouse model, onset of ataxia is at 7 months, which corresponds to mid-life onset of SCA6 in human at around 50 years of age (Fig 2). This is important because the interplay between normal aging and pathological changes needs to be considered. For example, autophagy, a process that maintains cellular health by degrading dysfunction proteins or organelles, is comprised in aging (Barbosa, Grosso, and Fader 2018). It is thought that the loss of autophagic activity in aging can exacerbate diseases (Aman et al. 2021). Second, this mouse model features late Purkinje cell degeneration, which resembles the clinical observation in patients. In SCA6, motor symptoms precede cerebellar degeneration, which suggests cellular dysfunctions, but not neuronal loss, lead to ataxia. The late degeneration in this model allows for investigation of molecular mechanisms in disease.

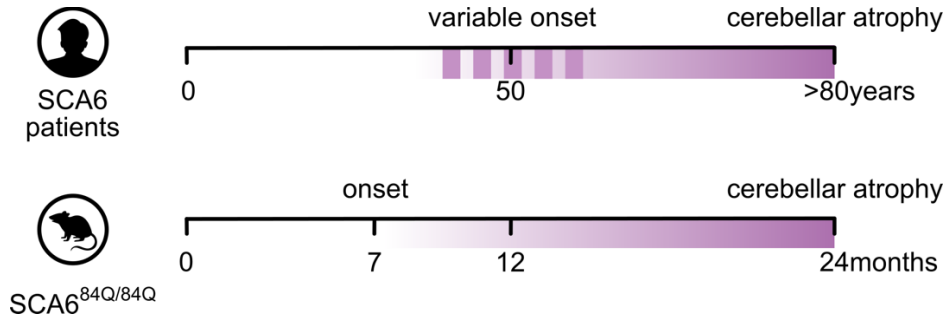

Figure 2 – SCA6 key disease features are recapitulated in SCA6$^{84Q/84Q}$ mouse model

2.6 Mitochondria and the cerebellum

Mitochondria are indispensable for the normal functioning of cells. They produce the majority of ATP through oxidative phosphorylation to sustain a cell's energy demand. They also play a role in Ca^{2+} homeostasis by acting as a Ca^{2+} reservoir, a function especially important in neurons at synaptic terminals. Normal mitochondrial activity also produce reactive oxygen species that act as signalling molecules and neurotransmitters (Kann and Kovacs 2007). Because of the vital functions mitochondria provide, it is important for the cell to maintain a healthy pool of the organelle. This is achieved by (1) biogenesis of mitochondria through expression of mitochondria proteins, (2) fusion and fission of mitochondria to facilitate exchange of healthy proteins and removal of damage fragments, and (3) mitophagy to degrade damaged mitochondria. These three processes constitute mitochondria quality control (Chen, Zhao, and Li 2023).

Mitochondrial impairment has been implicated in most neurodegenerative diseases (Lezi and Swerdlow 2012). They are known for their significant role in both programmed cell death and aging, which also made them the likely mediator of neurodegenerative diseases, diseases that are usually caused by neuronal cell death later in life (Lin and Beal 2006).

2.6.1 Mitochondrial impairments are common in SCAs

Impairment in mitochondria is also a common feature in many SCAs, for example in SCA1, 2, 3, 7 and 28 (Stucki et al. 2016; Ward et al. 2019; Mancini et al. 2019; Harmuth et al. 2022; Cornelius et al. 2017; Hsu et al. 2017; Kristensen et al. 2018; Harmuth et al. 2018). Some SCAs are caused by mutation in mitochondrial genes directly, including SCA28 and 31 and a new SCA subtype SCA49 (Aoki et al. 2023; Corral-Juan et al. 2022; Mancini et al. 2019). In fact, ataxia is one of the

most reported symptoms of mitochondria diseases (Zeviani, Simonati, and Bindoff 2012). In a mouse model of a mitochondria disease COQ8A-ataxia, Purkinje cell-specific knockout of COQ8A was sufficient to induce cerebellar ataxia, suggesting that mitochondria malfunction in Purkinje cells could play a critical role in causing ataxia (Manolaras et al. 2023).

Diverse types of mitochondrial impairments have been reported in SCAs, some of which are summarized in Table 2. The impairments span from morphological and functional changes to individual mitochondrion, to distribution of mitochondrial network within elaborately shaped neurons, and further to other cellular processes such as mitophagy/autophagy and oxidative stress that have broader implications to the cell. The kind(s) of impairment in a disease will help determine the appropriate mitochondria-targeting treatments, which are further discussed in the next section.

In SCAs, Purkinje cells are usually the cell type in the cerebellum to degenerate. Purkinje cells are among the largest and the most metabolically active neurons in the nervous system, and they are believed to be especially sensitive to disruption in mitochondria for a number of reasons: First, Purkinje cells sustain high spontaneous firing rate, which is energy demanding and calcium dependent, both are mitochondrial-dependent (Howarth, Gleeson, and Attwell 2012). Second, Purkinje cells have elaborate dendrite trees, where distal processes rely on a healthy network of mitochondria (Liu et al. 2018). Third, as a post-mitotic cell type, Purkinje cells are unable to eliminate energy-defective cells through cell division, such that a healthy pool of mitochondria within the cell is dependent on tight control of biogenesis, fusion/fission and mitophagy. Indeed, mitochondria impairments specifically within Purkinje cell were reported in SCAs and in even other diseases where the cerebellum is not the primary site of pathology, such as in Alzheimer's disease (Baloyannis 2011), suggesting that Purkinje cell mitochondria are a common target of disease insult.

Mitochondrial impairments have thus been hypothesized to contribute to SCA6 but have never been investigated until now. In this thesis, I explored this aspect of SCA6 pathology in chapter 3.

Table 2 – mitochondrial impairments in some SCAs

Disease	Model system	Mitochondria impairments	Ref
SCA1	Mouse ($SCA1^{154Q/2Q}$)	Mouse Purkinje cell findings: - Altered protein expression, majority downregulated; - Altered shape; - Reduced ETC activities; - Increased oxidative stress	(Stucki et al. 2016)
SCA2	Human (patient-derived fibroblast culture)	- Increased oxidative stress; - Altered shape; - Reduced ETC activities	(Cornelius et al. 2017)
SCA3	Mouse (HDPromMJD148-derived embryonic fibroblast cell) Human (patient-derived fibroblast culture)	Mouse findings: - Altered mitophagy and autophagy Human findings: - Altered shape - Reduced ETC activities - Altered mitophagy and autophagy	(Harmuth et al. 2022)
SCA7	Mouse ($SCA7^{266Q/5Q}$) Human (patient-derived neural progenitor cells)	Mouse Purkinje cell findings - Disrupted network; - Altered shape; Human finding: - Altered shape - Reduced respiratory capacity	(Ward et al. 2019)
SCA28	Mouse ($Afg3l2^{M665R}$-derived embryonic fibroblast cell)	Mouse findings: - Reduced mitochondria membrane potential; - Reduced respiratory capacity; - Reduced ETC activities; - Altered shape	(Mancini et al. 2019)

2.6.2 Mitochondria as a therapeutic target

Because of the central role they play in many cellular processes, mitochondria have been targeted for therapy for neurodegenerative diseases. To date, there are a number of molecules that have been tested to reverse specific mitochondrial impairments and have shown different levels of successes (reviewed extensively in (Murphy and Hartley 2018)). The study of mitochondrial impairment in SCAs can benefit from repurposing available drugs to accelerate treatment development.

Despite the high hope for mitochondria-targeting treatments, meticulous pre-clinical animal studies are still required to select the appropriate molecule for treating a specific disease. Two studies in SCA1 mouse models demonstrated this by testing two molecules as potential therapeutics for SCA1. In the first study, Stucki and colleagues administered the mitochondria-targeting antioxidant MitoQ to $SCA1^{154Q/2Q}$ animals chronically (from pre-symptomatic to mid-disease stage, p40-p150) or briefly (from post-symptomatic to mis-disease, p90-p110) (Stucki et al. 2016). They found that both treatment regimes prevented Purkinje cell loss and restored electron transport chain (ETC) function, while only chronic treatment slowed down motor incoordination (Stucki et al. 2016). In the second study, Sucha and colleagues tested the efficacy of another mitochondria-targeting antioxidant Edaravone on the same SCA1 mouse model. They found no appreciable improvement in a battery of motor, cognitive and behavioral tests nor in mitochondrial function, despite the early intervention (pre-symptomatic, p56-p165) and high dosage used (Sucha et al. 2023). This shows that despite targeting the same mitochondria-induced impairment – oxidative stress accumulation, there are many factors that could influence the effectiveness of the treatment such as choice of molecule, bioavailability, intervention start date and length of treatment.

Mitochondria impairments are likely the secondary pathology in some SCAs, especially when they are detected during disease progression. Mitochondria-targeting therapies may thus show the most promise in slowing down disease progression, as demonstrated in SCA1 and ARSACS animal models (Marquez et al. 2023; Stucki et al. 2016). However, towards the goal of restoring cell health and normal motor functioning, perhaps a combination of therapies targeting different pathologies would be a more promising strategy.

2.7 Purkinje cell selective vulnerability in the cerebellum

Purkinje cells are common targets of many neurological conditions. It is known that Purkinje cells selectively degenerate under neurological conditions – that is, specific populations of Purkinje cells are lost under neurological stress, sometimes forming striking patterns under immunohistochemistry staining (extensively reviewed in (Sarna and Hawkes 2003)). For a given neurological condition, the population of Purkinje cell that is lost tends to be consistent; however, across different conditions, it is not always the same population of Purkinje cells that is vulnerable.

A reasonable question to ask is then, what factors render some Purkinje cells to be vulnerable, the other resilient under a specific neurological stress?

2.7.1 Neurological conditions with patterned Purkinje cell degeneration

In many neurological conditions, Purkinje cells were found to selectively degenerate in a non-random manner. In some, Purkinje cells in the anterior lobe of the cerebellum are the first ones to succumb to disease insult. For example, in SCA6, severe Purkinje cell degeneration in patients was found in the anterior lobe of the cerebellar vermis while the nodular lobe appeared intact (Takahashi et al. 1998). This was recapitulated in the more progressive mouse model of SCA6 ($MPI^{118Q/118Q}$) that, when combined with loss of endosomal/lysosomal cysteine proteases CatB, Purkinje cells in the anterior lobe of the cerebellum died while the ones in the nodular lobe survived (Unno et al. 2012). This is also reported in Chapter 4 of this thesis in a different mouse model of SCA6.

This patterned degeneration is not only observed in cerebellar diseases. For instance, in a knock-out mouse model of Niemann-Pick disease type C1 (NPC1), a lysosomal disease that affect cholesterol transport in cells, Purkinje cells were reported to die in the anterior lobe at 7 weeks. By 9 weeks, the degeneration spread to the central lobe; yet, as observed in SCA6, the nodular lobe remained intact (Chung et al. 2016).

The other disease studies in either human or animal models that have reported anterior vulnerability include SCA1, autosomal-recessive spastic ataxia of Charlevoix-Saguenay (ARSACS), Christianson syndrome (CS), Niemann-Pick disease type A/B, Menkes Syndrome, Chédiak-Higashi syndrome (CHS) (White et al. 2021; Robitaille, Schut, and Kish 1995; Chopra et al. 2020; Toscano Marquez et al. 2021; Stromme et al. 2011; Iwata, Hirano, and French 1979; Sarna et al. 2001; Hedberg-Buenz et al. 2019).

Despite the many observations of anterior-specific degeneration in the cerebellum, there are neurological conditions where degeneration is specific to the posterior cerebellum. For example, in SCA10, patterned degeneration in patients were found to first appear in the posterior/flocculo-nodular cerebellum in a magnetic resonance imaging (MRI) study (Hernandez-Castillo et al. 2019). Interestingly, while animal models of SCA1 displayed anterior-specific degeneration, a longitudinal MRI study in patients revealed selective atrophy in the posterior lobe of the

cerebellum (Nigri et al. 2022). Other studies that reported posterior/flocculo-nodular specific vulnerability include SCA5 and SCA7 (Perkins et al. 2010; Perkins et al. 2016; Stoyas et al. 2020). Taken together, it is unlikely that one subpopulation of Purkinje cells is intrinsically more susceptible to any disease insults; rather, characteristics of different subpopulations of Purkinje cells render them more vulnerable under specific context.

2.7.2 Molecular signature as a source of selective vulnerability

Purkinje cells, despite seemingly identical, can be categorized into subpopulations along many axes. One of which is its expression of a respiratory enzyme aldolase c, also known as zebrin II. Staining of the cerebellum with zebrin II antibody reveals parasagittal bands along the rostro-caudal axis that are evolutionarily conserved and highly reproducible (Fujita et al. 2014). Importantly, majority of Purkinje cells in the anterior cerebellum do not express zebrin II (Z-), while in the posterior, majority of Purkinje cells express zebrin II (Z+). It was also found that the intrinsic firing properties of Z- Purkinje cells are distinct from that of Z+ Purkinje cells (Cerminara et al. 2015). This has led to the hypothesis that Purkinje cell vulnerability may be defined by zebrin identity. Indeed, in an animal model of ARSACS, Purkinje cell loss in the anterior cerebellum took place in regions corresponding to Z-, leaving behind Z+ Purkinje cells (Toscano Marquez et al. 2021). The same has been shown in *leaner* mouse, an animal model for dystonia and cerebellar degeneration due to a spontaneous mutation in the *Cacna1a* gene (Heckroth and Abbott 1994), and in an animal model of Niemann-Pick disease type A/B (Sarna et al. 2001).

Despite the ostensible correlation between Purkinje cell degeneration and zebrin identity, it does not paint the full picture. EAAT4, a glutamate excitatory amino acid transporter (EAAT), co-expresses with zebrin II in the same compartment. It is found on the post-synaptic membrane of Purkinje cell, and functions to uptake excess extracellular glutamate to protect cells from excitotoxicity. Perkins and colleagues showed that ablation of EAAT4 led to Purkinje cell loss in the posterior cerebellum, particularly the population that in normal condition expressed EAAT4, as revealed by zebrin immunopositivity (Perkins et al. 2018). This suggests that zebrin, while acts as a landmark in the cerebellum, may not be the sole molecule responsible for selective Purkinje cell vulnerability.

To add to the complexity, there are other molecules which expression form similar or opposite pattern as zebrin II, among others HNK-1, PLCβ3, PLCβ4, mGluR1β, GABABR2 (reviewed in

(Cerminara et al. 2015)). Their expression patterns, however, do not completely correspond to that of zebrin. The boundaries are slightly different, suggesting that there are many ways whereby the cerebellum map can be drawn. Recent single-cell RNA sequencing result has suggested that there could be even more granular classifications based on the molecular diversity (Kozareva et al. 2021). It is likely that selective vulnerability of Purkinje cell subpopulation can be traced back to their molecular signature or transcriptional landscape. However, future studies will still be required to delineate the mechanisms by which these molecules confer vulnerability.

2.7.3 Innervation onto Purkinje cell as a source of selective vulnerability

Purkinje cell input circuitry is uniform and well-organized: it receives large excitatory glutamatergic input from brainstem inferior olive via a single climbing fiber synapses onto the soma and the proximal dendrite, and small but numerous glutamatergic inputs via the estimated 100,000 synapses made with granule cell-originated parallel fibers synapsed onto its elaborate dendritic tree. Granule cells themselves receive inputs from mossy fibers from various origins in the cerebrum and spinal cord, and by means of parallel fibers these extra-cerebellar signals eventually converge onto Purkinje cells. This parallel fiber to Purkinje cell connection is sometimes interrupted by molecular layer interneurons, who receive excitatory input from parallel fiber, then exert inhibitory output onto Purkinje cells to modulate the final Purkinje cell output out of the cerebellar cortex.

In some cases, the input connection to Purkinje cells overlaps the zebrin topography. Sawada and colleagues discovered that a subtype of climbing fibers expressing corticotropin-releasing factor (CRF) innervates specifically Z+ Purkinje cell in the anterior lobe (Sawada, Fukui, and Hawkes 2008). However, strips of CRF immunopositive climbing fibers were also observed in lobule X, where zebrin expression is uniform, suggesting a more complex relationship between climbing fiber innervation and Purkinje cell molecular identity (Sawada, Fukui, and Hawkes 2008). It is therefore important to consider Purkinje cell afferent innervation pattern as another source of selective vulnerability.

There is mounting reports that reveal the Purkinje cell innervation topography. A study on climbing fiber innervation to zebrin zones revealed that more glutamate is release at climbing fiber-Purkinje cell synapses in the Z+ strips, resulting in more slowly-decayed excitatory post synaptic current and longer complex spikes in Purkinje cells (Paukert et al. 2010). Gao and

colleagues also showed that molecular layer interneurons, basket and stellate cells, in Crus II Z-strips respond weakly to parallel fiber excitation, thereby exerting weak inhibition on Z- Purkinje cells (Gao et al. 2006). A follow up study revealed that such differential inhibition corresponding to Crus II zebrin II strips is mediated by mGluR1-mediated increase of intracellular Ca^{2+} through internal release (Wang et al. 2011). The innervation topography, and how it may relate to cerebellar development are comprehensively reviewed in (Apps and Hawkes 2009; Reeber et al. 2012).

Taken together, it is likely that the interplay between extrinsic (e.g. synaptic connection) and intrinsic (e.g. calcium buffering capacity) properties of Purkinje cells eventually determine its vulnerability under a disease context. The study of selective Purkinje cell vulnerability in diseases will benefit from investigating both axes. In this thesis, I explored both molecular expression and parallel fiber to Purkinje cell connection, and their contribution to selective vulnerability in SCA6 in chapter 4.

2.8 Involvement of other cerebellar cell types in cerebellar ataxias

Despite most of the research in cerebellar ataxia focus on Purkinje cell pathophysiology, other cell types in the cerebellum have been shown to also contribute to disease.

Situated also in the Purkinje cell layer are Bergmann glia. They are responsible for glutamate reuptake at parallel fibre- and climbing fibre-Purkinje cell synapses and extracellular potassium ion homeostasis (Wang et al. 2012). It is shown in SCA7 that expressing the disease causing mutant protein ataxin-7 selectively in Bergmann glia was sufficient to cause ataxia and Purkinje cell degeneration, suggesting that glial dysfunction could play a direct role in causing cerebellar ataxias (Custer et al. 2006). In fact, Bergmann glia inflammation has been demonstrated in SCA1, 2 and 7, suggesting that glial reaction constitutes part of the cerebellar pathology in these diseases (Edamakanti, Mohan, and Opal 2023). Indeed, it is likely that without the glutamate clearance by Bergmann glia, Purkinje cells may suffer from excitotoxicity and thus undergo dark-cell degeneration, a common form of degeneration observed in multiple SCAs (Kasumu and Bezprozvanny 2012).

Molecular layer interneurons (MLI), including stellate cells and basket cells, have also been implicated in cerebellar pathologies. They exert strong inhibition on Purkinje cells and thereby

shape Purkinje cells activity. Therefore, while MLIs may not degenerate in diseases, they may lead to Purkinje cell dysfunction and degeneration. In SCA1, it was shown that MLIs were hyperexcitable in disease, and that enhancing MLIs activity in WT animals was sufficient to cause SCA1-like phenotypes (Pilotto et al. 2023).

Beyond these cell types, there are other cell populations in the cerebellum, such as granule cells, Golgi cells, Lugaro cells, unipolar brush cells and velate cells, whose dysfunction has been proposed or shown to cause cerebellar ataxias (Kreko-Pierce et al. 2020; Lee et al. 2023; Cerrato 2020). These lines of evidence together argue that cerebellar pathologies are not Purkinje cell-autonomous but are likely caused by dysfunction in multiple cell populations. This highlights the importance in considering different cell types when studying cerebellar ataxias.

In this thesis, I reported transcriptional changes in different cerebellar cells, mitochondria dysfunction in molecular and granule cell layer, and oxidative stress in molecular layer interneurons, demonstrating their involvement in SCA6 pathology.

CHAPTER 3: MITOCHONDRIAL DAMAGE AND IMPAIRED MITOPHAGY CONTRIBUTE TO DISEASE PROGRESSION IN SCA6

Manuscript published at *Acta Neuropathologica* (January 2024):

Mitochondrial damage and impaired mitophagy contribute to disease progression in SCA6

Tsz Chui Sophia Leung[1], Eviatar Fields[1,2], Namrata Rana[1], Ru Yi Louisa Shen[1], Alexandra E. Bernstein[1], Anna A. Cook[1], Daniel E. Phillips[1], Alanna J. Watt[1*]

[1]Biology Department, McGill University, Montreal, QC, Canada

[2]Integrated Program in Neuroscience, McGill University, Montreal, QC, Canada

[*]Correspondence: alanna.watt@mcgill.ca

Abstract

Spinocerebellar ataxia type 6 (SCA6) is a neurodegenerative disease that manifests in midlife and progressively worsens with age. SCA6 is rare, and many patients are not diagnosed until long after disease onset. Whether disease-causing cellular alterations differ at different disease stages is currently unknown, but it is important to answer this question in order to identify appropriate therapeutic targets across disease duration. We used transcriptomics to identify changes in gene expression at disease onset in a well-established mouse model of SCA6 that recapitulates key disease features. We observed both up- and down-regulated genes with the major down-regulated gene ontology terms suggesting mitochondrial dysfunction. We explored mitochondrial function and structure and observed that changes in mitochondrial structure preceded changes in function, and that mitochondrial function was not significantly altered at disease onset but was impaired later during disease progression. We also detected elevated oxidative stress in cells at the same disease stage. In addition, we observed impairment in mitophagy that exacerbates mitochondrial dysfunction at late disease stages. In post-mortem SCA6 patient cerebellar tissue, we observed metabolic changes that are consistent with mitochondrial impairments, supporting our results from animal models being translatable to human disease. Our study reveals that mitochondrial dysfunction and impaired mitochondrial degradation likely contribute to disease progression in SCA6 and suggests that these could be promising targets for therapeutic interventions in particular for patients diagnosed after disease onset.

Key words

Transcriptome, metabolomics, mitochondria, ataxia, Purkinje cell, disease progression

Introduction

Spinocerebellar ataxia type 6 (SCA6) is a neurodegenerative disease that typically first affects patients during midlife after which it progressively worsens with age [27, 66]. Post-mortem studies reveal extensive Purkinje cell death in the cerebellar vermis [26, 55, 78]. SCA6 is caused by CAG

repeat expansion mutation in the *CACNA1A* gene that encodes both the α1A subunit of the P/Q voltage-dependent calcium channel [80], and a transcription factor, α1ACT [17]. Despite its likely role in transcriptional dysregulation, we have an incomplete understanding of the transcriptional changes that contribute to SCA6, limiting the development of effective treatments.

We utilize a mouse model of SCA6 that contains a hyper-expanded CAG repeat tract that recapitulates several features of human disease ($SCA6^{84Q/84Q}$ mice, hereafter referred to as SCA6 mice): midlife onset, progressive motor impairment with age, and late Purkinje cell death [29, 76]. This allows us to examine cellular and molecular changes associated not only with disease onset, but also temporal alterations that are associated with disease progression. Given that SCA6 patients are often diagnosed post-onset [59, 60], it is important to understand the cellular pathophysiology that contributes to disease progression, since this may differ from mechanisms of disease onset.

To address this question, we used transcriptomics to explore the molecular changes underlying SCA6 at disease onset. We identified hundreds of significantly dysregulated genes, with both up- and down-regulated transcripts observed. Bioinformatic pathway analysis of these dysregulated genes revealed that the major families of downregulated genes were associated with impaired mitochondrial function and structure. Mitochondrial alterations have been implicated in many neurodegenerative diseases such as Alzheimer's disease and Parkinson disease [5, 22], as well as other SCA subtypes SCA1 and SCA7 [62, 75], although mitochondrial dysfunction has not previously been observed in SCA6.

To determine how transcriptional changes affect mitochondrial function, we measured mitochondrial membrane potential in cerebellar Purkinje cells and found that it was normal at disease onset but impaired as disease progressed. In agreement with this, we observed an increase in oxidative stress in cerebellar Purkinje cells at later disease stages although not at disease onset. Intriguingly, these cellular dysfunctions were not limited to cerebellar Purkinje cells but was also observed in molecular layer interneurons, suggesting that other cerebellar cell types are also affected in SCA6, as has been demonstrated in other forms of ataxia [32, 49]. Next, we confirmed that mitochondrial structure is impaired in cerebellar Purkinje cells both at early and late disease stages using transmission electron microscopy. Since cells maintain mitochondrial quality in part by the elimination of damaged mitochondria through mitophagy, we explored whether mitophagy

might be altered in SCA6. We observed that there was a reduction of markers of both autophagosomes and mitophagosomes, suggesting that the SCA6 cerebellum displays a progressive reduction in mitophagy that likely exacerbates mitochondrial dysfunction. To address whether our findings are representative of human disease, we analyzed post-mortem cerebellar tissues from SCA6 patients and non-neuropathological controls using metabolomics, and observed changes in metabolites that indicate mitochondrial dysfunction. Our findings uncover novel mitochondrial and mitophagy dysfunction that likely contributes to disease progression in SCA6, and highlight promising future avenues for therapeutic interventions for patients after disease onset.

Materials and Methods

Animals

We used a knock-in mouse model of SCA6 containing a humanized 84 CAG repeat expansion mutation at the *Cacna1a* locus ($SCA6^{84Q/84Q}$). To obtain homozygous SCA6 mice ($SCA6^{84Q/84Q}$) and litter-matched WT control mice, we bred heterozygous mice ($SCA6^{84Q/+}$) acquired from Jackson Laboratories (Bar Harbor, Maine; strain: B6.129S7-Cacna1atm3Hzo/J; stock number: 008683; RRID:IMSR_JAX:008683) [76]. Genotyping of the animals was performed using primer sequences provided by Jackson laboratories. Mice of both sexes were included in all experiments, and no animals were excluded from analysis. Breeding and animal procedures were carried out with the approval of the McGill Animal Care Committee in accordance with the Canadian Council on Animal Care guidelines.

RNA extraction and RNA sequencing

The experimental area and equipment were cleaned with RNAseZAP (Sigma #R2020) to remove RNAse contamination. Mice were anesthetised with isoflurane until loss of toe pinch reflex, then decapitated and cerebellar vermis were dissected out, flash frozen on dry ice, and stored at -80°C until extraction. Cerebellar tissues were mechanically homogenized in TRIzol reagent (Invitrogen #15596026) by passing through 18-gauge then 23-gauge needles. Chloroform (Sigma #288306) was then added to the homogenate to separate total RNA into the aqueous phase, which was then

recovered by precipitation with 70% ethanol. All procedures were performed on ice or at 4°C. To further remove any organic carryover and DNA, RNA extracts were purified using RNeasy Mini Kit (Qiagen #74104) with DNase I treatment as described in manufacturer's protocol.

RNA integrity was assessed with capillary electrophoresis (Agilent BioAnalyzer 2100) which generated an RNA integrity number (RIN). All samples have RIN over 9.3, indicating high RNA quality. Total RNA was sent to Genome Quebec for library preparation and sequencing. Library was created using NEB stranded mRNA library preparation, and sequencing was done on Illumina HiSeq 4000 generating 100bp paired-end reads. These samples had a median of 53 million reads (IQR, 47-63 million reads), and a median of 92.5% mapping rate (IQR, 92%-93%).

RNA sequencing data analysis

FASTQ files were transferred to Compute Canada cloud server for processing. Reads were aligned to mouse reference genome (GRCm38) using HISAT2 version 2.1.0 [33]. Reads were quantified using HTSeq version 0.11. [1] in union mode. Differential expression analysis was done with DESeq2 version 1.24.0 in RStudio [37]. DESeq2 adjusted P values for multiple testing with a target $\alpha = 0.05$, and genes were considered DEGs at FDR < 0.05. For principal component analysis, normalized read data generated using DESeq2 was then log2 transformed. Enriched gene pathways in GO databases and KEGG pathway database were identified using gProfiler [50]. To identify significantly disrupted pathways, a limit of 1000 genes were used to filter out more general GO terms.

Acute slice preparation and mitochondria membrane potential staining

Slice preparation was performed as previously described [14]. Mice were deeply anesthetised with intraperitoneal injection of 2,2,2-tribromoethanol (Avertin) until the loss of toe pinch reflex, followed by an intracardiac perfusion with approximately 30 ml of ice-cold partial sucrose replacement slicing solution (111 mM sucrose, 25 mM glucose, 50 mM NaCl, 2.5 mM KCl, 1.25 mM NaH_2PO_4, 25 mM $NaHCO_3$, 0.65 mM $CaCl_2$ and 10 mM $MgCl_2$, bubbled with 95% O2 and 5% CO2 to maintain pH at 7.3). Mice were then rapidly decapitated, and the brain was dissected out, which was then sectioned into 150μm thick slices using a VT 1200S vibratome (Leica Microsystems, Wetzlar, Germany). Slices were incubated in artificial cerebrospinal fluid (ACSF: 20 mM glucose, 125 mM NaCl, 2.5 mM KCl, 1.25 mM NaH_2PO_4, 25 mM $NaHCO_3$, 2mM $CaCl_2$

and 1 mM $MgCl_2$, bubbled with 95% O2 and 5% CO2 to maintain pH at 7.3; osmolality ~320 mOsm) at 37°C for 45 minutes for recovery.

To stain slices with Tetramethylrhodamine, Ethyl Ester, Perchlorate (TMRE, Invitrogen #T669), slices were transferred to a 24-well plate, one slice per well, and incubated in 10nM of TMRE (prepared fresh the day of experiment by serial dilution with ACSF from 200μM stock in DMSO) at 37°C for 30 minutes in dark. As a control, 40μM of carbonyl cyanide-p-trifluoromethoxyphenylhydrazone (FCCP) was added to collapse membrane potential which prevents TMRE accumulation in mitochondria. During image acquisition, slices were left in 10nM TMRE to prevent recalibration of the dye. Using an LSM800 confocal microscope (Zeiss) and excitation at 561nm, Z-stack images were acquired from 4-6 slices/animal. During each experimental session, cerebellum from two animals, one of each genotype, were used to manage uncontrolled variables. Blinding was achieved by pre-selecting the animal pairs for each session and referring to each animal only by their IDs.

Image analysis was performed in Fiji (ImageJ; US National Institutes of Health) [52, 57]. Z-projection of 11 optical slices (slice interval at 0.5μm, total section of 5μm) max intensity was used to measure signal intensity within regions of interest. Data were normalized to WT data from the same experimental session.

Immunohistochemistry

Tissue sections for immunohistochemistry was prepared as previously described [14]. Anesthesia of mice were induced and maintained with isoflurane through inhalation, confirmed with absence of toe pinch reflex. Then, intracardiac perfusion was performed with a flush of ice-cold phosphate-buffered saline (PBS; 0.1 M, pH 7.4) with heparin salt (5.6 μg/ml), followed by 40ml of 4% paraformaldehyde (PFA) in phosphate buffer (pH 7.4), both at the rate of 50 ml/min. Brain was rapidly removed and incubated in 4% PFA at 4°C overnight on an orbital shaker at 70rpm before being transferred to PBS with 0.05% sodium azide for short term storage at 4°C. The cerebellum was then sliced using a vibrating microtome (5100mz Vibratome, Campden Instruments, Loughborough, UK) into sections of 80 or 100μm thickness. Slices were collected serially and were suspended in 24-well plate containing PBS with 0.05% sodium azide.

For each experiment, slices from all animals were stained simultaneously in one setting, and master mixes of antibodies were made to minimize batch effects. All incubation steps were done on an orbital shaker at 70rpm to achieve even staining. Free-floating slices were first rinsed with washing solution (PBS with 0.4% Triton X-100), then incubated in primary antibody (Supplementary Table 2) and blocking solution (PBS, 0.4% Triton X-100, 5% Bovine serum albumin (BSA), 0.05% sodium azide) for 3 days at room temperature. Slices were then rinsed in washing solution and incubated for 90 minutes with secondary antibodies (Table 2). For experiments involving antibodies derived from mouse, an additional 30-minute incubation with Anti-Mouse IgG Fab fragments was added prior to secondary antibody incubation. After a final washing solution rinse, stained slices were mounted using ProLong Gold Antifade mounting medium (Thermo Fisher Scientific, Waltham, USA) and stored in dark at 4°C prior to imaging.

Image acquisition and analysis

Images were acquired using an LSM800 confocal microscope (Zeiss) on Zen Blue software. For analyses that detect signal intensity within the entire Purkinje cell body area (Fig. 3, 4 and 6e), images were acquired using a 20x objective at 1024 x 1024-pixel resolution. For analyses concerning subcellular structures (Fig. 6a-d), images were acquired using a 40x objective at 2048 x 2048-pixel resolution. Laser settings were kept identical for each experiment. All imaging and analysis were performed in lobule III of the anterior vermis, a region of the cerebellum where cellular deficits in SCA6 were shown [14, 29]. Both image acquisition and image analysis were carried out blinded to the experimental conditions.

Image analysis was done in Fiji [52, 57]. For Fig. 3, 4 and 6e, Purkinje cell and molecular layer interneurons bodies were delineated by hand using calbindin and parvalbumin as markers respectively, which were then overlaid onto regions of interest to measure signal intensity within these cells. For Fig. 6a-d, object-based colocalization were used. Images were pre-processed with *Background Subtraction*, then an auto-threshold protocols was applied to segment lysosome (stained by Lamp1, using *RenyiEntropy*) and mitochondria (stained by CoxIV, using *Moments*) from the background. Then, the area of the intersection of lysosome and mitochondria was calculated using the AND operator in *Image Calculator.*

To generate representative images, linear adjustments of the brightness and contrast were applied to improve the legibility. Identical adjustments were applied to all images within a data set.

Transmission electron microscopy

For tissue fixation, mouse anesthesia was induced and maintained with isoflurane through inhalation, confirmed with absence of toe pinch reflex. Then, intracardiac perfusion was performed with a flush of ice-cold phosphate-buffered saline (PBS; 0.1 M, pH 7.4) with heparin salt (5.6 µg/ml), followed by 40ml of 2% paraformaldehyde (Electron Microscopy Sciences) and 2% glutaraldehyde (Electron Microscopy Sciences) in 0.1M phosphate buffer in (pH 7.4), both at the rate of 50 ml/min. Brain was rapidly removed and incubated in 2.5% glutaraldehyde in 0.1 M sodium cacodylate (Electron Microscopy Sciences) at 4°C for one week on an orbital shaker at 70rpm. Lobule III of the cerebellar vermis were micro-dissected out under light microscope and sent for dehydration, embedding, sectioning, and staining processed by Facility for Electron Microscopy Research (FEMR) at McGill University, as described before [35].

Images were acquired using FEI Tecnai G2 Spirit Twin Cryo-TEM (FEI Company, Hillsboro, OR, USA) at 120 kV and visualized with an AMT XR80C 8-megapixel CCD camera (Advanced Microscopy Techniques, Woburn, MA, USA) at 1900x and 4800x resolutions. Only one cross section image was taken for each Purkinje cell body, thus each Purkinje cell is analysed only once. EM images from each timepoint were analysed in parallel by two independent analysts, who were blinded to genotypes. They identified and counted all mitochondria in the Purkinje cell body and annotated them individually as healthy or damaged based on the cristae content and the integrity of mitochondrial membrane. Data from one observer is shown and data from the other observer is provided in the supplementary material (Supplementary Fig. 4c-f).

Accelerating rotarod

We used an accelerating paradigm on a rotarod (Stoelting, IITC) as previously described [14, 28, 29], which robustly detects motor coordination deficits in SCA6 mice. Mice were allowed to acclimatize in the experimental room for 1 hour prior to testing. Mice were then placed on rotating rods, which accelerates from 4 rpm to 40 rpm over 5 minutes and stays at 40 rpm for another 5 minutes. Latency to fall off the rod was recorded. If a mouse fell off within 5 seconds, it was

considered as an invalid trial and the animal was immediately retested. Mice performed the assay four times per day with 10 minutes rest between trials, for five consecutive days. Average latencies of each day were shown.

Human post-mortem cerebellar tissues

SCA6 patients' post-mortem cerebellar tissues were donated by Dr. Arnulf Koeppen (Albany Stratton Veterans Affairs Medical Center, Albany, New York, USA). Age- and sex- matched non-neuropathological control cerebellar tissues were obtained from The Douglas Bell Canada Brain Bank. Tissues were shipped in pellet dry ice and stored at -80°C upon arrival.

Tissue extraction and LC-MS/MS

Post-mortem human cerebellar tissues were crushed to fine powder in liquid nitrogen using a pre-chilled mortar and pestle. Approximately 19mg of crushed tissue (19.2 ± 0.2mg) were quickly weighed out and transferred to tubes stored in dry ice to minimise tissue thawing. Tissues were then extracted with 31.6% methanol (Fisher Scientific, Ottawa, Ontario)/36.7% acetonitrile (Fisher Scientific, Ottawa, Ontario) in LC/MS grade water containing 1mg/ml of N-ethylmaleimide (Sigma-Aldrich, Oakville, Ontario) to protected free thiols [54]. Then, tissues were lysed and homogenized by bead-beating for 2 minutes at 30 Hz using 4 ceramic beads (2 mm) per sample (SpeedMill Plus, Jena Analytik). Tissue extracts were partitioned into an aqueous layer, a protein intermediate layer and an organic layer following dichloromethane treatment and centrifugation. The protein layers were dried by vacuum centrifugation and analyzed for total protein concentration using Bradford assay. The aqueous supernatants were dried by vacuum centrifugation with sample temperature maintained at -4°C (Labconco, Kansas City MO, USA). Dried extracts were subsequently re-suspended in 50 μL of chilled H_2O and clarified by centrifugation at 1°C.

Ion Pairing

For targeted metabolite analysis, samples were injected onto an Agilent 6470 Triple Quadrupole (QQQ)–LC–MS/MS (Agilent Technologies). Chromatographic separation of metabolites was achieved by using a 1290 Infinity ultra-performance quaternary pump liquid chromatography system (Agilent Technologies). The mass spectrometer was equipped with a Jet StreamTM electrospray ionization source, and samples were analyzed in negative mode. The source-gas

temperature and flow were set at 150 °C and 13 L/min, respectively, the nebulizer pressure was set at 45 psi, and capillary voltage was set at 2,000 V. Multiple reaction monitoring parameters (qualifier/quantifier ions and retention times) were obtained and optimized using authentic metabolite standards (Sigma-Aldrich, Oakville, Ontario).

Chromatographic separation of the isomers and other metabolites was achieved by using a Zorbax Extend C18 column 1.8 µm, 2.1 × 150mm^2 with guard column 1.8 µm, 2.1 × 5mm^2 (Agilent Technologies). The chromatographic gradient started at 100% mobile phase A (97% water, 3% methanol, 10 mM tributylamine, 15 mM acetic acid, 5 µM medronic acid) for 2.5 min, followed with a 5-min gradient to 20% mobile phase C (methanol, 10 mM tributylamine, 15 mM acetic acid, 5 µM medronic acid), a 5.5-min gradient to 45% C and a 7-min gradient to 99% C at a flow rate of 0.25 mL/min. This was followed by a 4-min hold time at 100% mobile phase C. The column was restored by back-washing with 99% mobile phase D (90% ACN) for 3 min at 0.25 mL/min, followed by increase of the flow rate to 0.8 mL/min over 0.5 min and a 3.85-min hold, after which the flow rate was decreased to 0.6 mL min−1 over 0.15 min. The column was then re-equilibrated at 100% A over 0.75 min, during which the flow rate was decreased to 0.4 mL/min, and held for 7.65 min. One minute before the next injection, the flow was brought back to forward flow at 0.25 mL/min. For all LC–MS analyses, 5 µL of sample was injected. The column temperature was maintained at 35°C.

Amino acids and derivatives

Since the above ion pairing method is limited to only negative ionization, amino acids and other related metabolites were collected using an Agilent 6470 Triple Quadrupole (QQQ)-LC-MS/MS. Chromatography was achieved using a 1290 Infinity ultra-performance LC system (Agilent Technologies, Santa Clara, CA, USA). Mass spectrometer was equipped with a Jet Stream electrospray ionization (ESI) source and samples were analyzed in positive mode. Multiple reaction monitoring was optimized and retention times confirmed on authentic metabolite standards. Source gas temperature and flow were set at 300°C and 5 L/min respectively, nebulizer pressure was set at 45 psi and capillary voltage was set at 3500V. The autosampler temperature was maintained at 4° C.

Chromatographic separation of creatine was achieved using an Intrada Amino Acid column 3 µm, 3.0×150mm (Imtakt Corp, JAPAN). The chromatographic gradient started at 100% mobile phase B (0.3% formic acid in ACN) with a 3 min gradient to 27% mobile phase A (100 mM ammonium

formate in 20% ACN / 80% water) followed with a 19.5 min gradient to 100% A at a flow rate of 0.6 ml/min. This was followed by a 5.5 min hold time at 100% mobile phase A and a subsequent re-equilibration time (7 min) before next injection. The column temperature was maintained at 10°C. Relative concentrations were determined from external calibration curves of standards dissolved in water.

All LC-MS/MS data were analyzed using MassHunter Quant (Agilent Technologies). No additional corrections were made for ion suppression; thus, concentrations are relative to the calibration curve and not absolute. Relative concentration of each compound was normalized to total protein amount and data are represented as fold change relative to the average of control.

Statistics

Data were first tested for normalcy and statistical comparisons were performed using Student's *t* test Mann-Whitney *U* test using JMP software (SAS, Cary, NC). Data are reported as box plots, where the box represents 1st quartile, median and 3rd quartile, and the whiskers represent one standard deviation from median.

Results

Transcriptional alterations in SCA6 cerebellum

To identify novel molecular targets that may contribute to SCA6 disease, we profiled gene expression changes using RNA sequencing (RNA-seq) in a knock-in mouse model of SCA6 [76]. We compared SCA6 and litter-matched wildtype (WT) control mouse cerebellar vermis at disease onset (7 months), an age when motor coordination deficits start to be observed but prior to Purkinje cell degeneration (Fig. 1a) [29]. Animals were selected based on rotarod performance to confirm that SCA6 mice included in this analysis displayed impaired motor coordination (Supplementary Fig. 1a), with both sexes included. We micro-dissected the cerebellar vermis from SCA6 and WT mice (N=5 per group; Fig. 1b), then extracted and sequenced the total mRNA from tissue homogenates. To gain insight into sources of variability among samples, we performed principal component analysis (PCA) on the RNA-seq data. PC1 (33.4%) and PC2 (24.5%) together accounted for slightly over half of the variability in the dataset (Supplementary Fig. 1b), suggesting that there could be more than two main sources of variability. The samples were loosely grouped into two clusters corresponding to the two genotypes (Supplementary Fig. 1c), suggesting that despite the appreciable level of variability, the expression profile of SCA6 animals was distinguishable from that of WT animals. Interestingly, however, data did not cluster based on sex, suggesting sex difference was not a main source of variability in transcription profile (Supplementary Fig. 1c).

To gain insight into disrupted molecular signatures, we next performed differential expression analysis, and found that there were 513 differentially expressed genes (DEGs) that showed significant differences in SCA6 mice (Padj < 0.05; Fig. 1c and Supplementary Table 1). Of these, ~half (54%) were upregulated, and ~half (46%) were downregulated (Fig. 1c). This suggests that widespread transcriptional dysregulation is present in SCA6, consistent with the mutated gene, *Cacna1a,* encoding a transcription factor [17]. The majority of dysregulated genes were altered by only moderate fold changes from WT level, with most genes dysregulated to between 50% – 150%, or -0.585 and 0.585 on log2 scale (Fig. 1d). Of these more than 500 DEGs, certain genes displayed changes as predicted: e.g., *Cacna1a* had reduced expression level in SCA6 than WT (fold change = 0.791; Padj = 0.0152; Supplementary Fig. 1d), suggesting that the CAG repeat expansion

mutation decreases expression of both the P/Q calcium channel and the transcription factor that it encodes (consistent with [76]). However, the function of many of the most highly dysregulated genes in the cerebellum is largely unknown (see Supplementary Table 1).

To interpret the list of DEGs in functional terms, we performed gene ontology (GO) term enrichment analysis on the list of DEGs to identify impacted biological processes, rather than investigating single genes or proteins. We mapped both up- and down-regulated genes onto biological process GO terms and detected the statistically over-represented terms. We found that the gene ratios (the number of mapped DEGs/the number of genes associated with the GO term) were higher for the downregulated terms compared to the upregulated terms (Fig. 2a, indicated by the size of the circles), suggesting that these downregulated biological processes may be more severely affected. Among the significantly upregulated GO terms, we found that the top terms were those involved in behavior, development, and synapse organization and signaling (Fig. 2a). This is interesting since synaptic dysregulation has been observed in SCA6 models [41], and developmental alterations have been observed previously in the same mouse model [30]. Since the RNA-seq was performed at a mid-life timepoint, our data suggest that either the gene expression changes that induce developmental deficits persist into adulthood, or the development GO terms upregulated in SCA6 may lack temporal specificity.

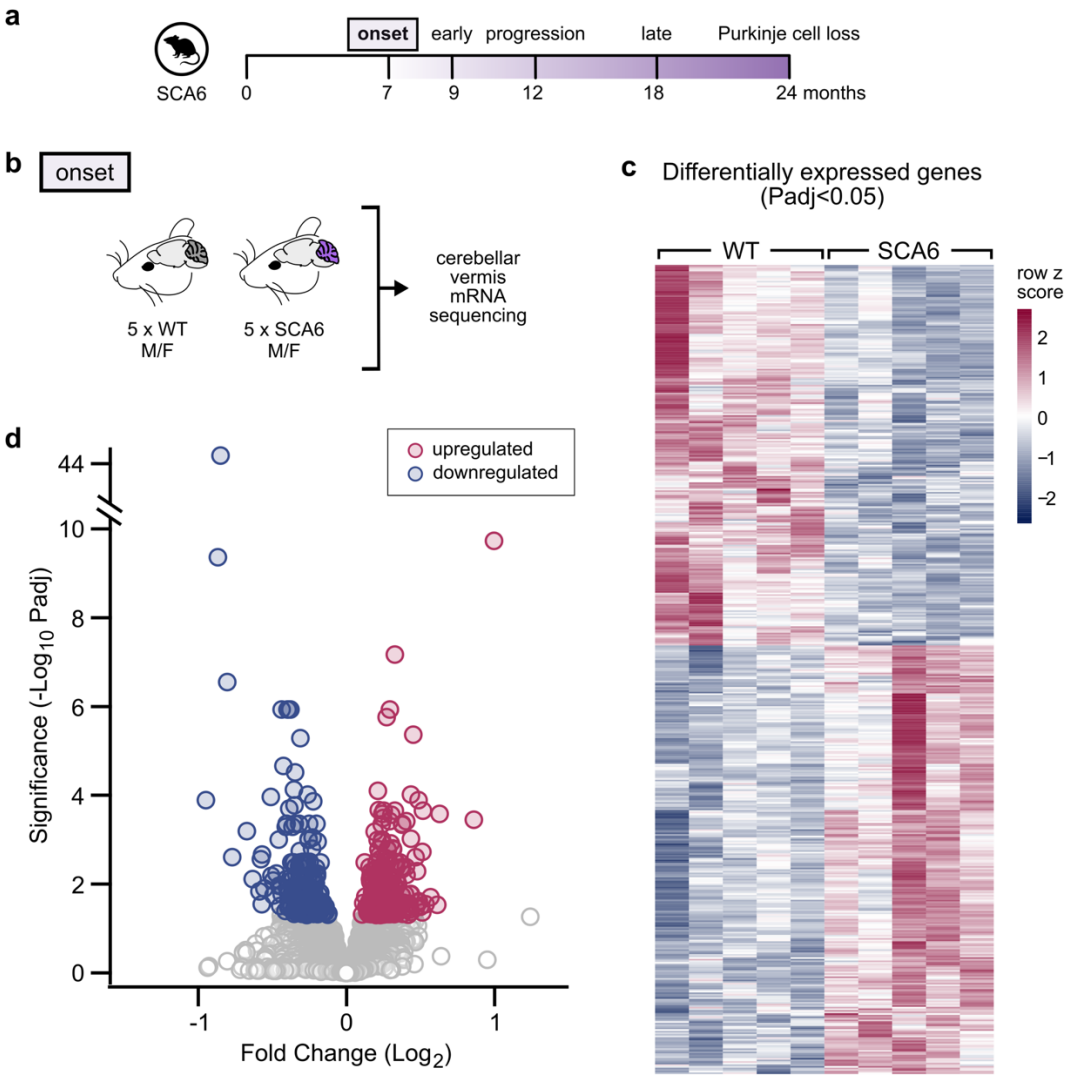

Fig. 1 Gene expression changes in SCA6 cerebellum at disease onset. (a) Timeline of disease progression in SCA6 mouse model. (b) Cerebellar vermis tissue was extracted from male and female WT and SCA6 mice (N = 5 per genotype) for sequencing. (c) RNA sequencing revealed 513 DEGs in SCA6 compared to WT (Padj < 0.05). Each column of the heatmap represents an animal, each row represents a gene. Refer to Supplementary Table 1 for complete list of genes. (d) Volcano plot shows the distribution of fold changes of the disrupted genes in SCA6. Colored markers represent significant genes, grey markers are non-significantly changed genes

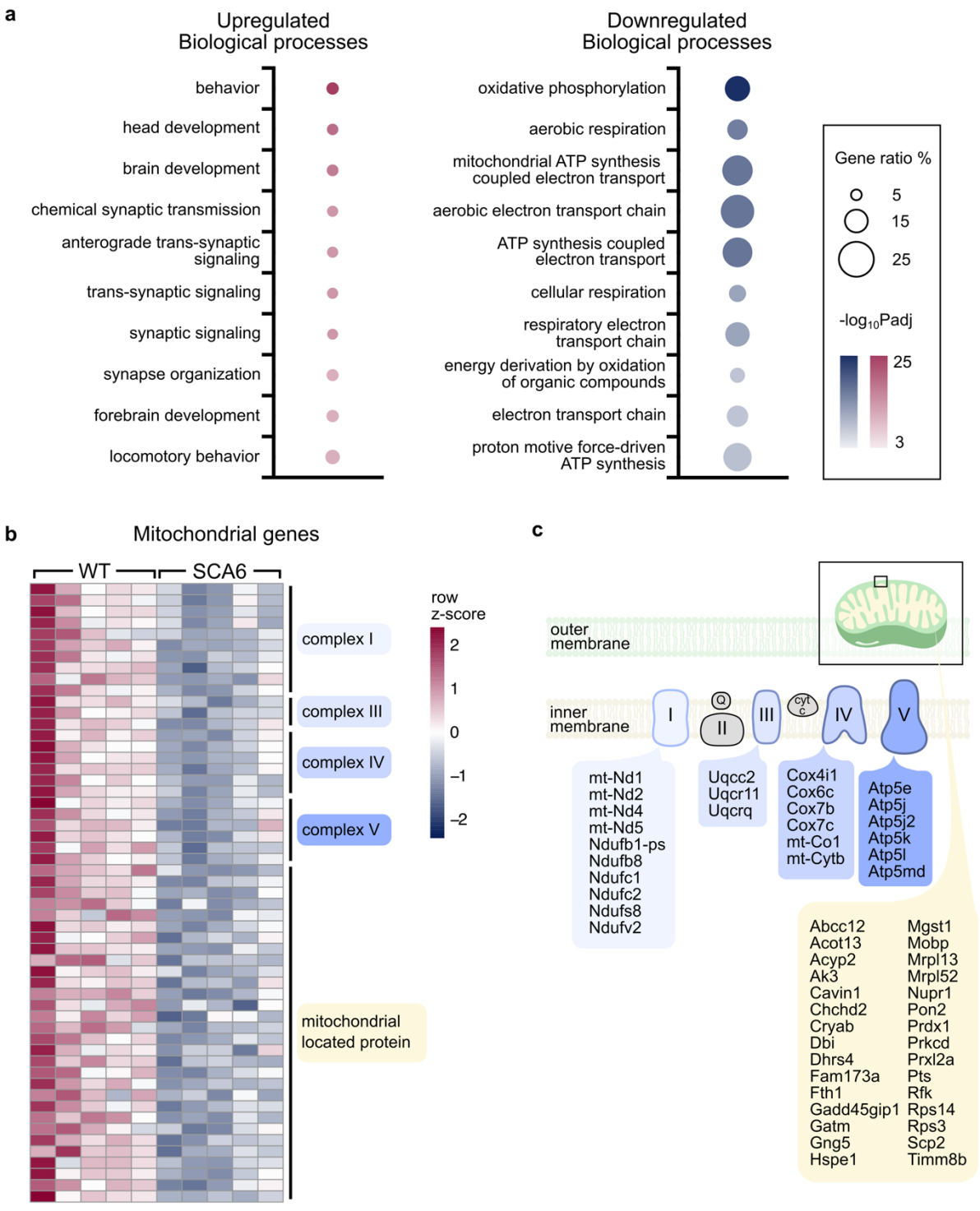

Fig. 2 Mitochondrial genes are downregulated in SCA6. (a) GO term enrichment analysis revealed the top biological processes that are up- (left) and down- (right) regulated. The proportion of dysregulated genes per GO term is larger for down-regulated compared to up-regulated GO terms

(gene ratio, indicated by size of the circle). (b) Heatmap showing down-regulated mitochondrial-related genes grouped by location within the mitochondria showed that these changes are consistent in same direction in all 5 SCA6 animals. (c) Genes encoding complexes of the electron transport chain and mitochondria membrane were downregulated

Mitochondrial genes are downregulated in SCA6

In contrast to the top upregulated GO terms, the top downregulated GO terms (Fig. 2a) included larger gene ratios that were significantly over-represented compared to the upregulated GO terms (indicated by larger and darker markers). Interestingly, these downregulated GO terms correspond to biological processes that have not previously been implicated in SCA6 that strongly suggest mitochondrial dysfunction. Genes mapped to these GO terms include both genomic (e.g. Atp5e) and mitochondrial (e.g. mt-Cytb) genes, and include genes that encode for complex subunits in the electron transport chain (ETC) (Fig. 2b-c). These genes were consistently downregulated in all 5 SCA6 RNA-seq samples (Fig. 2b). This suggests that there could be a reduction of mitochondria biogenesis, a global reduction of the pool size of mitochondria, and/or a disruption to mitochondrial respiratory capacity in SCA6. Since mitochondrial dysfunction is a novel impairment that has not previously been implicated in SCA6 disease pathology, we chose to study it further.

Lowered mitochondrial membrane potential as SCA6 progresses

Our RNA-seq data demonstrated reduced expression of ETC genes in SCA6 cerebellar vermis. Since ETC complexes are required to sustain mitochondrial respiration, we hypothesized that this may result in a lower respiratory capacity of SCA6 mitochondria. To test this, we examined the mitochondrial membrane potential ($\Delta\psi_m$) in individual neurons within live cerebellar tissue at two disease stages: disease onset (7 months) and disease progression (12 months; Fig. 3a). $\Delta\psi_m$ is generated by complexes in the ETC and, together with the mitochondrial pH gradient, it provides the bioenergetic driving force for respiration, or ATP production [81]. We loaded live acute cerebellar slices from WT and SCA6 animals with 10nM of Tetramethylrhodamine, Ethyl Ester

(TMRE), a fluorescent dye that accumulates within mitochondria in proportion to their $\Delta\psi_m$ (Fig. 3b), and then imaged the slices on a laser scanning confocal microscope to determine TMRE intensity within Purkinje cells. Purkinje cell bodies could be reliably identified based on their size and location between the molecular layer and granule cell layer under both bright field and laser microscopy (Fig. 3c). As a control, carbonyl cyanide-p-trifluoromethoxyphenylhydrazone (FCCP) was administered to collapse $\Delta\psi_m$ which reduced the TMRE signal to background level, confirming that the fluorescent signal indeed came from TMRE accumulated in mitochondria (Fig. 3c).

We collected TMRE images from the same location in the cerebellum, the anterior lobule, and from both genotypes in each experimental session to minimize technical variability (N=3 animals per genotype, n=16-26 cells per animal for each timepoint). TMRE signals were punctate, resembling the distribution of mitochondria in cells (Fig. 3d-g), and were observed across the cerebellar cortical layers (Fig. 3c). Thus, although SCA6 pathology has been thought to be primarily expressed in cerebellar Purkinje cells [25, 70], we had the opportunity to examine changes in $\Delta\psi_m$ in mitochondria within each cortical layer: we visually identified Purkinje cell bodies within the Purkinje cell layer (Fig. 3d, f), and also measured $\Delta\psi_m$ in the molecular layer, likely arising from a heterogenous population of mitochondria located in Purkinje cell dendrites, parallel fiber, molecular layer interneurons, and Bergmann glia; as well as in the granule cell layer, likely representing a mixed population of mitochondria located in granule cells, Golgi cells, and mossy fiber terminals (Fig. 3e, g).

At disease onset, the same timepoint at which RNA-seq was performed, we found that there were no significant differences in TMRE signals in Purkinje cells, as well as in molecular layer and granule cell layer from SCA6 and WT mice (Fig. 3d-e). This suggests that cellular respiration may be not affected at this age despite reduction in gene expression. However, since SCA6 is a progressive disease [27, 46], and disease alterations are thought to accumulate with disease progression, we also measured $\Delta\psi_m$ in SCA6 and WT mice at a later timepoint when disease had progressed (at 12 months, 5 months after disease onset). Strikingly, we observed a significant reduction in TMRE signals which indicated a reduction in mitochondrial $\Delta\psi_m$ in all cerebellar locations examined, including in Purkinje cell bodies, as well as in the molecular layer and granule cell layer in SCA6 cerebellar vermis compared to WT (Fig. 3f-g). While changes in the molecular

layer could reflect alterations in mitochondria in both molecular layer interneurons and Purkinje cell dendrites, the alterations observed in the granule cell layer must arise from cell types other than Purkinje cells, which suggests that mitochondria dysfunction may not be limited to Purkinje cells in SCA6. We wondered if such dysfunction is limited to the cerebellum, or can also be observed in other brain regions. To investigate this, we measured TMRE signals in the somatomotor cortex from SCA6 and WT mice at the same disease timepoint (at 12 months; Supplementary Fig. 2). We oberved no significant difference in TMRE signals between the two genotypes (Supplementary Fig. 2b-c), while on the same tissue slice as an internal control, the TMRE signals of SCA6 Purkinje cells were significantly lower than that in WT (Supplementary Fig. 2d-e). This suggests that at this timepoint, mitochondrial dysfunction is restricted to the cerebellum, in line with the understanding that SCA6 pathology is largely cerebellar. The $\Delta\psi_m$ reduction we observed in SCA6 mice suggests that mitochondria have reduced cellular respiration, that is, a reduced capacity to produce ATP, as the disease progresses. Since Purkinje cells show high spontaneous activity [13], and thus require a high level of energy to sustain cellular function [11], the perturbation of ATP production may be particularly deleterious. Interestingly, since the transcriptional alterations we observed at disease onset were not reflected in functional changes until later during disease progression, our findings suggest that Purkinje cells normally have surplus bioenergetic capacity, making them resilient to small perturbations in mitochondrial gene expression.

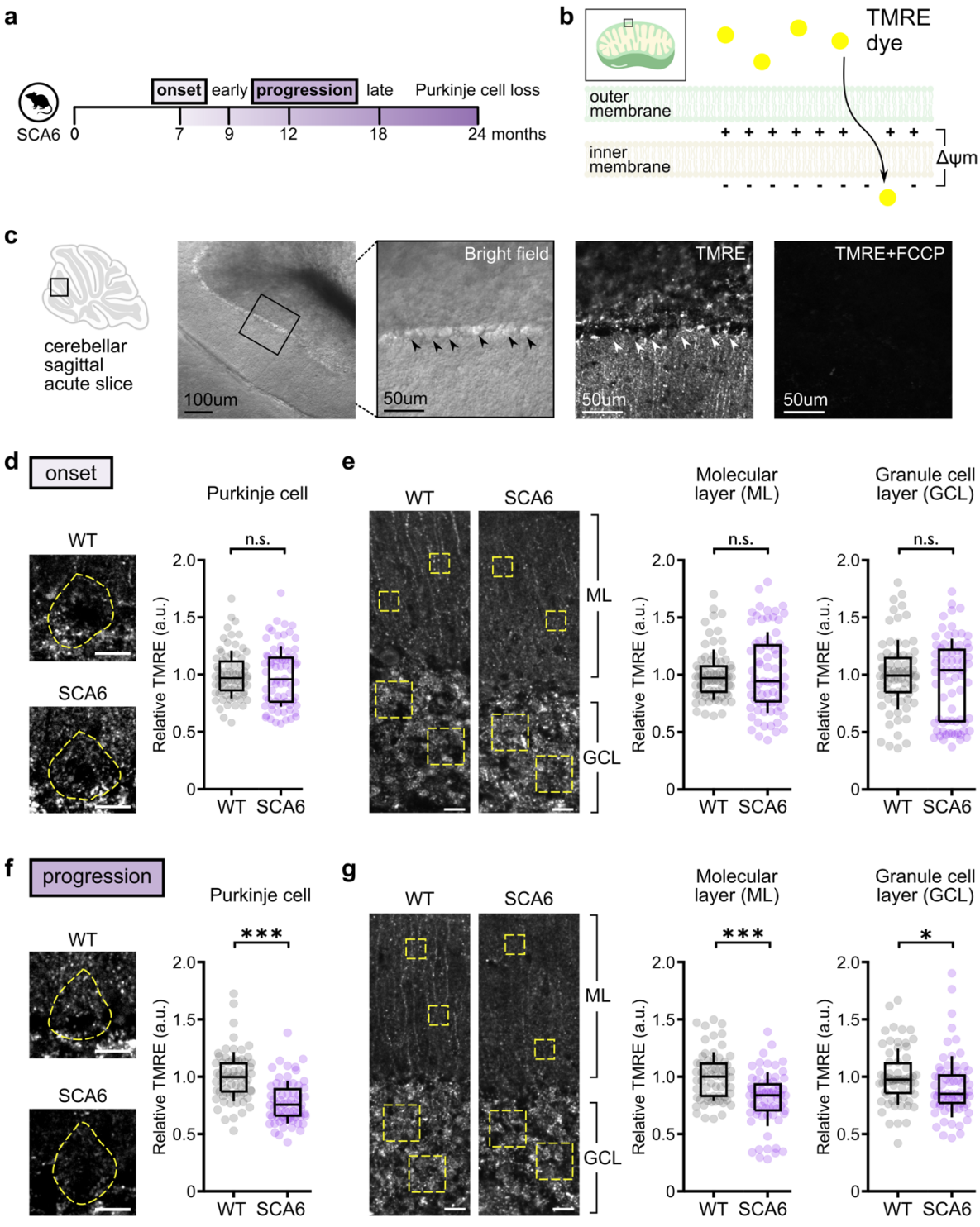

Fig. 3 SCA6 cerebellar mitochondria have a reduced membrane potential (Δψm), resulting in impaired cellular respiration as the disease progresses. (a) Δψm was assayed at disease onset and disease progression. (b) The fluorescent dye TMRE accumulates in mitochondria in proportion to

Δψm. (c) Purkinje cell bodies could be identified by their location between the molecular layer and granule cell layer under bright field and laser-scanning confocal microscopy. FCCP collapses mitochondrial Δψm and reduced TMRE signal to background levels as a negative control. (d-e) Data from disease onset (7 months). (d) Representative TMRE images of Purkinje cell bodies (outlined) in WT and SCA6. Relative TMRE signals showed no difference between genotypes (WT: n = 74 cells from N = 3 mice; SCA6: n = 74 cells from N = 3 mice; not significantly different, P = 0.617) (e) Representative TMRE images of a section of the cerebellar sagittal slice showing molecular and granule cell layer. Yellow dotted boxes illustrate regions of interest (ROIs). There were no differences in relative TMRE signal between genotypes at disease onset in either the molecular (WT: n = 74 ROI from N=3 mice; SCA6: n = 73 ROI from N = 3 mice; P = 0.802) or the granule cell layer (WT: n = 74 ROI from N = 3 mice; SCA6: n = 73 ROI from N = 3 mice; P = 0.795) (f-g) Data from a later timepoint as SCA6 progresses (12 months; progression). (f) Representative TMRE images of Purkinje cell bodies (outlined) in WT and SCA6. At this later age, TMRE signals were significantly reduced in SCA6 (WT: n = 68 cells from N = 3 mice; SCA6: n = 65 cells from N = 3 mice, P < 0.0001) (g) Representative TMRE images of a section of the cerebellar sagittal slice showing molecular layer and granule cell layer. Relative TMRE signal was reduced in SCA6 in both molecular layer (WT: n = 64 ROI from N = 3 mice; SCA6: n = 64 ROI from N = 3 mice; P < 0.0001) and granule cell layer (WT: n = 64 ROI from N = 3 mice; SCA6: n = 68 ROI from N = 3 mice; P < 0.05). Scale bar for (d)-(g) = 20 μm. Mann Whitney *U* test was used for all statistical comparisons. * P < 0.05, *** P < 0.0001, n.s. P > 0.05

Purkinje cells are under oxidative stress as SCA6 progresses

Previous studies have shown that reduction in $\Delta\psi_m$ leads to increases in reactive oxygen species (ROS) production [65]. There is also evidence that damaged mitochondria can induce ROS production from other sources, such as the endoplasmic reticulum [47]. ROS accumulation is typically considered to be deleterious to cell health [74], and Purkinje cells have been shown to be particularly susceptible to oxidative stress [10]. Indeed, antioxidant treatments that reduce oxidative stress have been shown to prevent Purkinje cell death in mouse models of disease such as spinocerebellar ataxia type 1 (SCA1) and in Autosomal recessive spastic ataxia of Charlevoix-

Saguenay (ARSACS) [43, 62]. Given that we observed a reduction in $\Delta\psi_m$ in the cerebellar vermis from SCA6 mice as disease progresses, we wondered if this would lead to excessive oxidative stress. To address this, we performed immunohistochemistry staining on acute cerebellar slices against a biomarker of cellular oxidative damage, 8-dihydro-2'-deoxyguanosine (8-OHdG), which is an oxidized form of the nucleotide guanine (Fig. 4b) [72]. We also labeled Purkinje cells with calbindin and interneurons with parvalbumin to localize these changes to specific cell types (Fig. 4c-f).

Since changes in $\Delta\psi_m$ were not detected at disease onset (Fig. 3), we chose to investigate two time points after onset: an early disease stage (9 months, 2 months after disease onset) and a later stage of disease progression (12 months; Fig. 4a). At the early disease stage, we observed robust labelling for the oxidative damage signal in both Purkinje cells as well as in molecular layer interneurons even in WT mice (Fig. 4c-d), which may represent oxidative damage related to normal aging. Staining in the granule cell layer was diffuse and not clearly localized to any cell type, so this was not quantified further. We observed no significant differences in the intensity of 8-OHdG in WT or SCA6 mice at this early disease stage (Fig. 4c-d), as expected given that we observed no significant changes in $\Delta\psi_m$ at disease onset (Fig. 3). However, as disease progressed, we observed a significant accumulation of the oxidative damage marker in both Purkinje cells bodies and molecular layer interneurons in SCA6 (Fig. 4e-f). This is also expected given the decrease in $\Delta\psi_m$ at the same progressive stage of disease (Fig. 3). Molecular layer interneurons have been classified into different subtypes [18] in part based on their location within the molecular layer of the cerebellum. To determine if a subtype of molecular layer interneurons was more susceptible to oxidative stress, we examined the upper- and lower- molecular layer interneuron subpopulations individually. We found that both populations had significantly elevated oxidative stress in SCA6 compared to WT (Supplementary Fig. 3). Taken together, the accumulation of oxidative stress we observe as SCA6 progresses suggests that mitochondrial dysfunctions could lead to broader negative consequences to cellular health.

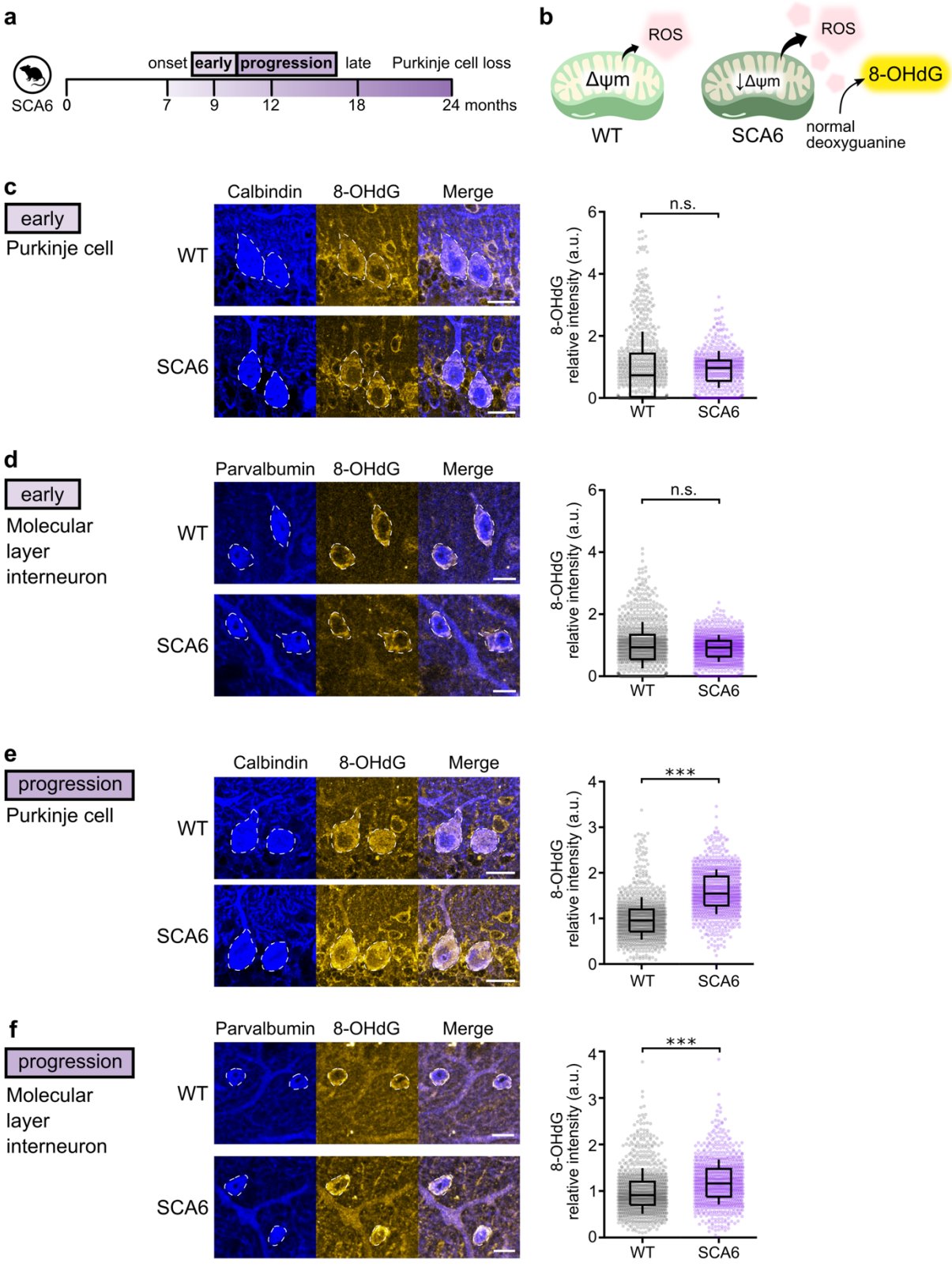

Fig. 4 SCA6 cerebellar neurons accumulate oxidative stress as disease progresses. (a) Oxidative

damage was measured at two disease timepoints: an early disease stage and disease progression stage. (b) Reduction in Δψm increases ROS production by mitochondria, which then oxidizes deoxyguanine to 8-OHdG. 8-OHdG is used as a biomarker for cellular oxidative stress (c-d) At an early disease stage, we did not observe a significant increase in oxidative stress (c) in SCA6 Purkinje cell bodies (WT: n = 695 cells from N = 3 WT mice; SCA6: n = 553 cells from N = 3 mice; P = 0.109) or (d) in molecular layer interneurons (WT and SCA6: n = 960 cells from N = 3 mice; P = 0.207). (e-f) At disease progression stage, we observed a significant accumulation of oxidative stress (e) in SCA6 Purkinje cells (WT: n = 952 cells from N = 3 WT mice; SCA6: n = 939 cells from N = 3 mice; P < 0.0001) and (f) in molecular layer interneurons (f) (WT: n = 960 cells from N = 3 WT mice; SCA6: n = 880 cells from N = 3 mice; P < 0.0001), a disease stage when Δψm was also significantly reduced. Scale bars for (c) and (e) = 20μm; for (d) and (f) = 10μm. Mann Whitney *U* test was used for all statistical comparisons. *** P < 0.0001, n.s. P > 0.05

Mitochondria are damaged in SCA6 Purkinje cells

There is a close relationship between mitochondrial function and morphology. For example, disrupted mitochondrial cristae is a hallmark morphological feature that is tightly associated with impaired mitochondrial respiration [12]. Given the functional deficits we observed in SCA6 mice as disease progressed, we wondered if morphological changes in mitochondria would be evident in the SCA6 cerebellum. We used transmission electronic microscopy to examine the ultrastructure of mitochondria in SCA6 and WT Purkinje cell bodies from two disease stages: an early disease timepoint (9 months) and a late disease timepoint when disease progression has advanced (18 months; Fig. 5a). Purkinje cells can be visibly identified within a sagittal cut of the cerebellar vermis – (1) they are localized in a single-cell thick layer between the outer molecular layer filled with cross section cut parallel fibres and the inner granule cell layer populated by granule cells with visually-distinctive nuclei, and (2) Purkinje cell bodies are larger than other surrounding cell types (Supplementary Fig. 4a).

Ultrastructural examination of Purkinje cell bodies early in disease in WT and SCA6 mice revealed several hallmark features. (1) First, we observed lipofuscin granules (Fig. 5ci and 5di), an aging-related structure common to post-mitotic cells. Its formation has been linked to oxidative damage

to proteins [51], mitochondrial impairment [34] and lysosomal dysfunction [64]. Interestingly, we observed no differences in the number of lipofuscin particles in WT and SCA6 Purkinje cells (Supplementary Fig. 4b), suggesting that its accumulation arises due to aging rather than disease. (2) Next, we observed putative autophagosomes (thick membranous structures enclosing disarrayed content) in proximity to a lysosome (dark, electron dense body) (Fig. 5cii). This association likely represents a snapshot showing the degradation of mitochondria and/or other cellular components. (3) We could also identify mitochondria-subsurface cisterna contact (Fig. 5ciii), and (4) mitochondria-endoplasmic reticulum (ER) contacts (Fig. 5dii). Both these last structures are thought to be enriched in Purkinje cells [20] and are involved in changes in calcium dynamics following synaptic stimulation [67]. Finally, we occasionally observed evidence of (5) synapses being made onto Purkinje cell bodies (Fig. 5diii).

At an early disease timepoint, we observed similar numbers of mitochondria in both WT and SCA6 Purkinje cells (Fig. 5f). We wondered whether morphological evidence for mitochondrial damage would be present at this early disease stage. Damaged mitochondria were identified as those with loss of cristae folding, and/or a rupture in the mitochondrial membrane (Fig. 5b). While damaged mitochondria were observed in WT Purkinje cells at this age, they were more common in SCA6 (Fig. 5e-f). This was surprising, since we lack functional evidence for mitochondrial impairment at this age (Fig. 3 and 4) and suggests that changes in morphology precede changes in function. We wondered if mitochondrial dysfunction worsens as disease progresses. To address this in more detail, we next examined mitochondrial morphology at a late stage of disease progression (18 months).

Notably, we observed dark cell degeneration at this late disease stage (Fig. 5g). Dark cell degeneration is a special form of cell death that Purkinje cells undergo, which has also been observed in other disease models that exhibit mitochondria dysfunctions [9, 39, 40]. Focusing only on Purkinje cell bodies which appeared healthy and did not display cytoplasmic darkening, we observed no significant difference in the number of mitochondria in WT and SCA6 Purkinje cells at this late stage of disease progression (Fig. 5h-j), similar to what we observed at an early stage of disease (Fig. 5f). However, the number of mitochondria in both genotypes decreased with age (compare Fig. 5f to 5j). We next examined damaged mitochondria in WT and SCA6 Purkinje cells, and found that the proportion of damaged mitochondria in SCA6 was elevated compared to in WT.

Although the absolute proportion of damaged mitochondria was similar to the early disease timepoint, there are nonetheless strong signs of increased severity of damage with age in SCA6. For example, at 18 months the loss of cristae was more severe (compare Fig. 5i to 5e). Taken together, these data suggest that mitochondria display progressive morphological impairment, and that mild impairment precedes functional deficits in SCA6 mice in early stages of disease.

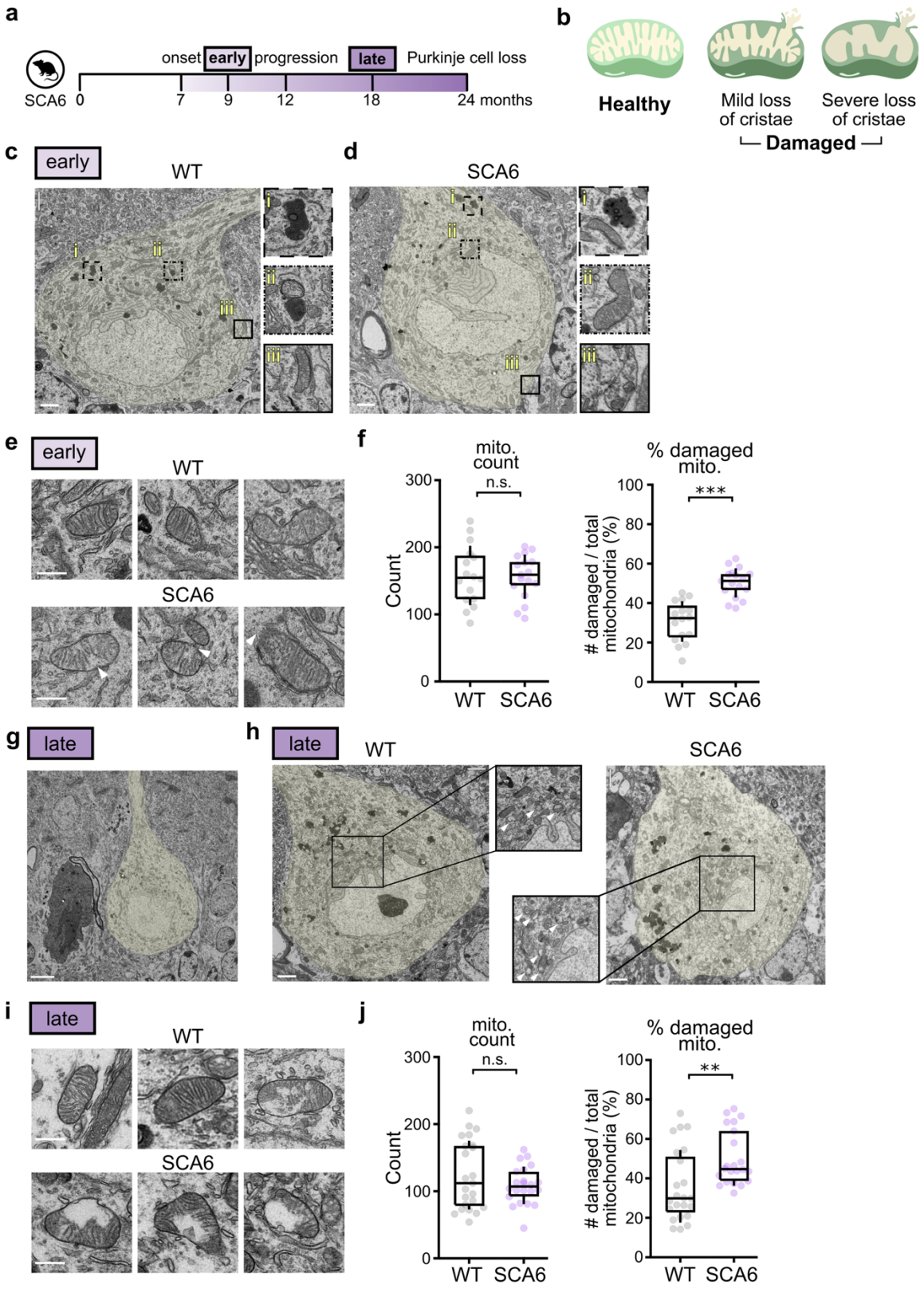
a
onset
early
progression
late
Purkinje cell loss
SCA6
0
7
9
12
18
24 months
b
Healthy
Mild loss of cristae
Severe loss of cristae
Damaged
c
early
WT
d
SCA6
e
early
WT
SCA6
f
mito. count
n.s.
Count
300
200
100
0
WT
SCA6
% damaged mito.
***
damaged / total mitochondria (%)
100
80
60
40
20
0
WT
SCA6
g
late
h
late
WT
SCA6
i
late
WT
SCA6
j
mito. count
n.s.
Count
300
200
100
0
WT
SCA6
% damaged mito.
**
damaged / total mitochondria (%)
100
80
60
40
20
0
WT
SCA6

Fig. 5 Ultrastructural features of WT and SCA6 Purkinje cell mitochondria. (a) The ultrastructure of mitochondria was studied at early and late disease time points. (b) Damaged mitochondria were identified by their loss of cristae, and/or ruptured mitochondrial membrane. (c-d) Representative images of WT and SCA6 Purkinje cells at early disease stage. (e) Representative images of mitochondria in WT and SCA6 Purkinje cells at early disease stage. White arrows show loss of cristae folding or rupture in mitochondrial membrane. (f) At early disease stage, we observed a similar number of mitochondria in both WT and SCA6 Purkinje cells (WT: 158 ± 11.1 mitochondria / cross-section of Purkinje cell body; SCA6: 156 ± 8.0 mitochondria / cross-section of Purkinje cell body; $P > 0.05$). There was a significantly higher proportion of damaged mitochondria in SCA6 Purkinje cells (WT: n = 16 Purkinje cell bodies from N = 3 mice, SCA6: n = 17 Purkinje cell bodies from N = 3 mice; $P < 0.0001$). (g) Dark cell degeneration of a Purkinje cell can be observed late in disease progression. (h) Representative images of Purkinje cells from WT and SCA6 cerebella. White arrows denote damaged mitochondria (i) Representative images of mitochondria in WT and SCA6 Purkinje cells at late disease stage. (j) At late disease stage, we observed similar number of mitochondria in both WT and SCA6 Purkinje cell (WT: 124 ± 10.7 mitochondria / cross-section of Purkinje cell body; SCA6: 109 ± 5.9 mitochondria / cross-section of Purkinje cell body; $P > 0.05$). There was a significantly higher proportion of damaged mitochondria in SCA6 Purkinje cells (WT: n = 23 Purkinje cell bodies from N = 3 mice, SCA6: n = 22 Purkinje cell bodies from N = 3 mice; $P < 0.005$). Scale bar in (c), (d) and (h) = 2μm; in (e) and (i) = 0.5μm; in (g) = 5μm. Mann Whitney *U* test was used for all statistical comparisons. ** $P < 0.005$, *** $P < 0.0001$, n.s. $P > 0.05$

Insufficient mitophagy in SCA6

The pool of mitochondria in a cell is maintained by a balance between mitochondria biogenesis, recycling through the fusion-fission process, and removal of the damaged mitochondria through mitophagy [42]. One puzzle in our data is that given the reduced expression of mitochondrial genes and the increase in damaged mitochondria with age, we might predict that we would observe a reduction in the total number of mitochondria. Yet this was not observed, suggesting that additional changes in mitochondrial removal may be present in the SCA6 cerebellum. To test this

hypothesis, we took two experimental approaches. (1) quantification of lysosome and mitochondria colocalization by immunohistochemistry, and (2) quantification of Purkinje cell LC3 by immunohistochemistry.

The last step of the process of mitophagy is the fusion of mitochondria-containing autophagosomes with lysosomes (Fig. 6b). Therefore, the colocalization of mitochondria with lysosomes is a direct indication of mitophagy. To determine the level of mitophagy in SCA6 Purkinje cells, we quantified the expression levels and the degree of colocalization of the lysosome marker Lamp1 and mitochondria marker CoxIV in Purkinje cells by immunohistochemistry. At the age of disease onset, we observed no difference between WT and SCA6 animals in the fluorescence intensity or area of Lamp1 and CovIV within Purkinje cell bodies (Fig. 6c-e, Supplementary Fig. 4a-b), as well as no difference in the area of colocalization of these proteins (Fig. 6f). However, at a late disease stage, we observed reductions in both Lamp1 and CoxIV staining (Fig. 6g-i) as well as a significant reduction in their colocalization in SCA6 Purkinje cells compared to WT (Fig. 6j). This suggests that there is a reduction in mitophagy at late disease stages in cerebellar Purkinje cells in SCA6. Interestingly, the reduction in CoxIV intensity but not CoxIV area (Supplementary Fig. 5c-d) at this disease stage was consistent both with our finding in the transcriptomics data (Fig. 2b-c, Supplementary Table 1) as well as in our EM data (Fig. 5) – since CoxIV resides in the cristae of mitochondria, the loss of cristae with no change in mitochondria count is consistent with the reduction in intensity but not the total area of CoxIV immunoreactivity.

Second, we quantified the expression of the autophagosome marker MAP1 light chain 3 (LC3) since it is important for regulating autophagic flux and its expression level has been shown to be dysregulated in disease states that lead to insufficient autophagy (Fig. 6b) [56]. We co-stained acute cerebellar slices with an antibody against LC3B, an isoform of LC3, and the Purkinje cell marker calbindin. At a late disease stage, we observed a significantly reduced level of LC3B in Purkinje cell body compared to WT (Fig. 6k-l). Interestingly, we also observed reduced level of LC3B in the molecular layer and granule cell layer (Supplementary Fig. 5e-f). This suggests that autophagy may be impaired not only in SCA6 Purkinje cells but also in other cerebellar cell types at late disease stages. Taken together, these data suggest that in addition to the accumulation of increasingly damaged mitochondria in SCA6 mouse cerebellum, an impairment in mitochondrial removal via mitophagy contributes to mitochondrial dysfunction in SCA6.

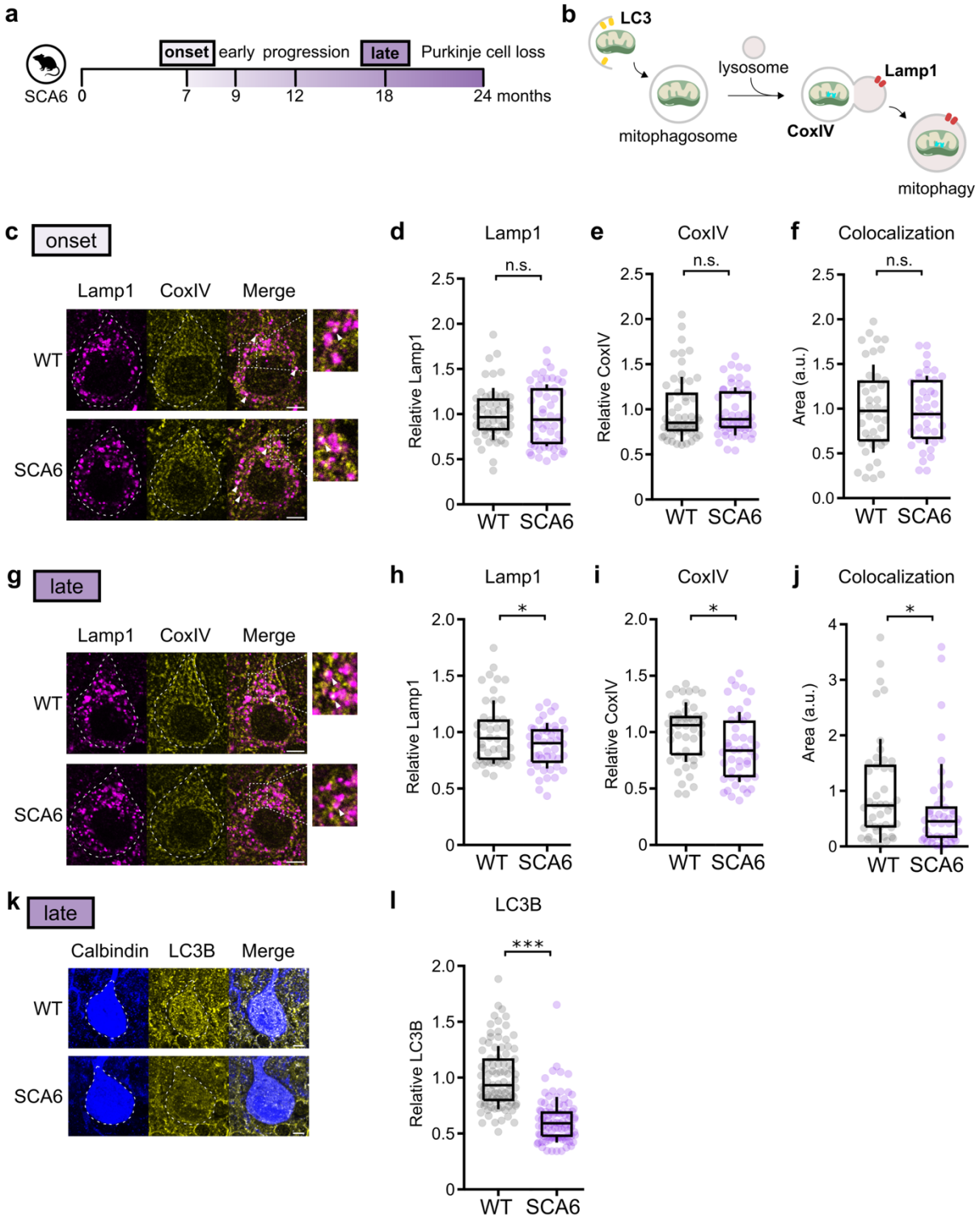

Fig. 6 Insufficient mitophagy in SCA6 at late disease state. (a) Extent of mitophagy was studied at early and late disease stages. (b) Illustration showing autophagy marker LC3, mitochondria marker CoxIV and lysosome marker Lamp1 in the mitophagy pathway. (c) Representative images

showing Lamp1 and CoxIV staining in Purkinje cell bodies (outlined) at early disease stage. Colocalization of the two markers can be observed (arrow heads). (d-e) Relative Lamp1 (d) and CoxIV (e) intensity within Purkinje cells were unchanged in SCA6 compared to WT controls (WT and SCA6: n = 54 cells from N = 3 mice; Student's t test; $P > 0.05$). (f) The area of colocalization of Lamp1 and CoxIV staining within Purkinje cells was unchanged in SCA6 compared to WT controls (WT and SCA6: n = 41 cells from N = 3 mice; Student's t test; $P > 0.05$). (g) Representative images showing Lamp1 and CoxIV staining in Purkinje cell bodies (outlined) at late disease stage. Zoomed in images shows that there was less colocalization in SCA6 Purkinje cells. (h-i) Relative Lamp1 (h) and CoxIV (i) intensity within Purkinje cells were reduced in SCA6 compared to WT controls (WT and SCA6: n = 46 cells from N = 3 mice; Student's t-test; $P < 0.05$). (j) The area of colocalization of Lamp1 and CoxIV staining within Purkinje cells was decreased in SCA6 compared to WT controls (WT and SCA6: n = 44 cells from N = 3 mice; Mann Whitney U test; $P < 0.05$). (k) Representative images showing Purkinje cell marker calbindin and autophagy marker LC3B staining in Purkinje cells at late disease stage. (l) Relative LC3B level within Purkinje cells was reduced in SCA6 compared to WT controls (WT and SCA6: n = 93 cells from N = 3 mice; Mann Whitney *U* test; $P < 0.0001$). Scale bars for all images = 5μm. * $P < 0.05$, *** $P < 0.0001$, n.s. $P > 0.05$

SCA6 patients' cerebellar tissues showed metabolic signature for mitochondrial dysfunction

One open question with these findings is whether the results from SCA6 mice are representative of human disease. To address this, we acquired post-mortem cerebellar tissues from SCA6 patients and age- and sex- matched non-neuropathological individuals (Supplementary Table 3) to determine whether signatures of mitochondrial dysfunction were present in SCA6 post-mortem cerebellum.

To examine this question, we used liquid chromatography-mass spectrometry (LC/MS) to analyze biomarkers from human post-mortem cerebellar tissue to look for evidence of mitochondrial dysfunctions and elevated oxidative stress (Fig. 7a). Classic biomarkers for mitochondrial dysfunction include lactate, pyruvate, creatine and carnitine, which are alternate energy metabolites that can be important for high-energy-demanding tissue like the brain. Previous work

has shown that brain levels of these biomarkers increase in response to oxidative phosphorylation dysfunction [24, 68, 73]. We also expected to observe the accumulation of succinate as a result of reduced enzymatic activity of succinate dehydrogenase, or ETC complex II, an important bioenergetic enzyme that functions both in the Krebs cycle and the ETC [7]; a reduction of ATP production and a disequilibrium of the ETC cofactors NAD+/NADH [69, 77].

We were able to detect many molecules relevant for mitochondrial function in SCA6 post-mortem cerebellar tissues, which we compared to control tissues (Supplementary Table 4). Overall, our findings support mitochondrial dysfunction in the cerebellum of SCA6 patients. First, we observed a significant 2-fold increase in the level of lactate (Fig. 7b). When mitochondria are damaged and the ETC fails, cells shift their energy production from mitochondrial oxidative phosphorylation towards the less efficient glycolysis, generating excess lactate as a result [36]. We also observed a significant increase in creatine (Fig. 7c), and a non-significant increase in carnitine (Fig. 7d). These features together suggest that oxidative phosphorylation dysfunction is observed in the human SCA6 cerebellum.

Furthermore, we found a non-significant but trending increase of succinate in SCA6 cerebellum (Fig. 7e), which has been shown to induce higher cellular oxidative stress and mitochondria dysfunctions [31, 38, 79]. Both ATP and NAD+ are known to be decreased with mitochondrial dysfunction and in mitochondrial diseases [8, 44, 61]. We thus quantified the level of ATP and NAD+ and found that both were present at a lower, though not statistically significant, level in SCA6 patients' cerebellum (Fig. 7f, g). To summarize, all biomarker changes we observed were in the direction predicted by mitochondrial dysfunction, although not all changes were significantly altered. It is noteworthy that some molecules are prone to undergo post-mortem changes, and to minimize the impact, we matched the post-mortem intervals (PMI) of control tissues with that of the SCA6 tissues (Supplementary Fig. 6a). For example, we observed variable levels of creatinine across individual samples, a metabolite that is commonly used in forensic analysis to estimate the PMI, which likely represent post-mortem changes and storage condition differences (Supplementary Fig. 6b) [3, 23]. However, some metabolites are known to be relatively stable despite long PMI, such as lactate [58], the biomarker that showed the most significant changes in our post-mortem SCA6 tissue. Taken together, the metabolic changes we observed in SCA6 patients' tissues are consistent with mitochondrial impairment, supporting our findings from our SCA6 mouse model.

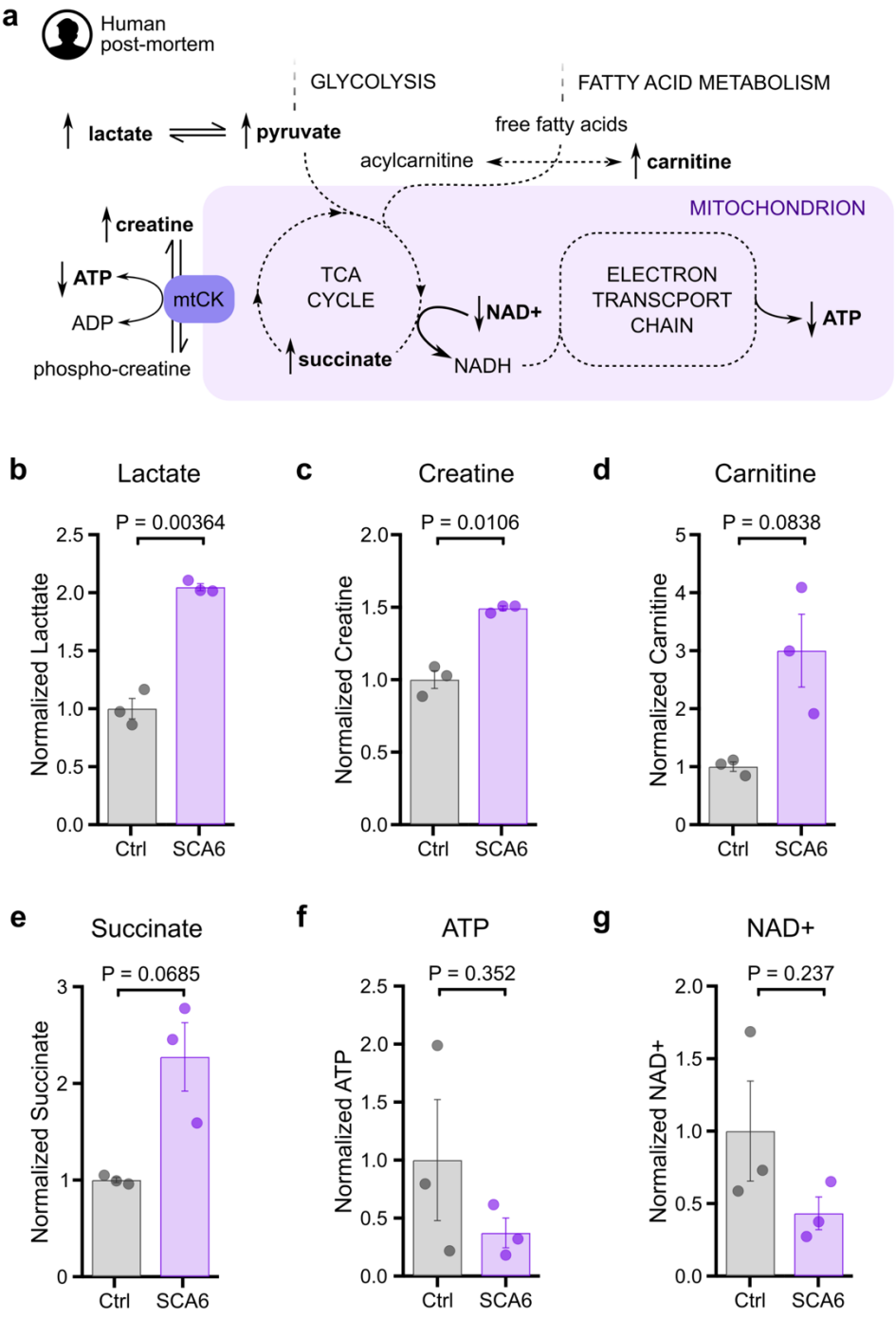

Fig. 7 Biomarkers for mitochondrial dysfunctions were detected in SCA6 patients' cerebellar tissues. (a) Simplified illustration of energy metabolism pathways, highlighting biomarkers for mitochondrial dysfunctions (bolded) and their predicted direction of change based on previous literature. Levels of lactate (b) and creatine (c) were significantly increased in SCA6 patients'

tissues, suggesting mitochondrial oxidative phosphorylation failure. There were non-significant but trending changes in the predicted direction detected in carnitine (d) and succinate (e). ATP (f) and NAD+ (g) changes were non-significant but were consistent with predicted changes under mitochondrial dysfunctions. Unpaired Student's *t* test was used for all statistical comparisons. Ctrl: Non-neuropathological controls

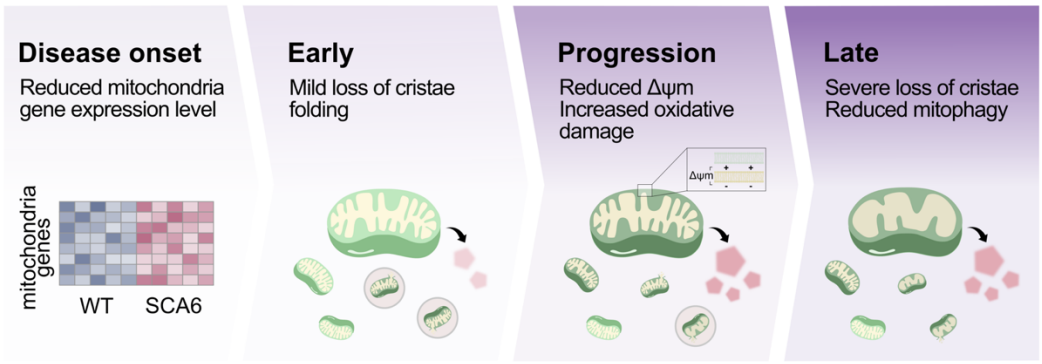

Fig. 8 Mitochondrial dysfunction and structural impairment worsen over the course of SCA6 disease progression

Discussion

Here we use multiple approaches to identify mitochondrial dysfunction as an important and hitherto unappreciated feature of SCA6 disease progression (Fig. 8). Bioinformatic analysis of transcriptomics data from disease onset revealed that mitochondrial-related genes were the most dysregulated gene families. Intriguingly, although transcriptional alterations were present at disease onset, a significant reduction in $\Delta\psi_m$ and a downstream increase in oxidative stress were not observed until later during disease progression, meaning that functional changes lagged behind transcriptional changes by several months. Structurally, Purkinje cell mitochondria were damaged both early and at a late stage of disease progression, with the degree of damage increasing with age. This accumulation of mitochondria with increasing structural damage appears to arise at least in part due to insufficient mitophagy at late disease stages, which will exacerbate mitochondrial impairment over time. Metabolomic analysis of SCA6 post-mortem cerebellar tissues revealed metabolic signatures of mitochondrial dysfunctions consistent with the findings from our mouse model.

Our data argue that mitochondrial dysfunction is an important feature of SCA6, yet it is one that has been previously unappreciated. However, fatigue, which is a hallmark feature of mitochondrial disease [21], is prevalent in SCA6 patients [4], and is often characterized as one of the worst symptoms of their disease by patients [4]. In fact, fatigue is a common comorbidity of many neurodegenerative diseases, and can describe both mental and/or physical exhaustion [48]. Recent work in human subjects has demonstrated a role for cerebellar activity in the perception of fatigue [6]. Perception of fatigue is difficult to study in animal models, but is linked to the mental exhaustion associated with fatigue [2]. This work suggests a link may exist between fatigue and cerebellar function. Future studies will be needed to determine whether a link between mitochondrial impairment in the cerebellum and fatigue exists in SCA6.

One of the surprises from our data is the difference in the timelines we observed between transcriptional, structural, and functional changes related to mitochondria. Transcriptional changes occurred first at disease onset, as did mild alterations in Purkinje cell mitochondrial structure. However, functional changes or resulting alterations in oxidative stress were not observed at this time. It was not until much later during disease progression that mitochondrial dysfunction was

observed, as well as a worsening of structural impairment. This shows that cerebellar neurons can maintain mitochondrial function even in the face of mild impairments, arguing that cerebellar neurons normally function with a large reserve of mitochondrial capacity.

Impaired Purkinje cell firing is a common feature of ataxias and other diseases affecting the cerebellum [13]. We have previously characterized altered Purkinje cell firing in SCA6 [14, 28]. Recent work has suggested a link between mitochondria and the regulation of neuronal firing [53, 63]. Thus, impaired mitochondrial respiration in SCA6 may contribute to Purkinje cell firing deficits at late stages of disease [14, 28], although other mechanisms, including mitochondrial Ca^{2+} buffering capacity, are likely to contribute to early impairment of firing rates.

Although a great deal of research in SCA6 has focused on Purkinje cells, which express the mutated protein at high levels and show late degeneration in mice [29] and patients [25], one notable discovery in our data is that mitochondrial impairment is not limited to cerebellar Purkinje cells but extends to other major classes of cells including molecular layer interneurons and granule cells. This finding is in line with recent studies showing the involvement of other cell classes that contribute to disease in other forms of ataxia, such as molecular layer interneurons in SCA1 [49]. Whether changes to other cells occur in parallel with changes in Purkinje cells, or arise as a consequence of changes in Purkinje cells, remains to be determined. However, the mutated *CACNA1A* gene is expressed not only in Purkinje cells, but also in cerebellar granule cells [16, 19] and our *in silico* cell-type analysis of our transcriptomics data reveals that altered genes in SCA6 are likely expressed in many cell types (Supplementary Fig. 1e).

We propose the accumulation of damaged mitochondria is due to insufficient mitophagy, which is in line with evidence from our lab that there are endo-lysosomal deficits in SCA6 [15]. Such deficits could lead to reduced quality control mechanisms for mitochondria that contribute to Purkinje cell deficits and eventual cell death. The combination of mitochondrial deficits, oxidative damage, and reduced mitophagy suggests a deleterious cycle that increases the pathophysiological stress on Purkinje cells and other cerebellar cell types as disease progresses.

Many SCA6 patients are not diagnosed until well past disease onset, meaning that it is imperative to study mechanisms that contribute to disease progression as well as onset. Previous work in our lab shows that around disease onset, BDNF-TrkB signaling contributes to SCA6, and that

activating this signaling pathway can reverse ataxia at early disease stages [14]. However, we found that as disease progresses, BDNF-TrkB signaling is no longer sufficient to reverse ataxia, suggesting that other mechanisms likely contribute to SCA6 as disease progresses. Mitochondrial dysfunction aligns with the timeline of disease progression: it worsens as the disease worsens. Mitochondrial function is important for the health of Purkinje cells, thus we propose that the mitochondrial dysfunction we describe here is likely to contribute to disease progression. This is important clinically because much biomedical research focuses on disease onset, but mechanisms that contribute to disease onset may not be appropriate therapeutic targets at late disease stages.

While SCA6 mice have been shown to recapitulate key properties of human disease [29, 76], it can be difficult to determine whether pathophysiological changes identified in animal models are representative of human disease. Even for a given mutation in human patients, disease presentation can vary widely. For example, in repeat expansion disorders such as SCA6, different repeat lengths can lead to different disease symptoms and pathology [66]. To tie these results more closely with human disease, we used metabolomics to determine whether signatures of mitochondrial deficits exist from post-mortem human tissue, representing a very late stage of disease progression. Our findings are consistent with deficits in mitochondrial function in human post-mortem cerebellar vermis, which validates findings from our mouse model. Taken together, findings from both mouse and human data argue that mitochondrial dysfunction is an important deficit that likely contributes increasingly to cerebellar damage as SCA6 progresses. How the CAG expansion mutation leads to these changes remains to be determined, although alterations in mitochondrial genes expression due to abnormal activity of the α1ACT transcription factor are likely to be involved [17]. Furthermore, our study suggests that by implementing therapeutic approaches to improve mitochondria health – for example, by inducing mitophagy or mitochondrial biogenesis [45, 71] – we could improve cerebellar cell health and function. This could lead to improvement in the progression or severity of ataxia in SCA6 [43] in particular at late disease stages that are unlikely to be ameliorated by other therapeutic approaches that target mechanisms of disease onset.

Acknowledgements

We are grateful for help and guidance from Dr. Anne McKinney, Dr. Rosemary Bagot, Dr. Siegfried Hekimi, Dr. Jesper Sjöström, Dr. Nam-Sung Moon, Dr. Ying Wang, and current and past members of the Watt lab, especially including Dr. Brenda Toscano-Márquez, Dr. Kim Gruver, Dr. Daneck Lang-Ouellete, Chloe Stewart and Lois Lau. We thank McGill Animal Resources Centre (CMARC) for excellent animal care and training, particularly Dr. T. Koch and Dr. B. Sartip who facilitated the research. We are grateful for help from the skilled staff in the Facility for Electron Microscopy Research (FEMR) as well as to those from the Advanced BioImaging Facility (ABIF), both at McGill University. We thank Dr. Daina Avizonis, Mariana Russo, Luc Choinière and Cian Monnin, who performed the metabolomics analysis in this study at the Rosalind and Morris Goodman Cancer Research Centre Metabolomics Core Facility supported by the Canada Foundation for Innovation, The Dr. John R. and Clara M. Fraser Memorial Trust, the Terry Fox Foundation (TFF Oncometabolism Team Grant 116128), and McGill University. We thank Dr. Arnulf Koeppen (Albany Stratton Veterans Affairs Medical Center, Albany, New York, USA) and The Douglas Bell Canada Brain Bank for providing post-mortem human cerebellar tissues. This research was enabled in part by support provided by Calcul Québec (calculquebec.ca) and the Digital Research Alliance of Canada (alliancecan.ca).

Declarations

Author Contributions

T.C.S.L designed and ran all experiments, analyzed data for all figures, and wrote the manuscript; E.F. contributed to the study design for Fig. 6; N.R. ran experiments for Fig. 4 and Supp. Fig. 3, and analyzed data for Fig. 4, 5, Supp. Fig. 3 and Supp. Fig. 4; R.L.L.S. and A.B. analyzed data for Fig.5 and Supp. Fig. 4; A.A.C. helped run experiment for Fig. 2 and edited the manuscript; D.E.P. analyzed data for Supp. Fig. 5e; A.J.W. conceived the project, designed experiments, supervised the project, and wrote the manuscript.

Funding

This study was supported by the following funding sources: Canadian Institutes of Health Research (CIHR) project grants (PJT-153150 and PJT-190151) (A.J.W.) and Fonds de recherche du Québec – Santé (FRQS) Doctoral Scholarship (T.C.S.L., E.F. and A.A.C.).

Competing interests

The authors declare no conflict of interests.

Ethics approval

The current study was approved by the Faculty of Medicine Institutional Review Board (IRB) at McGill University in compliance with the Cadre de reference ministériel pour la recherche avec des participants humains (MSSS, 2020), and the Food and Drugs Act (17 June 2001); and acts in accordance with the U.S. Code of Federal Regulations (FWA 00004545).

Data availability

The raw sequence data reported in this paper have been deposited in the Genome Sequence Archive (accession: CRA013247) that are publicly accessible at https://ngdc.cncb.ac.cn/gsa.

Chapter 3 Supplemental Information

Supplementary Figures 1-6

Supplementary Table 1 List of DEGs

Differentially expressed genes in SCA6 mice compared to WT controls, their fold changes and p values.

Supplementary Table 2 List of reagents and antibodies

Information of reagents and antibodies used in the current study and concentrations used

Supplementary Table 3 Human post-mortem tissues demographics

Age, sex, post-mortem delay, CAG repeat length (SCA6 patients only) and sources of post-mortem human tissues

Supplementary Table 4 LC/MS Raw data

Raw data and normalization factors for LC/MS datasets: amino acids and ion-pairing

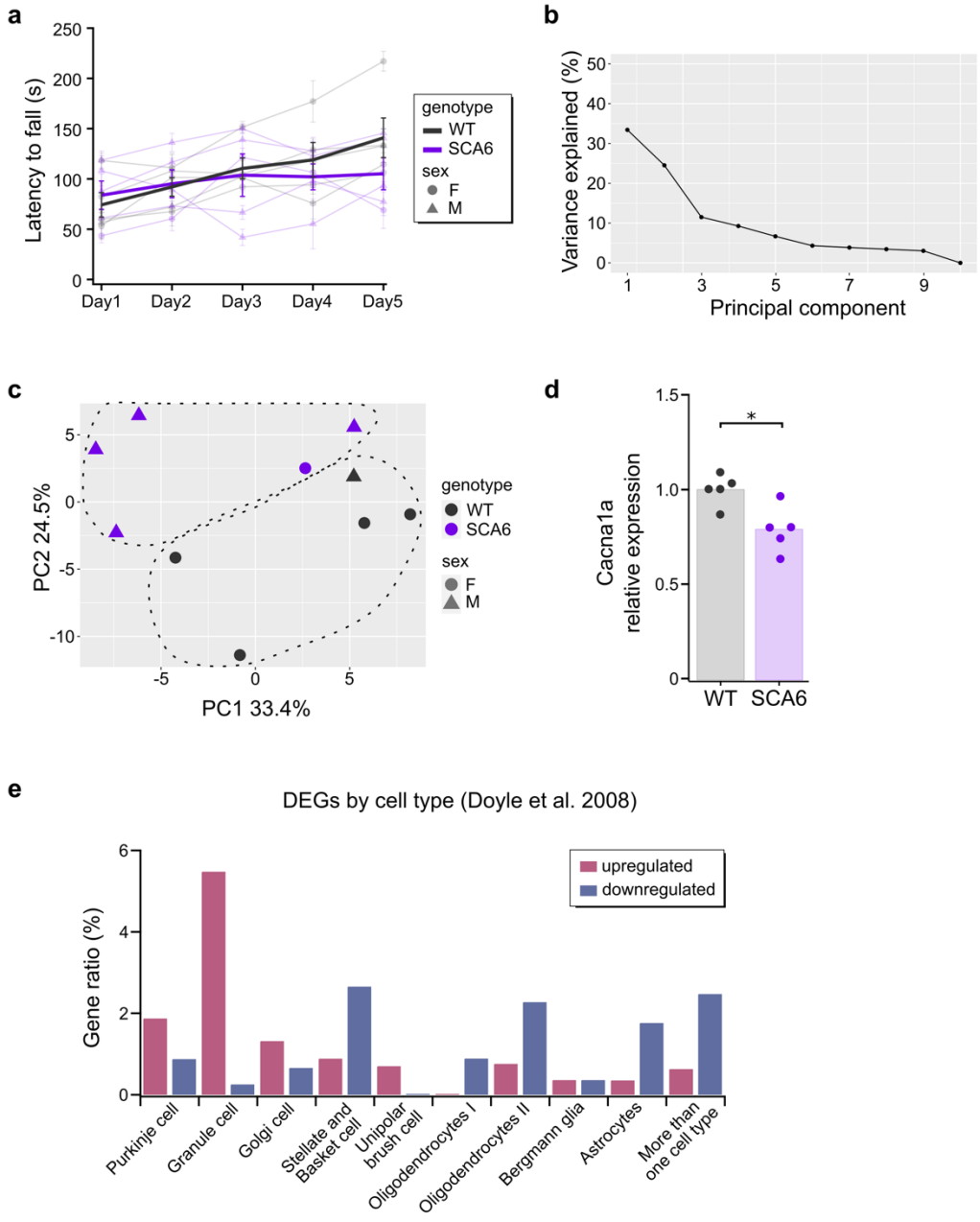

Supplementary Figure 1 (a) Motor coordination deficit of mice used for RNA-seq was assayed on rotarod. (b) Percentage of variance explained by each principal component (PC). (c) PC1 and PC2 together explain more than 50% of the variance, and animals of each genotype loosely cluster together (grouped with dashed line). (d) Relative expression level of *Cacna1a* in SCA6 is 20% lower than in WT (e) DEGs identified are specific for different cell types in the cerebellum. Gene ratios are defined as the number mapped DEGs to a cell type / the number of cell-specific genes to that cell type identified in (Doyle et al. 2008).

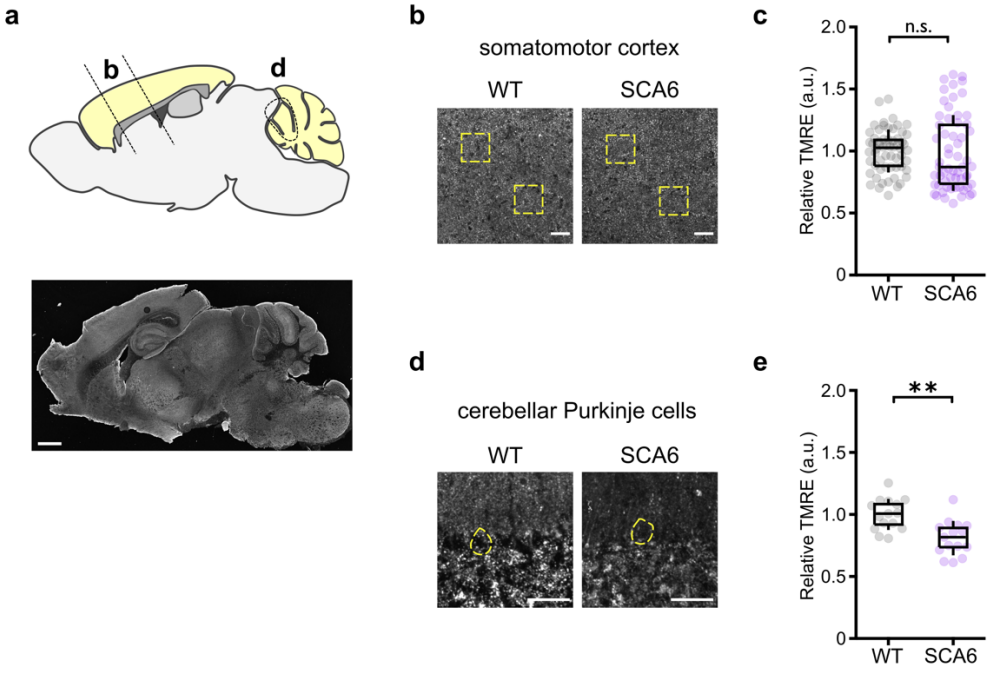

Supplementary Figure 2 Mitochondrial dysfunction was not detected in somatomotor cortex. (a) Top: Illustration showing regions where TMRE signals were measured from (regions within dashed lines). The somatomotor cortex is located using the corpus callosum, lateral ventricle and hippocampus as landmarks. Bottom: representative whole brain sagittal slice stained with TMRE. Image was taken at low magnification for reference purpose only. Analysis was performed on images taken on higher magnifications. (b) Representative TMRE images of somatomotor cortex in WT and SCA6 mice. (c) Relative TMRE signals showed no difference between genotypes (WT: n = 60 ROIs from N = 3 mice; SCA6: n = 60 ROIs from N = 3 mice; not significantly different, P = 0.724) (d) Representative TMRE images of Purkinje cells (outlined). (e) TMRE signals were significantly reduced in SCA6 (WT: n = 15 cells from N = 3 mice; SCA6: n = 15 cells from N = 3 mice, P = 0.000473). Scale bar for (a) = 100 μm, (b) and (d) = 50 μm. Mann Whitney *U* test was used for all statistical comparisons. ** $P < 0.005$, n.s. $P > 0.05$

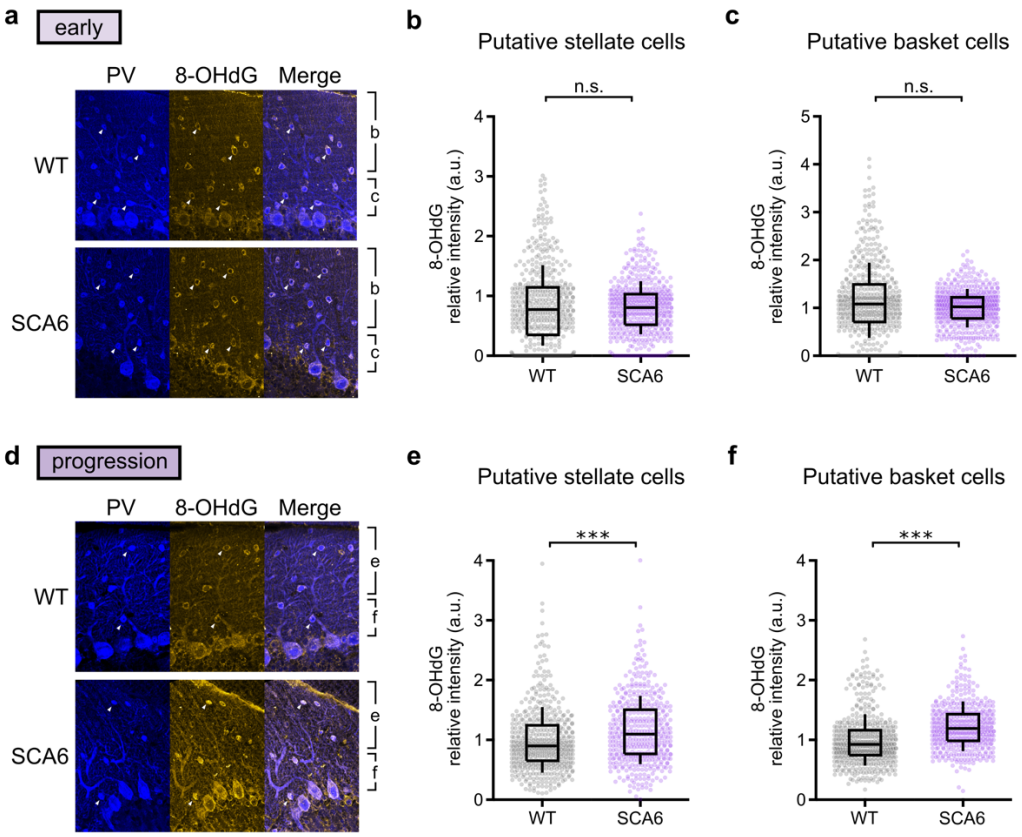

Supplementary Figure 3 Oxidative stress accumulates in both populations of molecular layer interneurons. (a) Representative images of molecular layer interneurons (stained with parvalbumin, PV) and oxidative stress marker (stained with 8-OHdG) at early disease stage. White arrows denote individual interneurons. The upper interneurons are putative stellate cells; the bottom interneurons are putative basket cells. Quantifications of oxidative stress staining of these two populations of interneurons are shown in (b) and (c) respectively. (b-c) Neither population shows significant difference in oxidative stress level compared to WT. (WT and SCA6: n = 480 cells from N = 3 mice; Mann Whitney *U* test, $P > 0.05$) (d) Representative images of molecular layer interneurons and oxidative stress staining at disease progression stage. (e-f) Both putative stellate cells and putative basket cells accumulated higher level of oxidative stress compared to WT. (WT and SCA6: n = 480 cells from N = 3 mice; Mann Whitney *U* test, $P < 0.0001$). *** $P < 0.0001$, n.s. $P > 0.05$.

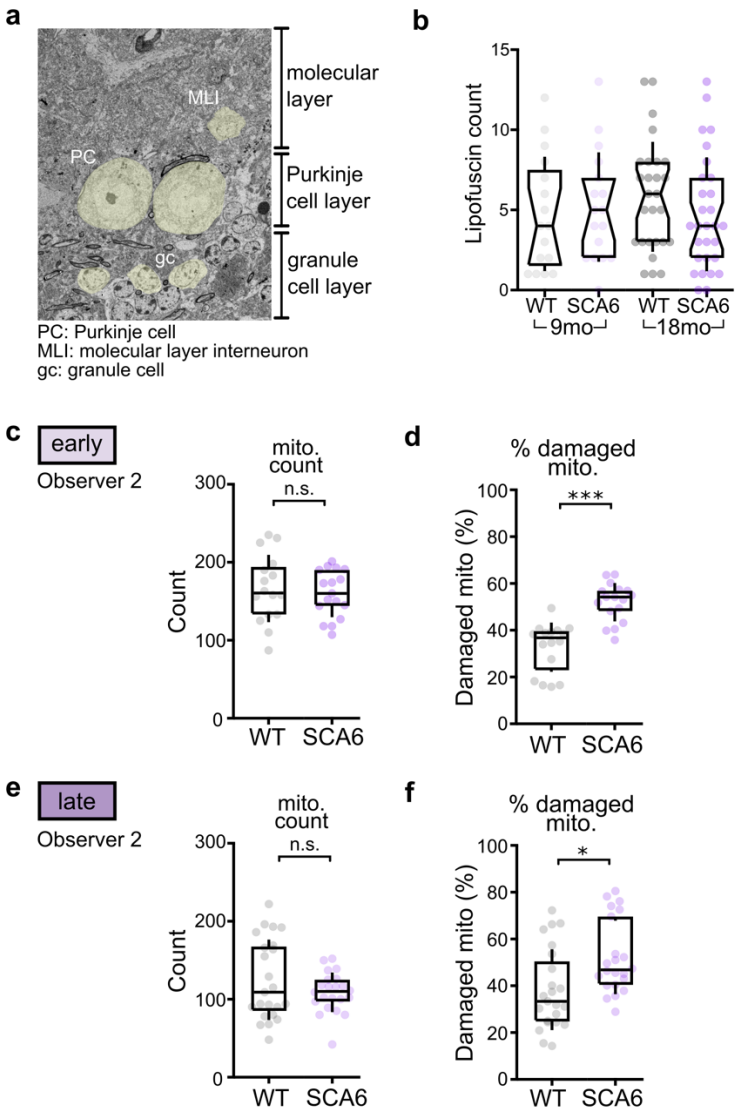

Supplementary Figure 4 (a) Location of Purkinje cells under electron microscope can be identified between the molecular layer interneurons and granule cells, which are both smaller. (b) Quantification of lipofuscin granules in Purkinje cell bodies. (c-d) Mitochondria count and damaged mitochondria percentage at early disease stage as quantified by observer 2. (e-f) Mitochondria count and damaged mitochondria percentage at late disease stage as quantified by observer 2. * $P < 0.05$, *** $P < 0.0001$, n.s. $P > 0.05$.

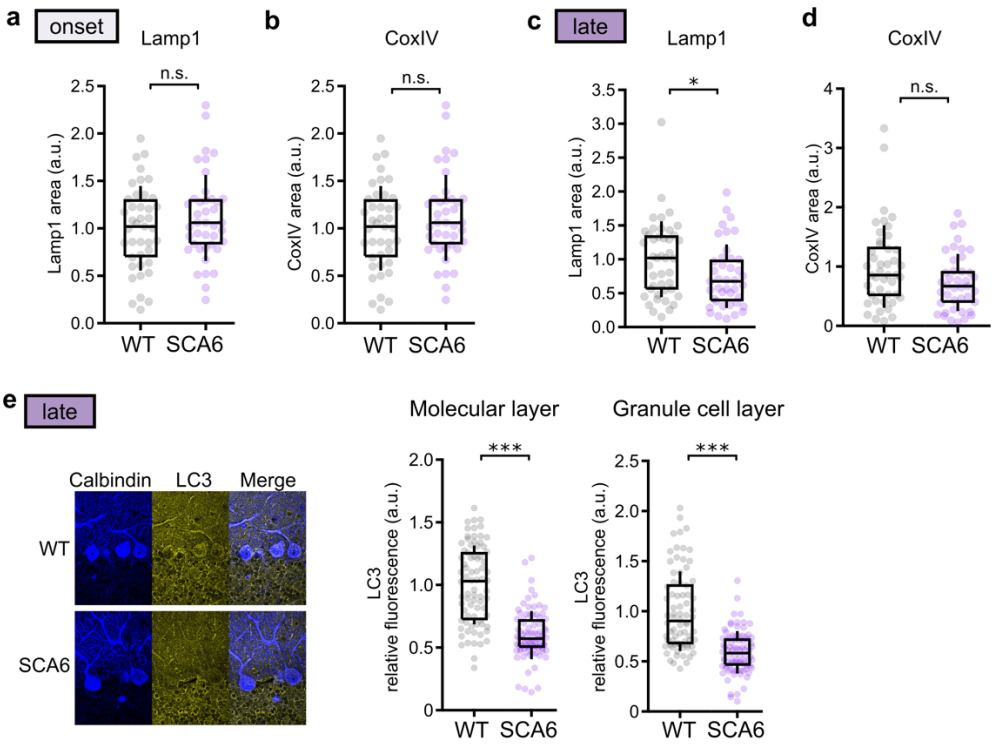

Supplementary Figure 5 (a-b) Lamp1 and CoxIV staining areas in Purkinje cell bodies are not altered in SCA6 at disease onset (c) Lamp1 area is reduced in Purkinje cell bodies in SCA6 at late disease stage, which is in line with the reduced fluorescence density. (d) CoxIV area is unchanged in Purkinje cell bodies in SCA6 at late disease stage, consistent with the EM data that there was no difference in mitochondria count between SCA6 and WT Purkinje cells at this disease stage. (e) LC3 fluorescence signals are reduced in both molecular layer and granule cell layer. * $P < 0.05$, *** $P < 0.0001$, n.s. $P > 0.05$.

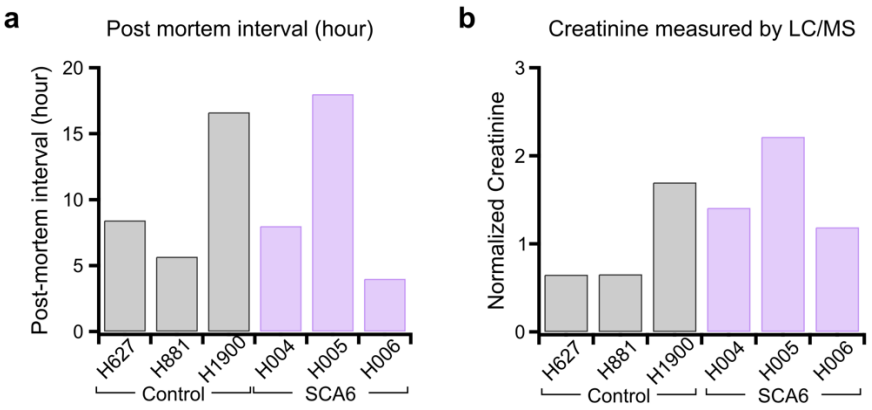

Supplementary Figure 6 Post-mortem delay of human post-mortem tissues (a) Post-mortem delay (hour) of control and SCA6 cerebellar tissues are matched to control for impact on metabolites cause by post-mortem delay. (b) Relative creatinine level in post-mortem human tissues used as an estimate for post-mortem-delay-related metabolic alterations.

Supplementary Table 1 – Differentially expressed genes in SCA6 mice compared to WT controls

Gene name	DESeq2 base mean	Log2 fold change	Adjusted P value
Scoc	1935.7	-0.853	6.30E-45
Gpr26	185.2	0.993	2.79E-10
Mri1	204.8	-0.870	6.48E-10
Epb41l4b	1544.4	0.323	1.88E-07
Abcc12	160.9	-0.806	4.19E-07
Rnf150	675.6	-0.440	1.00E-06
Jph4	3330.8	0.290	1.62E-06
Ablim1	6768.6	0.269	1.65E-06
Gm28437	17715.4	-0.382	1.72E-06
Gm28661	12801.2	-0.394	1.72E-06
mt-Rnr1	47368.2	-0.402	1.72E-06
D630045J12Rik	707.3	0.450	4.26E-06
Selenof	3969.4	-0.315	7.77E-06
Gm29216	10302.9	-0.428	2.99E-05
Gnao1	12948.4	0.209	3.63E-05
Ndufb8	1237.9	-0.349	3.63E-05
Fto	3285.1	-0.227	6.90E-05
S100a1	821.7	-0.358	8.59E-05
Cdh1	280.3	-0.513	8.74E-05
Spock3	2949.6	-0.265	8.74E-05
Cacna1c	1145.4	0.432	9.97E-05
Syt1	9441.6	0.215	0.000131
Gm19935	139.1	-0.950	0.000132
Kcnk9	2007.0	0.484	0.000132
Metrn	3840.4	-0.353	0.000172
Sez6	1770.8	0.249	0.000205
Heatr3	701.2	0.325	0.000220
Gm28439	7524.7	-0.390	0.000231
Fgf1	3155.4	-0.205	0.000262
Aloxe3	213.0	0.514	0.000264
Ebf1	1444.4	0.239	0.000277
Alpk2	355.9	0.625	0.000285
Diras2	12327.0	0.289	0.000285
Myt1	1149.3	0.301	0.000341
Cntn2	6655.3	0.235	0.000349
Kif26b	1517.6	0.401	0.000349
Prkcd	1847.6	-0.254	0.000349

Th	330.5	0.857	0.000349
Atp2b4	957.2	0.374	0.000353
Ndst3	2099.7	0.246	0.000404
Fat2	10041.2	0.374	0.000411
Gadd45gip1	568.4	-0.322	0.000411
Lypd6	844.6	-0.351	0.000411
Gm28438	2160.5	-0.407	0.000467
S100b	12010.4	-0.367	0.000510
Nkd1	355.1	-0.413	0.000514
Trp53inp2	3825.5	-0.198	0.000614
Islr	249.6	-0.675	0.000640
Tacc2	1770.4	0.189	0.000799
Aldh1a1	5690.1	-0.231	0.000812
Socs7	3234.9	0.234	0.000964
Tpm4	847.9	-0.258	0.000964
Sgsm1	1748.9	0.238	0.000989
Cadm3	16855.9	0.214	0.00102
Selenop	4830.8	-0.258	0.00103
Hook2	194.5	-0.460	0.00104
Cacna1e	3160.8	0.433	0.00104
Ajm1	4166.2	0.209	0.00133
Reln	6187.1	0.311	0.00149
Ccdc120	545.0	0.297	0.00154
Chmp5	1675.0	-0.235	0.00169
Dbi	3941.5	-0.318	0.00185
Epb41	5926.2	0.313	0.00185
Kcnb1	844.0	0.275	0.00185
Rere	3342.2	0.220	0.00203
Crhr1	1037.9	0.278	0.00221
Fam114a1	112.5	-0.573	0.00244
Gm37206	209.8	0.510	0.00245
Slc7a8	1048.7	0.261	0.00261
Adamts18	310.8	0.465	0.00271
Mast1	2364.8	0.225	0.00271
Slc47a1	104.6	-0.775	0.00271
Cabp7	1974.5	-0.374	0.00280
Mtcl1	5167.6	0.273	0.00280
Crtc1	2923.8	0.204	0.00287
Sestd1	2893.1	0.220	0.00287
D430041D05Rik	3351.1	0.324	0.00294
Lpcat2	145.0	-0.580	0.00297

Ppfia4	4081.3	0.280	0.00297
Atp5l	2660.7	-0.250	0.00316
Cpne2	563.1	-0.361	0.00316
Ablim3	1803.5	0.203	0.00321
Dhps	413.6	-0.318	0.00321
mt-Cytb	163594.0	-0.300	0.00321
Aktip	2189.3	-0.178	0.00324
Grk5	982.4	0.258	0.00324
Synpr	1352.7	0.265	0.00324
mt-Co1	361924.1	-0.269	0.00325
Efemp1	423.6	-0.310	0.00339
Gm10095	297.6	-0.357	0.00339
Plin3	542.8	-0.290	0.00339
Chn2	14025.9	0.161	0.00355
Gabra2	807.3	-0.278	0.00355
Smg1	8724.2	0.359	0.00355
Itpr3	585.5	0.334	0.00365
Cacnb2	1119.3	0.244	0.00412
Ccdc34	413.8	-0.322	0.00412
Sema4f	1109.7	0.229	0.00425
Vti1b	1687.8	-0.207	0.00455
Kcnc1	11378.3	0.244	0.00458
Mgst1	341.6	-0.347	0.00458
Grm2	340.7	0.399	0.00460
Zic1	17216.2	0.120	0.00481
Chgb	10532.0	0.153	0.00484
mt-Nd4	67438.7	-0.291	0.00489
Lgr5	308.1	0.365	0.00500
Epha3	261.0	0.334	0.00524
Brd4	1578.3	0.186	0.00526
Svep1	922.8	0.475	0.00526
Pclo	5541.3	0.373	0.00529
Pdcd10	831.2	-0.228	0.00558
Pla2g16	1338.1	-0.206	0.00588
Rfk	1422.3	-0.200	0.00598
Setbp1	1073.0	0.404	0.00600
Vegfb	1088.3	-0.202	0.00600
Camk2b	12110.2	0.159	0.00612
Cntn6	1455.3	0.197	0.00625
Crmp1	3594.7	0.170	0.00625
Gm10925	17860.8	-0.342	0.00625

Prss23	130.3	-0.475	0.00627
Uqcc2	806.5	-0.317	0.00627
mt-Nd1	117061.9	-0.311	0.00659
Cyld	2292.6	-0.282	0.00679
Tmem201	2489.2	0.229	0.00689
Cnnm1	3117.2	0.193	0.00700
mt-Rnr2	119055.5	-0.321	0.00700
Wscd2	3461.8	0.221	0.00700
Cox7c	2315.8	-0.262	0.00703
Celf2	3482.0	0.215	0.00711
Chd7	4134.4	0.276	0.00711
Nupr1	120.8	-0.509	0.00711
Fth1	26571.9	-0.364	0.00746
Neurl1a	2119.9	0.196	0.00746
Atf5	772.6	-0.410	0.00747
Vwf	364.6	-0.635	0.00757
Zmynd8	2218.6	0.210	0.00757
Slc6a13	219.5	-0.380	0.00757
Gng13	2387.0	-0.313	0.00759
Ptn	3824.1	-0.228	0.00766
Glrx3	1324.9	-0.221	0.00794
Cux1	2367.6	0.156	0.00802
Erbb4	625.6	0.334	0.00802
Tmem132c	533.2	0.306	0.00802
Gpatch8	1736.0	0.259	0.00833
Git2	1645.7	0.204	0.00833
Hspe1	991.3	-0.227	0.00882
Pde1c	1810.8	0.339	0.00889
Auts2	1407.5	0.217	0.00899
Ctxn3	1023.7	-0.285	0.00899
Zfp398	853.6	0.202	0.00902
Timm8b	994.1	-0.287	0.00929
Kank2	2691.8	0.236	0.00939
Grik2	1918.2	0.248	0.00951
Grin2a	1594.4	0.292	0.00958
Gm6204	169.4	-0.498	0.00969
Atp5md	2372.0	-0.285	0.00981
Chd8	2984.2	0.181	0.00981
Cntnap4	1083.2	0.346	0.00981
Fnip2	767.8	0.282	0.0102
Plekhb1	9309.6	-0.314	0.0102

Rbm33	2313.1	0.271	0.0102
Arhgap26	4211.1	0.158	0.0103
Apod	5643.5	-0.312	0.0104
Psma2	2020.6	-0.210	0.0104
Sez6l	3080.8	0.228	0.0104
Coro2b	5350.4	0.189	0.0106
Prdx1	3007.2	-0.213	0.0106
Nhsl2	1065.1	0.318	0.0108
Pkn1	924.8	-0.223	0.0108
Gm10033	479.8	-0.458	0.0109
Plekha1	2147.7	0.158	0.0111
Anxa2	230.8	-0.368	0.0113
Chka	1990.2	0.258	0.0113
Cry2	2199.2	0.198	0.0113
Rps14	4649.3	-0.281	0.0113
Serf1	129.0	-0.449	0.0113
Trim62	2811.7	0.185	0.0116
Fxyd6	1853.1	0.248	0.0117
Gm13340	1116.8	-0.444	0.0117
Tor4a	141.4	-0.556	0.0124
Trmt1	801.9	-0.267	0.0124
Gpm6b	33636.6	-0.227	0.0126
Tpt1	6923.1	-0.235	0.0128
Dand5	193.8	-0.392	0.0131
Parm1	1058.7	-0.247	0.0133
Ak3	1964.5	-0.179	0.0134
Rps3	5138.9	-0.235	0.0134
Rpl39	1267.3	-0.288	0.0137
Pcp4l1	1604.1	-0.367	0.0138
Mrpl13	587.8	-0.227	0.0138
Rpl22l1	1310.6	-0.302	0.0141
Ptpre	934.6	0.247	0.0141
Trim59	541.1	-0.268	0.0141
Pllp	975.6	-0.360	0.0142
Zfp704	1759.8	0.260	0.0142
Wdr83os	359.7	-0.398	0.0142
Acyp2	471.1	-0.277	0.0146
Adam22	5313.3	0.200	0.0146
Aldh1a2	278.3	-0.591	0.0146
Btbd1	2773.9	-0.221	0.0149
Gng11	489.4	-0.313	0.0149

Fam214a	1574.6	0.179	0.0152
Adgrl1	5482.0	0.201	0.0152
Cacna1a	5941.3	-0.338	0.0152
Trhde	852.9	0.255	0.0155
Evi2a	500.5	-0.303	0.0157
Cox4i1	7662.2	-0.269	0.0159
Krcc1	621.9	-0.296	0.0159
Prkcb	5671.3	0.170	0.0159
Rpl32	2239.3	-0.250	0.0159
Xpo6	1447.2	0.215	0.0159
Btaf1	1455.6	0.312	0.0159
Als2	4335.2	0.247	0.0161
Fam173a	1000.6	-0.260	0.0164
Cox7b	2683.3	-0.240	0.0167
S100a10	361.1	-0.330	0.0167
Sf3a2	801.8	0.205	0.0167
Cacna1i	1817.8	0.308	0.0168
Cntnap2	1503.9	0.241	0.0168
mt-Nd2	94965.4	-0.254	0.0168
Slc6a20a	497.0	-0.396	0.0168
Rps25	2989.2	-0.250	0.0173
Castor2	2319.1	0.206	0.0173
Cops9	919.0	-0.289	0.0173
Dhrs4	282.1	-0.314	0.0173
Mef2d	3237.4	0.177	0.0173
Nav2	816.9	0.432	0.0173
Psat1	2504.9	-0.246	0.0173
Rflnb	822.7	-0.335	0.0185
Slc22a6	159.3	-0.440	0.0188
Patj	4861.7	0.189	0.0188
Borcs8	243.7	-0.377	0.0190
Gm10222	1485.4	-0.349	0.0190
Hist1h2be	146.3	-0.495	0.0190
Mctp1	1653.2	0.208	0.0190
Usb1	136.6	0.393	0.0190
Srgap2	3460.5	0.262	0.0192
Tceal9	1445.3	-0.192	0.0193
Herc1	5345.0	0.272	0.0197
Ptpn22	607.6	0.430	0.0199
Pde9a	1105.4	0.234	0.0199
Sfpq	3774.4	0.257	0.0199

St8sia5	2961.4	0.200	0.0201
Neb	574.9	0.372	0.0201
S1pr5	546.7	-0.272	0.0201
Samd1	370.8	-0.316	0.0201
Rasl10b	2302.5	-0.174	0.0206
Nek7	1076.4	-0.209	0.0208
Ndrg3	11832.3	0.124	0.0213
Fam174a	951.4	-0.212	0.0214
Pts	459.9	-0.245	0.0214
Bud31	723.8	-0.208	0.0215
Ndufc1	734.4	-0.257	0.0215
Rps7	3341.9	-0.240	0.0218
Gjd2	264.4	-0.279	0.0222
Nsd3	1891.7	0.228	0.0225
Tmem242	946.9	-0.210	0.0225
Rasgrp1	1163.4	0.286	0.0227
Sema5a	926.5	0.297	0.0227
Pcid2	653.1	0.194	0.0230
Dop1a	1950.9	0.232	0.0230
Gm43300	114.2	0.565	0.0233
Lpar1	1059.7	-0.244	0.0233
Numa1	3284.9	0.228	0.0233
Chchd2	3705.5	-0.209	0.0235
Uqcrq	1653.0	-0.285	0.0235
Zic2	5726.6	0.162	0.0235
Snx33	267.6	-0.296	0.0235
Uqcr11	1146.6	-0.243	0.0235
Gsn	1200.3	-0.253	0.0235
Tmem164	692.7	0.195	0.0236
Eif3h	2415.9	-0.179	0.0237
Hsp90aa1	19041.5	-0.161	0.0237
Gabpb2	1444.8	0.258	0.0238
Csnk1g1	677.1	0.230	0.0239
Foxred2	901.0	0.186	0.0239
Tbc1d8	703.6	0.214	0.0240
Htt	3512.3	0.297	0.0241
Adcyap1r1	2727.1	0.254	0.0243
Cox6c	3639.1	-0.291	0.0243
Sept7	9181.1	-0.181	0.0243
Snx5	2110.7	-0.162	0.0243
Ndufs8	1162.8	-0.199	0.0245

Camkk2	3554.3	0.164	0.0245
Sec61g	623.4	-0.316	0.0245
Nhlh2	311.4	0.297	0.0246
Rap1a	1515.7	-0.160	0.0247
Slc8a1	2298.8	0.284	0.0251
Cblb	513.0	0.250	0.0251
Bsn	5175.7	0.363	0.0252
Dclk1	6853.9	0.150	0.0252
Nol4l	715.9	0.185	0.0252
Tmsb4x	5390.0	-0.245	0.0252
Gng5	330.6	-0.322	0.0254
Ndufv2	3221.4	-0.222	0.0254
Ubr4	4139.4	0.279	0.0257
Per2	492.8	0.487	0.0264
Uncx	531.4	0.210	0.0266
Lgals1	279.1	-0.385	0.0267
Sipa1l2	950.0	0.231	0.0267
Dcn	717.1	-0.317	0.0270
Psg16	364.7	0.243	0.0273
Dnmt3a	2154.0	0.243	0.0273
Naa20	1270.5	-0.194	0.0273
Sik3	2548.4	0.230	0.0273
Pcif1	1865.1	0.154	0.0274
Cavin1	523.4	-0.277	0.0277
Iws1	1307.6	0.210	0.0279
Acvr2b	104.8	0.484	0.0281
Astn1	1815.7	0.151	0.0286
Braf	2803.2	0.204	0.0286
Chil5	158.2	0.382	0.0286
Kcnn3	217.2	0.357	0.0286
Olfm1	6852.7	0.112	0.0286
Speg	2053.3	0.249	0.0286
Skor1	537.4	-0.220	0.0287
Rpl10a-ps1	199.9	-0.310	0.0291
Dr1	1013.9	-0.244	0.0293
Eef2k	1250.2	0.201	0.0293
Lrig2	1000.0	0.197	0.0296
Ryr2	3238.5	0.312	0.0298
Edc4	1252.8	0.160	0.0298
Ep400	2029.3	0.258	0.0302
Gm15500	674.3	-0.292	0.0302

Mgp	269.9	-0.575	0.0302
Npm1	3567.5	-0.200	0.0302
Pon2	959.6	-0.251	0.0302
Acot13	784.0	-0.217	0.0304
1700109H08Rik	171.5	0.415	0.0305
Rps27a	3612.6	-0.237	0.0307
Syne1	18752.2	0.533	0.0307
Grm7	476.6	0.223	0.0309
Camk2n1	6604.0	-0.173	0.0310
Atp5e	1496.2	-0.277	0.0311
Kmt2a	3356.9	0.350	0.0311
Per3	1084.4	0.340	0.0313
Eps8	1778.6	0.162	0.0313
Gm21781	409.7	0.419	0.0313
Rps5	2287.0	-0.198	0.0313
Sf3b3	1978.3	0.143	0.0313
Ercc6	498.0	0.240	0.0314
Gjb2	202.7	-0.343	0.0314
Nfat5	2388.2	0.323	0.0314
Serac1	364.2	0.311	0.0314
Atp5j2	2195.0	-0.247	0.0314
Atp5k	1490.4	-0.285	0.0316
Zfhx2os	244.8	0.612	0.0316
Atp8a2	1234.6	0.262	0.0318
Arhgef7	4203.0	0.141	0.0319
Prr18	910.9	-0.286	0.0319
Rims1	3559.5	0.210	0.0319
Strada	611.6	0.264	0.0319
Cacna2d1	1214.9	0.242	0.0319
Tpt1-ps3	830.4	-0.285	0.0321
Scp2	2227.6	-0.169	0.0322
Laptm4a	5411.2	-0.144	0.0324
Tnc	237.7	-0.372	0.0324
Arl6	601.1	-0.217	0.0326
Cfdp1	1341.0	-0.165	0.0326
Gmeb1	425.9	0.219	0.0326
Klhl23	1554.8	0.160	0.0326
Pbdc1	276.7	-0.393	0.0326
Stc2	135.3	-0.450	0.0326
Cebpzos	366.8	-0.288	0.0327
Crebbp	1364.2	0.208	0.0331

Fbxo41	1140.3	0.214	0.0331
Nsd1	3532.0	0.226	0.0331
Ocrl	1344.4	0.196	0.0331
Klf7	1133.8	0.205	0.0334
Acyp1	483.4	-0.236	0.0335
Ago3	1382.3	0.336	0.0335
Cmpk1	1375.8	-0.162	0.0335
Pax6	1889.7	0.174	0.0335
Bcap29	978.4	-0.184	0.0335
Ubr5	4828.9	0.195	0.0335
Rictor	2848.9	0.223	0.0336
Cplane1	1268.1	0.253	0.0340
Dnmbp	345.8	0.245	0.0340
Fam107a	15439.5	-0.294	0.0340
Hpcal1	4831.7	0.193	0.0340
Sidt1	512.3	0.282	0.0340
Sptssa	468.2	-0.226	0.0340
Tef	6300.0	0.259	0.0342
Ost4	606.5	-0.200	0.0343
Ndufc2	2211.0	-0.174	0.0344
Csrp1	5355.3	-0.206	0.0346
Ndufb1-ps	815.8	-0.318	0.0348
Aak1	9902.1	0.215	0.0350
Arap1	958.9	0.188	0.0350
Cryab	1350.5	-0.288	0.0350
Cyb5b	2797.1	-0.124	0.0350
Gas5	1213.0	-0.257	0.0350
Gatm	2984.4	-0.190	0.0350
Iqsec2	1932.1	0.223	0.0350
Mdfi	269.5	-0.353	0.0350
Mmp15	307.0	0.352	0.0350
Nrip1	1249.2	0.219	0.0350
Ramp1	755.3	-0.277	0.0350
Rps27	2485.2	-0.251	0.0350
Tmem63c	1287.6	0.191	0.0350
Tsc2	2022.2	0.156	0.0350
Uqcrb	1621.6	-0.245	0.0350
Zfp318	1097.2	0.154	0.0350
Mtus2	1969.0	0.223	0.0356
Cd300a	123.7	0.496	0.0358
Cry1	967.4	0.206	0.0358

Xpo4	909.2	0.201	0.0364
Gm9856	98.3	0.425	0.0366
Ptprk	918.2	-0.264	0.0366
Alms1	990.2	0.311	0.0367
Atad2b	864.2	0.227	0.0367
Heatr6	484.0	0.254	0.0367
Peli2	979.0	0.186	0.0367
Ccdc124	1025.6	-0.189	0.0368
Gls	5998.0	0.160	0.0368
Gm10275	190.3	-0.395	0.0368
Gm39465	200.2	0.468	0.0368
Prxl2a	4347.9	-0.219	0.0368
Lpp	585.9	0.358	0.0368
Oaz1-ps	377.9	-0.229	0.0370
Mapk14	1752.1	0.131	0.0372
Osbpl6	2586.9	0.189	0.0372
Eef1e1	462.5	-0.258	0.0372
Kcnk13	160.8	-0.355	0.0372
Dcdc2a	167.7	-0.356	0.0380
Rad54l2	835.0	0.236	0.0380
Unc5d	312.1	0.320	0.0380
Wdfy3	4943.7	0.318	0.0380
BC005561	481.3	0.273	0.0382
Cers6	1166.3	0.218	0.0382
Atp5j	3008.9	-0.196	0.0390
Kcnq1ot1	869.0	0.403	0.0390
Rpl12	1793.7	-0.240	0.0390
Eftud2	1678.7	0.145	0.0394
Ralgapa2	683.1	0.227	0.0394
Aff1	1183.2	0.209	0.0397
Clasp2	6656.3	0.149	0.0397
Dynlt3	3026.7	-0.162	0.0397
Golga7	2332.5	-0.145	0.0397
Igfbp4	238.2	-0.280	0.0397
Jarid2	1488.4	0.186	0.0397
Nkx6-2	251.4	-0.350	0.0397
Trp73	182.8	0.427	0.0397
Rps20	1450.0	-0.183	0.0399
Eif2s2	2253.9	-0.179	0.0399
Kmt2c	3169.4	0.332	0.0405
Ogn	318.3	-0.415	0.0407

Dnajb9	1216.4	-0.181	0.0410
Vps13c	2513.7	0.326	0.0412
Tanc2	836.5	0.264	0.0414
Asgr1	260.9	-0.313	0.0419
Etnppl	2937.9	0.152	0.0419
Gm13493	165.1	-0.330	0.0419
Ube2e1	1648.7	-0.158	0.0419
Runx1t1	385.4	0.316	0.0424
Cacna2d3	1069.1	-0.206	0.0437
Isyna1	364.5	-0.304	0.0437
mt-Nd5	99668.0	-0.225	0.0437
Rassf3	523.2	-0.223	0.0437
Rpl36a	1166.1	-0.239	0.0437
Rps24	4526.9	-0.191	0.0437
Stum	276.4	0.298	0.0437
Trim3	3587.4	0.143	0.0437
Trio	5146.4	0.234	0.0452
Csmd1	263.8	0.315	0.0453
Cttnbp2	1508.6	0.207	0.0453
Dgkg	2855.1	0.310	0.0453
Ehmt1	758.0	0.215	0.0453
Fam163b	257.6	0.315	0.0453
Flnb	1448.7	0.304	0.0453
Gm38020	416.5	0.510	0.0453
Ormdl1	302.6	-0.251	0.0453
Ptpru	516.2	0.261	0.0453
Rps27l	293.2	-0.344	0.0453
Herc2	4366.3	0.260	0.0454
Anxa5	1668.4	-0.198	0.0455
Fam32a	1658.8	-0.185	0.0455
Gstm7	305.6	-0.304	0.0455
Mobp	16091.6	-0.300	0.0456
Mrpl52	241.7	-0.301	0.0456
Khdrbs3	368.0	-0.254	0.0457
Paics	2747.7	-0.128	0.0459
Srp14	1094.9	-0.227	0.0460
Bgn	339.0	-0.355	0.0462
Phf2	1606.9	0.198	0.0464
A930017K11Rik	456.3	0.286	0.0468
Scmh1	787.1	0.185	0.0468
Gm20342	141.2	0.433	0.0469

Dock3	3514.9	0.234	0.0476
Ece1	2171.5	0.165	0.0476
Elk1	1236.1	0.224	0.0476
N4bp1	1190.9	0.224	0.0481
Gpx4	3444.9	-0.238	0.0482
Car2	3773.2	-0.217	0.0484
Dgkh	1909.0	0.250	0.0484
Kmt2d	2271.1	0.376	0.0484
Fry	3613.8	0.264	0.0488
Amer3	1026.9	0.213	0.0488
Hivep2	3086.0	0.291	0.0488
Il20rb	929.7	0.335	0.0488
Cnksr2	2438.8	0.321	0.0488
Nae1	1618.9	0.169	0.0494
Capn15	1691.9	0.192	0.0495
Atox1	358.9	-0.270	0.0498
Mtmr3	1997.5	0.146	0.0498
Celf1	4230.8	0.179	0.0498

Supplementary Table 2 – Reagents and antibodies

Reagent	Host	Clonality	Supplier	Catalog Number	RRID	Dilution/ Concentration	Figure
TMRE	n.a.	n.a.	Sigma Aldrich	87917		10nM	3
8-OHdG	Mouse	Monoclonal	Abcam	ab62623	AB_940049	1:700	4
LC3B	Rabbit	Polyclonal	ABClonal	A7198	AB_2863546	1:200	6
Lamp1	Rat	Monoclonal	DSHB (University of Iowa)*	1D4B	AB_2134500	1:400	6
CoxIV	Mouse	Monoclonal	Abcam	ab33985	AB_879754	1:300	6
Calbindin	Rabbit	n.a.	Swant	CB38a	AB_10000340	1:500	4, 6
Calbindin	Mouse	Monoclonal	Swant	CB300	AB_10000347	1:500	6
Parvalbumin	Guinea pig	n.a.	Swant	GP72	AB_2665495	1:1000	4
Anti-Mouse IgG Fab Fragment	Donkey	Polyclonal	Jackson Immunoresearch	715-007-003	AB_2307338	1:200	4, 6
Anti-mouse secondary (Alexa 488)	Goat	Polyclonal	Jackson Immunoresearch	115-545-003	AB_2338840	1:1000	4, 6
Anti-rabbit secondary (Alexa 594)	Donkey	Polyclonal	Jackson Immunoresearch	711-585-152	AB_2340621	1:1000	4, 6
Anti-mouse secondary (Alexa 594)	Goat	Polyclonal	Jackson Immunoresearch	115-585-003	AB_2338871	1:1000	6

Anti-rabbit secondary (Alexa 488)	Donkey	Polyclonal	Jackson Immunoresearch	711-545-152	AB_2313584	1:1000	6
Anti-rat secondary (Alexa 488)	Goat	Polyclonal	Invitrogen	A11006	AB_2534074	1:1000	6
Anti-guinea pig secondary (DyLight 405)	Goat	Polyclonal	Jackson Immunoresearch	106-475-003	AB_2337432	1:1000	4

Supplementary Table 3 – Human post-mortem tissues demographics

Sample ID	Age (year)	Sex	Post Mortem Delay (hour)	Group	*CACNA1A* CAG repeat length	Source of the tissues
H627	78	M	8.42	Non-neuropathological control	n.a.	The Douglas Bell Canada Brain Bank
H881	85	M	5.67	Non-neuropathological control	n.a.	
H1900	67	F	16.62	Non-neuropathological control	n.a.	
H004	68	F	8	SCA6	10 / 21	Donation from Dr. Arnulf Koeppen (Veterans Affairs Medical Center, Albany, New York)
H005	81	M	18	SCA6	10 / 21	
H006	85	M	4	SCA6	12 / 26	

Supplementary Table 4 – Raw data of LC/MS (Amino acids)

Compound	Fold Change (Log2)	P value
2-Aminoadipic acid	0.965	0.292
5-Deoxy-5-(methylthio)adenosine	2.112	0.183
5-Methyluridine	-0.015	0.970
Adenine (bA)	-0.151	0.606
Adenosine (A)	2.908	0.272
Alanine (7.8)	1.224	0.117
AMP	-2.034	0.143
Arginine	1.242	0.456
Argininosuccinic acid	0.727	0.062
Asparagine	0.438	0.694
Aspartic acid	0.225	0.811
b-Alanine	1.032	0.307
Betaine	0.492	0.471
Carnitine	1.585	0.084
Carnosine	1.902	0.076
Choline	1.518	0.186
Citrulline	0.652	0.581
Creatine	0.577	0.011
Creatinine	0.682	0.267
Cystathionine	0.519	0.634
Cystine	1.601	0.350
Cytidine (C)	0.425	0.611
Cytosine (bC)	1.215	0.450
deoxy-Cytidine (dC)	1.435	0.400
FAD	0.492	0.113
GABA	1.384	0.168
Glutamic acid	0.734	0.025
Glutamine	0.864	0.002
Glutathione (oxidized)	2.012	0.184
GlycP-Choline	0.687	0.008
GMP	-0.533	0.578
Guanine (bG)	-1.329	0.078
Guanosine (G)	0.760	0.030
Histidine	1.764	0.384
Hydroxy-Proline	0.691	0.333
Inosine (I)	1.236	0.053
Isoleucine (6.3)	1.823	0.434

Itaconic acid	0.174	0.675
Kynurenine	1.911	0.018
Lactic acid	1.033	0.004
Leucine (6.1)	1.538	0.413
Lysine	1.966	0.438
Malonic acid	0.752	0.012
Methionine	0.733	0.502
N-Ac-Aspartic acid	0.334	0.408
N-Ac-Glutamic acid	0.098	0.837
N-Carbamyl-Glutamic acid	0.702	0.508
NAc-Neuraminic acid	0.577	0.173
NAD	-1.207	0.237
NADP	-0.709	0.400
NEM-Cysteine	-1.788	0.088
NEM-Cysteinylglycine	-1.083	0.217
NEM-g-Glu-Cys	-0.933	0.381
NEM-Glutathione	-1.128	0.233
NEM-Homocysteine	-2.396	0.349
Ornithine	0.935	0.455
Pantothenic acid	1.805	0.163
Phenylalanine	1.659	0.400
Phospho-choline	-0.247	0.614
Proline	1.253	0.463
Pyridoxine	0.725	0.180
Riboflavin (B2)	0.008	0.986
Ribonic acid gamma lactone	0.778	0.125
S-5-Adenosyl-L-Homocysteine (SAH)	0.557	0.273
S-5-Adenosyl-L-Methionine (SAM)	2.084	0.151
Sarcosine (7.4)	0.783	0.229
Serine	0.640	0.487
Succinic acid	1.185	0.069
Taurine	0.923	0.026
Threonine	0.328	0.695
Tryptophan	1.761	0.411
Tyrosine	0.934	0.454
UDP-Glucose	0.394	0.328
Uridine (U)	0.800	0.145
Valine	0.992	0.253

The following compounds are not detected or do not pass quality control filter

deoxy-Guanosine (dG)	Dihydroorotic acid
Gluconic acid	DOPA
Hypotaurine	dUMP
IMP	F-1,6-bisP
N,N-dimethylglycine	Fumaric acid
Niacin (Nicotinic acid)	GA3P (7.7)
Pyroglutamic acid	Galactosamine
Uracil (bU)	g-Glu-Cys
cis-Aconitic acid / trans-Aconitic acid	Glutathione (reduced)
Erythrose-4P	Glyceric acid
2,3-Dihydroxybenzoic acid	Glycine
3-Hydroxy-Phenylacetic acid	Homocysteine
3-Indoleacetic acid	Homocystine
4-Pyridoxic acid	Malic acid
5-Aminolevulinc acid	o-Hydroxy hippuric acid
5-Hydroxy-Tryptophan	O-Phospho-Serine
5-Methoxy-Tryptamine	Orotic acid
5-Methylcytosine	Phosphoenolpyruvic acid
Ac-Choline	Pyruvic acid
Allantoin	Sedoheptulose-7P
alpha-Ketoglutaric acid	Taurocholic acid
cAMP	Thymidine (T)
CMP	Thymine (bT)
Creatine phosphate	TMP
Cysteine	trans-trans Muconic acid
dAMP	UMP
dCMP	Xanthine
deoxy-Adenosine (dA)	O-Phosphorylethanolamine
dGMP	Hypoxanthine
DHAP (7.0)	

Sample ID	H627	H881	H1900	H004	H005	H006
Normalization factor (total protein quantified by Bradford assay)	**1.34**	**1.06**	**1.10**	**0.82**	**0.87**	**0.80**
Group	**Control**	**Control**	**Control**	**SCA6**	**SCA6**	**SCA6**
2-Aminoadipic acid	39613.3	64418.1	41743.6	42192.1	87256.4	155137.0
5-Deoxy-5-(methylthio)adenosine	1918.5	1087.6	2459.0	13119.6	2574.1	7934.8
5-Methyluridine	12141.2	18702.4	20520.5	24511.1	13731.4	12577.0
Adenine (bA)	56363.2	95302.8	68391.8	55713.7	71751.7	70668.1
Adenosine (A)	28623.4	81062.4	68638.9	1694.1	441271.1	895861.9
Alanine (7.8)	88910.1	58674.7	118545.5	157990.4	302021.8	161564.6
AMP	30479.3	74103.8	28678.0	18833.6	9781.4	3919.0
Arginine	682014.0	261151.7	1255821.9	844542.5	3892267.7	465386.1
Argininosuccinic acid	8189.3	9896.4	5303.7	10530.4	15556.5	12635.4
Asparagine	73772.3	49563.5	151780.3	55220.7	259695.1	57691.0
Aspartic acid	24317.4	37039.2	53883.9	24741.8	90640.5	19273.0
b-Alanine	1166.2	1433.5	1428.7	2281.9	1232.9	4721.6
Betaine	2601963.5	3046295.0	1612311.2	5532059.4	2762687.9	1916695.6
Carnitine	1274192.6	1360420.2	1028726.4	3656511.5	4994709.8	2336929.2
Carnosine	8728.4	8523.4	26729.6	81251.0	41894.6	41279.6
Choline	236271.9	403119.0	180485.5	1282958.5	668002.6	396726.0
Citrulline	117514.1	51665.1	79179.4	72447.5	272303.0	45575.0
Creatine	6642657.0	8174600.5	7710693.5	10956667.4	11320375.6	11321869.7
Creatinine	2301896.6	2317729.0	6014090.3	4992507.1	7853361.6	4211829.6
Cystathionine	97364.1	144241.7	602970.8	729466.8	342625.9	137881.9
Cystine	8839.5	5757.6	7627.9	6894.4	47121.2	13390.8
Cytidine (C)	16891.6	33651.5	30590.2	7276.9	58180.5	43461.5
Cytosine (bC)	4558.8	7084.3	10450.8	1284.9	36783.3	13235.5
deoxy-Cytidine (dC)	11930.1	19494.3	21680.3	4488.6	101333.4	37725.9
FAD	4074.1	4588.7	3325.5	5799.0	4416.6	6643.8
GABA	5664535.4	9372654.0	4361807.3	26564326.3	14505089.7	9544332.0
Glutamic acid	1072494.2	1329048.9	1259575.6	1910299.2	2359056.2	1818717.8
Glutamine	2289730.8	2662533.3	2730121.0	4750734.7	4657908.5	4573129.6
Glutathione (oxidized)	12557.2	76035.3	11501.1	112493.8	56788.6	234567.4
GlycP-Choline	6477260.5	7367587.7	5976184.6	10229179.0	11840693.3	9843328.7
GMP	1906.6	6674.2	1888.6	2969.3	1246.7	3018.1
Guanine (bG)	113917.2	69306.3	138628.7	76129.7	12675.9	39312.6
Guanosine (G)	425471.3	373642.2	500566.5	678680.0	652420.8	870326.5
Histidine	86341.4	68282.0	206329.6	167427.8	929677.3	129231.3
Hydroxy-Proline	112575.8	178361.9	66679.7	303651.8	133707.0	139964.4
Inosine (I)	433374.3	502813.0	418636.6	1145195.8	768709.2	1277831.5

Isoleucine (6.3)	106399.0	38753.3	204735.2	135213.6	1021307.6	81857.1
Itaconic acid	1324.2	2896.3	1759.2	1938.2	1949.6	2857.8
Kynurenine	6285.7	2954.9	7505.6	24962.9	22543.8	15450.9
Lactic acid	84762.2	74939.2	101390.3	183361.3	175695.0	175351.8
Leucine (6.1)	284969.3	112078.5	649443.2	448963.5	2300228.1	289405.6
Lysine	415623.0	94739.6	1207760.5	829151.8	5678156.0	207214.2
Malonic acid	1439116.3	1879956.9	1717992.9	2431274.2	3008276.0	3046186.8
Methionine	177738.2	98778.3	386407.6	214146.2	709707.1	177756.1
N-Ac-Aspartic acid	29911.1	56993.6	28921.6	40770.0	58515.8	46756.7
N-Ac-Glutamic acid	154406.6	191443.8	316714.0	139152.0	311106.1	258905.0
N-Carbamyl-Glutamic acid	49909.7	26660.8	104091.9	57109.1	187333.8	49446.8
NAc-Neuraminic acid	40096.5	45999.2	54045.0	66989.8	90748.8	51335.4
NAD	60609.6	174255.2	75422.1	28209.1	38800.8	67353.0
NADP	4209.8	9518.5	3133.5	4350.1	1363.1	4603.6
NEM-Cysteine	359996.4	143658.7	367356.6	44372.1	158338.6	49525.0
NEM-Cysteinylglycine	57979.0	98394.7	153314.0	21515.1	26331.2	98369.2
NEM-g-Glu-Cys	15008.1	34588.0	7657.7	6355.2	7042.5	16595.3
NEM-Glutathione	185262.4	360754.1	122444.9	64995.7	56650.3	184288.1
NEM-Homocysteine	4637.8	2731.8	25728.3	1813.2	3684.9	791.5
Ornithine	83799.5	157663.8	237090.0	203029.2	613339.9	98638.8
Pantothenic acid	42685.3	33193.2	29179.6	201646.0	97910.1	67505.8
Phenylalanine	181410.4	82885.2	486088.5	290762.9	1803152.4	274972.2
Phospho-choline	1301204.7	1338154.4	2059880.2	654530.9	1942269.2	1362499.2
Proline	1669184.6	942337.0	3094071.5	1809000.2	10334604.6	1450762.8
Pyridoxine	63821.0	62402.5	42632.7	113958.4	109490.2	55640.8
Riboflavin (B2)	11841.4	10548.5	12994.1	12505.1	16917.3	6155.5
Ribonic acid gamma lactone	64691.9	41739.3	53842.2	88477.0	65734.7	120686.4
S-5-Adenosyl-L-Homocysteine (SAH)	40778.7	32619.6	69008.3	88071.3	78278.0	43196.8
S-5-Adenosyl-L-Methionine (SAM)	35621.2	27408.2	83022.7	277538.9	63710.2	277970.5
Sarcosine (7.4)	1527.1	1467.5	4127.6	5650.8	3749.4	2854.1
Serine	238743.0	166319.5	420285.3	294224.1	778646.2	213699.0
Succinic acid	28089.5	26555.9	25678.5	65705.0	74318.9	42580.5
Taurine	54510.3	81421.5	65935.4	142095.8	101063.8	139645.0
Threonine	87560.5	83754.6	221013.1	101889.3	293082.6	97600.1
Tryptophan	59605.2	28871.0	114550.0	73116.7	542505.4	72338.0
Tyrosine	97487.9	70429.9	227805.3	122545.7	507237.4	126274.1
UDP-Glucose	11571.5	15706.9	13432.3	21966.8	11275.9	20247.1
Uridine (U)	6181.3	4607.6	13215.0	11187.4	17014.1	13585.9
Valine	1632021.5	925201.3	2839588.2	3026284.0	5741158.7	1967947.8

Supplementary Table 5 – Raw data of LC/MS (Ion Pairing)

Compound	Fold Change (Log2)	P value
2-Aminoadipic acid	1.311998416	0.20485695
2-Hydroxyglutaric acid	0.88267562	0.1566423
2-Isopropylmalic acid	0.184223935	0.80962046
2-Phosphoglyceric acid / 3-Phosphoglyceric acid	1.334278263	0.13583468
2,3-BPG	-1.961411226	0.16513698
2,3-Pyridinedicarboxylic acid	1.952153633	0.44348596
4-Pyridoxic acid	-0.170354279	0.73728498
5-Hydroxymethylcytosine	-0.76148393	0.50475325
5-Methyluridine	0.949020285	0.1762888
a-Hydroxy-Butyric acid	2.100873687	0.17654752
Acetoacetate	-0.245372551	0.72470657
Adenine	-1.001529898	0.34053159
Adenosine	3.345559803	0.41979678
Adenylosuccinic acid	0.034287821	0.98315085
ADP	-1.39943611	0.36416429
ADPR	0.471318463	0.58923354
Alanine/Sarcosine	0.331130954	0.34824107
alpha-Ketoglutaric acid	0.740775964	0.25398106
AMP	-3.476361032	0.27793516
Arginine	0.462283865	0.5959367
Argininosuccinic acid	0.738820063	0.09781979
Asparagine	0.406871017	0.71338299
Aspartic Acid	-0.210421699	0.68230757
ATP / dGTP	-1.424967392	0.35177875
b-Hydroxy-Butyric acid	0.725309777	0.29338626
b-Hydroxy-Isobutyric acid	1.42059438	0.15925763
Carnitine	1.130611101	0.07940987
CDP-Choline	-0.166066774	0.77517827
cis-Aconitic acid	0.574771709	0.48065379
Citramalic acid	0.887055252	0.1548202
Citric acid / Isocitric acid	0.787071495	0.39090876
CMP	0.984104875	0.63278368
Creatine	0.275147267	0.54245605
Creatinine	0.388970307	0.29934897
Cystathionine	0.20422616	0.87232869
Cytidine	0.257356261	0.75116443
dC	0.509022609	0.44427616

dGMP	0.103038168	0.84011913
DHAP	-0.885149492	0.52391631
dI	2.245637956	0.39433054
dU	2.017341181	0.21164979
F6P	0.899042248	0.47618753
FAD	0.193173121	0.79964884
Fumaric acid	0.558134791	0.4155602
G1P	3.355502696	0.36164364
G6P	1.163916379	0.14888684
GABA	-0.036736878	0.93457934
Gluconic acid	1.782737882	0.08891988
Glutamic acid	0.608706753	0.2589413
Glutamine	0.223965742	0.49149201
Glutathione (oxidized)	2.572799645	0.36662178
Glyceric acid	3.191647939	0.16378466
GMP	-0.81481619	0.61840141
Guanine	-0.284030936	0.71934711
Guanosine	1.331398095	0.29424915
Homocitrate	0.433475218	0.71734127
Homocysteine	-0.792686857	0.48119583
Homoserine	0.241840518	0.74585602
Hypoxanthine	0.221622705	0.74408395
IMP	-0.952230282	0.61867383
Inosine	1.203016413	0.31386851
Isoleucine	0.853963235	0.13725564
Kynurenine	1.758599533	0.15264599
Lactic acid	0.679974513	0.17437101
Leucine	0.801205315	0.06944054
Malic acid	0.995210948	0.33765224
Methionine	0.689112312	0.11464518
N-Carbamyl-Glutamic acid	-0.862768172	0.30966047
N,N-Dimethylglycine	-0.349718469	0.53841919
NAc-Aspartic acid	0.169388405	0.82285096
NAc-Glucosamine	0.724556311	0.10129227
NAc-Glutamic acid	0.375750612	0.59307322
NAc-Neuraminic acid	0.742225431	0.23795547
NAD	-1.965968495	0.28430924
NEM-Glutathione	-2.119839661	0.36172846
NEM-Homocysteine	-2.491476856	0.16779932
O-Phospho-Serine	1.825676173	0.10069243
O-Phosphorylethanolamine	-0.822466759	0.48207971

Pantothenic acid	1.262852593	0.40791688
Pentose alcohols	0.271417555	0.59815252
Phenylalanine	0.960792207	0.01670554
Phosphoenolpyruvic acid	1.330871545	0.14571419
Pyridoxal	1.314055598	0.23058367
Pyridoxine	0.312930257	0.7277362
Pyroglutamic acid	-0.373809569	0.69130303
Riboflavin (B2)	1.070924702	0.14921768
Ribose-5P	-0.8052074	0.5323349
Ribulose-5P	-3.512432971	0.16766009
S-5-Adenosyl-L-homocysteine (SAH)	0.678448749	0.44157858
Sedoheptulose-7P	-0.266680261	0.77412103
Sphinganine	-0.038154336	0.95778361
Succinic acid	0.561012207	0.46382759
Taurine	0.797193606	0.35361222
Threonine	0.563270906	0.46910605
Thymidine	1.362297335	0.159849
Thymine	0.916282909	0.55593074
trans-Aconitic acid	0.187947193	0.72262958
Tryptophan	0.796179807	0.08764225
TTP	-0.596171775	0.65445792
Tyrosine	0.678723264	0.08710516
UDP-Glucose / UDP-Galactose	0.668306412	0.34661288
UDP-Glucuronic acid	-0.105048128	0.90643349
UDP-NAc-Glucosamine	0.470330932	0.61546326
UMP	-1.95238663	0.35739552
Uracil	-0.343713349	0.67447276
Uric acid	1.313791309	0.042284
Uridine	0.804182833	0.34263164
UTP	-1.528969709	0.3425167
Valine	0.645211863	0.16125867
Xanthine	0.846709745	0.32092222
Xanthosine	1.161632249	0.20424279

The following compounds are not detected or do not pass quality control filter

1,3-BPG	CoA-Isovaleryl	ITP
2-Deoxy-Ribose	CoA-Malonyl	Ketoisovaleric acid-14.3 / Ketovaleric acid-14.7
2-Deoxy-Ribose 5P	CoA-Methylmalonyl	Lipoamide
2-Ketobutyrate	CoA-Propionyl	Lipoic acid
2,2-Dimethyl Succinic acid	CoA-Succinyl	Lipoic acid (reduced)
2,3-Dihydroxybenzoic acid	Creatine phosphate	M6P
2,3-Dihydroxyisovaleric acid	CTP	Maleic acid
2,3-Dimethyl Succinic acid	Cysteine	Malonic acid
3-Hydroxy-Anthranilic acid	Cystine	Mevalonic acid
3-Hydroxy-Kynurenine	Cytosine	Mevalonic acid-5P
3-Hydroxy-Phenylacetic acid	dA	Mevalonolactone
3-Indoleacetic acid	dADP	N-Carbamoyl-Aspartic acid
3-Methylglutaric acid	dAMP	NAc-Galactosamine
3,2-Hydroxyethylindole	dATP	NAc-Glucosamine-1P
4-Aminobenzoic acid	dCDP	NAc-Glucosamine-6P
4-Guanidobutyric acid	dCMP	NADH
4-Hydroxyphenyl-Pyruvic acid	dCTP	NADP
4-Methyl-2-Oxovaleric acid	dG	NADPH
5-Deoxy-5-(methylthio)adenosine	dGDP	NaMN
5-Hydroxy-3-indoleacetic acid	DHF	NEM-Cysteine
5-Hydroxy-Tryptophan	Dihydroorotic acid	NEM-Cysteine1
5-Methoxy-Tryptamine	Disaccharides	NEM-g-Glu-Cys
5-Methylcytosine	DOPA	NEM-Lipoic acid (reduced)
6-Hydroxy-Nicotinic acid	dUMP	NEM-NAc-Cysteine
6-Methyladenine	dUTP	Nicotinamide
a-Hydroxy-Isobutyric acid	Erythrose-4P	Nicotinic acid
a-P-Glycerol	F-1,6-bisP	Nicotinic acid mononucleotide
Adipic acid	Folic acid	o-Hydroxy hippuric acid
AICAR	Folinic acid	O-Succinyl-L-homoserine
AICAR-P	GA3P	Ornithine
Allantoin	Galactonic acid	Orotic acid
Arabinose-5P	Galactosamine	Oxaloacetic acid
b-P-Glycerol	gamma-Glu-Cys	Oxamic acid
Bile_C_Cholesterol	GDP	Pentoses
Bile_Deoxycholic acids (DCA, UDCA, ChDCA, HDCA)	Glucoheptonic acid	Phenylpyruvic acid
Bile_GCA_Glycocholic acid	Gluconic acid-6P	Prephenic acid
Bile_GChDCA_Glycochenodeoxycholic acid	Gluconolactone	Proline
Bile_LCA_Lithocholic acid	Glucosamine-1P	PRPP

Bile_TCA_Taurocholic acid	Glucosamine-6P	Pyridoxal-5P
Bile_TChDCA_Taurochenodeoxycholic acid	Glutamine	Pyridoxamine
Bile_TUDCA_Tauroursodeoxycholic acid	Glutathione (reduced)	Pyruvic acid
cADPR	Glyoxylic acid	Quinic acid
cAMP	GTP	Ribonic acid gamma lactone
Carnosine	Hexoses	Ribulose-1,5-bisP
CDP	Histidine	Serine
cGAMP	Homocystine	Succinic semialdehyde
cGMP	Hydroxy-Proline	TDP
Citrulline	Hydroxybenzoic acid	THF
CoA	Hydroxybenzoic acid (oxidized)	Thiamine (B1)
CoA-Acetoacetyl	Hypotaurine	TMP
CoA-Acetyl	IDP	trans-trans Muconic acid
CoA-Butyryl / CoA-Isobutyryl	Isopentenyl pyrophosphate	UDP
CoA-HMG	Itaconic acid	Xylulose-5P
CoA-Hydroxybutyryl		

Sample ID	H627	H881	H1900	H004	H005	H006
Normalization factor (total protein quantified by Bradford assay)	**1.34**	**1.06**	**1.10**	**0.82**	**0.87**	**0.80**
Group	**Control**	**Control**	**Control**	**SCA6**	**SCA6**	**SCA6**
2-Aminoadipic acid	24733.4	34665.4	23410.5	34083.3	61348.0	110172.0
2-Hydroxyglutaric acid	1284781.3	702003.5	465725.6	1797120.5	894068.2	1830729.4
2-Isopropylmalic acid	96620.7	164973.0	28866.3	131587.2	45692.4	152742.6
2-Phosphoglyceric acid / 3-Phosphoglyceric acid	186881.2	287608.4	66662.5	539552.3	217578.1	607380.8
2,3-BPG	720021.2	435375.7	175573.7	39850.7	151366.4	150545.8
2,3-Pyridinedicarboxylic acid	12997.9	5233.1	44290.4	25647.8	206234.2	10045.9
4-Pyridoxic acid	9037.8	14467.2	22554.0	18352.6	9424.2	13152.3
5-Hydroxymethylcytosine	1648486.6	4633887.5	819610.0	925036.9	814841.8	2449505.5
5-Methyluridine	4530.5	9080.0	5095.5	9623.2	17869.1	8620.7
a-Hydroxy-Butyric acid	1043868.6	403834.3	589984.0	5117303.2	1843212.7	1780530.9
Acetoacetate	10051.9	16231.4	3885.0	12466.2	6512.5	6471.1
Adenine	1063047.8	2146529.8	462294.2	898196.5	323230.1	612563.4
Adenosine	32677.4	62950.6	26103.1	4956.1	83091.0	1149368.0
Adenylosuccinic acid	3593.2	33565.5	597.6	29113.8	1421.9	8128.7
ADP	38830.4	94351.3	8782.2	35420.4	7147.4	11247.4
ADPR	65291.4	71360.6	18200.9	51934.4	34473.0	128277.1
Alanine/Sarcosine	2600943.4	3451262.3	1719201.6	3514854.1	2527506.9	3734062.8
alpha-Ketoglutaric acid	130929.6	157533.4	132355.3	313735.3	117517.9	271965.3
AMP	793539.9	2583207.7	153859.9	256538.7	29676.2	31005.0
Arginine	15172.2	9658.3	22208.1	17243.9	39193.8	8368.5
Argininosuccinic acid	2063.2	2360.5	906.3	2766.5	3489.0	2639.1
Asparagine	10975.0	6306.6	24814.7	9002.7	38436.7	8372.2
Aspartic Acid	1336672.2	2323988.4	871946.6	1282603.9	1478014.2	1156844.4
ATP / dGTP	53378.4	133488.2	14566.7	41332.3	12186.2	21500.9
b-Hydroxy-Butyric acid	435336.0	467142.1	132061.0	837176.9	321074.2	552106.5
b-Hydroxy-Isobutyric acid	26095.7	51839.0	10233.5	75780.0	39516.4	120726.2
Carnitine	3312.9	4030.2	2588.5	8314.1	8729.4	4701.8
CDP-Choline	26048.7	36252.0	12469.8	28720.3	11187.2	26733.2
cis-Aconitic acid	73898.3	98666.8	34415.4	102387.2	37963.2	167935.1
Citramalic acid	187352.4	103640.1	71411.2	268527.7	131333.4	270367.4
Citric acid / Isocitric acid	1790599.9	3638889.4	875781.8	3297247.9	1525459.2	6057468.2
CMP	24035.5	63000.7	6222.7	168004.7	5080.3	11389.1
Creatine	1840230.8	2679722.9	1087091.1	2510356.3	1540827.9	2733999.3
Creatinine	63526.5	81432.9	60519.4	113596.5	61389.5	94079.9

Cystathionine	1907.3	3301.7	20832.0	18492.3	9130.4	2378.2
Cytidine	15080.4	30967.9	13162.5	10045.9	18502.8	42225.1
dC	3426.9	4843.8	11467.6	5088.5	11763.3	11237.5
dGMP	372.1	728.6	841.1	1025.0	610.7	449.8
DHAP	482442.2	1126966.8	75224.7	693004.4	77443.8	141665.4
dI	4579.7	8118.1	40386.4	24231.8	206828.7	20689.5
dU	10709.5	15552.9	5751.9	79356.5	24118.9	26130.6
F6P	126265.6	12209.7	17708.4	124496.1	11878.5	154881.0
FAD	2533.7	3889.4	695.3	4227.5	1309.0	2601.9
Fumaric acid	9670389.3	14480229.2	3529911.3	16708617.4	6407884.6	17639325.1
G1P	65164.7	0.0	32167.4	117787.5	37414.7	841034.9
G6P	1046917.5	702252.0	411287.6	1603227.5	907375.5	2330221.9
GABA	1158.0	1748.2	874.6	1305.5	752.4	1627.7
Gluconic acid	957214.0	353835.2	644613.9	3164129.3	1274188.2	2290699.3
Glutamic acid	5029435.2	7129454.0	2775037.9	8864580.8	4555388.3	9352652.0
Glutamine	132370.9	166403.6	255807.0	228582.3	222853.1	196282.4
Glutathione (oxidized)	6440.8	81189.1	1092.8	92699.6	10740.1	424427.1
Glyceric acid	107996.1	75781.1	54637.2	1255067.6	215404.9	707810.1
GMP	15286.2	79633.7	3550.0	25969.6	2503.8	27504.8
Guanine	654044.6	280628.1	532514.8	254460.8	785005.5	165524.6
Guanosine	533462.9	607679.6	134989.0	1133550.5	243461.0	1834327.8
Homocitrate	799886.8	1046880.5	338374.3	2166052.2	492386.0	292557.9
Homocysteine	357536.6	930250.2	154432.1	299067.3	123687.0	409792.5
Homoserine	8903.6	8952.4	18305.0	10246.2	24917.4	7596.9
Hypoxanthine	3480707.7	4846065.4	1196283.0	5661137.6	1994981.2	3448187.3
IMP	15491.3	101136.9	3992.7	55977.3	3307.0	3056.6
Inosine	3802054.2	6678618.9	924444.4	11057579.1	1543644.0	13655697.5
Isoleucine	2547.1	1555.4	685.4	2867.3	3630.7	2155.8
Kynurenine	11233.0	5660.2	5240.4	38808.7	11099.6	24984.9
Lactic acid	1892891.9	2252531.3	1176608.1	3361092.4	1782645.8	3382749.1
Leucine	10268.1	7132.5	4301.5	13664.9	13846.6	10305.6
Malic acid	863590.7	1378041.6	189737.6	1927861.2	414109.1	2504654.3
Methionine	148969.4	98498.6	61953.6	172874.6	180249.8	145753.3
N-Carbamyl-Glutamic acid	325872.5	376825.8	91102.4	218611.7	106399.8	111496.6
N,N-Dimethylglycine	65999.8	123854.4	57910.1	52066.8	45453.9	96909.2
NAc-Aspartic acid	7633835.4	12909933.0	2339631.9	10384662.8	3570870.9	11778718.3
NAc-Glucosamine	36233.3	25970.0	32453.5	48738.0	66820.1	40852.1
NAc-Glutamic acid	328041.6	663022.4	167624.5	531195.8	255731.3	716487.9
NAc-Neuraminic acid	134094.8	188302.8	42323.0	258620.3	123751.6	227716.1

NAD	504937.9	1284398.1	155954.1	126276.5	131089.1	240565.1
NEM-Glutathione	1985756.8	6768812.4	203409.8	394939.0	58599.9	1607445.5
NEM-Homocysteine	11816.8	6425.7	25653.1	3081.0	3799.0	925.7
O-Phospho-Serine	753.8	1341.8	280.7	4308.8	2165.1	1949.5
O-Phosphorylethanolamine	850471.3	2375596.7	407911.4	442202.7	417245.6	1195473.6
Pantothenic acid	157606.8	211043.9	20737.8	640822.2	53315.7	240276.9
Pentose alcohols	14887.3	16421.3	12746.0	27419.7	12465.0	13288.9
Phenylalanine	642924.9	459724.2	455805.3	868434.2	1189598.2	975309.7
Phosphoenolpyruvic acid	161238.8	197328.9	75786.9	545973.1	205373.4	341292.7
Pyridoxal	94203.4	79494.8	16338.5	220982.3	45419.4	206104.6
Pyridoxine	21852.3	17741.4	6369.4	35953.6	12811.9	8331.2
Pyroglutamic acid	15096.1	21051.6	64222.5	41536.3	14677.3	21246.1
Riboflavin (B2)	8007.4	3606.9	5610.7	17474.6	11198.7	7512.4
Ribose-5P	136962.5	391443.2	43710.1	187837.8	16306.6	123265.9
Ribulose-5P	482377.3	977959.7	170251.0	104372.8	9317.1	29198.4
S-5-Adenosyl-L-homocysteine (SAH)	91817.3	133114.9	29432.2	210614.6	41150.3	155324.6
Sedoheptulose-7P	1696805.1	383343.1	478225.3	948589.8	412033.9	765973.2
Sphinganine	137832.6	68423.7	36148.3	120186.0	44933.1	70958.8
Succinic acid	3547889.3	4837603.4	882323.2	6696193.3	1964597.5	5012054.6
Taurine	457181.6	692939.5	439300.1	1504801.8	376731.3	880432.0
Threonine	52086.2	45248.9	110509.3	114070.1	155895.9	37148.1
Thymidine	1630.0	1807.7	1732.0	2580.7	6777.5	3932.6
Thymine	12681.0	16132.2	19052.9	13844.6	70218.1	6272.3
trans-Aconitic acid	151332.3	218512.8	101246.3	266526.3	112019.4	158094.2
Tryptophan	78050.0	68148.8	29520.0	91632.1	107951.9	105551.0
TTP	489.1	518.8	3033.9	676.4	1547.5	449.8
Tyrosine	196470.0	185952.7	97548.7	245667.1	256102.4	266531.7
UDP-Glucose / UDP-Galactose	299023.7	305752.4	167619.0	615148.9	187537.8	424808.6
UDP-Glucuronic acid	55426.7	114369.1	15160.6	83032.6	21481.4	67453.6
UDP-NAc-Glucosamine	135524.1	276334.2	36518.6	319670.3	53129.1	248394.4
UMP	182713.8	541065.4	17825.2	146964.5	17306.8	27350.7
Uracil	443654.3	624799.2	109702.6	506701.7	256785.6	164912.0
Uric acid	21357.9	22740.2	21905.7	59725.0	40900.2	63456.4
Uridine	488995.5	849684.8	210891.8	986733.0	351650.3	1367412.2
UTP	4748.9	13032.7	1561.8	3783.0	1236.4	1683.6
Valine	2038968.2	1386927.0	1192369.0	2661889.5	2957526.3	1603406.0
Xanthine	547559.9	1005188.4	238953.3	1681753.3	484066.8	1056366.6
Xanthosine	322303.2	356173.9	242956.9	1063140.8	352244.9	645957.8

Chatper 3 References

1 Anders S, Pyl PT, Huber W (2015) HTSeq--a Python framework to work with high-throughput sequencing data. Bioinformatics 31: 166-169 Doi 10.1093/bioinformatics/btu638

2 Azzollini V, Hayward W (2023) What Role Does the Cerebellum Have in a Fatigue Network? J Neurosci 43: 7599-7600 Doi 10.1523/JNEUROSCI.1168-23.2023

3 Brion F, Marc B, Launay F, Gailledreau J, Durigon M (1991) Postmortem interval estimation by creatinine levels in human psoas muscle. Forensic Sci Int 52: 113-120 Doi 10.1016/0379-0738(91)90103-p

4 Brusse E, Brusse-Keizer MG, Duivenvoorden HJ, van Swieten JC (2011) Fatigue in spinocerebellar ataxia: patient self-assessment of an early and disabling symptom. Neurology 76: 953-959 Doi 10.1212/WNL.0b013e31821043a4

5 Calvo-Rodriguez M, Bacskai BJ (2021) Mitochondria and Calcium in Alzheimer's Disease: From Cell Signaling to Neuronal Cell Death. Trends Neurosci 44: 136-151 Doi 10.1016/j.tins.2020.10.004

6 Casamento-Moran A, Mooney RA, Chib VS, Celnik PA (2023) Cerebellar Excitability Regulates Physical Fatigue Perception. J Neurosci 43: 3094-3106 Doi 10.1523/JNEUROSCI.1406-22.2023

7 Cecchini G (2003) Function and structure of complex II of the respiratory chain. Annu Rev Biochem 72: 77-109 Doi 10.1146/annurev.biochem.72.121801.161700

8 Cerutti R, Pirinen E, Lamperti C, Marchet S, Sauve AA, Li W, Leoni V, Schon EA, Dantzer F, Auwerx Jet al (2014) NAD(+)-dependent activation of Sirt1 corrects the phenotype in a mouse model of mitochondrial disease. Cell Metab 19: 1042-1049 Doi 10.1016/j.cmet.2014.04.001

9 Chakrabarti L, Eng J, Ivanov N, Garden GA, La Spada AR (2009) Autophagy activation and enhanced mitophagy characterize the Purkinje cells of pcd mice prior to neuronal death. Mol Brain 2: 24 Doi 10.1186/1756-6606-2-24

10 Chen P, Peng C, Luff J, Spring K, Watters D, Bottle S, Furuya S, Lavin MF (2003) Oxidative stress is responsible for deficient survival and dendritogenesis in purkinje neurons from ataxia-telangiectasia mutated mutant mice. J Neurosci 23: 11453-11460

11 Chow HM, Cheng A, Song X, Swerdel MR, Hart RP, Herrup K (2019) ATM is activated by ATP depletion and modulates mitochondrial function through NRF1. J Cell Biol 218: 909-928 Doi 10.1083/jcb.201806197

12 Cogliati S, Frezza C, Soriano ME, Varanita T, Quintana-Cabrera R, Corrado M, Cipolat S, Costa V, Casarin A, Gomes LCet al (2013) Mitochondrial cristae shape determines respiratory chain

supercomplexes assembly and respiratory efficiency. Cell 155: 160-171 Doi 10.1016/j.cell.2013.08.032

13 Cook AA, Fields E, Watt AJ (2021) Losing the Beat: Contribution of Purkinje Cell Firing Dysfunction to Disease, and Its Reversal. Neuroscience 462: 247-261 Doi 10.1016/j.neuroscience.2020.06.008

14 Cook AA, Jayabal S, Sheng J, Fields E, Leung TCS, Quilez S, McNicholas E, Lau L, Huang S, Watt AJ (2022) Activation of TrkB-Akt signaling rescues deficits in a mouse model of SCA6. Sci Adv 8: eabh3260 Doi 10.1126/sciadv.abh3260

15 Cook AA, Leung TCS, Rice M, Nachman M, Zadigue-Dube É, Watt AJ (2023) Endosomal dysfunction contributes to cerebellar deficits in spinocerebellar ataxia type 6. Elife 12: Doi 10.7554/eLife.90510

16 Doyle JP, Dougherty JD, Heiman M, Schmidt EF, Stevens TR, Ma G, Bupp S, Shrestha P, Shah RD, Doughty MLet al (2008) Application of a translational profiling approach for the comparative analysis of CNS cell types. Cell 135: 749-762 Doi 10.1016/j.cell.2008.10.029

17 Du X, Wang J, Zhu H, Rinaldo L, Lamar KM, Palmenberg AC, Hansel C, Gomez CM (2013) Second cistron in CACNA1A gene encodes a transcription factor mediating cerebellar development and SCA6. Cell 154: 118-133 Doi 10.1016/j.cell.2013.05.059

18 Eccles JC, Ito M, Szentágothai Jn (1967) The cerebellum as a neuronal machine. Springer-Verlag, City

19 Fagerberg L, Hallstrom BM, Oksvold P, Kampf C, Djureinovic D, Odeberg J, Habuka M, Tahmasebpoor S, Danielsson A, Edlund Ket al (2014) Analysis of the human tissue-specific expression by genome-wide integration of transcriptomics and antibody-based proteomics. Mol Cell Proteomics 13: 397-406 Doi 10.1074/mcp.M113.035600

20 Fecher C, Trovo L, Muller SA, Snaidero N, Wettmarshausen J, Heink S, Ortiz O, Wagner I, Kuhn R, Hartmann Jet al (2019) Cell-type-specific profiling of brain mitochondria reveals functional and molecular diversity. Nat Neurosci 22: 1731-1742 Doi 10.1038/s41593-019-0479-z

21 Filler K, Lyon D, Bennett J, McCain N, Elswick R, Lukkahatai N, Saligan LN (2014) Association of Mitochondrial Dysfunction and Fatigue: A Review of the Literature. BBA Clin 1: 12-23 Doi 10.1016/j.bbacli.2014.04.001

22 Franco-Iborra S, Cuadros T, Parent A, Romero-Gimenez J, Vila M, Perier C (2018) Defective mitochondrial protein import contributes to complex I-induced mitochondrial dysfunction and neurodegeneration in Parkinson's disease. Cell Death Dis 9: 1122 Doi 10.1038/s41419-018-1154-0

23 GonzaleZ-Riano C, Tapia-Gonzalez S, Garcia A, Munoz A, DeFelipe J, Barbas C (2017) Metabolomics and neuroanatomical evaluation of post-mortem changes in the hippocampus. Brain Struct Funct 222: 2831-2853 Doi 10.1007/s00429-017-1375-5

24 Hubens WHG, Vallbona-Garcia A, de Coo IFM, van Tienen FHJ, Webers CAB, Smeets HJM, Gorgels T (2022) Blood biomarkers for assessment of mitochondrial dysfunction: An expert review. Mitochondrion 62: 187-204 Doi 10.1016/j.mito.2021.10.008

25 Ishikawa K, Tanaka H, Saito M, Ohkoshi N, Fujita T, Yoshizawa K, Ikeuchi T, Watanabe M, Hayashi A, Takiyama Yet al (1997) Japanese families with autosomal dominant pure cerebellar ataxia map to chromosome 19p13.1-p13.2 and are strongly associated with mild CAG expansions in the spinocerebellar ataxia type 6 gene in chromosome 19p13.1. Am J Hum Genet 61: 336-346 Doi 10.1086/514867

26 Ishikawa K, Watanabe M, Yoshizawa K, Fujita T, Iwamoto H, Yoshizawa T, Harada K, Nakamagoe K, Komatsuzaki Y, Satoh Aet al (1999) Clinical, neuropathological, and molecular study in two families with spinocerebellar ataxia type 6 (SCA6). J Neurol Neurosurg Psychiatry 67: 86-89 Doi 10.1136/jnnp.67.1.86

27 Jacobi H, Bauer P, Giunti P, Labrum R, Sweeney MG, Charles P, Durr A, Marelli C, Globas C, Linnemann Cet al (2011) The natural history of spinocerebellar ataxia type 1, 2, 3, and 6: a 2-year follow-up study. Neurology 77: 1035-1041 Doi 10.1212/WNL.0b013e31822e7ca0

28 Jayabal S, Chang HH, Cullen KE, Watt AJ (2016) 4-aminopyridine reverses ataxia and cerebellar firing deficiency in a mouse model of spinocerebellar ataxia type 6. Sci Rep 6: 29489 Doi 10.1038/srep29489

29 Jayabal S, Ljungberg L, Erwes T, Cormier A, Quilez S, El Jaouhari S, Watt AJ (2015) Rapid Onset of Motor Deficits in a Mouse Model of Spinocerebellar Ataxia Type 6 Precedes Late Cerebellar Degeneration. eNeuro 2: Doi 10.1523/ENEURO.0094-15.2015

30 Jayabal S, Ljungberg L, Watt AJ (2017) Transient cerebellar alterations during development prior to obvious motor phenotype in a mouse model of spinocerebellar ataxia type 6. J Physiol 595: 949-966 Doi 10.1113/JP273184

31 Kamarauskaite J, Baniene R, Trumbeckas D, Strazdauskas A, Trumbeckaite S (2020) Increased Succinate Accumulation Induces ROS Generation in In Vivo Ischemia/Reperfusion-Affected Rat Kidney Mitochondria. Biomed Res Int 2020: 8855585 Doi 10.1155/2020/8855585

32 Kasumu A, Bezprozvanny I (2012) Deranged calcium signaling in Purkinje cells and pathogenesis in spinocerebellar ataxia 2 (SCA2) and other ataxias. Cerebellum 11: 630-639 Doi 10.1007/s12311-010-0182-9

33 Kim D, Paggi JM, Park C, Bennett C, Salzberg SL (2019) Graph-based genome alignment and genotyping with HISAT2 and HISAT-genotype. Nat Biotechnol 37: 907-915 Doi 10.1038/s41587-019-0201-4

34 Konig J, Ott C, Hugo M, Jung T, Bulteau AL, Grune T, Hohn A (2017) Mitochondrial contribution to lipofuscin formation. Redox Biol 11: 673-681 Doi 10.1016/j.redox.2017.01.017

35 Lang-Ouellette D, Gruver KM, Smith-Dijak A, Blot FGC, Stewart CA, de Vanssay de Blavous P, Li CH, Van Eitrem C, Rosen C, Faust PLet al (2021) Purkinje cell axonal swellings enhance action potential fidelity and cerebellar function. Nat Commun 12: 4129 Doi 10.1038/s41467-021-24390-4

36 Li X, Yang Y, Zhang B, Lin X, Fu X, An Y, Zou Y, Wang JX, Wang Z, Yu T (2022) Lactate metabolism in human health and disease. Signal Transduct Target Ther 7: 305 Doi 10.1038/s41392-022-01151-3

37 Love MI, Huber W, Anders S (2014) Moderated estimation of fold change and dispersion for RNA-seq data with DESeq2. Genome Biol 15: 550 Doi 10.1186/s13059-014-0550-8

38 Lu YT, Li LZ, Yang YL, Yin X, Liu Q, Zhang L, Liu K, Liu B, Li J, Qi LW (2018) Succinate induces aberrant mitochondrial fission in cardiomyocytes through GPR91 signaling. Cell Death Dis 9: 672 Doi 10.1038/s41419-018-0708-5

39 Maltecca F, Magnoni R, Cerri F, Cox GA, Quattrini A, Casari G (2009) Haploinsufficiency of AFG3L2, the gene responsible for spinocerebellar ataxia type 28, causes mitochondria-mediated Purkinje cell dark degeneration. J Neurosci 29: 9244-9254 Doi 10.1523/JNEUROSCI.1532-09.2009

40 Manolaras I, Del Bondio A, Griso O, Reutenauer L, Eisenmann A, Habermann BH, Puccio H (2023) Mitochondrial dysfunction and calcium dysregulation in COQ8A-ataxia Purkinje neurons are rescued by CoQ10 treatment. Brain 146: 3836-3850 Doi 10.1093/brain/awad099

41 Mark MD, Krause M, Boele HJ, Kruse W, Pollok S, Kuner T, Dalkara D, Koekkoek S, De Zeeuw CI, Herlitze S (2015) Spinocerebellar ataxia type 6 protein aggregates cause deficits in motor learning and cerebellar plasticity. J Neurosci 35: 8882-8895 Doi 10.1523/JNEUROSCI.0891-15.2015

42 Markaki M, Tavernarakis N (2020) Mitochondrial turnover and homeostasis in ageing and neurodegeneration. FEBS Lett 594: 2370-2379 Doi 10.1002/1873-3468.13802

43 Marquez BT, Leung TCS, Hui J, Charron F, McKinney RA, Watt AJ (2023) A mitochondrial-targeted antioxidant (MitoQ) improves motor coordination and reduces Purkinje cell death in a mouse model of ARSACS. Neurobiol Dis 183: 106157 Doi 10.1016/j.nbd.2023.106157

44 Massudi H, Grant R, Braidy N, Guest J, Farnsworth B, Guillemin GJ (2012) Age-associated changes in oxidative stress and NAD+ metabolism in human tissue. PLoS One 7: e42357 Doi 10.1371/journal.pone.0042357

45 Mishra E, Thakur MK (2023) Mitophagy: A promising therapeutic target for neuroprotection during ageing and age-related diseases. Br J Pharmacol 180: 1542-1561 Doi 10.1111/bph.16062

46 Moriarty A, Cook A, Hunt H, Adams ME, Cipolotti L, Giunti P (2016) A longitudinal investigation into cognition and disease progression in spinocerebellar ataxia types 1, 2, 3, 6, and 7. Orphanet J Rare Dis 11: 82 Doi 10.1186/s13023-016-0447-6

47 Murphy MP (2013) Mitochondrial dysfunction indirectly elevates ROS production by the endoplasmic reticulum. Cell Metab 18: 145-146 Doi 10.1016/j.cmet.2013.07.006

48 Penner IK, Paul F (2017) Fatigue as a symptom or comorbidity of neurological diseases. Nat Rev Neurol 13: 662-675 Doi 10.1038/nrneurol.2017.117

49 Pilotto F, Douthwaite C, Diab R, Ye X, Al Qassab Z, Tietje C, Mounassir M, Odriozola A, Thapa A, Buijsen RAMet al (2023) Early molecular layer interneuron hyperactivity triggers Purkinje neuron degeneration in SCA1. Neuron 111: 2523-2543 e2510 Doi 10.1016/j.neuron.2023.05.016

50 Raudvere U, Kolberg L, Kuzmin I, Arak T, Adler P, Peterson H, Vilo J (2019) g:Profiler: a web server for functional enrichment analysis and conversions of gene lists (2019 update). Nucleic Acids Res 47: W191-W198 Doi 10.1093/nar/gkz369

51 Reeg S, Grune T (2015) Protein Oxidation in Aging: Does It Play a Role in Aging Progression? Antioxid Redox Signal 23: 239-255 Doi 10.1089/ars.2014.6062

52 Rueden CT, Schindelin J, Hiner MC, DeZonia BE, Walter AE, Arena ET, Eliceiri KW (2017) ImageJ2: ImageJ for the next generation of scientific image data. BMC Bioinformatics 18: 529 Doi 10.1186/s12859-017-1934-z

53 Ruggiero A, Katsenelson M, Slutsky I (2021) Mitochondria: new players in homeostatic regulation of firing rate set points. Trends Neurosci 44: 605-618 Doi 10.1016/j.tins.2021.03.002

54 Russo MST, Napylov A, Paquet A, Vuckovic D (2020) Comparison of N-ethyl maleimide and N-(1-phenylethyl) maleimide for derivatization of biological thiols using liquid chromatography-mass spectrometry. Anal Bioanal Chem 412: 1639-1652 Doi 10.1007/s00216-020-02398-x

55 Sasaki H, Kojima H, Yabe I, Tashiro K, Hamada T, Sawa H, Hiraga H, Nagashima K (1998) Neuropathological and molecular studies of spinocerebellar ataxia type 6 (SCA6). Acta neuropathologica 95: 199-204

56 ScherZ-Shouval R, Weidberg H, Gonen C, Wilder S, Elazar Z, Oren M (2010) p53-dependent regulation of autophagy protein LC3 supports cancer cell survival under prolonged starvation. Proc Natl Acad Sci U S A 107: 18511-18516 Doi 10.1073/pnas.1006124107

57 Schindelin J, Arganda-Carreras I, Frise E, Kaynig V, Longair M, Pietzsch T, Preibisch S, Rueden C, Saalfeld S, Schmid Bet al (2012) Fiji: an open-source platform for biological-image analysis. Nat Methods 9: 676-682 Doi 10.1038/nmeth.2019

58 Scholefield M, Church SJ, Xu J, Robinson AC, Gardiner NJ, Roncaroli F, Hooper NM, Unwin RD, Cooper GJS (2020) Effects of Alterations of Post-Mortem Delay and Other Tissue-Collection Variables on Metabolite Levels in Human and Rat Brain. Metabolites 10: Doi 10.3390/metabo10110438

59 Schols L, Kruger R, Amoiridis G, Przuntek H, Epplen JT, Riess O (1998) Spinocerebellar ataxia type 6: genotype and phenotype in German kindreds. J Neurol Neurosurg Psychiatry 64: 67-73 Doi 10.1136/jnnp.64.1.67

60 Sinke RJ, Ippel EF, Diepstraten CM, Beemer FA, Wokke JH, van Hilten BJ, Knoers NV, van Amstel HK, Kremer HP (2001) Clinical and molecular correlations in spinocerebellar ataxia type 6: a study of 24 Dutch families. Arch Neurol 58: 1839-1844 Doi 10.1001/archneur.58.11.1839

61 Srivastava S (2016) Emerging therapeutic roles for NAD(+) metabolism in mitochondrial and age-related disorders. Clin Transl Med 5: 25 Doi 10.1186/s40169-016-0104-7

62 Stucki DM, Ruegsegger C, Steiner S, Radecke J, Murphy MP, Zuber B, Saxena S (2016) Mitochondrial impairments contribute to Spinocerebellar ataxia type 1 progression and can be ameliorated by the mitochondria-targeted antioxidant MitoQ. Free Radic Biol Med 97: 427-440 Doi 10.1016/j.freeradbiomed.2016.07.005

63 Styr B, Gonen N, Zarhin D, Ruggiero A, Atsmon R, Gazit N, Braun G, Frere S, Vertkin I, Shapira Iet al (2019) Mitochondrial Regulation of the Hippocampal Firing Rate Set Point and Seizure Susceptibility. Neuron 102: 1009-1024 e1008 Doi 10.1016/j.neuron.2019.03.045

64 Sulzer D, Mosharov E, Talloczy Z, Zucca FA, Simon JD, Zecca L (2008) Neuronal pigmented autophagic vacuoles: lipofuscin, neuromelanin, and ceroid as macroautophagic responses during aging and disease. J Neurochem 106: 24-36 Doi 10.1111/j.1471-4159.2008.05385.x

65 Suski JM, Lebiedzinska M, Bonora M, Pinton P, Duszynski J, Wieckowski MR (2012) Relation between mitochondrial membrane potential and ROS formation. Methods Mol Biol 810: 183-205 Doi 10.1007/978-1-61779-382-0_12

66 Takahashi H, Ishikawa K, Tsutsumi T, Fujigasaki H, Kawata A, Okiyama R, Fujita T, Yoshizawa K, Yamaguchi S, Tomiyasu Het al (2004) A clinical and genetic study in a large cohort of patients with spinocerebellar ataxia type 6. J Hum Genet 49: 256-264 Doi 10.1007/s10038-004-0142-7

67 Tao-Cheng JH (2018) Stimulation-induced structural changes at the nucleus, endoplasmic reticulum and mitochondria of hippocampal neurons. Mol Brain 11: 44 Doi 10.1186/s13041-018-0387-2

68 Thompson Legault J, Strittmatter L, Tardif J, Sharma R, Tremblay-Vaillancourt V, Aubut C, Boucher G, Clish CB, Cyr D, Daneault Cet al (2015) A Metabolic Signature of Mitochondrial Dysfunction Revealed through a Monogenic Form of Leigh Syndrome. Cell Rep 13: 981-989 Doi 10.1016/j.celrep.2015.09.054

69 Tretter L, Adam-Vizi V (2000) Inhibition of Krebs cycle enzymes by hydrogen peroxide: A key role of [alpha]-ketoglutarate dehydrogenase in limiting NADH production under oxidative stress. J Neurosci 20: 8972-8979 Doi 10.1523/JNEUROSCI.20-24-08972.2000

70 Tsuchiya K, Oda T, Yoshida M, Sasaki H, Haga C, Okino H, Tominaga I, Matsui K, Akiyama H, Hashizume Y (2005) Degeneration of the inferior olive in spinocerebellar ataxia 6 may depend on disease duration: report of two autopsy cases and statistical analysis of autopsy cases reported to date. Neuropathology 25: 125-135 Doi 10.1111/j.1440-1789.2005.00596.x

71 Uittenbogaard M, Chiaramello A (2014) Mitochondrial biogenesis: a therapeutic target for neurodevelopmental disorders and neurodegenerative diseases. Curr Pharm Des 20: 5574-5593 Doi 10.2174/1381612820666140305224906

72 Valavanidis A, Vlachogianni T, Fiotakis C (2009) 8-hydroxy-2' -deoxyguanosine (8-OHdG): A critical biomarker of oxidative stress and carcinogenesis. J Environ Sci Health C Environ Carcinog Ecotoxicol Rev 27: 120-139 Doi 10.1080/10590500902885684

73 Virmani MA, Cirulli M (2022) The Role of l-Carnitine in Mitochondria, Prevention of Metabolic Inflexibility and Disease Initiation. Int J Mol Sci 23: Doi 10.3390/ijms23052717

74 Wang X, Michaelis EK (2010) Selective neuronal vulnerability to oxidative stress in the brain. Front Aging Neurosci 2: 12 Doi 10.3389/fnagi.2010.00012

75 Ward JM, Stoyas CA, Switonski PM, Ichou F, Fan W, Collins B, Wall CE, Adanyeguh I, Niu C, Sopher BLet al (2019) Metabolic and Organelle Morphology Defects in Mice and Human Patients Define Spinocerebellar Ataxia Type 7 as a Mitochondrial Disease. Cell Rep 26: 1189-1202 e1186 Doi 10.1016/j.celrep.2019.01.028

76 Watase K, Barrett CF, Miyazaki T, Ishiguro T, Ishikawa K, Hu Y, Unno T, Sun Y, Kasai S, Watanabe Met al (2008) Spinocerebellar ataxia type 6 knockin mice develop a progressive neuronal dysfunction with age-dependent accumulation of mutant CaV2.1 channels. Proc Natl Acad Sci U S A 105: 11987-11992 Doi 10.1073/pnas.0804350105

77 Xie N, Zhang L, Gao W, Huang C, Huber PE, Zhou X, Li C, Shen G, Zou B (2020) NAD(+) metabolism: pathophysiologic mechanisms and therapeutic potential. Signal Transduct Target Ther 5: 227 Doi 10.1038/s41392-020-00311-7

78 Yang Q, Hashizume Y, Yoshida M, Wang Y, Goto Y, Mitsuma N, Ishikawa K, Mizusawa H (2000) Morphological Purkinje cell changes in spinocerebellar ataxia type 6. Acta Neuropathol 100: 371-376 Doi 10.1007/s004010000201

79 Zhang Y, Zhang M, Zhu W, Yu J, Wang Q, Zhang J, Cui Y, Pan X, Gao X, Sun H (2020) Succinate accumulation induces mitochondrial reactive oxygen species generation and promotes status epilepticus in the kainic acid rat model. Redox Biol 28: 101365 Doi 10.1016/j.redox.2019.101365

80 Zhuchenko O, Bailey J, Bonnen P, Ashizawa T, Stockton DW, Amos C, Dobyns WB, Subramony SH, Zoghbi HY, Lee CC (1997) Autosomal dominant cerebellar ataxia (SCA6) associated with small polyglutamine expansions in the alpha 1A-voltage-dependent calcium channel. Nat Genet 15: 62-69 Doi 10.1038/ng0197-62

81 Zorova LD, Popkov VA, Plotnikov EY, Silachev DN, Pevzner IB, Jankauskas SS, Babenko VA, Zorov SD, Balakireva AV, Juhaszova Met al (2018) Mitochondrial membrane potential. Anal Biochem 552: 50-59 Doi 10.1016/j.ab.2017.07.009

CHAPTER 4: ADAPTATION OF THE POSTERIOR CEREBELLUM TO DISEASE INSULT IN SCA6

Foreword

In the previous chapter, I have demonstrated that mitochondrial damage and impaired mitophagy contribute to SCA6 progression. For consistency, all the experiments were performed in lobule III of the cerebellum, an area that is historically considered to be involved in motor coordination. Furthermore, lobule III is within the anterior zone of the cerebellum that showed severe atrophy in SCA6 patients. Therefore, our findings are in line with the hypothesis that dysfunction of cells in this region leads to motor incoordination, and the accumulation of various dysfunctions eventually leads to cell death.

However, one open question is that why is the anterior zone of the cerebellum especially vulnerable in SCA6? The cerebellum is known to have a uniform cytoarchitecture: different cell types are organized into three distinct layers across all lobules. The circuitry of the cerebellum is also thought to be consistent across different regions. On top, the mutated gene *CACNA1A* in SCA6, is expressed everywhere in the cerebellum. What could be the factors that confer selective vulnerability to the anterior zone, and selective resilience to the other regions? This is an important question to ask because this represents a unique approach in developing treatment: can we tap into the innate mechanisms of resilience and apply that to vulnerable regions to halt disease progression or even reverse disease damage?

To begin investigating selective vulnerability in SCA6, in the next chapter, I first validated that the pattern of cerebellar atrophy observed in patients were recapitulated in our mouse model. This then allowed me to further investigate electrophysiological and molecular alterations in the mouse model that will likely be informative for the human disease. There are known molecular markers in the cerebellum that correlate with Purkinje cell vulnerability, the most prominent being aldolase c (zebrin II). However, I discovered that Purkinje cell death in SCA6 mouse model did not correlate with zebrin II identity, which prompted me to explore other frameworks. I performed RNA sequencing to gain a comprehensive view of gene expression differences between the vulnerable and resilient regions. Bioinformatics analysis of differentially expressed genes strongly suggested alterations at synapses. Surprisingly, these changes were found in the resilient region of the cerebellum.

Together, my work in these two chapters showed that while it is likely that substantial pathological alterations can be found in regions that degenerate, unconventional insights can also be drawn from examining spared regions. The work in chapter 4 represents the first step of many in understanding how the cerebellum respond as a whole to disease.

Manuscript in preparation

Adaptation of the posterior cerebellum to disease insult in SCA6

Tsz Chui Sophia Leung, Lois Lau, Chanelle Lawson Lartego, Maya Nachman, Alanna Watt

Department of Biology, McGill University

Correspondence: alanna.watt@mcgill.ca

Abstract

Cerebellar heterogeneity is important for normal function and can be disturbed in disease models. Whether there are regional specific changes in SCA6, and how they correlate with degeneration pattern are unclear but are important to inform therapeutics development. In this study, we showed that SCA6 mouse model recapitulated degeneration pattern as observed in patients: the anterior zone Purkinje cell degenerated while those in nodular zone persisted at late disease stages, although this degeneration pattern did not correlate with Purkinje cell subtype marker zebrin. Long before degeneration takes place, at disease onset, these vulnerable Purkinje cells lost their signature pacemaker firing pattern, while resilient Purkinje cells in the nodular showed normal firing, suggesting dysfunction preceded degeneration. We thus explored the molecular signature differences between anterior and posterior cerebellum using RNA sequencing. Surprisingly, we discovered the posterior cerebellum underwent the most substantial transformation in SCA6: many genes showed altered expression compared to WT, and within SCA6 cerebellum, many genes gained regional expression pattern. Gene ontology analysis showed that excitatory synapse genes, specifically at parallel fiber to Purkinje cell synapse, were implicated. We then investigated the density of parallel fiber to Purkinje cell synapses and found that they were unchanged in the anterior zone but reduced specifically in the nodular zone. Taken together, we presented unexpected molecular and synaptic adaptations of the posterior cerebellum to disease insult in SCA6, highlighting the interconnected nature of the cerebellum.

Introduction

Although the cerebellum has a uniform cytoarchitecture and circuitry, molecular heterogeneity of Purkinje cells suggests that distinct cell populations have distinct functions. For example, alternative patterns of expressing and non-expressing Purkinje cell populations of several molecules (e.g. aldolase c or zebrin, Hsp25, Plcβ4) form parasagittal strips that correlate with distinct firing properties or cell death patterns (Cerminara et al. 2015; Zhou et al. 2014). In fact, innervation patterns differ in different regions of the cerebellum: corticotropin-releasing factor (CRF)-expressing climbing fibers innervate subset of Purkinje cells that form parasagittal boundaries similar but not entirely overlapping with Hsp52 (Sawada, Fukui, and Hawkes 2008). Purkinje cells in different transverse zones also showed different intrinsic firing properties (Cerminara et al. 2015). It is thought that this innate heterogeneity confers cerebellum the complex

computation ability for the cerebellum. This also argues that the innate heterogeneity is vital for the normal functioning of the cerebellum.

Is cerebellar heterogeneity altered in disease? Regional degeneration is common in neurodegenerative diseases (Pandya and Patani 2021; Sarna and Hawkes 2003). In the cerebellum, regional specific Purkinje cell degeneration has been observed in many diseases, including diseases in which the cerebellum is not the primary target, suggesting that degeneration is not solely mutation specific (Chen et al. 2023). Interestingly, it is not always the same population of Purkinje cells that are vulnerable – cell in the anterior zone that degenerate in one disease may persist in another disease (Perkins et al. 2016; Toscano Marquez et al. 2021). This suggests that it is the interaction between the intrinsic properties of cells and disease that confer vulnerability.

Spinocerebellar ataxia type 6 (SCA6) is a rare, mid-life onset neurodegenerative disease that primarily affects the cerebellum (Solodkin and Gomez 2012). In patients, cerebellum atrophy is typically observed long after disease onset, indicating that instead of cell loss, cellular dysfunction may be driving pathogenesis (Takahashi et al. 1998; Gomez et al. 1997). In post-mortem studies, most of the cell loss were found to be Purkinje cells in the anterior zone, suggesting that dysfunction in the anterior Purkinje cells later lead to degeneration (Yang et al. 2000). SCA6 is caused by CAG repeat expansion mutation in the *CACNA1A* gene, which encodes the α1A subunit of the P/Q type voltage gated calcium channel and the α1ACT transcription factor, both highly expressed across the cerebellum (Zhuchenko et al. 1997; Du et al. 2013). It remains unclear how selective vulnerability of Purkinje cell is mediated in SCA6. That is, what makes anterior Purkinje cells susceptible, when all Purkinje cells express the mutant proteins?

In this study, we use a well-established mouse model of SCA6 ($SCA6^{84Q/84Q}$, hereafter referred to as SCA6 mice), to study the selective Purkinje cell vulnerability. This mouse model of SCA6 recapitulates many aspects of the human disease: (1) mid-life onset of motor incoordination (Watase et al. 2008), (2) late Purkinje cell degeneration (Jayabal et al. 2015), (3) mitochondrial impairment (Leung et al. 2024). In this study, we showed that, consistent with previous studies (Jayabal et al. 2016), Purkinje cells in lobule III displayed firing deficits at disease onset and later degenerate at advance disease stage. However, firing properties of Purkinje cells in the nodular zone were indistinguishable between SCA6 and wildtype (WT) animals at disease onset, suggesting that this region is spared at this timepoint. At later disease stages, we found Purkinje cell death in anterior lobule III, consistent with previous studies (Jayabal et al. 2015) while

Purkinje cells in the nodular persisted, again consistent with the nodular zone being spared from neurodegeneration. We further showed that Purkinje cell survival did not correlate with zebrin identity, in contrast to what has been observed in other animal models of other forms of ataxia (Toscano Marquez et al. 2021). To explore the possible contributors for selective vulnerability in the anterior and resilience in the nodular, we performed RNA sequencing on anterior and posterior cerebellum separately in SCA6 and WT animals. To our surprise, we found that there was a higher number of differentially expressed genes in the posterior cerebellum of SCA6 compared to WT. Additionally, the anterior-to-posterior expression pattern of many genes was altered in SCA6. Gene ontology enrichment analysis of these genes suggested synaptic changes, specifically in the parallel fiber to Purkinje cell (PF-PC) synapses. We quantified the density of PF-PC synapses and found that there was no change in the anterior zone but surprisingly a reduction in the nodular zone of SCA6 cerebellum. Our findings uncover that the cerebellum adapts to SCA6 disease insult using an unexpected coping mechanism of molecular reprogramming in the posterior cerebellum that leads to a reduction of excitatory PF-PC synapses. This suggests that different regions of the cerebellum do not work in isolation; instead, they orchestrate to dynamically adapt to disease alterations.

Result

Anterior Purkinje cells later degenerate but nodular Purkinje cells remain

In SCA6 patients, the anterior lobe in the cerebellar vermis is selectively atrophied, marked by extensive Purkinje cell loss (Takahashi et al. 1998). The nodular lobe in the vermis, on the other hand, appears to be largely spared (Yang et al. 2000). Previous study in our lab demonstrated that in our mouse model of SCA6, Purkinje cells degeneration in lobule III was not observed until 24 months of age in mice, corresponding to a late stage of human disease (Jayabal et al. 2015). While this late degeneration timepoint aligns well with the human disease, it is unknown whether degeneration occurs in other parts of the cerebellum.

To address this, we performed immunohistochemistry staining against Purkinje cell marker calbindin on sagittal cerebellum slices so that both anterior and nodular transverse zones are captured on the same tissue slice. We then quantified Purkinje cell density and molecular layer height in lobule III in anterior zone and lobule X in nodular zone from SCA6 mice at two disease stages: early disease stage at 12 months and at late disease stage at 24 months. We found that

consistent with previous report, both Purkinje cells density and molecular layer height were significantly reduced at 24 months in lobule III (Fig 1a-c)(Jayabal et al. 2015; Watase et al. 2008). In contrast, in lobule X, both Purkinje cell density and molecular layer height were not significantly reduced at late ages in SCA6 (Fig 1d-f). This suggests that the anterior zone of the cerebellum is vulnerable, and the nodular zone is resilient against SCA6, recapitulating findings in human post-mortem studies.

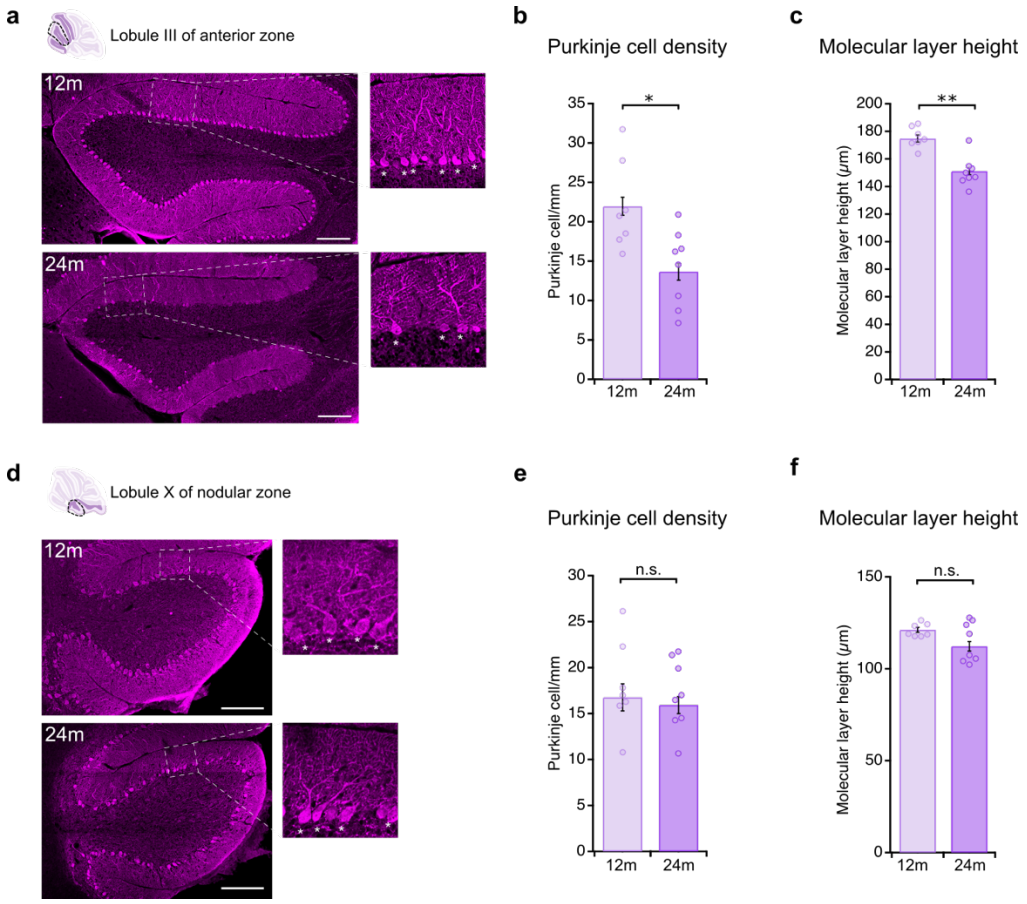

Figure 1 Degeneration of anterior Purkinje cells while nodular Purkinje cells survive. (a) Representative images of lobule III in SCA6 cerebellum at 12 months (12m) and 24 months (24m) of age. There was evident loss of Purkinje cell soma at 24m. (b) Reduced Purkinje cell density at 24m compared to 12m animals ($P = 0.0205$). (c) Reduced molecular layer height at 24m compared to 12m animals ($P = 0.00218$). (d) Representative images of lobule X in SCA6 cerebellum at 12 months (12m) and 24 months (24m) of age. (e) Purkinje cell densities are comparable between 12m and 24m ($P > 0.05$). (f) Molecular layer height is not significantly different between 12m and

24m ($P > 0.05$). Scale bar = 200 µm. N = 7-8 mice per group. n = 2-4 slices per animal were sampled. Each marker represents the averages of 2-4 slices for each animal and height of the bar represent the average across all animals. Mann Whitney *U* test was used for all comparisons. * $P < 0.05$, ** $P < 0.005$, n.s. $P > 0.05$

Anterior Purkinje cells display firing deficits but not nodular Purkinje cells

There is evidence from studies in different disease model that deficits in spontaneous firing of Purkinje cells is a common feature of many neurological diseases affecting the cerebellum (reviewed in (Cook, Fields, and Watt 2021)). Indeed, study in our lab has previously reported firing deficits in Purkinje cells in SCA6 cerebellum (Jayabal et al. 2016). However, experiments in the previous study were performed strictly in lobule III of the anterior zone for consistency. We wondered if Purkinje cells in the nodular zone, despite persisting until late in disease in SCA6 patients and animal model, display alteration in function such as firing deficits. To investigate this, we performed extracellular electrophysiological recording of Purkinje cells to measure their spontaneous firing frequency and regularity (Fig. 2a).

On an acute sagittal slice of the cerebellum, extracellular recordings of Purkinje cells were taken both from lobule III in the anterior zone and lobule X in the nodular zone. Consistent with previous reports, SCA6 Purkinje cells in the lobule III showed lower spontaneous firing frequency (Fig. 2b) and reduced regularity, manifest as an increase in coefficient of variation (CV; Fig. 2c) compared to litter-matched WT mice at disease onset (7 months). However, in lobule X, both the firing frequency and regularity of SCA6 Purkinje cell were similar to that of WT (Fig. 2d-e). Purkinje cells are known to have different range of firing frequencies depending on their location in the cerebellum, with cells in anterior fire at higher frequencies than those in the posterior and nodular (Cerminara et al. 2015). This is also evident in our data as well (compare Fig. 2b to 2d). Taken together, our shows that Purkinje cells in lobule X, a region where cells survive under disease insult, do not display alteration to their spontaneous electrophysiological properties.

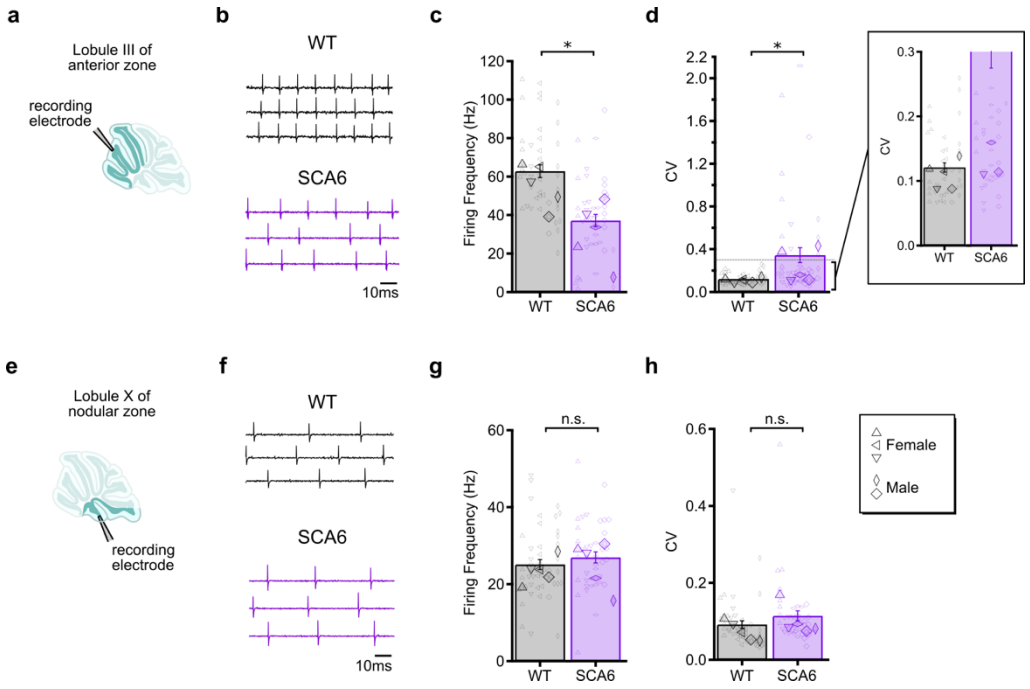

Figure 2 Firing deficit in SCA6 lobule III Purkinje cells but not in lobule X. (a) Extracellular recording of Purkinje cells was made in lobule III of the anterior zone in WT and SCA6 cerebellar acute slices (b) Sample traces of extracellular Purkinje cell recording from WT and SCA6 animals. SCA6 Purkinje cell firing (c) SCA6 Purkinje cells in lobule III fire at lower frequency compared to WT ($P = 0.0176$) (d) SCA6 Purkinje cells fire with higher irregularity compared to WT as measured by coefficient of variation (CV) ($P = 0.0296$) (e) Extracellular recording of Purkinje cells was made in lobule X in WT and SCA6 cerebellar acute slices (f) Sample traces of extracellular Purkinje cell recording from WT and SCA6 animals. SCA6 Purkinje cell firing (g) SCA6 Purkinje cells in lobule X of the nodular zone fire at similar frequency compared to WT ($P = 0.4552$) (h) SCA6 Purkinje cells fire with similar regularity compared to WT as measured by CV ($P = 0.405$). n = 40-48 cells from N = 5 mice per group. Linear mixed model was used for all comparisons, with genotype as fixed effect and individual mouse as random effect. * $P < 0.05$, n.s. $P > 0.05$

Purkinje cell loss does not correspond to zebrin identity

Aldolase c, also known as zebrin II, is a well-documented molecular marker that define subpopulations of Purkinje cells (Brochu, Maler, and Hawkes 1990). Zebrin II immunostaining in the mouse cerebellum reveals a striking stripped pattern, which inspired the name of the molecule

(Sillitoe and Hawkes 2002). Of note, in the anterior zone, there is only a small portion of Purkinje cells expressing zebrin II, in contrast to near complete expression of zebrin II in the nodular lobe. It has been described in several animal models of neurological conditions, including autosomal-recessive spastic ataxia of Charlevoix-Saguenay (ARSACS), ischemia, Niemann-Pick disease type A/B and dystonia, that cells undergo patterned degeneration: Purkinje cells that express zebrin II (Z+ cells) remains while Purkinje cells lacking zebrin II degenerate (Z– cells) (Toscano Marquez et al. 2021; Slemmer et al. 2007; Heckroth and Abbott 1994; Sarna et al. 2001).

We wondered if Purkinje cell degeneration in SCA6 can also be described by the same pattern, which might then support the hypothesis that Z+ cells possess intrinsic properties that confer resilience (Hernández-Pérez, Weruaga, and Díaz 2023). To explore this, we performed immunohistochemistry staining against zebrin II and calbindin as Purkinje cell markers on coronal slices from 24 months old SCA6 and WT control animals. We quantified the surviving Purkinje cells and recorded their zebrin II identity. Since no Purkinje cell in lobule X is Z–, we opted to analyse nodular lobule IX to better relate cell survival to zebrin II identity.

In this analysis of coronal tissue slices, extensive Purkinje cell loss in SCA6 lobule III is observed, in line with observation from sagittal slices (Fig 3a-b). Three Z+ bands can be observed in SCA6 animals, indicating normal boundaries of zebrin II expression is maintained in SCA6 (Fig 3a). The majority of cells in both WT and SCA6 lobule III were Z–, consistent with the canonical zebrin expression pattern in the anterior lobe (Fig 3c). However, the proportion of surviving Z+ cells in SCA6 lobule III was not significantly different from that in WT, suggesting that Z+ cells were not preferentially protected from SCA6 mutation (Fig 3c).

Normal zebrin stripes were also observed in SCA6 lobule IX (Fig 3d). There is no significant Purkinje cell loss in the nodular lobule IX (region indicated with dashed line in Fig 3e), nor difference in the proportion of Z+ and Z– population between SCA6 and WT (Fig 3f). Taken together, Z+ Purkinje cells are not more resilient than non-expressing cells in mouse model of SCA6. Instead, selective Purkinje cell vulnerability is better described by the transverse zones they locate in: cells in anterior zone are more vulnerable while cells in nodular are resilient.

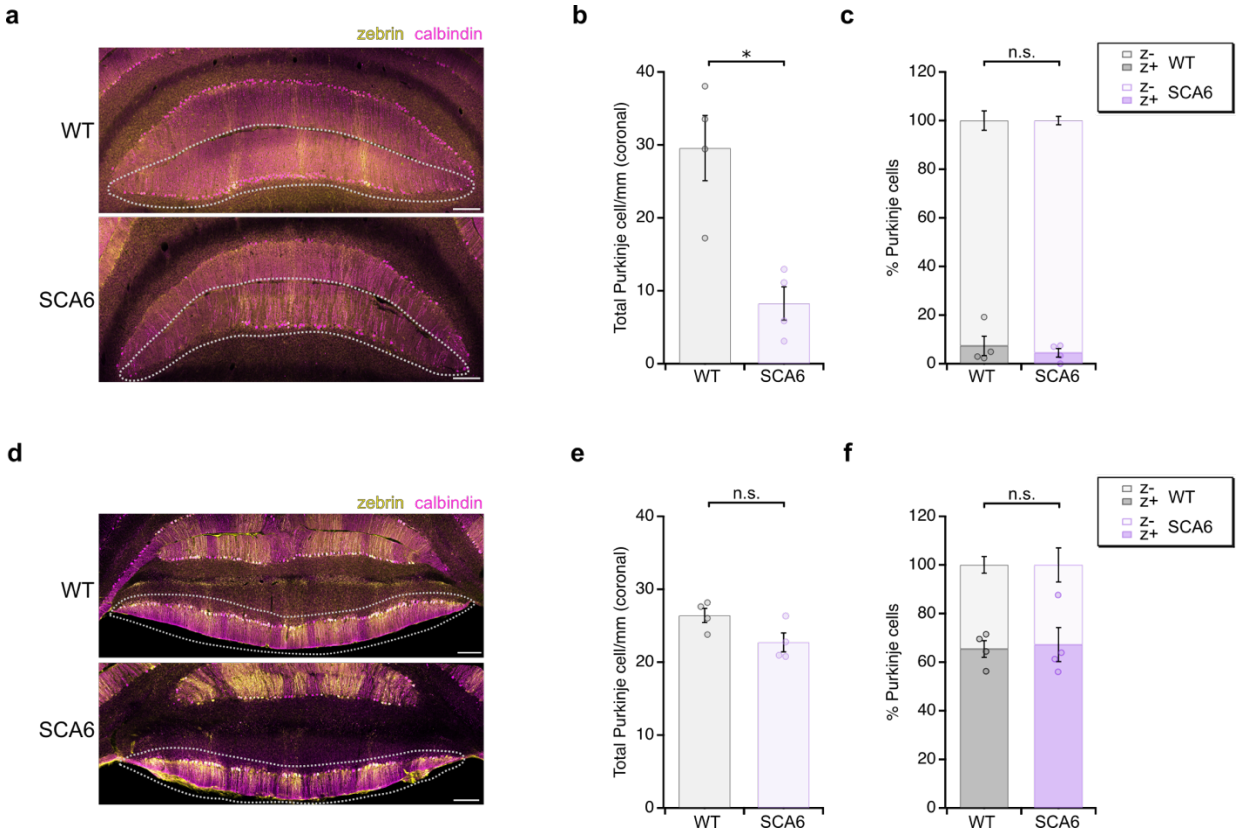

Figure 3 Survival of Purkinje cells is not defined by their zebrin identity (a) Representative images of lobule III in WT and SCA6 cerebellum at 24 months of age. (b) Reduced Purkinje cell density in SCA6 compared to WT (P = 0.0286). (c) Purkinje cell proportions by zebrin identity are comparable between SCA6 and WT (P > 0.05). (d) Representative images of lobule IX in WT and SCA6 cerebellum at 24 months of age (e) Purkinje cell densities are comparable between SCA6 and WT (P > 0.05). (f) Purkinje cell proportions by zebrin identity are comparable between SCA6 and WT (P > 0.05). Scale bar = 200µm. N = 4 mice per group. Each marker represents the averages of 3 slices for each animal. Mann Whitney *U* test was used for all comparisons. * P < 0.05, n.s. P > 0.05

The majority of transcriptional changes are found in the posterior cerebellum of SCA6

Cacna1a is highly expressed across the whole cerebellum (Westenbroek et al. 1995); However, our data and previous reports suggest that in SCA6 patients and animal models, the anterior zone is more affected than posterior (Unno et al. 2012; Yang et al. 2000; Takahashi et al. 2004). We thus wondered if mutation in *Cacna1a* induces different molecular responses in different regions

of the cerebellum. Since one of the two gene products of *Cacna1a* is a transcription factor, α1ACT (Du et al. 2013), we hypothesized that the differences could be transcriptional.

To explore this comprehensively, we decided to perform bulk RNA sequencing (RNA-seq) on anterior-central and posterior-nodular zone separately from WT and SCA6 mice cerebellum vermis (Fig 4a) (Hamel and Cvetanovic 2020). We chose to investigate 12 months old animals, 5 months after disease onset and many months before cell loss is recorded. Previous studies recorded pathological changes in all three cerebellar cortical layers, the molecular layer, Purkinje cell layer and granule cell layer, therefore we opted to perform bulk RNA-seq to capture changes in the whole vermis region. The method offers sufficient sensitivity to resolve genes expressed in anterior and posterior region of the cerebellar vermis (Fig 4b), as demonstrated by the relative expression of known regionally enriched markers such as *Kcng4* (voltage-gated potassium channel subunit K_v6.4; high in anterior) and *Aldoc* (zebrin II; high in posterior) (Rodriques et al. 2019) (Supp Fig 3).

We have previously shown that there are over 500 genes that have altered expression level in SCA6 mouse whole cerebellum at disease onset. At this later disease stage, curiously, in the most affected region the anterior cerebellum, we identified only 107 differentially expressed genes (DEGs; Fig 4c-d, Supp Table 1). In contrast, in the spared posterior lobes, we identified ten times more DEGs, in total 1077 genes (Fig. 4c, e, Supp Table 2). This suggests that it is cells in the posterior lobes that preferentially underwent transcriptional reprogramming in response to disease insult. What kinds of cellular adaptation do these genes represent? We first were interested in whether these changes are related to intracellular signalling or synaptic transmission. To answer this, we performed gene ontology (GO) enrichment analysis, with an emphasis on the cellular component (GO:CC) aspect of the analysis. For the anterior DEGs, there are only six GO:CC terms that showed enrichment (Fig 4f), and they are related to astrocyte projections and dendrites, indicating potential synaptic changes. For posterior DEGs, the top six GO:CC terms are synapse related (Fig 4g). Strikingly, the term *parallel fiber to Purkinje cell synapse* is the most statistically significant and has the highest gene ratio (the number of mapped DEGs/the number of genes associated with the GO term). This suggests that at this progressive disease stage, the SCA6 cerebellum is likely undergoing circuit level changes in response to the disease, with most of the changes taking place in the posterior cerebellum.

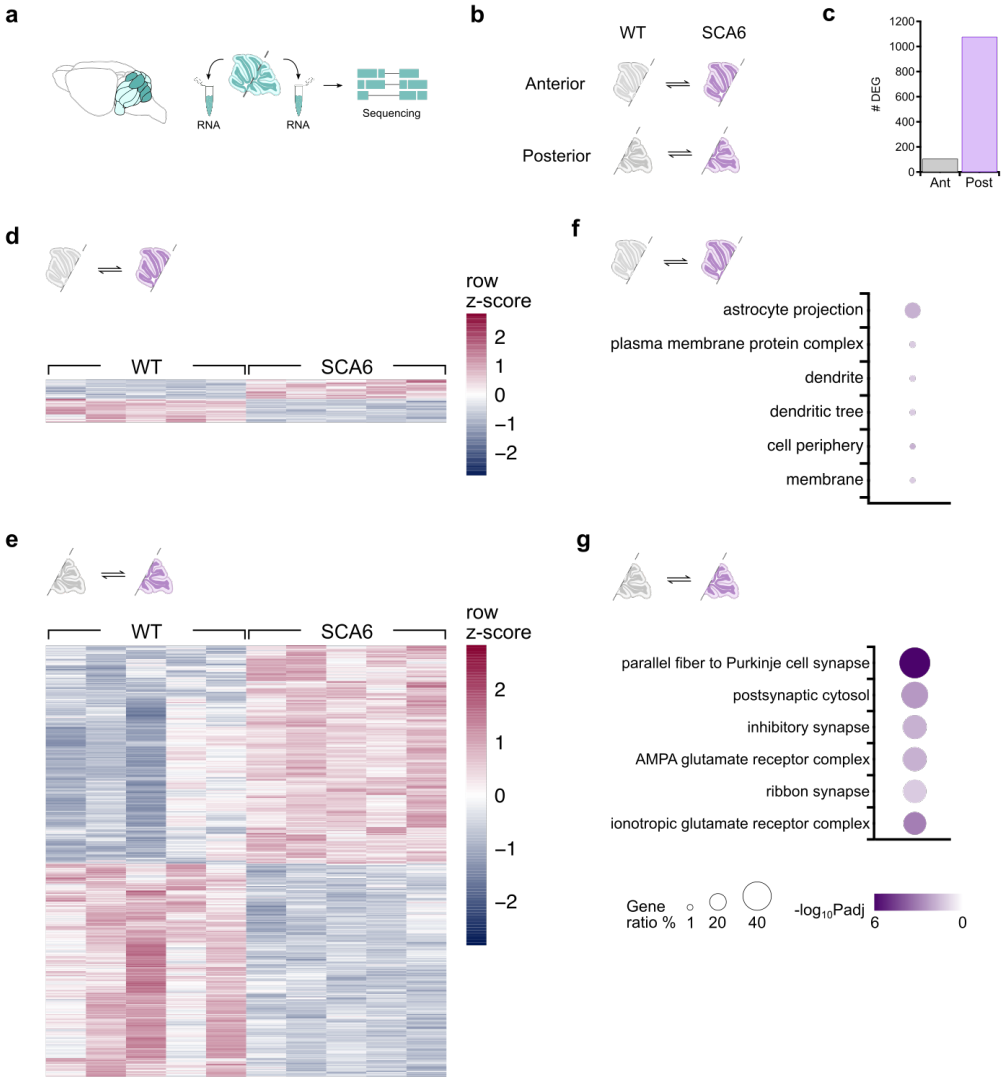

Figure 4 SCA6 posterior cerebellum undergoes extensive transcriptional changes (a) Schematic of experimental design. Cerebellar vermis of SCA6 and WT animals were extracted and dissected into anterior (Ant) and posterior (Post) portion. RNA from these regions were then sequenced separately. N = 5 mice were used per genotype. (b) Comparison performed for differential expression analysis. WT anterior cerebellum was compared to SCA6 anterior cerebellum, and vice versa. (c) Number of differentially expressed genes (DEG) from each comparison. (d-e) Heatmap showing the DEGs in anterior and posterior cerebellum respectively. Each column represents an animal, and each row represents a gene. (f-g) Gene ontology term enrichment analysis of DEGs list from anterior and posterior cerebellum respectively. Marker size denotes gene ratio (the

number of mapped DEGs/the number of genes associated with the GO term), and marker shade denotes significance.

Anterior-posterior transcription signature is not preserved in SCA6

A number of studies have shown that cells in the anterior are transcriptionally distinct from those in the posterior (Martin et al. 2019). It is also established that Purkinje cells in particular are physiologically and molecularly different in these two regions (Albergaria and Carey 2014). We wondered if the molecular heterogeneity is captured in our dataset. We thus compared gene expressed in anterior to posterior cerebellum within WT samples and identified 1842 DEGs that showed regional expression (Fig 5a). Within these genes, 901 (48.9%) of them were expressed significantly higher in the anterior and 941 (51.1%) of them were significant higher in the posterior (Fig 5a). These include previously reported genes that showed patterned expression such as *Plcb3*, *Plcb4*, *Aldoc, Fgf7*, *Cck,* (Martin et al. 2019; Cerminara et al. 2015) (Supp Table 3). We also inspected the anterior-to-posterior gene expression differences in SCA6 (Fig 5a), and discovered that there were in total 3339 DEGs, with 1506 (45.1%) genes expressed significantly higher in the anterior and 1833 (54.9%) genes significant higher in the posterior (Fig 5a). The number of genes that showed regional enrichment is higher in SCA6 than in WT, suggesting that there may be an expanded regional heterogeneity of molecular signature in SCA6 (Supp Table 4). Interestingly, expression pattern of *Cacna1a* is unchanged in SCA6, only the expression level is further reduced from a 20% reduction at 7 months old to 40% reduction in both anterior and posterior cerebellum compared to WT at 12 months (Supp Fig 2; Chapter 3 Supp Fig 1d).

Interestingly, not all regionally enriched genes in WT maintained their patterned expression in SCA6. There were 143 genes that lost their anterior enrichment, and 167 that lost their posterior enrichment in SCA6 (Fig 5b-c). For example, the gene *Prkcd* that was highly expressed in the posterior in WT, had expression level in the SCA6 posterior cerebellum that was similar to in the anterior. On the other hand, there were genes that acquired regional enrichment in SCA6. Specially, there are 748 genes that gained anterior enrichment, and 1059 genes that gained posterior enrichment (Fig 5b, d). This includes genes that are relevant to ataxia, such as *Itpr1* (inositol 1,4,5-trisphosphate receptor type 1), *Cbln1* (cerebellin 1)*, Slc1a3* (EAAT1).

To interpret these genes that had diminished or enhanced regional enrichment in SCA6, we performed GO term enrichment analysis. We found that genes that had diminished regional

enrichment in SCA6 are related to cell-cell junction and synapse (Fig 5e). However, only a small percentage of genes associated to these GO terms were found to be changed in our analysis, reported as gene ratio indicated by small size of the marker, suggesting the alteration at cell junction and synapse as a result of diminished regional enrichment may be limited. For genes that had enhanced regional enrichment in SCA6, we found that they are related to excitatory synapse and cytoskeleton (Fig 5f). This was interesting because in another analysis in Fig 4, we also identified *parallel fibre to Purkinje cell synapse*, an excitatory synapse, to be one of the most significantly altered GO term. Parallel fibre to Purkinje cell (PF-PC) synapse is one of the most abundant synaptic connections in the brain, with an estimate of 100,000 billion PF-PC synapses estimated to exist in the human cerebellum (Azevedo et al. 2009; Huang et al. 2014), making this an important synapse in the cerebellum cortex. We thus decided to investigate this synapse further.

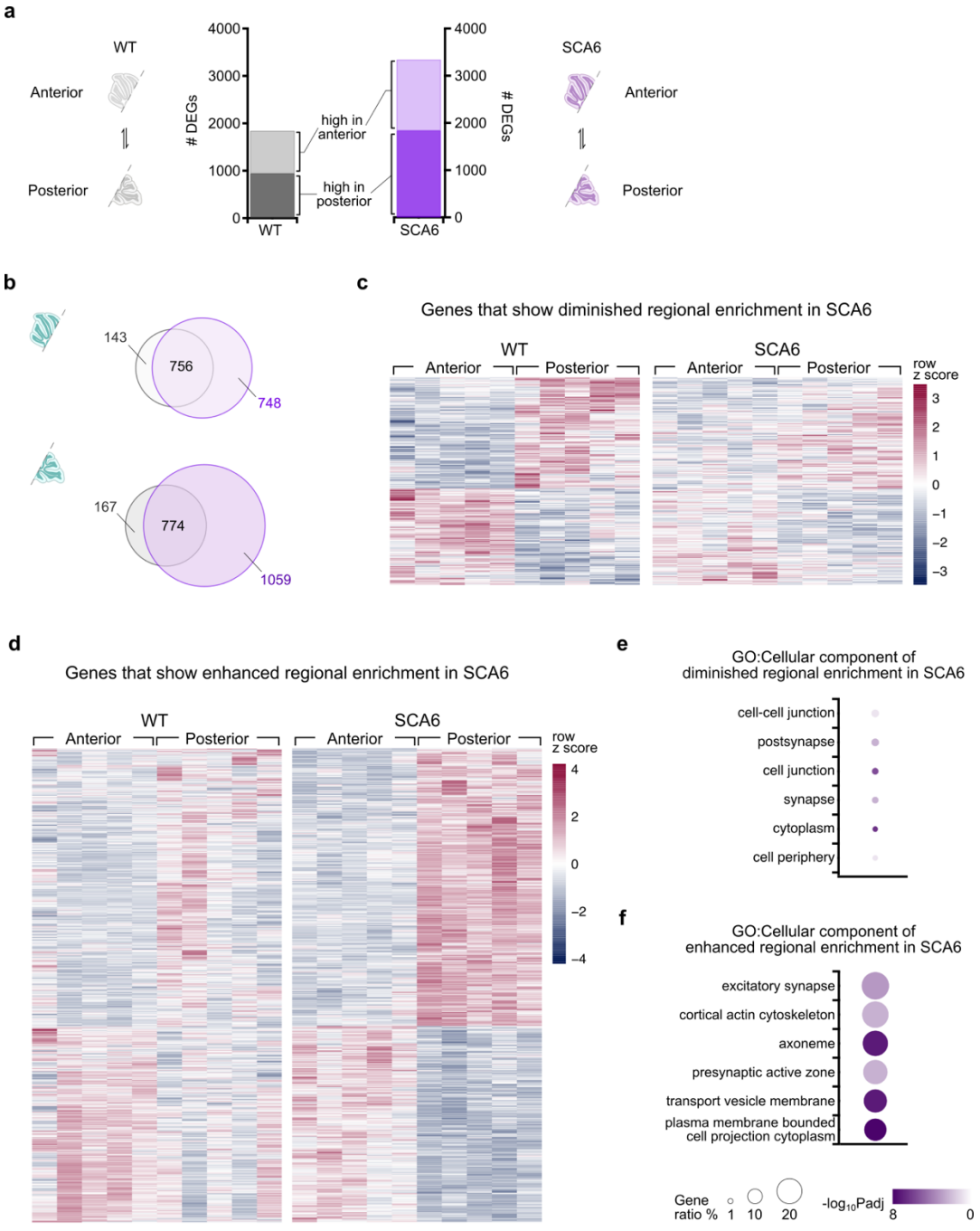

Figure 5 SCA6 cerebellum has expended regional heterogeneity. (a) Comparison performed for differential expression analysis. WT anterior cerebellum was compared to WT posterior cerebellum to obtain the regionally enriched genes. Close to 2000 genes were found to be either highly expressed in WT anterior or posterior cerebellum. Same was performed for SCA6 samples, and 50% more genes were found to display regional enrichment. (b) Venn diagram showing

regionally enriched genes that were unique to either WT or SCA6 cerebellum. (c) Heatmap showing expression of genes that were regionally enriched in WT, but not in SCA6 (d) Heatmap showing expression of genes that were regionally enriched in SCA6, but not in WT (e) GO term enrichment analysis showing genes that had diminished regional enrichment in SCA6 were related to cell junction and synapse (f) GO term enrichment analysis showing genes that had enhanced regional enrichment in SCA6 were related to synapse and cytoskeleton. Marker size denotes gene ratio (the number of mapped DEGs/the number of genes associated with the GO term) and marker shade denotes significance.

PF-PC synaptic changes in the posterior lobule

Downregulation of PF-PC synaptic gene expression have also been reported in other subtypes of SCAs, such as SCA1, SCA2 and SCA7 (Niewiadomska-Cimicka et al. 2021). Gene expression reduction has been shown to coincide with impaired synaptic properties, such as in the case of SCA1, where both PF-PC genes downregulation and impaired PF-PC synaptic plasticity were reported at 5 weeks and worsen at 12 weeks (Robinson, Watchon, and Laird 2020; Ingram et al. 2016; Shuvaev et al. 2017). This suggests that there could be alterations to PF-PC synapses in SCA6.

Aside from genes mapped to the *parallel fiber to Purkinje cell synapse* GO term, other known genes important for the PF-PC synapse are also found to be downregulated, such as *Slc17a7* (vGlut1), *Slc1a3* (EAAT1/GLAST), *Trpc3* (TRPC3) and *Nrxn1* (neurexin I) (Fig 6a). Importantly, the Nrx-Cbln1-GluD2 complex is essential in the formation and maintenance of PF-PC synapse (Ito-Ishida et al. 2008; Kakegawa et al. 2009). The components had normal expression in the SCA6 anterior cerebellum, but two out of three components showed reduced expression in the posterior (Fig 6a). Since RNA-seq was performed in the whole posterior cerebellum which consists of the posterior zone and nodular zone, it is unclear whether PF-PC synapse genes reduction was driven by changes in the posterior zone or if the nodular zone was also affected.

To determine if PF-PC synapses were reduced in the nodular zone, we performed immunohistochemistry staining against presynaptic marker vGlut1 and postsynaptic marker Psd95 on cerebellum slices from SCA6 and WT animals at 13 months of age, one month after gene reduction was quantified (Fig 6a). We quantified the colocalization of the two markers in lobule III of the anterior zone and lobule X in the nodular zone as a measure of PF-PC synapse density,

focusing on the upper portion of the molecular layer where synapses are largely PF-PC synapses (Fig 6b, d). We found that, in lobule III, there was no significant difference in the colocalization of Psd95 and vGlut1, indicating that there was similar number of PF-PC synapses in SCA6 compared to WT animals (Fig 6c). However, in lobule X, there was a significant reduction in the colocalization of Psd95 and vGlut1 in SCA6, indicating that there was a reduction in PF-PC synapses in the nodular of SCA6 compared to WT animals (Fig 6e).

Interestingly, while there was a reduction in *Slc17a7* transcript level in the SCA6 posterior cerebellum, immunohistochemistry staining showed similar vGlut1 immunopositivity intensities in the posterior cerebellum of SCA6 and WT (Supp Fig 3). The vGlut1 intensities were also similar between SCA6 and WT in the anterior cerebellum (Supp Fig 3). This suggest that protein level changes may lag or be decoupled from changes at the transcript level changes.

Taken together, our data showed that as suggested by the transcriptomic data, there is a reduction of PF-PC synapses in the SCA6 posterior cerebellum.

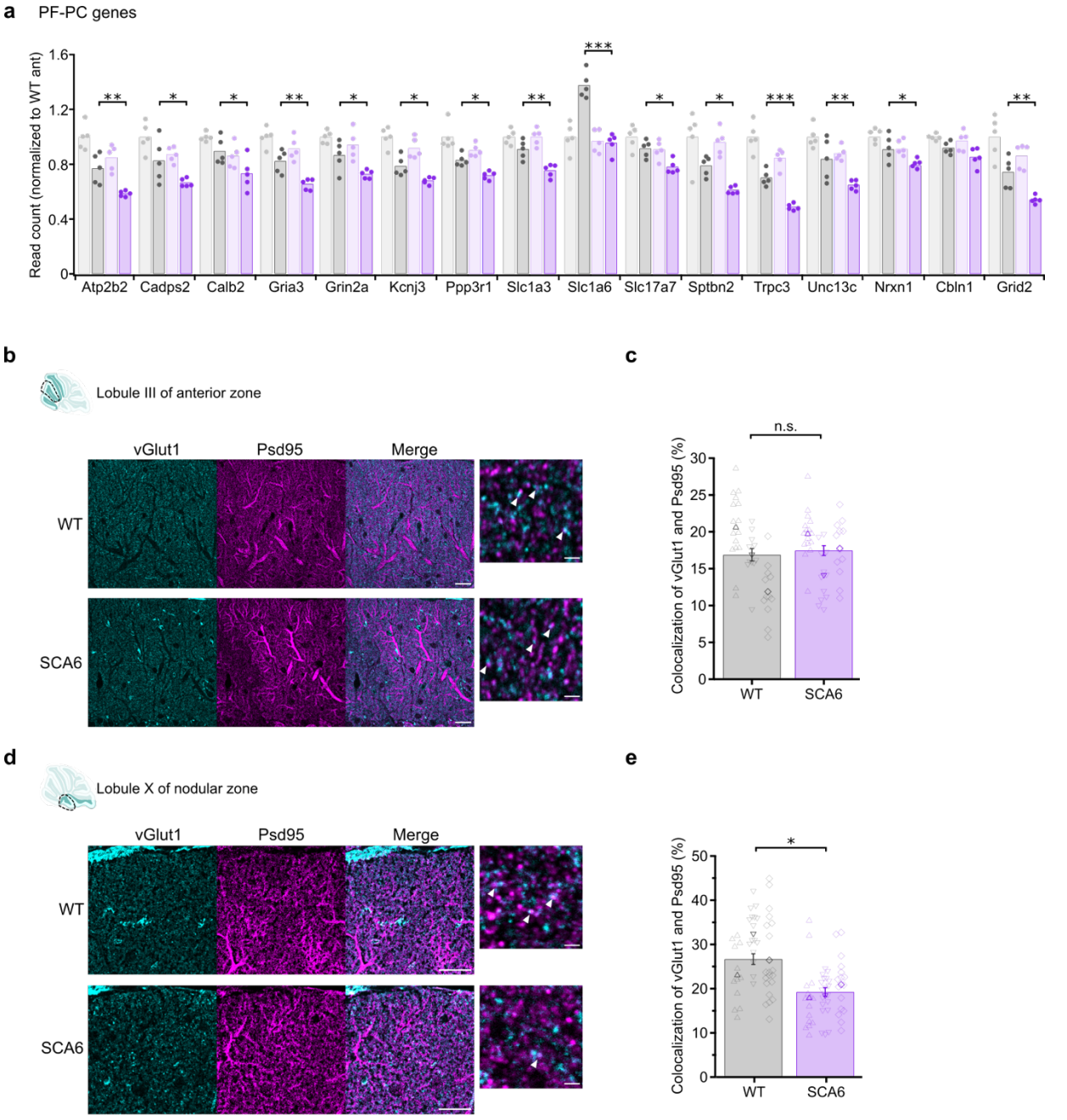

Figure 6 SCA6 posterior cerebellum has reduced PF-PC synapses (a) PF-PC genes were unchanged in anterior cerebellum but downregulated in posterior cerebellum in SCA6. Each marker represents RNA-seq read count from a single animal and each bar represents the group average. Statistics shown were adjusted P values for comparisons between WT and SCA6 posterior cerebellum. Comparison is not significant when statistic is not shown. (b, d) Representative images of PF-PC synapses staining using vGlut1 as pre-synaptic marker and Psd95 as post-synaptic

marker. (c) Colocalization of vGlut1 and Psd95 markers were not significantly different between WT and SCA6 lobule III of the anterior zone ($P > 0.05$) (e) Colocalization of vGlut1 and Psd95 was reduced in SCA6, indicating a reduction in PF-PC synapse density ($P = 0.00333$). Scale bars = 20μm except for zoom-in images = 1μm. N = 3 mice per group, n = 3 slices from each animal. Each unfilled marker represents a region of interest drawn from 3 slices per animal and the filled marker represents the average by animal. Linear mixed model was used for comparisons in (c) and (e), with genotype as fixed effect and individual mouse as random effect. * $P < 0.05$, ** $P < 0.05$ n.s. $P > 0.05$.

Discussion

Here we have shown that Purkinje cells showed regional specific alterations under SCA6 disease insult. Parallel to what was observed in patients, in our mouse model of SCA6, Purkinje cells in the anterior zone degenerated while those in the nodular survived. The degeneration was preceded by functional deficits – Purkinje cells in the anterior zone fired at lower frequency and with reduced regularity, but cells in nodular zone fired normally. This pattern of vulnerability is not unique to SCA6. In fact, in many disorders, the anterior zone of the cerebellum is the first to succumb to disease insult while the nodular is spared (Hernández-Pérez, Weruaga, and Díaz 2023). Example includes Niemann Pick disease type C (NPC), ARSACS and Christianson syndrome (Martin et al. 2019; Toscano Marquez et al. 2021; Xu et al. 2017). In the case of ARSACS, it was also reported that Purkinje cell firing deficits preceded degeneration (Ady et al. 2018). Our finding in SCA6 suggests that the anterior Purkinje cells may possess intrinsic properties that render them susceptible to perturbation.

One way of dividing Purkinje cells into subpopulation is by their zebrin expression identity. It has been shown that Z+ Purkinje cells are more resilient and persist in diseases (Martin et al. 2019; Toscano Marquez et al. 2021), a potential point of breakthrough into characterizing vulnerable and resilient Purkinje cell subtypes. However, our data showed that Purkinje cell degeneration in SCA6 did not correlate with zebrin identity, suggesting that there could be other approaches to define selectively vulnerable Purkinje cell subtypes in the SCA6 cerebellum. Recent single cell RNA-seq experiments have reported over 9 subtypes of Purkinje cells differentiated by expression level of

a collection of molecules (Kozareva et al. 2021). It remains to be determined if vulnerable Purkinje cells could be segregated based on different molecular classifications in SCA6.

We employ the broad-scope approach to characterize the molecular signature of vulnerable and resilient regions of the cerebellum by conducting bulk RNA-seq. There are limitations to this approach, the most overt being the inability to deconvolute cell type specific dysregulations. However, previous study in SCA6 reported that cerebellar cell types other than Purkinje cells are likely to be affected in the same manner (Leung et al. 2024). Therefore, we believe that bulk RNA-seq could provide valuable insight in revealing substantial changes across different cell types.

We performed RNA-seq on anterior and posterior cerebellum separately in both WT and SCA6 animals. The comparisons between WT and SCA6 yielded the understanding that majority of gene expression changes took place in the posterior cerebellum unexpectedly. Gene ontology term enrichment analysis indicated that genes at synaptic compartments, specifically at PF-PC synapse, were overrepresented. This data suggests that the PF-PC synapse may be one of the among the most vulnerable synapses in the cerebellum. Dysfunction of this synapse has been reported in SCA1, 3, 5, and 27, although the exact contribution of this vulnerability to diseases remains unclear (Hoxha et al. 2016).

Comparing anterior cerebellum to posterior cerebellum, there were over 1500 genes that showed alterations in SCA6 that led to regional enrichment while in WT did not show significantly different expression across anterior and posterior cerebellum. Such a wide extent of alteration to regional gene expression enrichment has not been reported before in cerebellar ataxias. In an NPC1 mouse model study, RNA-seq analysis comparing lobule III to lobule X yielded only about 200 genes different between WT and NPC1 animals, despite disease progresses much more rapidly than in our SCA6 model (Martin et al. 2019). In another study in SCA1, there was even a shrinkage in SCA1 cerebellum heterogeneity (Hamel et al. 2023). These data suggest that the SCA6 cerebellum undergoes molecular reprogramming that maybe unique to its disease context.

Interestingly, the regionally enriched genes in SCA6 appear to include many gene products that are preferentially located at excitatory synapse. A more in-depth analysis of gene expression

showed normal expression level in the SCA6 anterior cerebellum but a widespread downregulation of genes whose protein products function at the PF-PC synapse that are restricted only to the SCA6 posterior cerebellum. Using immunohistochemistry, we discovered that, in line with the RNA-seq data, the number of PF-PC synapse was unchanged in the anterior zone, but a reduction in number of synapses was observed only in the posterior zone of SCA6 cerebellum compared to WT. This was unexpected considering our previous data indicated that nodular Purkinje cells were spared in functional impairment and degeneration. It is possible that the changes in PF-PC synapse represents an adaptive mechanism undertaken by the posterior nodular zone of SCA6 cerebellum to ensure vitality and maintain optimal Purkinje cell functional output. This could be an example of neuronal homeostasis – feedback mechanism to adjust individual neuron output to achieve a stable network level function. In this case, the reduction of PF-PC synapses in the nodular may ensure a stable Purkinje cell output to the deep cerebellar nuclei. Future work is required to test the role of PF-PC alteration in SCA6 pathology.

Taken together, we showed that in SCA6, while Purkinje cells in the anterior zone were the vulnerable cell population, resilient Purkinje cells in the posterior underwent drastic changes at the molecular level that manifest as changes in synaptic connectivity in response to disease insult. This highlights the need to also investigate regions outside of the regions of degeneration in disease research, as they may be altered under disease and these alterations may reveal mechanisms of resilience that can be applied for therapeutic developments.

Materials and methods

Animals

Breeding and animal procedures were performed with the approval of the McGill Animal Care Committee in accordance with the Canadian Council on Animal Care guidelines. We obtained the SCA6 mouse model ($SCA6^{84Q/84Q}$) from Jackson Laboratories (Bar Harbor, Maine; strain: B6.129S7-Cacna1atm3Hzo/J; stock number: 008683; RRID:IMSR_JAX:008683). This mouse contains a humanized 84 CAG repeat expansion mutation knocked in at the endogenous *Cacna1a* locus. We bred heterozygous mice to obtain litter-matched WT control mice, heterogenous mice ($SCA6^{84Q/+}$) and homozygous mice ($SCA6^{84Q/84Q}$). We genotyped the animals in-house by PCR using primer sequences provided by Jackson laboratories. Experiments in this study used both male and female mice. No animal was excluded from the study.

Immunohistochemistry

Tissue sections for immunohistochemistry was prepared as previously described (Leung et al. 2024). Mice were anesthetised with isoflurane through inhalation, confirmed with absence of toe pinch reflex. Then, mice were perfused transcardiacally first with ice-cold phosphate-buffered saline (PBS; 0.1 M, pH 7.4) containing heparin salt (5.6 μg/ml), then with 40ml of 4% paraformaldehyde (PFA) in phosphate buffer (pH 7.4), both at the rate of 50 ml/min. Brain was rapidly extracted and incubated in 4% PFA at 4°C on an orbital shaker at 70rpm overnight. Brain was then transferred to PBS with 0.05% sodium azide for short term storage at 4°C. Sectioning of the cerebellum was performed using a vibrating microtome (5100mz Vibratome, Campden Instruments, Loughborough, UK), producing sections of 80 or 100μm thickness. Tissue slices were collected serially and stored in PBS with 0.05% sodium azide on 24-well plate containing.

To avoid batch effect, master mixes of antibodies were made to stain slices from all animals simultaneously. Free floating staining of slices was performed on 24-well plates, one slice per well, on an orbital shaker at 70rpm to achieve even staining. Slices were first rinsed with washing solution (PBS with 0.4% Triton X-100) and then blocked with blocking solution (PBS, 0.4% Triton X-100, 5% Bovine serum albumin (BSA), 0.05% sodium azide), then incubated in primary antibody (Supp Table 5) for 3 days at room temperature. Slices were then rinsed in washing

solution and incubated for 30 minutes with anti-Mouse IgG Fab fragments. Then, the slices were rinsed again with washing buffer, followed by a 90-minute incubation with secondary antibodies (Supp Table 5). After a final washing solution rinse, slices were mounted onto glass slides using ProLong Gold Antifade mounting medium (Thermo Fisher Scientific, Waltham, USA) and stored in dark at 4°C prior to imaging.

Image acquisition and analysis

Images were acquired using an LSM800 confocal microscope (Zeiss) on Zen Blue software. For cell counting experiments (Fig 1 and 3), images were acquired using a 20x objective at 1024 x 1024-pixel resolution. For colocalization experiments (Fig 6), images were acquired using a 40x objective at 2048 x 2048-pixel resolution using pinhole of 1 Airy width. For each experiment, laser settings were kept identical for all slices. Experimenters were blinded to genotypes for both image acquisition and image analysis.

Image analysis was done in Fiji (Schindelin et al. 2012). For Fig 1 and 3, Purkinje cell bodies were delineated by hand using calbindin as markers. For molecular layer height measurement, four measurements were made per image, three images were measured per animal. For Fig. 6, images were pre-processed with *Background Subtraction* function in Fiji using a rolling ball radius of 30 pixels, then the Mander's overlap coefficient for vGlut1 and Psd95 staining was generated using the JACoP plugin.

To generate representative images, identical adjustments of the brightness and contrast were applied to all images within a data set to improve the image clarity.

RNA extraction and sequencing

Experimental mice were first tested on rotarod to assay their motor coordination, which was used to select animals that were representative of their genotype. RNAseZap (Sigma #R2020) was used to remove RNAse in experimental area and tools. Mice were anesthetised with isoflurane, then rapidly decapitated and the cerebellar vermis was dissected out. Cerebellum tissues were then separated into anterior and posterior using fissure between lobule VI and VII and white matter between lobule II and X as landmark. Tissues were flash frozen on dry ice then stored at -80°C until RNA extraction.

RNA was extracted from 5 WT (2 males, 3 females) and 5 SCA6 (3 males, 2 females) mice at 12 months of age. RNA extraction was performed as previously described (Leung et al. 2024). Briefly, TRIzol-Chloroform-ethanol RNA extraction was performed on homogenized tissue (TRIzol: Invitrogen #15596026; Chloroform: Sigma #288306). RNA extracts purification was performed using the RNeasy Mini Kit (Qiagen #74104) with DNase I treatment as described in the manufacturer's protocol.

Extracted RNA samples were assayed on Agilent BioAnalyzer 2100 to quantify their RNA integrity. RNA integrity number (RIN) generated for all samples were over 7.5, suggesting high RNA quality. Library preparation and sequencing were performed by Genome Quebec (Montreal, Quebec, Canada) using NEB stranded mRNA library preparation protocol. Sequencing was performed on the Illumina NovaSeq 6000 S4 platform generating 100bp paired end reads. Sequencing depth of samples had a median of 53 million reads (IQR, 42-64 million reads), and a median of 92% mapping rate (IQR, 92%-92%).

RNA sequencing data analysis

Raw read FASTQ files were processed on cloud computing service provided by the Digital Research Alliance of Canada. Alignment of reads to mouse reference genome (GRCm38) were performed using HISAT2 version 2.1.0 (Kim et al., 2019). Read counting was carried out with HTSeq version 0.11. (Anders et al., 2015) in union mode. Differential expression analysis was performed with DESeq2 version 1.24.0 in RStudio (Love et al., 2014). Adjusted P values of 0.05 was used to determine significant genes. Gene ontology term enriched analysis was performed using gProfiler (Raudvere et al., 2019) (Database version of GO:MP, CC and BP releases/2023-07-27).

Slice Electrophysiology

Acute slice preparation was performed as previously described (Leung et al. 2024). Deep anesthesia of animals was achieved with intraperitoneal injection of 2,2,2-tribromoethanol (Avertin). Intracardiac perfusion was performed with approximately 30 ml of ice-cold partial sucrose replacement slicing solution (111 mM sucrose, 25 mM glucose, 50 mM NaCl, 2.5 mM KCl, 1.25 mM NaH2PO4, 25 mM NaHCO3, 0.65 mM CaCl2 and 10 mM MgCl2, bubbled with

95% O2 and 5% CO2 to maintain pH at 7.3). The brain was then rapidly dissected out and sectioned into 200μm slices using a VT 1200S vibratome (Leica Microsystems, Wetzlar, Germany). Slices recovered in artificial cerebrospinal fluid (ACSF: 20 mM glucose, 125 mM NaCl, 2.5 mM KCl, 1.25 mM NaH2PO4, 25 mM NaHCO3, 2mM CaCl2 and 1 mM MgCl2, bubbled with 95% O2 and 5% CO2 to maintain pH at 7.3; osmolality ~320 mOsm) at 37°C for 45 minutes before electrophysiology.

Electrophysiology protocol was performed as previously described (Jayabal et al. 2016). Slices were kept at around 33°C in ACSF during recording. Purkinje cells spontaneous firing was recorded using borosilicate pipettes with tip size of 1-2 μm pulled using a P-1000 puller (Sutter Instruments, Novato, CA, USA). Recordings of lobule III and X Purkinje cells were taken from every slice in random order. Data acquisition and analysis were performed in IGOR Pro version 7.0 and 8.0 (Wavemetrics, Portland, OR, USA) using custom program.

Statistics

Comparisons in this manuscript were performed in JMP (SAS, Cary, NC). For Fig 1 and 3, data were first assessed for normality, and for non-normal data, Mann-Whitney *U* test was performed. For Fig 2 and 6, linear mixed effect model analysis was performed, using individual animal as random effect.

Acknowledgements

We are grateful for help and guidance from Dr. Anne McKinney, Dr. Rosemary Bagot, Dr. Jesper Sjöström and current and past members of the Watt lab, especially including Dr. Anna Cook and Dr. Brenda Toscano-Márquez. This research is made possible by the excellent animal care provided by McGill Animal Resources Centre (CMARC), particularly Dr. T. Koch and Dr. B. Sartip. We thank the staff from Advanced BioImaging Facility (ABIF) at McGill University, particularly Dr. Joel Ryan who facilitated confocal acquisition. This research was enabled in part by support provided by Calcul Québec (calculquebec.ca) and the Digital Research Alliance of Canada (alliancecan.ca).

Declarations

Author Contributions

T.C.S.L designed and ran all experiments, analyzed data for all figures, and wrote the manuscript; L. L. and M.N. analyzed data for Fig. 1; C. L. L. analyzed data for Fig. 3; A.J.W. conceived the project, designed experiments, supervised the project, and editted the manuscript.

Funding

This study was supported by the following funding sources: Canadian Institutes of Health Research (CIHR) project grants (PJT-153150 and PJT-190151) (A.J.W.) and Fonds de recherche du Québec – Santé (FRQS) Doctoral Scholarship (T.C.S.L.).

Competing interests

The authors declare no conflict of interests.

Chapter 4 Supplementary Information

Supplementary figure 1-3

Supplementary Table 1 Top DEG of WT versus SCA6 in anterior cerebellum

Supplementary Table 2 Top DEG of WT versus SCA6 in posterior cerebellum

Supplementary Table 3 Top DEG of anterior versus posterior cerebellum in WT

Supplementary Table 4 Top DEG of anterior versus posterior cerebellum in SCA6

Supplementary Table 5 List of antibodies

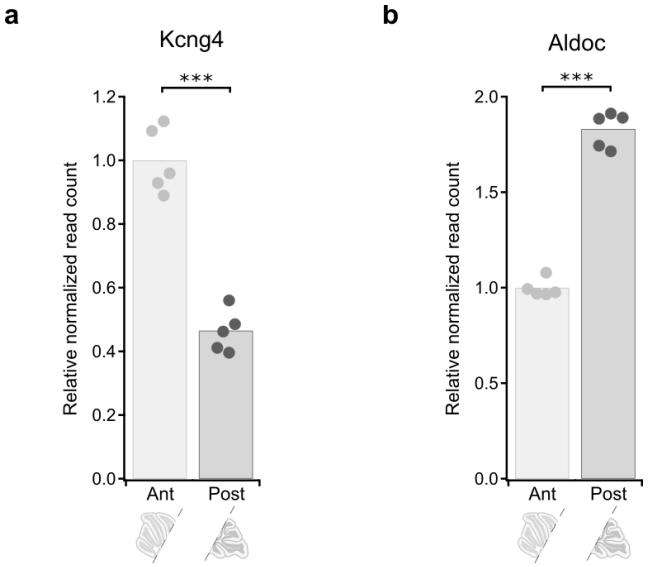

Supp Fig 1 Known regionally enriched genes could be resolved by RNA sequencing experimental design. Data shown is the normalised read count relative to anterior sample average. (a) *Kcng4* is known to be expressed highly in the anterior cerebellum and showed over 2 folds differences between anterior and posterior (b) *Aldoc* is known to be expressed highly in the posterior cerebellum, and showed almost 2 folds differences between anterior and posterior. *** Padj < 0.0005

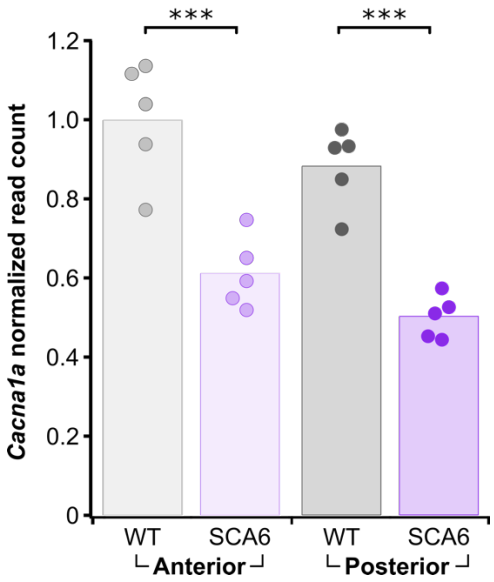

Supp Fig 2 Expression of *Cacna1a* in SCA6 at 12 months show similar anterior-posterior expression pattern. Expression level of *Cacna1a* is further reduced from 20 % lower than in WT at 7 months to 40% lower at 12 months, in both anterior and posterior cerebellum. *** Padj < 0.0005. n.s. when comparison is not shown. All data are normalized to WT anterior cerebellum.

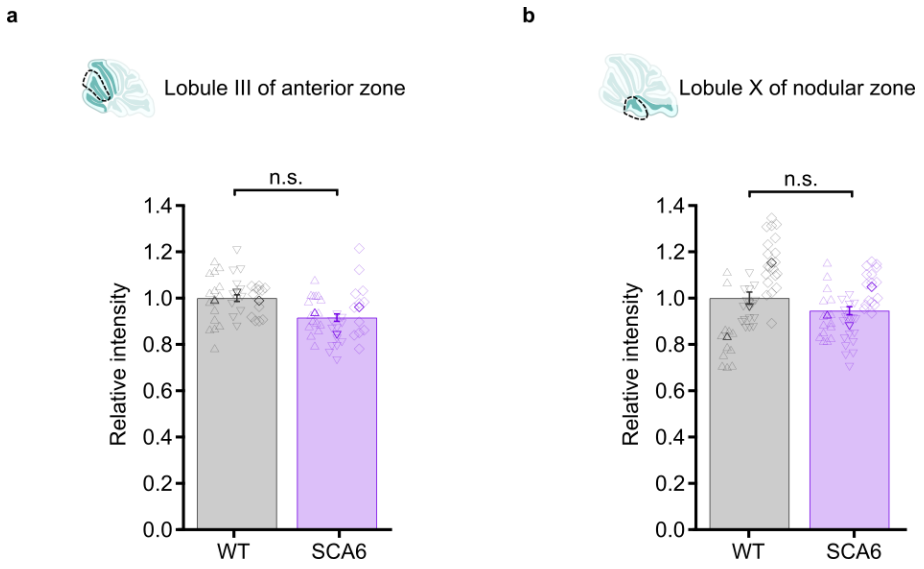

Supp Fig 3 vGlut1 staining intensities similar between WT and SCA6 (a) vGlut1 intensities in lobule III of WT and SCA6 (b) vGlut1 intensities in lobule X of WT and SCA6

Supp Table 1 Top DEG of WT versus SCA6 in anterior cerebellum

Gene name	DESeq2 baseMean	Log2 fold change	Padj
Comp	1278.09	-2.13	1.08E-106
Prdx2-ps1	82.69	-5.89	2.92E-37
Gm10654	86.43	6.78	3.86E-29
Gm10033	1433.86	1.05	3.33E-26
Scoc	5989.00	0.73	7.49E-17
Ccdc194	95.71	-4.22	6.25E-16
Gm45640	40.05	5.07	5.72E-14
Abcc12	800.41	1.05	1.11E-13
Il15	97.06	1.97	1.11E-13
Gm45643	46.45	6.87	2.00E-13
Gm7335	52.12	-4.44	1.87E-12
Usb1	588.85	-0.64	4.58E-12
Zfp963	275.60	-1.03	1.69E-11
Gm18180	80.88	-2.19	1.83E-11
Mri1	926.87	0.84	3.52E-09
Gm7785	66.19	-1.62	5.99E-09
Crnde	117.16	1.63	2.58E-08
Ndrg4	92555.83	0.33	3.61E-08
Cacna1a	26952.46	0.71	1.24E-07
Fcho1	4335.09	-0.49	1.61E-07
Gm45854	20.33	7.82	1.71E-07
Tmem59l	20207.93	0.39	2.10E-07
Gm15784	16.26	-5.79	2.10E-07
Fto	15091.74	0.27	2.63E-07
B3gnt3	33.48	2.41	9.01E-07
Zfp869	4051.63	0.30	1.10E-06
Plvap	1688.11	-0.55	1.90E-06
Gm2573	19.84	-2.85	2.45E-06
Gmip	511.06	-0.66	7.97E-06
Gm45694	92.32	1.43	7.98E-06
Mef2b	43.58	-1.97	9.56E-06
Pgpep1	1466.72	0.39	1.95E-05
H2-K1	4339.25	-0.57	1.95E-05
Tnc	791.43	0.79	4.31E-05
Cyld	8558.89	0.29	4.31E-05
Hbb-bs	3469.05	-0.74	5.27E-05
Tmem255a	5094.28	0.40	2.15E-04
Hba-a1	1732.85	-0.71	2.19E-04

Nrip3	7682.76	0.26	2.74E-04
Lyz2	1083.21	-0.80	3.60E-04
Fam129c	298.18	-0.87	7.74E-04
Ecm2	1428.28	-0.39	8.01E-04
Rnf150	2796.61	0.37	9.38E-04
D130040H23Rik	330.55	0.73	1.00E-03
Gfap	24255.73	-0.59	1.03E-03
Zfp868	1875.31	-0.30	1.32E-03
Kndc1	16067.91	0.36	1.63E-03
Plpp6	4683.33	0.28	1.85E-03
Mylk3	21.64	-2.49	2.03E-03
Ifi30	365.41	-0.56	2.11E-03
Clec7a	156.66	-1.42	2.11E-03
Eomes	1471.23	0.49	2.41E-03
Ptger1	64.64	-1.38	2.45E-03
Gabbr1	58909.94	0.19	2.48E-03
Mex3a	537.05	-0.47	2.75E-03
Rasd2	2043.22	0.35	4.09E-03
Aqp6	3323.93	0.36	4.59E-03
Mcam	3900.61	0.27	5.06E-03
Bdnf	971.98	0.39	5.14E-03
Insrr	217.09	-0.83	5.78E-03
Fbxw9	1050.92	-0.35	5.83E-03
Trem2	617.68	-0.56	5.83E-03
Heatr3	2737.96	-0.24	5.83E-03
Gm3365	165.65	0.68	5.83E-03
Adam23	15105.04	0.34	6.17E-03
Coq9	4984.13	-0.20	6.19E-03
Gatad2a	3994.36	0.24	6.91E-03
Gm44284	28.82	2.74	7.33E-03
Cpne2	2396.00	0.41	8.21E-03
2210011C24Rik	38.90	1.51	8.60E-03
D130017N08Rik	1457.57	0.26	8.69E-03
Nptn	38612.20	0.22	9.24E-03
Slc35e1	4530.30	0.33	1.03E-02
H2-Q4	818.86	-0.70	1.09E-02
Pcdha8	99.58	1.38	1.11E-02
Nr4a3	808.85	0.92	1.19E-02
Mlc1	19267.60	-0.16	1.30E-02
Ssbp4	4950.65	-0.30	1.30E-02
Asb11	58.68	-0.85	1.40E-02

Synpr	5668.39	-0.29	1.42E-02
Colgalt1	4918.11	-0.28	1.66E-02
Lpcat2	604.55	0.47	1.80E-02
Ttll5	12031.29	0.29	1.94E-02
mt-Co2	1920.92	-0.67	1.95E-02
Armc6	1914.46	-0.32	2.09E-02
Fbxw23	69.57	-1.14	2.12E-02
Uba52	483.07	0.74	2.12E-02
Itgax	59.12	-1.43	2.15E-02
Gm9899	2285.54	0.28	2.16E-02
Slc35f1	2853.03	0.32	2.36E-02
Nptxr	17465.93	0.24	2.36E-02
Wdr83	1649.16	-0.31	2.42E-02
Lama2	2461.25	-0.26	2.80E-02
Kcnk2	1915.20	-0.29	3.10E-02
Gm3294	691.41	0.53	3.10E-02
Lat2	127.67	-0.80	3.94E-02
Etnppl	12184.43	-0.26	4.20E-02
Inpp5f	12158.40	0.17	4.28E-02
Cybb	123.25	-0.84	4.45E-02
Cacna2d2	17270.58	0.23	4.49E-02
Fgf1	11995.94	0.38	4.68E-02
Lgr6	1180.99	0.39	4.68E-02
Hsdl2	5381.66	0.22	4.80E-02
Thy1	25553.63	0.25	4.80E-02
Dner	57278.46	0.25	4.80E-02
Gm26633	16.54	2.40	4.80E-02
Rem2	293.22	0.57	4.95E-02

Supp Table 2 Top DEG of WT versus SCA6 in posterior cerebellum

Gene name	DESeq2 baseMean	Log2 fold change	Padj
Comp	1278.09	-1.59	8.40E-60
Prdx2-ps1	82.69	-7.27	1.32E-23
Gm10654	86.43	8.20	1.66E-23
Ccdc194	95.71	-4.90	1.66E-23
Gm10033	1433.86	0.96	2.32E-21
Scoc	5989.00	0.76	1.12E-18
Mmp2	351.14	-2.19	2.96E-17
Gm45643	46.45	6.65	6.62E-17
Gm7335	52.12	-5.34	4.03E-15
Abcc12	800.41	1.09	5.43E-15
Tnc	791.43	1.26	6.12E-14
Mri1	926.87	1.00	1.80E-13
Il15	97.06	1.92	2.26E-13
Prkcg	36795.44	0.60	4.31E-13
Gm45640	40.05	4.60	1.04E-12
Car7	3414.19	0.62	2.98E-12
Ptprr	9221.14	0.45	9.90E-12
Calb1	82838.81	0.53	9.90E-12
Muc3a	909.41	0.78	1.37E-11
Usb1	588.85	-0.59	1.35E-10
Ppp1r17	18370.24	0.51	1.36E-10
Nrk	4439.57	0.59	1.36E-10
Cacna1a	26952.46	0.81	1.44E-10
Dner	57278.46	0.50	1.64E-10
Cep76	12435.35	0.57	3.03E-10
Tmem59l	20207.93	0.45	4.27E-10
Gmip	511.06	-0.82	1.58E-09
Cpne9	3103.50	0.53	2.01E-09
Clstn2	5442.66	0.59	2.37E-09
B3gnt3	33.48	2.94	5.66E-09
Trpc3	11396.14	0.52	6.85E-09
Slc1a6	15341.05	0.53	7.92E-09
Gabbr1	58909.94	0.29	8.17E-09
Mdfi	1250.92	0.78	1.07E-08
Zfp385c	3847.22	0.53	1.13E-08
Kcnab1	11397.83	0.47	1.13E-08
Zfp869	4051.63	0.33	1.13E-08
Doc2b	9872.41	0.55	1.20E-08
Plvap	1688.11	-0.62	1.28E-08
Car8	128419.12	0.48	1.64E-08

Casq2	3427.18	0.48	2.49E-08
Cyld	8558.89	0.35	2.53E-08
Cacna2d2	17270.58	0.42	2.77E-08
Fto	15091.74	0.28	4.25E-08
Mmp15	1707.36	-0.76	5.13E-08
Tnfrsf11b	640.74	0.68	5.19E-08
Nell1	3822.63	0.46	6.00E-08
Plxdc1	6061.73	0.48	6.06E-08
Fcho1	4335.09	-0.49	6.06E-08
Ndrg4	92555.83	0.32	7.17E-08
Plcb3	5761.05	0.45	7.47E-08
Acacb	1704.63	-0.78	7.74E-08
Ecm2	1428.28	-0.50	1.28E-07
Mef2b	43.58	-2.06	1.69E-07
Plpp6	4683.33	0.38	2.13E-07
Flt3	3367.90	0.39	4.20E-07
Plekhd1	8872.65	0.44	4.20E-07
Tmem98	1246.09	-1.04	5.67E-07
Dpp10	14847.22	0.47	6.41E-07
Pkp3	1173.45	0.59	7.12E-07
Gfap	24255.73	-0.74	1.06E-06
Aqp6	3323.93	0.48	1.20E-06
Prkcd	7309.47	0.43	1.40E-06
Camk2a	9615.38	0.44	1.52E-06
Fam189a2	1373.13	-0.68	1.52E-06
Grik1	2130.52	0.39	1.57E-06
Ubash3b	9915.38	0.45	1.98E-06
Armh4	12863.11	0.42	2.41E-06
C4b	3591.08	-0.85	3.04E-06
Zfp868	1875.31	-0.36	4.42E-06
Opcml	7285.73	0.32	4.42E-06
Lgr6	1180.99	0.61	4.46E-06
Gfra2	1946.22	0.40	4.94E-06
Asph	26038.95	0.35	4.95E-06
Rspo3	510.13	0.58	6.08E-06
H2-K1	4339.25	-0.57	6.10E-06
B3gnt5	2030.58	0.52	6.91E-06
Xk	3309.64	0.46	6.95E-06
Foxj1	1853.63	-0.66	7.80E-06
Icmt	51146.27	0.51	8.43E-06
Cap2	10059.68	0.28	8.69E-06
Lpl	193.35	-1.67	8.87E-06
Pbxip1	6172.69	-0.59	9.03E-06
Gm18180	80.88	-1.51	1.05E-05

Akain1	3370.95	0.34	1.09E-05
Slc41a3	3743.65	0.48	1.14E-05
Zfp963	275.60	-0.71	1.51E-05
Kcnma1	21893.76	0.34	1.60E-05
Fam78b	3167.08	0.36	1.61E-05
Gm7785	66.19	-1.22	1.87E-05
Espn	726.89	0.55	2.01E-05
Prkg1	3180.38	0.53	2.03E-05
Sdk1	353.55	-0.59	2.04E-05
Crnde	117.16	1.29	2.10E-05
Slc9a3	1334.44	0.47	2.16E-05
Ipo5	13319.80	0.27	2.48E-05
Lhx1	5847.74	0.48	2.91E-05
Ccdc88c	2234.00	-0.40	2.96E-05
Gabbr2	24322.17	0.40	2.99E-05
Gad1	58043.56	0.30	3.06E-05
Mpped2	1486.27	0.31	3.06E-05
Hbegf	1924.59	0.29	3.33E-05
Sod3	2791.35	-1.24	3.87E-05
Unc119	1829.07	-0.38	3.93E-05
Slc38a3	7330.26	-0.35	3.93E-05
Adam23	15105.04	0.41	3.99E-05
Sybu	7433.41	0.24	4.20E-05
Tmem255a	5094.28	0.42	4.20E-05
Aldoc	175312.69	0.38	4.79E-05
Lyz2	1083.21	-0.83	5.53E-05
5730409E04Rik	6576.01	0.22	5.73E-05
Clec7a	156.66	-1.60	6.62E-05
Wnt3	1638.43	0.36	6.64E-05
Kcnip1	4686.98	0.45	6.72E-05
Stk17b	6777.64	0.42	6.81E-05
Sept9	1151.03	-0.82	6.81E-05
Ipcef1	5195.63	0.35	6.81E-05
Mtss1	17068.56	0.34	6.99E-05
Lipa	1458.08	-0.54	7.24E-05
Ccdc114	516.44	-0.68	7.24E-05
Slc5a1	1033.70	0.49	7.36E-05
Sept11	8407.29	0.27	7.64E-05
Bcar1	13673.72	0.34	8.11E-05
Inpp4a	16457.00	0.35	9.80E-05
Postn	111.30	-1.62	9.85E-05
Arhgap26	15110.53	0.37	1.09E-04
Dlec1	327.98	-1.03	1.14E-04
Sbk1	58390.06	0.47	1.14E-04

Ctsd	16355.12	-0.48	1.15E-04
Lingo3	7475.03	0.39	1.15E-04
Entpd3	407.91	-0.69	1.36E-04
Cacng5	5428.27	0.29	1.36E-04
Dgkh	6515.26	0.44	1.39E-04
Abca9	644.63	-0.50	1.39E-04
Pdgfra	2176.87	-0.46	1.48E-04
Klhdc7a	1740.77	-0.64	1.48E-04
Ackr4	320.48	-1.22	1.58E-04
Acsf2	1780.39	-0.30	1.73E-04
Arhgap20	6553.17	0.41	1.82E-04
Nwd2	2347.04	0.51	1.85E-04
Jak3	378.67	-0.60	1.88E-04
Susd4	6329.70	0.25	1.96E-04
Atp11a	9868.60	-0.30	1.98E-04
Adra2b	158.45	0.80	2.15E-04
Gata2	432.28	-0.55	2.17E-04
Efemp2	1736.02	-0.40	2.19E-04
Syt7	32201.80	0.32	2.19E-04
Dsg2	308.44	-1.10	2.27E-04
Crip2	2567.92	-0.50	2.52E-04
P3h4	1422.74	-0.34	2.67E-04
Myo7a	2632.42	-0.73	2.70E-04
Hk2	1221.22	0.46	2.78E-04
Cdk16	27699.86	0.21	2.80E-04
Cntnap5b	1958.98	0.82	2.80E-04
Nptxr	17465.93	0.29	2.91E-04
Ciapin1	3710.64	-0.23	2.92E-04
Cx3cl1	7359.46	-0.30	2.97E-04
Vcam1	1789.52	-0.57	3.08E-04
Ctdspl	1214.45	-0.53	3.09E-04
Pld1	728.41	-0.58	3.42E-04

Supp Table 3 Top DEG of anterior versus posterior cerebellum in WT

Gene name	DESeq2 baseMean	Log2 fold change	Padj
Inhbb	1014.04	-1.96	7.48E-59
Otx2	1936.12	-3.78	6.05E-44
Col17a1	659.73	-1.63	2.31E-42
Syndig1l	3075.19	-2.93	1.52E-40
Sp5	781.33	-1.98	3.68E-40
F2r	631.43	-2.32	4.93E-40
Snca	2378.08	-1.31	2.49E-39
Il17re	842.39	-1.54	4.40E-37
Far2	2662.39	1.18	1.74E-35
Ttr	218965.52	-9.19	2.74E-34
Pmepa1	1577.97	-1.23	4.97E-32
Sybu	7433.41	0.59	6.14E-32
Phldb2	1638.14	-1.63	4.91E-31
Kcnab1	11397.83	0.84	8.53E-31
Nek2	1164.94	1.25	4.94E-29
Alpk2	1455.87	1.75	1.19E-28
Aldoc	175312.69	-0.87	2.88E-28
Cplx2	69406.13	0.86	6.47E-28
Rprml	266.07	3.37	1.68E-27
Muc3a	909.41	1.12	1.71E-27
Rcor2	408.19	-2.22	3.87E-27
Cck	2812.32	1.50	5.31E-27
Kcng4	16716.54	1.10	5.55E-27
Kcnc4	7101.03	-1.00	1.12E-26
Car7	3414.19	-0.89	2.10E-26
Car8	128419.12	0.81	1.06E-25
Col27a1	1840.32	1.52	2.02E-25
Ptprt	6682.61	1.39	5.88E-24
Kitl	13034.40	0.99	8.27E-24
Syt6	837.01	1.65	1.22E-23
Shroom3	1305.67	-1.03	4.20E-23
Sept6	6340.03	0.52	4.35E-23
Garnl3	17104.01	0.76	6.32E-23
Gprin3	1565.62	-1.79	6.50E-23
Kcnip1	4686.98	0.92	4.07E-22
Plod2	1140.79	-1.11	1.92E-21
Chst8	1971.33	1.01	2.80E-21
Pde1b	3271.63	-1.35	5.66E-21
Dkk3	2754.03	-0.80	3.27E-20
Ebf2	1180.03	1.45	3.40E-20
Kcnd2	16995.05	0.73	5.08E-20

Sv2c	6106.93	1.24	8.26E-20
Col2a1	641.16	-1.05	7.04E-19
Ogfrl1	17612.64	-0.57	7.27E-19
Colq	560.13	-2.19	7.81E-19
Ccdc136	7705.16	-0.45	8.74E-19
Plcd1	820.86	-0.76	1.19E-18
Maf	3440.23	0.82	5.95E-18
Tmem255a	5094.28	0.74	8.57E-18
Spag5	2853.89	-1.00	9.83E-18
Kcne2	2008.93	-9.16	1.01E-17
Rgs8	105217.09	0.97	1.42E-17
Wif1	294.87	-2.20	1.52E-17
6430548M08Rik	25695.30	0.64	1.75E-17
Sln	144.70	-2.52	2.13E-17
Lhpp	2481.21	0.90	2.35E-17
Calm1	131634.14	0.33	2.96E-17
Plppr5	1533.11	0.78	4.31E-17
Nxph3	1721.23	-0.78	4.51E-17
Lox	200.64	-1.81	4.79E-17
1500009L16Rik	457.86	1.23	6.19E-17
Atp6ap1l	591.73	1.01	6.36E-17
Fxyd6	10200.94	-0.56	7.68E-17
Trabd2b	2127.88	0.91	8.48E-17
Tmem72	2626.40	-8.37	1.76E-16
Ankrd6	1468.77	-1.35	1.77E-16
Gask1b	310.46	1.39	3.10E-16
Aox1	1114.81	-0.97	6.11E-16
Arhgef3	4921.66	0.52	2.26E-15
Spry3	2570.66	1.01	2.93E-15
Prkcg	36795.44	0.62	3.14E-15
Adamts6	1082.11	-0.86	3.27E-15
Sstr3	1101.56	0.73	1.03E-14
Itgb7	497.68	-1.04	1.03E-14
Sema7a	20018.26	0.67	1.03E-14
Lancl1	9974.99	0.40	1.12E-14
Hmcn1	571.17	-1.27	3.04E-14
Plcb3	5761.05	-0.59	3.32E-14
Hapln4	14202.53	0.53	5.56E-14
Lmo2	1458.37	0.68	5.57E-14
Lrrn3	4848.50	0.74	5.71E-14
Mpped2	1486.27	-0.50	7.40E-14
Gnmt	544.11	-0.85	8.36E-14
Prkg1	3180.38	0.81	9.04E-14
Sh3bgrl2	3581.48	-0.64	9.12E-14

Th	2576.12	-2.28	1.13E-13
Plk5	6419.47	-0.62	1.21E-13
Mef2c	3168.71	0.60	1.40E-13
Sh3bgr	964.96	0.83	1.76E-13
Samd3	97.43	-2.49	1.78E-13
Rnf152	7937.84	0.70	1.99E-13
Moxd1	289.62	-4.07	2.18E-13
Zfp658	1678.92	0.68	2.19E-13
Ncald	11255.68	0.60	2.54E-13
Qsox1	1855.16	-0.62	2.98E-13
Fgf7	1278.32	1.11	3.69E-13
Tigd2	1941.40	-0.54	4.28E-13
Cep72	1467.03	0.60	5.52E-13
Synpo	1375.10	0.56	6.70E-13
Sorcs2	1733.96	-1.02	7.09E-13
Folr1	1376.44	-6.16	8.48E-13
Tlx3	599.08	-3.16	9.66E-13
Lsmem1	244.64	1.30	1.02E-12
Aqp1	1472.55	-6.94	1.02E-12
Camk2a	9615.38	0.60	1.02E-12
Nrk	4439.57	0.62	1.26E-12
Vat1l	11392.11	-0.91	1.26E-12
Enpp2	122546.43	-3.56	1.32E-12
Sostdc1	1780.99	-6.81	1.45E-12
Kl	9210.91	-6.31	1.51E-12
Mdga1	2109.42	-0.94	1.68E-12
Eomes	1471.23	-0.84	1.77E-12
Mfrp	2070.61	-7.95	2.11E-12
Itga8	157.92	-1.24	2.21E-12
Car12	2380.96	-5.61	3.06E-12
Icmt	51146.27	0.71	3.51E-12
Chst7	180.12	1.23	4.44E-12
Nlrp10	311.14	1.44	4.44E-12
Ankrd33b	1381.18	0.88	4.78E-12
Ptpn5	2775.68	-0.92	5.68E-12
Bspry	99.91	-1.67	5.94E-12
Abhd3	6582.70	0.44	6.84E-12
Wnt10b	56.43	-3.84	7.92E-12
Cds1	12681.00	0.40	1.03E-11
Gm48898	226.47	-5.27	1.20E-11
Mab21l2	512.10	-2.65	1.20E-11
Rasgrf1	21900.78	0.60	1.39E-11
Tgm5	126.48	1.88	1.79E-11
Gsg1l	1829.62	1.04	2.28E-11

Ttll5	12031.29	0.56	2.36E-11
Doc2g	348.28	-1.33	2.61E-11
Gm14033	1716.06	0.93	2.74E-11
Wnt10a	47.79	-2.28	3.26E-11
B3gnt5	2030.58	0.68	3.34E-11
Stk17b	6777.64	0.61	3.50E-11
Mir124-2hg	2902.10	0.66	4.01E-11
Barhl1	1262.67	0.72	4.65E-11
Pcsk6	11369.33	0.52	4.65E-11
Rasa3	10546.21	0.40	5.59E-11
Dnah11	3172.69	-0.67	6.29E-11
Ptprr	9221.14	0.42	6.51E-11
Myoc	610.18	1.49	6.76E-11
F5	2632.03	-5.86	6.77E-11
Gm13944	545.60	1.02	6.77E-11
Gpr26	975.86	1.46	7.52E-11
Adamts3	1514.66	0.96	7.89E-11
Cep76	12435.35	0.57	1.11E-10
Ifngr2	2552.09	0.54	1.62E-10
Gm2115	2698.99	0.58	1.73E-10
Ecm2	1428.28	-0.58	1.89E-10
Col4a5	996.28	-0.94	1.94E-10
Obscn	176.64	-1.63	2.00E-10
Cemip	2626.46	-0.76	2.13E-10
Unc13d	931.05	-0.69	2.58E-10
Opn3	943.21	1.45	2.73E-10
Ina	19842.99	0.35	3.01E-10
Igfn1	426.22	-6.33	3.13E-10
Plcb4	27295.15	0.58	3.14E-10
Large1	8841.10	0.52	3.34E-10
Cldn2	1272.72	-4.19	3.39E-10

Supp Table 4 Top DEG of anterior versus posterior cerebellum in SCA6

Gene name	DESeq2 baseMean	Log2 fold change	Padj
Muc3a	909.41	1.61	1.09E-55
Otx2	1936.12	-4.03	4.50E-51
Inhbb	1014.04	-1.80	4.50E-51
Kcnab1	11397.83	1.07	3.78E-50
Car8	128419.12	1.11	2.83E-48
Far2	2662.39	1.36	5.88E-48
Sybu	7433.41	0.70	4.96E-47
Col17a1	659.73	-1.58	1.81E-42
Nek2	1164.94	1.49	2.57E-42
Phldb2	1638.14	-1.83	2.71E-40
Alpk2	1455.87	2.04	9.64E-40
Ttr	218965.52	-9.71	1.50E-38
Prkcg	36795.44	0.98	3.20E-38
Kitl	13034.40	1.23	2.87E-37
Atp6ap1l	591.73	1.47	4.36E-37
Kcnip1	4686.98	1.18	7.30E-37
Pmepa1	1577.97	-1.30	1.29E-36
Camk2a	9615.38	1.00	3.03E-36
Kcng4	16716.54	1.27	6.52E-36
Cck	2812.32	1.70	1.84E-35
Syndig1l	3075.19	-2.71	4.22E-35
Nrk	4439.57	1.01	1.08E-33
F2r	631.43	-2.10	3.24E-33
Il17re	842.39	-1.41	8.99E-33
Fgf7	1278.32	1.69	4.70E-31
Garnl3	17104.01	0.88	5.67E-31
Sept6	6340.03	0.59	9.62E-31
Ptprr	9221.14	0.69	7.80E-30
Zfp658	1678.92	1.00	9.29E-30
Th	2576.12	-3.33	1.80E-29
Ppp1r17	18370.24	0.81	5.95E-29
Lhpp	2481.21	1.14	1.06E-28
Shroom3	1305.67	-1.13	1.83E-28
Snca	2378.08	-1.08	1.24E-27
Rgs8	105217.09	1.20	1.27E-27
Lmx1a	276.76	-3.87	1.46E-27
Stk17b	6777.64	0.95	2.62E-27
Sh3bgrl2	3581.48	-0.88	2.93E-27
Cplx2	69406.13	0.85	3.06E-27
Icmt	51146.27	1.06	3.43E-27
Cep76	12435.35	0.88	2.10E-26

Gm14033	1716.06	1.40	7.08E-26
Calb1	82838.81	0.76	1.37E-25
Vat1l	11392.11	-1.28	1.61E-25
Casq2	3427.18	0.80	6.93E-25
Plcd1	820.86	-0.83	9.46E-25
Calm1	131634.14	0.39	3.25E-24
B3gnt5	2030.58	1.00	3.85E-24
Kcnd2	16995.05	0.80	7.42E-24
Slc29a4	3864.02	-1.37	1.38E-23
Enpp2	122546.43	-4.84	1.67E-23
Aox1	1114.81	-1.16	1.67E-23
Prkg1	3180.38	1.04	5.17E-23
Inpp5a	38777.05	0.75	6.40E-23
Trpc3	11396.14	0.79	1.16E-22
Tmem72	2626.40	-9.64	2.36E-22
Mmp2	351.14	-2.40	5.08E-22
Trabd2b	2127.88	1.03	5.92E-22
Pcsk6	11369.33	0.72	1.28E-21
Plekhd1	8872.65	0.73	2.21E-21
Sp5	781.33	-1.40	3.07E-21
Itpka	6236.73	1.06	3.15E-21
Sema7a	20018.26	0.80	3.51E-21
Rprml	266.07	2.82	7.59E-21
Nxph3	1721.23	-0.85	1.04E-20
Colq	560.13	-2.29	1.09E-20
F5	2632.03	-8.01	2.17E-20
Tmem98	1246.09	-1.71	2.17E-20
Spry3	2570.66	1.15	2.17E-20
Pbxip1	6172.69	-1.06	2.43E-20
Moxd1	289.62	-4.92	2.75E-20
Nlrp10	311.14	1.85	2.85E-20
Mef2c	3168.71	0.72	3.89E-20
Pgpep1	1466.72	-0.69	3.90E-20
Kcnma1	21893.76	0.62	4.41E-20
Acacb	1704.63	-1.20	6.20E-20
Ptprt	6682.61	1.24	2.57E-19
Qsox1	1855.16	-0.73	2.70E-19
Col27a1	1840.32	1.31	3.79E-19
Barhl1	1262.67	0.92	4.41E-19
Chrdl1	876.85	1.16	1.01E-18
Sema3a	1905.97	1.34	1.20E-18
Marveld3	65.69	-5.53	1.22E-18
Tmem255a	5094.28	0.76	1.25E-18
Tspan11	2617.85	0.92	1.88E-18

Tpd52l1	629.16	-1.55	1.96E-18
Zfp385c	3847.22	0.74	2.13E-18
Cacna2d2	17270.58	0.60	2.16E-18
Hapln4	14202.53	0.60	2.30E-18
Kcne2	2008.93	-8.80	2.84E-18
Ooep	66.04	-6.29	3.29E-18
Gask1b	310.46	1.41	5.42E-18
Aqp1	1472.55	-8.14	6.07E-18
Slc38a3	7330.26	-0.62	6.13E-18
Rcor2	408.19	-1.77	7.23E-18
Pla2g5	356.78	-1.63	7.56E-18
Dkk3	2754.03	-0.74	8.13E-18
Lancl1	9974.99	0.44	9.12E-18
Cep72	1467.03	0.69	1.18E-17
Trip10	856.02	-0.86	1.39E-17
Ccdc114	516.44	-1.23	1.60E-17
Lsmem1	244.64	1.47	2.15E-17
Folr1	1376.44	-7.07	2.61E-17
Atl2	15545.09	0.56	2.73E-17
Mfrp	2070.61	-9.27	2.86E-17
Klhdc7a	1740.77	-1.19	2.95E-17
Plod2	1140.79	-0.98	3.06E-17
Cmya5	2627.61	0.97	4.35E-17
Gfra2	1946.22	0.63	5.06E-17
Cldn2	1272.72	-5.37	5.06E-17
Bzw2	2597.94	0.50	5.24E-17
Gprin3	1565.62	-1.52	5.41E-17
Syt17	524.72	-1.36	6.28E-17
Lmo7	1454.38	0.56	6.41E-17
Ankrd33b	1381.18	1.03	6.76E-17
Llgl2	261.36	-2.24	8.96E-17
Dner	57278.46	0.61	1.07E-16
Sostdc1	1780.99	-7.73	1.34E-16
Pcolce2	701.16	-1.95	1.40E-16
Slc12a2	14192.24	-0.70	1.46E-16
Sod3	2791.35	-2.12	1.67E-16
Lrrn3	4848.50	0.79	1.80E-16
Ngfr	825.31	-1.44	1.89E-16
Car12	2380.96	-6.41	2.47E-16
Slit2	1063.69	-3.33	2.50E-16
Serpinb1b	677.31	-1.32	2.53E-16
Plppr5	1533.11	0.75	2.63E-16
Stk39	7246.15	-1.19	2.87E-16
Galm	535.99	-1.26	2.87E-16

Wnt10a	47.79	-2.66	3.05E-16
Slc16a8	336.04	-9.64	3.46E-16
Abca4	2194.44	-5.44	3.79E-16
Ecm2	1428.28	-0.69	4.51E-16
Plxdc1	6061.73	0.65	6.79E-16
Ctnnal1	2976.08	-0.95	8.27E-16
Hpcal1	22464.45	0.67	8.27E-16
Itga8	157.92	-1.33	8.41E-16
Acaa2	2245.36	-1.27	8.41E-16
Kl	9210.91	-7.01	8.68E-16
Kcnc4	7101.03	-0.76	9.50E-16
Tbc1d2	578.67	-2.62	1.22E-15
Polr3k	5043.62	0.53	1.27E-15
Rnf152	7937.84	0.74	1.41E-15
Igsf5	35.32	-3.73	1.95E-15
Samd3	97.43	-2.55	2.09E-15
Trp73	1095.36	-0.96	2.38E-15
Slco1c1	4521.25	-1.64	2.43E-15
Arl6ip1	21875.99	-0.81	2.53E-15
Doc2b	9872.41	0.70	3.31E-15
Chst8	1971.33	0.84	3.90E-15
Mab21l2	512.10	-2.99	3.94E-15
Slc4a5	2566.25	-5.88	3.95E-15
Oca2	246.72	-8.24	4.66E-15
Adgra3	1528.12	-1.16	4.67E-15
Gm48898	226.47	-5.77	5.05E-15
Atp11a	9868.60	-0.53	5.49E-15
Slc9a3	1334.44	0.73	6.10E-15
Unc119	1829.07	-0.62	6.51E-15
Inf2	4779.00	-0.79	6.97E-15
Syt6	837.01	1.27	7.06E-15

Supp Table 5 List of antibodies

Reagent	Host	Supplier	Catalog Number	RRID	Dilution	Figure
Calbindin	Rabbit	Swant	CB38a	AB_10000340	1:500	1, 3
Aldolase c	Mouse	Abcam	ab190368	AB_2747771	1:200	3
vGlut1	Mouse	DSHB (University of Iowa)	N28/9	AB_10673111	1:100	6
PSD95	Rabbit	Abcam	ab18258	AB_444362	1:100	6
Anti-Mouse IgG Fab Fragment	Donkey	Jackson Immunoresearch	715-007-003	AB_2307338	1:200	3, 6
Anti-mouse secondary (Alexa 488)	Goat	Jackson Immunoresearch	115-545-003	AB_2338840	1:1000	3, 6
Anti-rabbit secondary (Alexa 594)	Donkey	Jackson Immunoresearch	711-585-152	AB_2340621	1:1000	1, 3, 6

Chapter 4 References

Ady, V., B. Toscano-Marquez, M. Nath, P. K. Chang, J. Hui, A. Cook, F. Charron, R. Lariviere, B. Brais, R. A. McKinney, and A. J. Watt. 2018. 'Altered synaptic and firing properties of cerebellar Purkinje cells in a mouse model of ARSACS', *J Physiol*, 596: 4253-67.

Albergaria, C., and M. R. Carey. 2014. 'All Purkinje cells are not created equal', *Elife*, 3: e03285.

Azevedo, F. A., L. R. Carvalho, L. T. Grinberg, J. M. Farfel, R. E. Ferretti, R. E. Leite, W. Jacob Filho, R. Lent, and S. Herculano-Houzel. 2009. 'Equal numbers of neuronal and nonneuronal cells make the human brain an isometrically scaled-up primate brain', *J Comp Neurol*, 513: 532-41.

Brochu, G., L. Maler, and R. Hawkes. 1990. 'Zebrin II: a polypeptide antigen expressed selectively by Purkinje cells reveals compartments in rat and fish cerebellum', *J Comp Neurol*, 291: 538-52.

Cerminara, N. L., E. J. Lang, R. V. Sillitoe, and R. Apps. 2015. 'Redefining the cerebellar cortex as an assembly of non-uniform Purkinje cell microcircuits', *Nat Rev Neurosci*, 16: 79-93.

Chen, Y., S. Spina, P. Callahan, L. T. Grinberg, W. W. Seeley, H. J. Rosen, J. H. Kramer, B. L. Miller, and K. P. Rankin. 2023. 'Pathology-specific patterns of cerebellar atrophy in neurodegenerative disorders', *Alzheimers Dement*.

Cook, A. A., E. Fields, and A. J. Watt. 2021. 'Losing the Beat: Contribution of Purkinje Cell Firing Dysfunction to Disease, and Its Reversal', *Neuroscience*, 462: 247-61.

Du, X., J. Wang, H. Zhu, L. Rinaldo, K. M. Lamar, A. C. Palmenberg, C. Hansel, and C. M. Gomez. 2013. 'Second cistron in CACNA1A gene encodes a transcription factor mediating cerebellar development and SCA6', *Cell*, 154: 118-33.

Gomez, C. M., R. M. Thompson, J. T. Gammack, S. L. Perlman, W. B. Dobyns, C. L. Truwit, D. S. Zee, H. B. Clark, and J. H. Anderson. 1997. 'Spinocerebellar ataxia type 6: gaze-evoked and vertical nystagmus, Purkinje cell degeneration, and variable age of onset', *Ann Neurol*, 42: 933-50.

Hamel, K. A., and M. Cvetanovic. 2020. 'Cerebellar Regional Dissection for Molecular Analysis', *J Vis Exp*.

Hamel, Katherine, Emmanuel Labrada Moncada, Carrie Sheeler, Juao-Guilherme Rosa, Stephen Gilliat, Ying Zhang, and Marija Cvetanovic. 2023. 'Loss of intracerebellar heterogeneity and selective vulnerability in Spinocerebellar ataxia type 1 neurodegeneration', *bioRxiv*: 2022.02.24.481789.

Heckroth, J. A., and L. C. Abbott. 1994. 'Purkinje cell loss from alternating sagittal zones in the cerebellum of leaner mutant mice', *Brain Res*, 658: 93-104.

Hernández-Pérez, Carlos, Eduardo Weruaga, and David Díaz. 2023. 'Lobe X of the Cerebellum: A Natural Neuro-Resistant Region', *Anatomia*, 2: 43-62.

Hoxha, E., F. Tempia, P. Lippiello, and M. C. Miniaci. 2016. 'Modulation, Plasticity and Pathophysiology of the Parallel Fiber-Purkinje Cell Synapse', *Front Synaptic Neurosci*, 8: 35.

Huang, C., S.J. Gammon, M. Dieterle, R.H. Huang, L. Lee, and R.E. Ricklefs. 2014. 'Dramatic increases in number of cerebellar granule-cell-Purkinje-cell synapses across several mammals', *Mammalian Biology*, 79: 163–69.

Ingram, M., E. A. L. Wozniak, L. Duvick, R. Yang, P. Bergmann, R. Carson, B. O'Callaghan, H. Y. Zoghbi, C. Henzler, and H. T. Orr. 2016. 'Cerebellar Transcriptome Profiles of ATXN1 Transgenic Mice Reveal SCA1 Disease Progression and Protection Pathways', *Neuron*, 89: 1194-207.

Ito-Ishida, A., E. Miura, K. Emi, K. Matsuda, T. Iijima, T. Kondo, K. Kohda, M. Watanabe, and M. Yuzaki. 2008. 'Cbln1 regulates rapid formation and maintenance of excitatory synapses in mature cerebellar Purkinje cells in vitro and in vivo', *J Neurosci*, 28: 5920-30.

Jayabal, S., H. H. Chang, K. E. Cullen, and A. J. Watt. 2016. '4-aminopyridine reverses ataxia and cerebellar firing deficiency in a mouse model of spinocerebellar ataxia type 6', *Sci Rep*, 6: 29489.

Jayabal, S., L. Ljungberg, T. Erwes, A. Cormier, S. Quilez, S. El Jaouhari, and A. J. Watt. 2015. 'Rapid Onset of Motor Deficits in a Mouse Model of Spinocerebellar Ataxia Type 6 Precedes Late Cerebellar Degeneration', *eNeuro*, 2.

Kakegawa, W., T. Miyazaki, K. Kohda, K. Matsuda, K. Emi, J. Motohashi, M. Watanabe, and M. Yuzaki. 2009. 'The N-terminal domain of GluD2 (GluRdelta2) recruits presynaptic terminals and regulates synaptogenesis in the cerebellum in vivo', *J Neurosci*, 29: 5738-48.

Kozareva, V., C. Martin, T. Osorno, S. Rudolph, C. Guo, C. Vanderburg, N. Nadaf, A. Regev, W. G. Regehr, and E. Macosko. 2021. 'A transcriptomic atlas of mouse cerebellar cortex comprehensively defines cell types', *Nature*, 598: 214-19.

Leung, Tsz Chui Sophia, Eviatar Fields, Namrata Rana, Ru Yi Louisa Shen, Alexandra E. Bernstein, Anna A. Cook, Daniel E. Phillips, and Alanna J. Watt. 2024. 'Mitochondrial damage and impaired mitophagy contribute to disease progression in SCA6', *Acta Neuropathologica*, 147: 26.

Martin, K. B., I. M. Williams, C. V. Cluzeau, A. Cougnoux, R. K. Dale, J. R. Iben, N. X. Cawley, C. A. Wassif, and F. D. Porter. 2019. 'Identification of Novel Pathways Associated with Patterned Cerebellar Purkinje Neuron Degeneration in Niemann-Pick Disease, Type C1', *Int J Mol Sci*, 21.

Niewiadomska-Cimicka, A., F. Doussau, J. B. Perot, M. J. Roux, C. Keime, A. Hache, F. Piguet, A. Novati, C. Weber, B. Yalcin, H. Meziane, M. F. Champy, E. Grandgirard, A. Karam, N. Messaddeq, A. Eisenmann, E. Brouillet, H. H. P. Nguyen, J. Flament, P. Isope, and Y. Trottier. 2021. 'SCA7 Mouse Cerebellar Pathology Reveals Preferential Downregulation of Key Purkinje Cell-Identity Genes and Shared Disease Signature with SCA1 and SCA2', *J Neurosci*, 41: 4910-36.

Pandya, V. A., and R. Patani. 2021. 'Region-specific vulnerability in neurodegeneration: lessons from normal ageing', *Ageing Res Rev*, 67: 101311.

Perkins, E. M., D. Suminaite, Y. L. Clarkson, S. K. Lee, A. R. Lyndon, J. D. Rothstein, D. J. Wyllie, K. Tanaka, and M. Jackson. 2016. 'Posterior cerebellar Purkinje cells in an SCA5/SPARCA1 mouse model are especially vulnerable to the synergistic effect of loss of beta-III spectrin and GLAST', *Hum Mol Genet*, 25: 4448-61.

Robinson, K. J., M. Watchon, and A. S. Laird. 2020. 'Aberrant Cerebellar Circuitry in the Spinocerebellar Ataxias', *Front Neurosci*, 14: 707.

Rodriques, S. G., R. R. Stickels, A. Goeva, C. A. Martin, E. Murray, C. R. Vanderburg, J. Welch, L. M. Chen, F. Chen, and E. Z. Macosko. 2019. 'Slide-seq: A scalable technology for measuring genome-wide expression at high spatial resolution', *Science*, 363: 1463-67.

Sarna, J., S. R. Miranda, E. H. Schuchman, and R. Hawkes. 2001. 'Patterned cerebellar Purkinje cell death in a transgenic mouse model of Niemann Pick type A/B disease', *Eur J Neurosci*, 13: 1873-80.

Sarna, J. R., and R. Hawkes. 2003. 'Patterned Purkinje cell death in the cerebellum', *Prog Neurobiol*, 70: 473-507.

Sawada, K., Y. Fukui, and R. Hawkes. 2008. 'Spatial distribution of corticotropin-releasing factor immunopositive climbing fibers in the mouse cerebellum: analysis by whole mount immunohistochemistry', *Brain Res*, 1222: 106-17.

Schindelin, J., I. Arganda-Carreras, E. Frise, V. Kaynig, M. Longair, T. Pietzsch, S. Preibisch, C. Rueden, S. Saalfeld, B. Schmid, J. Y. Tinevez, D. J. White, V. Hartenstein, K. Eliceiri, P. Tomancak, and A. Cardona. 2012. 'Fiji: an open-source platform for biological-image analysis', *Nat Methods*, 9: 676-82.

Shuvaev, A. N., N. Hosoi, Y. Sato, D. Yanagihara, and H. Hirai. 2017. 'Progressive impairment of cerebellar mGluR signalling and its therapeutic potential for cerebellar ataxia in spinocerebellar ataxia type 1 model mice', *J Physiol*, 595: 141-64.

Sillitoe, R. V., and R. Hawkes. 2002. 'Whole-mount immunohistochemistry: a high-throughput screen for patterning defects in the mouse cerebellum', *J Histochem Cytochem*, 50: 235-44.

Slemmer, J. E., E. D. Haasdijk, D. C. Engel, N. Plesnila, and J. T. Weber. 2007. 'Aldolase C-positive cerebellar Purkinje cells are resistant to delayed death after cerebral trauma and AMPA-mediated excitotoxicity', *Eur J Neurosci*, 26: 649-56.

Solodkin, A., and C. M. Gomez. 2012. 'Spinocerebellar ataxia type 6', *Handb Clin Neurol*, 103: 461-73.

Takahashi, H., T. Ikeuchi, Y. Honma, S. Hayashi, and S. Tsuji. 1998. 'Autosomal dominant cerebellar ataxia (SCA6): clinical, genetic and neuropathological study in a family', *Acta Neuropathol*, 95: 333-7.

Takahashi, H., K. Ishikawa, T. Tsutsumi, H. Fujigasaki, A. Kawata, R. Okiyama, T. Fujita, K. Yoshizawa, S. Yamaguchi, H. Tomiyasu, F. Yoshii, K. Mitani, N. Shimizu, M. Yamazaki, T. Miyamoto, T. Orimo, S. Shoji, K. Kitamura, and H. Mizusawa. 2004. 'A clinical and genetic study in a large cohort of patients with spinocerebellar ataxia type 6', *J Hum Genet*, 49: 256-64.

Toscano Marquez, B., A. A. Cook, M. Rice, A. Smileski, K. Vieira-Lomasney, F. Charron, R. A. McKinney, and A. J. Watt. 2021. 'Molecular Identity and Location Influence Purkinje Cell Vulnerability in Autosomal-Recessive Spastic Ataxia of Charlevoix-Saguenay Mice', *Front Cell Neurosci*, 15: 707857.

Unno, T., M. Wakamori, M. Koike, Y. Uchiyama, K. Ishikawa, H. Kubota, T. Yoshida, H. Sasakawa, C. Peters, H. Mizusawa, and K. Watase. 2012. 'Development of Purkinje cell degeneration in a knockin mouse model reveals lysosomal involvement in the pathogenesis of SCA6', *Proc Natl Acad Sci U S A*, 109: 17693-8.

Watase, K., C. F. Barrett, T. Miyazaki, T. Ishiguro, K. Ishikawa, Y. Hu, T. Unno, Y. Sun, S. Kasai, M. Watanabe, C. M. Gomez, H. Mizusawa, R. W. Tsien, and H. Y. Zoghbi. 2008. 'Spinocerebellar ataxia type 6 knockin mice develop a progressive neuronal dysfunction with age-dependent accumulation of mutant CaV2.1 channels', *Proc Natl Acad Sci U S A*, 105: 11987-92.

Westenbroek, R. E., T. Sakurai, E. M. Elliott, J. W. Hell, T. V. Starr, T. P. Snutch, and W. A. Catterall. 1995. 'Immunochemical identification and subcellular distribution of the alpha 1A subunits of brain calcium channels', *J Neurosci*, 15: 6403-18.

Xu, M., Q. Ouyang, J. Gong, M. F. Pescosolido, B. S. Pruett, S. Mishra, M. Schmidt, R. N. Jones, E. D. Gamsiz Uzun, S. B. Lizarraga, and E. M. Morrow. 2017. 'Mixed Neurodevelopmental and Neurodegenerative Pathology in Nhe6-Null Mouse Model of Christianson Syndrome', *eNeuro*, 4.

Yang, Q., Y. Hashizume, M. Yoshida, Y. Wang, Y. Goto, N. Mitsuma, K. Ishikawa, and H. Mizusawa. 2000. 'Morphological Purkinje cell changes in spinocerebellar ataxia type 6', *Acta Neuropathol*, 100: 371-6.

Zhou, H., Z. Lin, K. Voges, C. Ju, Z. Gao, L. W. Bosman, T. J. Ruigrok, F. E. Hoebeek, C. I. De Zeeuw, and M. Schonewille. 2014. 'Cerebellar modules operate at different frequencies', *Elife*, 3: e02536.

Zhuchenko, O., J. Bailey, P. Bonnen, T. Ashizawa, D. W. Stockton, C. Amos, W. B. Dobyns, S. H. Subramony, H. Y. Zoghbi, and C. C. Lee. 1997. 'Autosomal dominant cerebellar ataxia (SCA6) associated with small polyglutamine expansions in the alpha 1A-voltage-dependent calcium channel', *Nat Genet*, 15: 62-9.

DISCUSSION

Purkinje cell electrophysiological properties and mitochondria damage

The P/Q channels and mitochondria both play vital roles in Purkinje cells. The interplay between the two ensures normal firing properties and synaptic transmission. Therefore, it is likely that the mutated P/Q channel in SCA6 and mitochondrial damage may together form a vicious cycle to exacerbate disease.

Although I have not directly demonstrated this in mice at disease onset, there was likely reduced Ca^{2+} current in SCA6 Purkinje cells based on previous studies at younger age (Watase et al. 2008). In the literature review section of this thesis, I discussed in detail that there were inconsistent evidence supporting the hypothesis that CAG repeat expansion mutation in *CACNA1A* altered P/Q channel function. On the other hand, an earlier study in $SCA6^{84Q/84Q}$, the mouse model used in this thesis, showed that SCA6 Purkinje cells have reduced current density which could be attributed to reduced expression of the channel (Watase et al. 2008). Reduced channel expression was also shown in another more progressive SCA6 mouse model, $SCA6^{118Q/118Q}$, suggesting that instead of altered channel function, altered channel abundance is likely a consequence of the mutation (Unno et al. 2012). Consistent with these findings, data from my RNA-seq at disease onset (7 month) also showed a reduction in *CACNA1A* transcripts (Chapter 3 Supp Fig 1d). Furthermore, a recent study in $SCA6^{118Q/118Q}$ showed that P/Q channels were found to be mislocalized – instead of being on the plasma membrane, P/Q channels were found to be in the cytoplasm, in close proximity to Golgi apparatus (Wang et al. 2024). Collectively, reduced expression and mistrafficking of the mutant P/Q channel limit the number of available, functional channels which then could compromise the normal functioning of Purkinje cells.

It is known that there are compensatory mechanisms among classes of calcium channels – dysfunction in one type of channel will stimulate functional upregulation in another (Etheredge et al. 2007; Inchauspe et al. 2004; Poetschke et al. 2015). Could there be other channels compensating for the loss of P/Q channel? Purkinje cells express many classes of voltage-gated calcium channels, but P/Q- and T-type channels mediate the majority of Ca^{2+} entry following action potential, each contributing half of the current (Raman and Bean 1999). However, I found that both of these channels showed reduced transcripts at 12 months in SCA6 animals, suggesting that there could

be a breakdown in the compensatory mechanism at mid-disease stage, and that calcium entry into Purkinje cell could be reduced (Chapter 4 Supp Table 1).

This reduced Ca^{2+} current into Purkinje cells may then influence normal functioning of mitochondria. In mitochondria, Ca^{2+} plays important role by stimulating activities of enzymes within the citric acid cycle and ETC to generate ATP through oxidative phosphorylation (Balaban 2009). The proton pump in the ETC partially generates mitochondria membrane potential and establishes an electrochemical gradient such that Ca^{2+} uptake into mitochondria an energetically favorable process. In turn, mitochondria also act to buffer cytosolic Ca^{2+} in a spatially restricted manner. Calcium dyshomeostasis in cell can lead to reduced oxidative phosphorylation and mitochondria damage, which then in turn diminish their Ca^{2+} buffering ability (Ryan, Ashkavand, and Norman 2020). In fact, mitochondrial Ca^{2+} dysregulation has been frequently implicated in normal aging and in neurodegenerative diseases (Jung et al. 2020).

The loss of Ca^{2+} and subsequent mitochondria damage may offer part of explanation to the late disease onset in SCA6. It is interesting that SCA6 animals and patients only display motor symptoms at mid-life, despite carrying the mutation since birth. In SCA6 mice, spontaneous firing deficit was also observed at the same time of motor deficits (7 months) but not earlier at a young age when reduced P/Q channel expression was observed (Jayabal et al. 2016; Watase et al. 2008). One possible explanation to the late onset would be the existence of an ion channel reserve such that mild perturbation to ion channel function or expression is tolerated; yet when disease deficits exceed the reserve, disease symptoms emerge (Bushart and Shakkottai 2022). It is possible that at 7 months in disease mice, this calcium channel reserve was overcome, which then led to perturbation to Ca^{2+} current and spontaneous firing that also exerted stress on mitochondria. This secondary damage to mitochondria in turn exacerbated calcium dyshomeostasis and on top reduced their bioenergetic capability, which was evident at 12 months (Chapter 3 Fig 3). Future study is required to verify this working model. It will offer insights into the causal and temporal relationships of these deficits which will be valuable in devising effective treatment regimen.

Mitochondrial damage and synaptic transmission

In Chapter 3 of this thesis, I have discussed in detail mitochondrial impairment in SCA6 during disease progression. Despite my study mainly focused on Purkinje cell autonomous changes, these

changes likely alter Purkinje cells interaction with neighbouring cell type, such as at synaptic terminals.

Mitochondria support normal synaptic transmission. As discussed, aside from their ATP production capability, mitochondria are critical to neuronal function for their Ca^{2+} buffering function. At synaptic terminal, mitochondria provide the energy required for synaptic vesicle docking, recruitment of reserve pool of synaptic vesicles to active zone, endocytosis of ion channels and local protein translation. Mitochondria also sequester and release Ca^{2+} at synaptic terminal that is important for vesicle release and synaptic plasticity (Vos, Lauwers, and Verstreken 2010). Specifically, in Purkinje cells, mitochondria express unique tethering protein RMDN3 to promote contact with endoplasmic reticulum for enhanced Ca^{2+} buffering capacity, highlighting the central role of healthy mitochondria in normal synaptic transmission in Purkinje cells (Fecher et al. 2019).

I have shown that mitochondria in Purkinje cell soma are evidently damaged at mid-disease stage. I have also indirectly showed that there was likely mitochondria dysfunction at synaptic terminal: mitochondrial membrane potential was lowered in the molecular layer of SCA6 cerebellum (Chapter 3 Fig. 3). While the measurement represents signals from a mix of Purkinje cell dendrites, cross-section of parallel fibers, synaptic terminals and molecular layer interneurons, PF-PC synapses are the most abundant synaptic contacts in the cerebellar cortex, making it likely that mitochondria at these synapses to have lowered membrane potential. Since both ATP production through electron transport chain and Ca^{2+} uptake into mitochondria depend on mitochondrial membrane potential, loss of membrane potential disrupts both of these processes, leading to impaired synaptic transmission.

One likely consequence of dysfunction in synapses is their elimination. Synaptic pruning which removes weakened or damaged synapses in neurodegenerative diseases is common (Cardozo et al. 2019). Nonetheless, when I quantified PF-PC synapse in lobule III of SCA6 cerebellum, I did not detect a reduction in synaptic connection (Chapter 4 Fig 6). One possible explanation for this apparent lack of change in synapses made onto Purkinje cell dendrites is because the quantification was performed at 13 months, only briefly after mitochondrial damage was evident at 12 months. Future work is required to investigate if PF-PC synapse elimination takes place later in disease.

Therapeutics potential of mitochondria targeting therapy

Owing to the involvement of mitochondria in nearly all cellular processes, mitochondrial damage has been implicated in many neurodegenerative diseases (Lin and Beal 2006). In diseases where mitochondria damage is a secondary pathology, mitochondria targeting therapies have led to symptoms alleviation (Golpich et al. 2017). Therefore, it is likely that restoring mitochondria health could ameliorate SCA6 pathology and slow down progression.

Drugs designed to act on mitochondria can be categorised into five main strategies: (1) stimulating mitochondria biogenesis, (2) enhancing mitochondria fusion/fission, (3) inducing mitophagy, (4) protecting mitochondria from oxidative stress and (5) altering mitochondria signalling cascades (Murphy and Hartley 2018). Some mitochondria targeting drugs have only a single mode of action, whereas many affect more than one of these actions. Therefore, when selecting drugs to test on, the type of mitochondrial impairments observed should be considered. In SCA6 mice, we observed reduction in mitochondria membrane potential, loss of cristae and oxidative stress earlier in disease, with reduced mitophagy emerging at more advanced disease stages (Chapter 3 Fig 3-6). Interestingly, we observed similar number of mitochondria between SCA6 and WT animals at both early and advanced disease stages, suggesting that mitochondria biogenesis may be relatively intact. This suggests that for SCA6, treatments targeting mitochondrial fusion/fusion and oxidative stress protect may be effective at early disease stage, whereas mitophagy-inducing drugs may be more fitting for later in disease.

One of the drugs that showed promising result in cerebellar ataxia is the mitochondria-targeting antioxidant MitoQ (Stucki et al. 2016; Marquez et al. 2023; Jauslin et al. 2003a). MitoQ was shown to slow down disease progression and reduce cell loss in SCA1 and ARSACS. However, it is noteworthy that MitoQ uptake by mitochondria is dependent on mitochondria membrane potential (Solesio et al. 2013). Since mitochondria membrane potential is reduced as SCA6 progresses, MitoQ may have diminishing effects in SCA6. Instead, another small molecule antioxidant, mitochondria-targeting vitamin E (MitoVit-E) may be a more promising candidate, since the antioxidant effect of MitoVit-E is not affected by mitochondria membrane potential (Jauslin et al. 2003b).

There are various other mitochondria targeting drugs that may be effective in treating SCA6. For instance, nicotinamide riboside was shown to prevent Purkinje cell loss and improve motor deficits

in mouse model of ataxia telangiectasia by inducing mitophagy (Yang et al. 2021). Other drugs and their mechanisms of action have been extensively reviewed in (Xu et al. 2022).

While mitochondria-targeting treatments may be a promising therapeutic avenue, since mitochondria impairment is likely a secondary pathology in SCA6, targeting mitochondria may only hold the promise of slowing down disease progression but not delaying disease onset. Previous study in the lab revealed the involvement of BDNF-TrkB signalling at disease onset and the therapeutic value of its reversal in SCA6 mouse model (Cook et al. 2022). The most effective treatment regime may thus require a combination of different therapies targeting disease onset and progression.

SCA6 Pathology in cells other than Purkinje cells

Studies in cerebellar ataxias focus heavily on Purkinje cells, for they are usually the most apparent degenerating cell type. However, it is likely that other cells types are also affected in diseases.

In this thesis, I presented some evidence that granule cells and molecular layer interneurons also suffered some damages in SCA6. When there was accumulation of oxidative stress in Purkinje cell, the same could be observed in molecular layer interneurons though to a smaller extent (Chapter 3 Fig 4). I also showed granule cell-originating parallel fibers lost synaptic connection with Purkinje cells in SCA6 animal (Chapter 4 Fig 6). Indeed, granule cell loss is occasionally observed in human patients (Ikeuchi et al. 1997; Yang et al. 2000). This is not unexpected because *CACNA1A* is also highly expressed in granule cells, and its mutation in SCA6 may also exert detrimental effect to granule cell functions. Granule cell specific *CACNA1A* knock-out resulted in reduced granule cell synaptic output and absent PF-PC long term synaptic plasticity (Galliano et al. 2013). Surprisingly, a small population of *CACNA1A*-expressing granule cell was sufficient to sustain normal motor function, consistent with the finding that majority of PF-PC synapses are silent (Isope and Barbour 2002). This property of PF-PC synapse makes it challenging to define the contribution of granule cell deficits to SCA6 pathology; on top its contribution may only be apparent at later stage of disease.

Transcriptomic data generated in this thesis also provided some insights into changes in other cerebellar cell types in SCA6. At disease onset at 7 months, the proportion of granule cell-specific genes that were dysregulated was highest among cerebellar cell types (Fig 3b, adapted from Chapter 3 Supp Fig 1e). The transcriptional landscape shifted as disease progresses that by 12

months, where a larger proportion of Purkinje cell specific genes showed dysregulation, same for granule cell, oligodendrocyte and astrocyte specific genes (Fig 3c). This suggests that as disease progresses, more and more cell types are affected. Future studies are required to better understand the alterations in other cerebellar cell types and how they contribute to SCA6 disease progression.

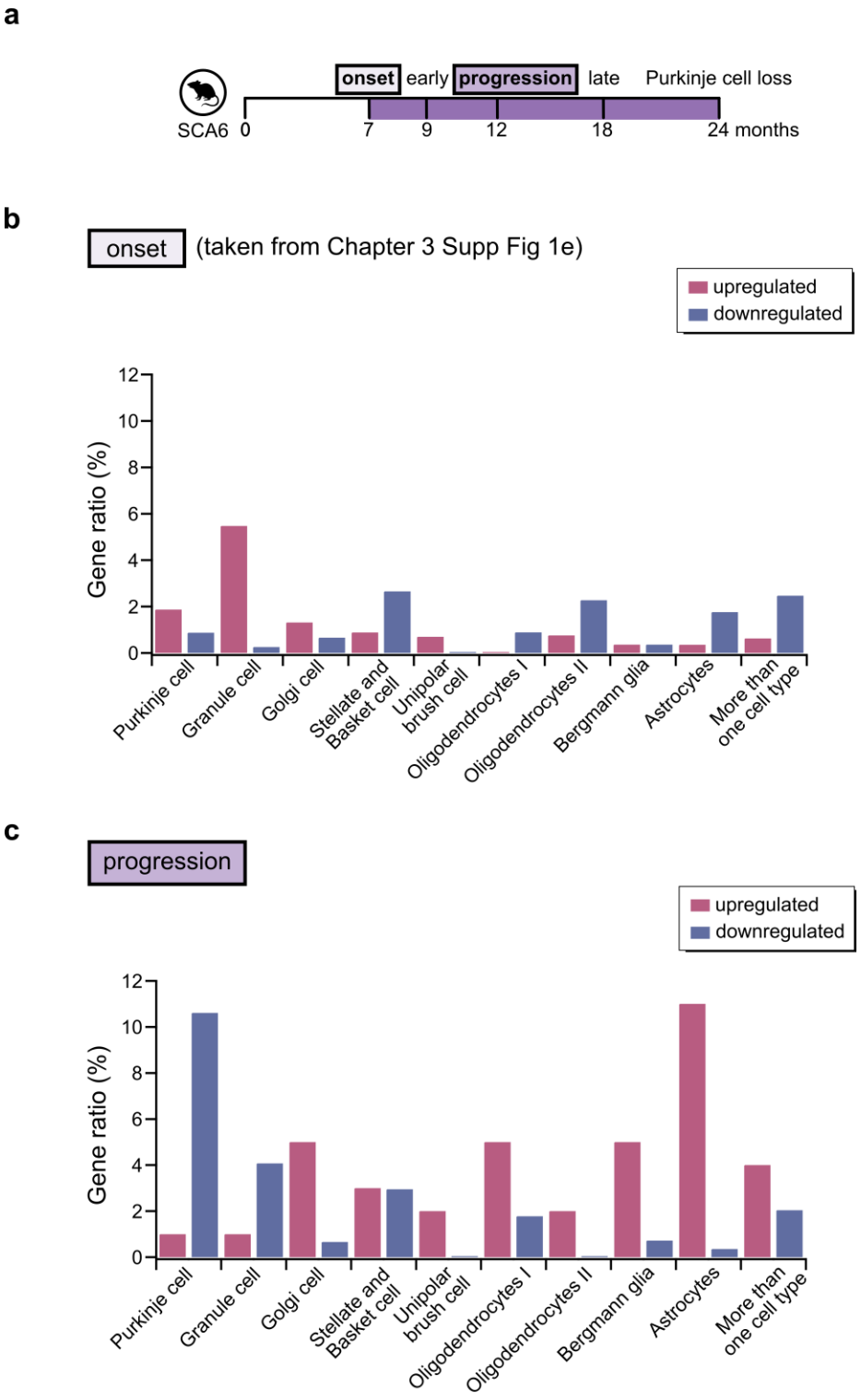

Figure 1 – RNA-seq data set from two stages of SCA6 disease showed different cell type specific expression

Mismatch between transcript level and pathology

One interesting observation in this thesis is that there is a mismatch in the timepoints when transcript level changes and functional level changes were observed. In the example of mitochondria, mitochondrial genes downregulation was observed at disease onset at 7 months by RNA-seq; yet functional changes such as membrane potential reduction and morphological damage were only observed months later. Furthermore, only a smaller subset of mitochondrial genes was found to be dysregulated at 12 months RNA-seq (Chapter 4 Supp Table 1), in contrast to the multiple lines of evidences showing mitochondria deficits at that age (Chapter 3).

One possible explanation maybe that the sensitivity of assays performed were insufficient in detecting mild disruption to mitochondria functions at an earlier age. However, this cannot reconcile the lack of mitochondria dysregulated genes at 12 months. There is a theory that neurodegenerative diseases are a form of accelerated aging disorder (Statsenko et al. 2023). Indeed, there are many parallels between neurodegenerative diseases and aging, mitochondria damage and cell loss are amongst the most prominent ones. It is thus plausible that the supposed reduction of mitochondrial transcript in aging took place earlier in SCA6 at 7 months. By 12 months, the normal aging-related reduction took place such as the levels of mitochondrial gene expression between WT and SCA6 were no longer distinguishable. And at this later timepoint, the damage in SCA6 mitochondria accumulated enough that caused widespread cellular consequences. Future work will be needed to test this speculation.

A second, and perhaps more likely explanation for this temporal mismatch is that processes like protein translation, post translational modification, trafficking and turnover could together supersede transcriptional dysregulation. In fact, it is known that mRNA level does not always correlate with protein level of a given gene (Maier, Guell, and Serrano 2009). When under stress, cell activates homeostatic responses which include the processes mentioned. Therefore, transcriptional changes can sometimes be uncoupled from functional changes.

Taken together, while transcriptomic studies offer comprehensive picture of genes expressed in a brain region, it represents a snapshot in time in which dynamic changes in cellular biology may be obscured. Transcriptional data is best used as a tool to inspire further investigation of biological processes on protein and function levels.

Open questions: posterior cerebellum compensation in SCA6?

In Chapter 4 of this thesis, I described the surprising finding that the spared nodular zone in SCA6 showed lost PF-PC synapses while the vulnerable anterior zone was unaffected. This is in stark contrast to the understanding that lobule X in the nodular is a naturally resilient region in the cerebellum (Hernández-Pérez, Weruaga, and Díaz 2023). This finding also opens up many questions: what cellular process mediated the retraction of PF-PC synapses? Does this shift in connectivity exert neuroprotective effect onto the cerebellum? If so, are there any mechanisms that could be tapped into for other brain regions where cell death is more prevalent?

Inputs into the cerebellar cortex from various sources converge onto Purkinje cells, which then form the sole output of the cortex onto the cerebellar nuclei. Each neuron in the cerebellar nuclei receives input from multiple Purkinje cells. Studies have shown that populations of Purkinje cells encode motor functions (Thier et al. 2000; Heck et al. 2013). Purkinje cells have also been hypothesized to fire in synchrony to influence spiking in postsynaptic cerebellar nuclear neurons (Person and Raman 2011). Recent study in the lab demonstrate that some cerebellar nuclear neurons receive input from Purkinje cells in different transverse zones, such as from the anterior and nodular zone (Gruver et al., 2024). This suggests that it is anatomically possible that changes in the nodular Purkinje cell outputs may compensate for deficits in anterior Purkinje cells.

However, it remains to be reconciled why the nodular zone showed reduced, but not increased, number of PF-PC synapses? Does this result in reduced excitatory inputs onto nodular Purkinje cells support nodular Purkinje cell function or hinder it? Future work is required to determine the downstream effect of changes in the SCA6 posterior cerebellum.

There are exciting research questions prompted by work in this thesis. Nevertheless, this work has offered a novel view into how the cerebellum could be affected in disease: regions other than the degenerating part of the cerebellum may also undergo adaptive changes. This also illustrates the importance of defining the region examined such that pathological and adaptive changes would not be convoluted. Any advances in understanding both of these processes in the SCA6 cerebellum will bring us one step closer to finding cure to this devastating disease.

CONCLUSION AND SUMMARY

In this thesis, I have identified restoring mitochondria health as a possible target for SCA6 therapy. I have also identified that while the anterior cerebellum is the main target of disease insult, alterations could also be found in the posterior cerebellum, adding nuances to SCA6 pathology. This is also valuable information to guide future studies and to accurately track disease progression, knowing certain region of the cerebellum is susceptible while the other is resilient.

However, I was not able to provide a mechanistic link between mutation in *CACNA1A,* mitochondria impairment and eventual Purkinje cell degeneration, nor could I test the effectiveness in treating SCA6 by targeting mitochondria. There are also open questions as to why the posterior cerebellum undergoes drastic transcriptional reprogramming, and what are the cellular consequences of these changes bring about that contribute to resilience. However, in these studies, I opted to perform omics analysis, such as transcriptomics and metabolomics, not only for the unbiased screening of a large number of targets, but also in hopes to generate datasets that could be referenced for future research. All raw data will be published and made available to all researchers.

The work here was carried out with the eventual goal of fully understand SCA6 pathology and the cerebellum. There is still much work to do before we can identify a cure for SCA6, and so much more before we unravel the mystery of the cerebellum. It is my hope that discoveries in this study add some missing pieces to the puzzles of SCA6 and cerebellum, and that future researchers in the field will find this work helpful.

REFERENCES

Ady, V., B. Toscano-Marquez, M. Nath, P. K. Chang, J. Hui, A. Cook, F. Charron, R. Lariviere, B. Brais, R. A. McKinney, and A. J. Watt. 2018. 'Altered synaptic and firing properties of cerebellar Purkinje cells in a mouse model of ARSACS', *J Physiol*, 596: 4253-67.

Aikawa, T., K. Mogushi, K. Iijima-Tsutsui, K. Ishikawa, M. Sakurai, H. Tanaka, H. Mizusawa, and K. Watase. 2015. 'Loss of MyD88 alters neuroinflammatory response and attenuates early Purkinje cell loss in a spinocerebellar ataxia type 6 mouse model', *Hum Mol Genet*, 24: 4780-91.

Albergaria, C., and M. R. Carey. 2014. 'All Purkinje cells are not created equal', *Elife*, 3: e03285.

Aman, Y., T. Schmauck-Medina, M. Hansen, R. I. Morimoto, A. K. Simon, I. Bjedov, K. Palikaras, A. Simonsen, T. Johansen, N. Tavernarakis, D. C. Rubinsztein, L. Partridge, G. Kroemer, J. Labbadia, and E. F. Fang. 2021. 'Autophagy in healthy aging and disease', *Nat Aging*, 1: 634-50.

Anders, S., P. T. Pyl, and W. Huber. 2015. 'HTSeq--a Python framework to work with high-throughput sequencing data', *Bioinformatics*, 31: 166-9.

Aoki, H., M. Higashi, M. Okita, N. Ando, S. Murayama, K. Ishikawa, and T. Yokota. 2023. 'Thymidine Kinase 2 and Mitochondrial Protein COX I in the Cerebellum of Patients with Spinocerebellar Ataxia Type 31 Caused by Penta-nucleotide Repeats (TTCCA)(n)', *Cerebellum*, 22: 70-84.

Apps, R., and R. Hawkes. 2009. 'Cerebellar cortical organization: a one-map hypothesis', *Nat Rev Neurosci*, 10: 670-81.

Azevedo, F. A., L. R. Carvalho, L. T. Grinberg, J. M. Farfel, R. E. Ferretti, R. E. Leite, W. Jacob Filho, R. Lent, and S. Herculano-Houzel. 2009. 'Equal numbers of neuronal and nonneuronal cells make the human brain an isometrically scaled-up primate brain', *J Comp Neurol*, 513: 532-41.

Azzollini, V., and W. Hayward. 2023. 'What Role Does the Cerebellum Have in a Fatigue Network?', *J Neurosci*, 43: 7599-600.

Balaban, R. S. 2009. 'The role of Ca(2+) signaling in the coordination of mitochondrial ATP production with cardiac work', *Biochim Biophys Acta*, 1787: 1334-41.

Baloyannis, S. J. 2011. 'Mitochondria are related to synaptic pathology in Alzheimer's disease', *Int J Alzheimers Dis*, 2011: 305395.

Barbosa, M. C., R. A. Grosso, and C. M. Fader. 2018. 'Hallmarks of Aging: An Autophagic Perspective', *Front Endocrinol (Lausanne)*, 9: 790.

Brion, F., B. Marc, F. Launay, J. Gailledreau, and M. Durigon. 1991. 'Postmortem interval estimation by creatinine levels in human psoas muscle', *Forensic Sci Int*, 52: 113-20.

Brochu, G., L. Maler, and R. Hawkes. 1990. 'Zebrin II: a polypeptide antigen expressed selectively by Purkinje cells reveals compartments in rat and fish cerebellum', *J Comp Neurol*, 291: 538-52.

Brusse, E., M. G. Brusse-Keizer, H. J. Duivenvoorden, and J. C. van Swieten. 2011. 'Fatigue in spinocerebellar ataxia: patient self-assessment of an early and disabling symptom', *Neurology*, 76: 953-9.

Bunting, E. L., J. Hamilton, and S. J. Tabrizi. 2022. 'Polyglutamine diseases', *Curr Opin Neurobiol*, 72: 39-47.

Bushart, D. D., and V. G. Shakkottai. 2022. 'Vulnerability of Human Cerebellar Neurons to Degeneration in Ataxia-Causing Channelopathies', *Front Syst Neurosci*, 16: 908569.

Calvo-Rodriguez, M., and B. J. Bacskai. 2021. 'Mitochondria and Calcium in Alzheimer's Disease: From Cell Signaling to Neuronal Cell Death', *Trends Neurosci*, 44: 136-51.

Cardozo, P. L., I. B. Q. de Lima, E. M. A. Maciel, N. C. Silva, T. Dobransky, and F. M. Ribeiro. 2019. 'Synaptic Elimination in Neurological Disorders', *Curr Neuropharmacol*, 17: 1071-95.

Casamento-Moran, A., R. A. Mooney, V. S. Chib, and P. A. Celnik. 2023. 'Cerebellar Excitability Regulates Physical Fatigue Perception', *J Neurosci*, 43: 3094-106.

Casey, H. L., and C. M. Gomez. 1993. 'Spinocerebellar Ataxia Type 6.' in M. P. Adam, J. Feldman, G. M. Mirzaa, R. A. Pagon, S. E. Wallace, L. J. H. Bean, K. W. Gripp and A. Amemiya (eds.), *GeneReviews((R))* (Seattle (WA)).

Cecchini, G. 2003. 'Function and structure of complex II of the respiratory chain', *Annu Rev Biochem*, 72: 77-109.

Cerminara, N. L., E. J. Lang, R. V. Sillitoe, and R. Apps. 2015. 'Redefining the cerebellar cortex as an assembly of non-uniform Purkinje cell microcircuits', *Nat Rev Neurosci*, 16: 79-93.

Cerutti, R., E. Pirinen, C. Lamperti, S. Marchet, A. A. Sauve, W. Li, V. Leoni, E. A. Schon, F. Dantzer, J. Auwerx, C. Viscomi, and M. Zeviani. 2014. 'NAD(+)-dependent activation of Sirt1 corrects the phenotype in a mouse model of mitochondrial disease', *Cell Metab*, 19: 1042-9.

Chakrabarti, L., J. Eng, N. Ivanov, G. A. Garden, and A. R. La Spada. 2009. 'Autophagy activation and enhanced mitophagy characterize the Purkinje cells of pcd mice prior to neuronal death', *Mol Brain*, 2: 24.

Chen, H., and E. S. Piedras-Renteria. 2007. 'Altered frequency-dependent inactivation and steady-state inactivation of polyglutamine-expanded alpha1A in SCA6', *Am J Physiol Cell Physiol*, 292: C1078-86.

Chen, P., C. Peng, J. Luff, K. Spring, D. Watters, S. Bottle, S. Furuya, and M. F. Lavin. 2003. 'Oxidative stress is responsible for deficient survival and dendritogenesis in purkinje neurons from ataxia-telangiectasia mutated mutant mice', *J Neurosci*, 23: 11453-60.

Chen, Y., S. Spina, P. Callahan, L. T. Grinberg, W. W. Seeley, H. J. Rosen, J. H. Kramer, B. L. Miller, and K. P. Rankin. 2023. 'Pathology-specific patterns of cerebellar atrophy in neurodegenerative disorders', *Alzheimers Dement*.

Chopra, R., D. D. Bushart, J. P. Cooper, D. Yellajoshyula, L. M. Morrison, H. Huang, H. P. Handler, L. J. Man, W. Dansithong, D. R. Scoles, S. M. Pulst, H. T. Orr, and V. G. Shakkottai. 2020. 'Altered Capicua expression drives regional Purkinje neuron vulnerability through ion channel gene dysregulation in spinocerebellar ataxia type 1', *Hum Mol Genet*, 29: 3249-65.

Chow, H. M., A. Cheng, X. Song, M. R. Swerdel, R. P. Hart, and K. Herrup. 2019. 'ATM is activated by ATP depletion and modulates mitochondrial function through NRF1', *J Cell Biol*, 218: 909-28.

Chung, C., M. J. Elrick, J. M. Dell'Orco, Z. S. Qin, S. Kalyana-Sundaram, A. M. Chinnaiyan, V. G. Shakkottai, and A. P. Lieberman. 2016. 'Heat Shock Protein Beta-1 Modifies Anterior to Posterior Purkinje Cell Vulnerability in a Mouse Model of Niemann-Pick Type C Disease', *PLoS Genet*, 12: e1006042.

Cogliati, S., C. Frezza, M. E. Soriano, T. Varanita, R. Quintana-Cabrera, M. Corrado, S. Cipolat, V. Costa, A. Casarin, L. C. Gomes, E. Perales-Clemente, L. Salviati, P. Fernandez-Silva, J. A. Enriquez, and L. Scorrano. 2013. 'Mitochondrial cristae shape determines respiratory chain supercomplexes assembly and respiratory efficiency', *Cell*, 155: 160-71.

Cook, A. A., E. Fields, and A. J. Watt. 2021. 'Losing the Beat: Contribution of Purkinje Cell Firing Dysfunction to Disease, and Its Reversal', *Neuroscience*, 462: 247-61.

Cook, A. A., S. Jayabal, J. Sheng, E. Fields, T. C. S. Leung, S. Quilez, E. McNicholas, L. Lau, S. Huang, and A. J. Watt. 2022. 'Activation of TrkB-Akt signaling rescues deficits in a mouse model of SCA6', *Sci Adv*, 8: eabh3260.

Cook, A. A., T. C. S. Leung, M. Rice, M. Nachman, É. Zadigue-Dube, and A. J. Watt. 2023. 'Endosomal dysfunction contributes to cerebellar deficits in spinocerebellar ataxia type 6', *Elife*, 12.

Cornelius, N., J. H. Wardman, I. P. Hargreaves, V. Neergheen, A. S. Bie, Z. Tumer, J. E. Nielsen, and T. T. Nielsen. 2017. 'Evidence of oxidative stress and mitochondrial dysfunction in spinocerebellar ataxia type 2 (SCA2) patient fibroblasts: Effect of coenzyme Q10 supplementation on these parameters', *Mitochondrion*, 34: 103-14.

Corral-Juan, M., P. Casquero, N. Giraldo-Restrepo, S. Laurie, A. Martinez-Pineiro, R. C. Mateo-Montero, L. Ispierto, D. Vilas, E. Tolosa, V. Volpini, R. Alvarez-Ramo, I. Sanchez, and A. Matilla-Duenas.

2022. 'New spinocerebellar ataxia subtype caused by SAMD9L mutation triggering mitochondrial dysregulation (SCA49)', *Brain Commun*, 4: fcac030.

Diallo, A., H. Jacobi, A. Cook, R. Labrum, A. Durr, A. Brice, P. Charles, C. Marelli, C. Mariotti, L. Nanetti, M. Panzeri, M. Rakowicz, A. Sobanska, A. Sulek, T. Schmitz-Hubsch, L. Schols, H. Hengel, B. Melegh, A. Filla, A. Antenora, J. Infante, J. Berciano, B. P. van de Warrenburg, D. Timmann, S. Boesch, M. Pandolfo, J. B. Schulz, P. Bauer, P. Giunti, J. S. Kang, T. Klockgether, and S. Tezenas du Montcel. 2018. 'Survival in patients with spinocerebellar ataxia types 1, 2, 3, and 6 (EUROSCA): a longitudinal cohort study', *Lancet Neurol*, 17: 327-34.

Doyle, J. P., J. D. Dougherty, M. Heiman, E. F. Schmidt, T. R. Stevens, G. Ma, S. Bupp, P. Shrestha, R. D. Shah, M. L. Doughty, S. Gong, P. Greengard, and N. Heintz. 2008. 'Application of a translational profiling approach for the comparative analysis of CNS cell types', *Cell*, 135: 749-62.

Du, X., J. Wang, H. Zhu, L. Rinaldo, K. M. Lamar, A. C. Palmenberg, C. Hansel, and C. M. Gomez. 2013. 'Second cistron in CACNA1A gene encodes a transcription factor mediating cerebellar development and SCA6', *Cell*, 154: 118-33.

Eccles, John C., Masao Ito, and János Szentágothai. 1967. *The cerebellum as a neuronal machine* (Springer-Verlag: Berlin, New York etc.).

Etheredge, J. A., D. Murchison, L. C. Abbott, and W. H. Griffith. 2007. 'Functional compensation by other voltage-gated Ca2+ channels in mouse basal forebrain neurons with Ca(V)2.1 mutations', *Brain Res*, 1140: 105-19.

Fagerberg, L., B. M. Hallstrom, P. Oksvold, C. Kampf, D. Djureinovic, J. Odeberg, M. Habuka, S. Tahmasebpoor, A. Danielsson, K. Edlund, A. Asplund, E. Sjostedt, E. Lundberg, C. A. Szigyarto, M. Skogs, J. O. Takanen, H. Berling, H. Tegel, J. Mulder, P. Nilsson, J. M. Schwenk, C. Lindskog, F. Danielsson, A. Mardinoglu, A. Sivertsson, K. von Feilitzen, M. Forsberg, M. Zwahlen, I. Olsson, S. Navani, M. Huss, J. Nielsen, F. Ponten, and M. Uhlen. 2014. 'Analysis of the human tissue-specific expression by genome-wide integration of transcriptomics and antibody-based proteomics', *Mol Cell Proteomics*, 13: 397-406.

Fecher, C., L. Trovo, S. A. Muller, N. Snaidero, J. Wettmarshausen, S. Heink, O. Ortiz, I. Wagner, R. Kuhn, J. Hartmann, R. M. Karl, A. Konnerth, T. Korn, W. Wurst, D. Merkler, S. F. Lichtenthaler, F. Perocchi, and T. Misgeld. 2019. 'Cell-type-specific profiling of brain mitochondria reveals functional and molecular diversity', *Nat Neurosci*, 22: 1731-42.

Filler, K., D. Lyon, J. Bennett, N. McCain, R. Elswick, N. Lukkahatai, and L. N. Saligan. 2014. 'Association of Mitochondrial Dysfunction and Fatigue: A Review of the Literature', *BBA Clin*, 1: 12-23.

Franco-Iborra, S., T. Cuadros, A. Parent, J. Romero-Gimenez, M. Vila, and C. Perier. 2018. 'Defective mitochondrial protein import contributes to complex I-induced mitochondrial dysfunction and neurodegeneration in Parkinson's disease', *Cell Death Dis*, 9: 1122.

Fujioka, S., C. Sundal, and Z. K. Wszolek. 2013. 'Autosomal dominant cerebellar ataxia type III: a review of the phenotypic and genotypic characteristics', *Orphanet J Rare Dis*, 8: 14.

Fujita, H., H. Aoki, I. Ajioka, M. Yamazaki, M. Abe, A. Oh-Nishi, K. Sakimura, and I. Sugihara. 2014. 'Detailed expression pattern of aldolase C (Aldoc) in the cerebellum, retina and other areas of the CNS studied in Aldoc-Venus knock-in mice', *PLoS One*, 9: e86679.

Galliano, E., Z. Gao, M. Schonewille, B. Todorov, E. Simons, A. S. Pop, E. D'Angelo, A. M. van den Maagdenberg, F. E. Hoebeek, and C. I. De Zeeuw. 2013. 'Silencing the majority of cerebellar granule cells uncovers their essential role in motor learning and consolidation', *Cell Rep*, 3: 1239-51.

Gao, W., G. Chen, K. C. Reinert, and T. J. Ebner. 2006. 'Cerebellar cortical molecular layer inhibition is organized in parasagittal zones', *J Neurosci*, 26: 8377-87.

Giunti, P., E. Mantuano, M. Frontali, and L. Veneziano. 2015. 'Molecular mechanism of Spinocerebellar Ataxia type 6: glutamine repeat disorder, channelopathy and transcriptional dysregulation. The multifaceted aspects of a single mutation', *Front Cell Neurosci*, 9: 36.

Golpich, M., E. Amini, Z. Mohamed, R. Azman Ali, N. Mohamed Ibrahim, and A. Ahmadiani. 2017. 'Mitochondrial Dysfunction and Biogenesis in Neurodegenerative diseases: Pathogenesis and Treatment', *CNS Neurosci Ther*, 23: 5-22.

Gomez, C. M., R. M. Thompson, J. T. Gammack, S. L. Perlman, W. B. Dobyns, C. L. Truwit, D. S. Zee, H. B. Clark, and J. H. Anderson. 1997. 'Spinocerebellar ataxia type 6: gaze-evoked and vertical nystagmus, Purkinje cell degeneration, and variable age of onset', *Ann Neurol*, 42: 933-50.

Gonzalez-Riano, C., S. Tapia-Gonzalez, A. Garcia, A. Munoz, J. DeFelipe, and C. Barbas. 2017. 'Metabolomics and neuroanatomical evaluation of post-mortem changes in the hippocampus', *Brain Struct Funct*, 222: 2831-53.

Hamel, K. A., and M. Cvetanovic. 2020. 'Cerebellar Regional Dissection for Molecular Analysis', *J Vis Exp*.

Hamel, Katherine, Emmanuel Labrada Moncada, Carrie Sheeler, Juao-Guilherme Rosa, Stephen Gilliat, Ying Zhang, and Marija Cvetanovic. 2023. 'Loss of intracerebellar heterogeneity and selective vulnerability in Spinocerebellar ataxia type 1 neurodegeneration', *bioRxiv*: 2022.02.24.481789.

Harmuth, T., C. Prell-Schicker, J. J. Weber, F. Gellerich, C. Funke, S. Driessen, J. C. D. Magg, G. Krebiehl, H. Wolburg, S. N. Hayer, S. Hauser, R. Kruger, L. Schols, O. Riess, and J. Hubener-Schmid. 2018. 'Mitochondrial Morphology, Function and Homeostasis Are Impaired by Expression of an N-terminal Calpain Cleavage Fragment of Ataxin-3', *Front Mol Neurosci*, 11: 368.

Harmuth, T., J. J. Weber, A. J. Zimmer, A. S. Sowa, J. Schmidt, J. C. Fitzgerald, L. Schols, O. Riess, and J. Hubener-Schmid. 2022. 'Mitochondrial Dysfunction in Spinocerebellar Ataxia Type 3 Is Linked to VDAC1 Deubiquitination', *Int J Mol Sci*, 23.

Heck, D. H., C. I. De Zeeuw, D. Jaeger, K. Khodakhah, and A. L. Person. 2013. 'The neuronal code(s) of the cerebellum', *J Neurosci*, 33: 17603-9.

Heckroth, J. A., and L. C. Abbott. 1994. 'Purkinje cell loss from alternating sagittal zones in the cerebellum of leaner mutant mice', *Brain Res*, 658: 93-104.

Hedberg-Buenz, A., L. M. Dutca, D. R. Larson, K. J. Meyer, D. A. Soukup, C. J. van der Heide, H. E. Mercer, K. Wang, and M. G. Anderson. 2019. 'Mouse models and strain-dependency of Chediak-Higashi syndrome-associated neurologic dysfunction', *Sci Rep*, 9: 6752.

Hernandez-Castillo, C. R., R. Diaz, I. Vaca-Palomares, D. L. Torres, A. Chirino, A. Campos-Romo, A. Ochoa, A. Rasmussen, and J. Fernandez-Ruiz. 2019. 'Extensive cerebellar and thalamic degeneration in spinocerebellar ataxia type 10', *Parkinsonism Relat Disord*, 66: 182-88.

Hernández-Pérez, Carlos, Eduardo Weruaga, and David Díaz. 2023. 'Lobe X of the Cerebellum: A Natural Neuro-Resistant Region', *Anatomia*, 2: 43-62.

Howarth, C., P. Gleeson, and D. Attwell. 2012. 'Updated energy budgets for neural computation in the neocortex and cerebellum', *J Cereb Blood Flow Metab*, 32: 1222-32.

Hoxha, E., F. Tempia, P. Lippiello, and M. C. Miniaci. 2016. 'Modulation, Plasticity and Pathophysiology of the Parallel Fiber-Purkinje Cell Synapse', *Front Synaptic Neurosci*, 8: 35.

Hsu, J. Y., Y. L. Jhang, P. H. Cheng, Y. F. Chang, S. H. Mao, H. I. Yang, C. W. Lin, C. M. Chen, and S. H. Yang. 2017. 'The Truncated C-terminal Fragment of Mutant ATXN3 Disrupts Mitochondria Dynamics in Spinocerebellar Ataxia Type 3 Models', *Front Mol Neurosci*, 10: 196.

Huang, C., S.J. Gammon, M. Dieterle, R.H. Huang, L. Lee, and R.E. Ricklefs. 2014. 'Dramatic increases in number of cerebellar granule-cell-Purkinje-cell synapses across several mammals', *Mammalian Biology*, 79: 163–69.

Hubens, W. H. G., A. Vallbona-Garcia, I. F. M. de Coo, F. H. J. van Tienen, C. A. B. Webers, H. J. M. Smeets, and Tgmf Gorgels. 2022. 'Blood biomarkers for assessment of mitochondrial dysfunction: An expert review', *Mitochondrion*, 62: 187-204.

Ikeuchi, T., H. Takano, R. Koide, Y. Horikawa, Y. Honma, Y. Onishi, S. Igarashi, H. Tanaka, N. Nakao, K. Sahashi, H. Tsukagoshi, K. Inoue, H. Takahashi, and S. Tsuji. 1997. 'Spinocerebellar ataxia type 6: CAG repeat expansion in alpha1A voltage-dependent calcium channel gene and clinical variations in Japanese population', *Ann Neurol*, 42: 879-84.

Inchauspe, C. G., F. J. Martini, I. D. Forsythe, and O. D. Uchitel. 2004. 'Functional compensation of P/Q by N-type channels blocks short-term plasticity at the calyx of Held presynaptic terminal', *J Neurosci*, 24: 10379-83.

Ingram, M., E. A. L. Wozniak, L. Duvick, R. Yang, P. Bergmann, R. Carson, B. O'Callaghan, H. Y. Zoghbi, C. Henzler, and H. T. Orr. 2016. 'Cerebellar Transcriptome Profiles of ATXN1 Transgenic Mice Reveal SCA1 Disease Progression and Protection Pathways', *Neuron*, 89: 1194-207.

Ishiguro, T., K. Ishikawa, M. Takahashi, M. Obayashi, T. Amino, N. Sato, M. Sakamoto, H. Fujigasaki, F. Tsuruta, R. Dolmetsch, T. Arai, H. Sasaki, K. Nagashima, T. Kato, M. Yamada, H. Takahashi, Y. Hashizume, and H. Mizusawa. 2010. 'The carboxy-terminal fragment of alpha(1A) calcium channel preferentially aggregates in the cytoplasm of human spinocerebellar ataxia type 6 Purkinje cells', *Acta Neuropathol*, 119: 447-64.

Ishikawa, K., K. Owada, K. Ishida, H. Fujigasaki, M. Shun Li, T. Tsunemi, N. Ohkoshi, S. Toru, T. Mizutani, M. Hayashi, N. Arai, K. Hasegawa, T. Kawanami, T. Kato, T. Makifuchi, S. Shoji, T. Tanabe, and H. Mizusawa. 2001. 'Cytoplasmic and nuclear polyglutamine aggregates in SCA6 Purkinje cells', *Neurology*, 56: 1753-6.

Ishikawa, K., H. Tanaka, M. Saito, N. Ohkoshi, T. Fujita, K. Yoshizawa, T. Ikeuchi, M. Watanabe, A. Hayashi, Y. Takiyama, M. Nishizawa, I. Nakano, K. Matsubayashi, M. Miwa, S. Shoji, I. Kanazawa, S. Tsuji, and H. Mizusawa. 1997. 'Japanese families with autosomal dominant pure cerebellar ataxia map to chromosome 19p13.1-p13.2 and are strongly associated with mild CAG expansions in the spinocerebellar ataxia type 6 gene in chromosome 19p13.1', *Am J Hum Genet*, 61: 336-46.

Ishikawa, K., M. Watanabe, K. Yoshizawa, T. Fujita, H. Iwamoto, T. Yoshizawa, K. Harada, K. Nakamagoe, Y. Komatsuzaki, A. Satoh, M. Doi, T. Ogata, I. Kanazawa, S. Shoji, and H. Mizusawa. 1999. 'Clinical, neuropathological, and molecular study in two families with spinocerebellar ataxia type 6 (SCA6)', *J Neurol Neurosurg Psychiatry*, 67: 86-9.

Isope, P., and B. Barbour. 2002. 'Properties of unitary granule cell-->Purkinje cell synapses in adult rat cerebellar slices', *J Neurosci*, 22: 9668-78.

Ito-Ishida, A., E. Miura, K. Emi, K. Matsuda, T. Iijima, T. Kondo, K. Kohda, M. Watanabe, and M. Yuzaki. 2008. 'Cbln1 regulates rapid formation and maintenance of excitatory synapses in mature cerebellar Purkinje cells in vitro and in vivo', *J Neurosci*, 28: 5920-30.

Iwata, M., A. Hirano, and J. H. French. 1979. 'Degeneration of the cerebellar system in X-chromosome-linked copper malabsorption', *Ann Neurol*, 5: 542-9.

Jacobi, H., P. Bauer, P. Giunti, R. Labrum, M. G. Sweeney, P. Charles, A. Durr, C. Marelli, C. Globas, C. Linnemann, L. Schols, M. Rakowicz, R. Rola, E. Zdzienicka, T. Schmitz-Hubsch, R. Fancellu, C. Mariotti, C. Tomasello, L. Baliko, B. Melegh, A. Filla, C. Rinaldi, B. P. van de Warrenburg, C. C. Verstappen, S. Szymanski, J. Berciano, J. Infante, D. Timmann, S. Boesch, S. Hering, C. Depondt, M. Pandolfo, J. S. Kang, S. Ratzka, J. Schulz, S. Tezenas du Montcel, and T. Klockgether. 2011. 'The natural history of spinocerebellar ataxia type 1, 2, 3, and 6: a 2-year follow-up study', *Neurology*, 77: 1035-41.

Jauslin, M. L., T. Meier, R. A. Smith, and M. P. Murphy. 2003a. 'Mitochondria-targeted antioxidants protect Friedreich Ataxia fibroblasts from endogenous oxidative stress more effectively than untargeted antioxidants', *FASEB J*, 17: 1972-4.

Jauslin, Matthias L., Thomas Meier, Robin A. J. Smith, and P. Michael Murphy. 2003b. 'Mitochondria-targeted antioxidants protect Friedreich Ataxia fibroblasts from endogenous oxidative stress more effectively than untargeted antioxidants', *The FASEB Journal*, 17: 1-10.

Jayabal, S., H. H. Chang, K. E. Cullen, and A. J. Watt. 2016. '4-aminopyridine reverses ataxia and cerebellar firing deficiency in a mouse model of spinocerebellar ataxia type 6', *Sci Rep*, 6: 29489.

Jayabal, S., L. Ljungberg, T. Erwes, A. Cormier, S. Quilez, S. El Jaouhari, and A. J. Watt. 2015. 'Rapid Onset of Motor Deficits in a Mouse Model of Spinocerebellar Ataxia Type 6 Precedes Late Cerebellar Degeneration', *eNeuro*, 2.

Jayabal, S., L. Ljungberg, and A. J. Watt. 2017. 'Transient cerebellar alterations during development prior to obvious motor phenotype in a mouse model of spinocerebellar ataxia type 6', *J Physiol*, 595: 949-66.

Jung, H., S. Y. Kim, F. S. Canbakis Cecen, Y. Cho, and S. K. Kwon. 2020. 'Dysfunction of Mitochondrial Ca(2+) Regulatory Machineries in Brain Aging and Neurodegenerative Diseases', *Front Cell Dev Biol*, 8: 599792.

Kakegawa, W., T. Miyazaki, K. Kohda, K. Matsuda, K. Emi, J. Motohashi, M. Watanabe, and M. Yuzaki. 2009. 'The N-terminal domain of GluD2 (GluRdelta2) recruits presynaptic terminals and regulates synaptogenesis in the cerebellum in vivo', *J Neurosci*, 29: 5738-48.

Kamarauskaite, J., R. Baniene, D. Trumbeckas, A. Strazdauskas, and S. Trumbeckaite. 2020. 'Increased Succinate Accumulation Induces ROS Generation in In Vivo Ischemia/Reperfusion-Affected Rat Kidney Mitochondria', *Biomed Res Int*, 2020: 8855585.

Kasumu, A., and I. Bezprozvanny. 2012. 'Deranged calcium signaling in Purkinje cells and pathogenesis in spinocerebellar ataxia 2 (SCA2) and other ataxias', *Cerebellum*, 11: 630-9.

Keller, J. L., and A. J. Bastian. 2014. 'A home balance exercise program improves walking in people with cerebellar ataxia', *Neurorehabil Neural Repair*, 28: 770-8.

Kim, D., J. M. Paggi, C. Park, C. Bennett, and S. L. Salzberg. 2019. 'Graph-based genome alignment and genotyping with HISAT2 and HISAT-genotype', *Nat Biotechnol*, 37: 907-15.

Konig, J., C. Ott, M. Hugo, T. Jung, A. L. Bulteau, T. Grune, and A. Hohn. 2017. 'Mitochondrial contribution to lipofuscin formation', *Redox Biol*, 11: 673-81.

Kordasiewicz, H. B., R. M. Thompson, H. B. Clark, and C. M. Gomez. 2006. 'C-termini of P/Q-type Ca2+ channel alpha1A subunits translocate to nuclei and promote polyglutamine-mediated toxicity', *Hum Mol Genet*, 15: 1587-99.

Kozareva, V., C. Martin, T. Osorno, S. Rudolph, C. Guo, C. Vanderburg, N. Nadaf, A. Regev, W. G. Regehr, and E. Macosko. 2021. 'A transcriptomic atlas of mouse cerebellar cortex comprehensively defines cell types', *Nature*, 598: 214-19.

Kristensen, L. V., F. S. Oppermann, M. J. Rauen, K. Fog, T. Schmidt, J. Schmidt, T. Harmuth, R. Hartmann-Petersen, and K. Thirstrup. 2018. 'Mass spectrometry analyses of normal and polyglutamine expanded ataxin-3 reveal novel interaction partners involved in mitochondrial function', *Neurochem Int*, 112: 5-17.

Lang-Ouellette, D., K. M. Gruver, A. Smith-Dijak, F. G. C. Blot, C. A. Stewart, P. de Vanssay de Blavous, C. H. Li, C. Van Eitrem, C. Rosen, P. L. Faust, M. Schonewille, and A. J. Watt. 2021. 'Purkinje cell axonal swellings enhance action potential fidelity and cerebellar function', *Nat Commun*, 12: 4129.

Lee, A., S. T. Wong, D. Gallagher, B. Li, D. R. Storm, T. Scheuer, and W. A. Catterall. 1999. 'Ca2+/calmodulin binds to and modulates P/Q-type calcium channels', *Nature*, 399: 155-9.

Leung, Tsz Chui Sophia, Eviatar Fields, Namrata Rana, Ru Yi Louisa Shen, Alexandra E. Bernstein, Anna A. Cook, Daniel E. Phillips, and Alanna J. Watt. 2024. 'Mitochondrial damage and impaired mitophagy contribute to disease progression in SCA6', *Acta Neuropathologica*, 147: 26.

Lezi, E., and R. H. Swerdlow. 2012. 'Mitochondria in neurodegeneration', *Adv Exp Med Biol*, 942: 269-86.

Li, X., Y. Yang, B. Zhang, X. Lin, X. Fu, Y. An, Y. Zou, J. X. Wang, Z. Wang, and T. Yu. 2022. 'Lactate metabolism in human health and disease', *Signal Transduct Target Ther*, 7: 305.
Lieberman, A. P., V. G. Shakkottai, and R. L. Albin. 2019. 'Polyglutamine Repeats in Neurodegenerative Diseases', *Annu Rev Pathol*, 14: 1-27.
Lin, M. T., and M. F. Beal. 2006. 'Mitochondrial dysfunction and oxidative stress in neurodegenerative diseases', *Nature*, 443: 787-95.
Liu, F., J. Lu, A. Manaenko, J. Tang, and Q. Hu. 2018. 'Mitochondria in Ischemic Stroke: New Insight and Implications', *Aging Dis*, 9: 924-37.
Love, M. I., W. Huber, and S. Anders. 2014. 'Moderated estimation of fold change and dispersion for RNA-seq data with DESeq2', *Genome Biol*, 15: 550.
Lu, Y. T., L. Z. Li, Y. L. Yang, X. Yin, Q. Liu, L. Zhang, K. Liu, B. Liu, J. Li, and L. W. Qi. 2018. 'Succinate induces aberrant mitochondrial fission in cardiomyocytes through GPR91 signaling', *Cell Death Dis*, 9: 672.
Maier, T., M. Guell, and L. Serrano. 2009. 'Correlation of mRNA and protein in complex biological samples', *FEBS Lett*, 583: 3966-73.
Maltecca, F., R. Magnoni, F. Cerri, G. A. Cox, A. Quattrini, and G. Casari. 2009. 'Haploinsufficiency of AFG3L2, the gene responsible for spinocerebellar ataxia type 28, causes mitochondria-mediated Purkinje cell dark degeneration', *J Neurosci*, 29: 9244-54.
Mancini, C., E. Hoxha, L. Iommarini, A. Brussino, U. Richter, F. Montarolo, C. Cagnoli, R. Parolisi, D. I. Gondor Morosini, V. Nicolo, F. Maltecca, L. Muratori, G. Ronchi, S. Geuna, F. Arnaboldi, E. Donetti, E. Giorgio, S. Cavalieri, E. Di Gregorio, E. Pozzi, M. Ferrero, E. Riberi, G. Casari, F. Altruda, E. Turco, G. Gasparre, B. J. Battersby, A. M. Porcelli, E. Ferrero, A. Brusco, and F. Tempia. 2019. 'Mice harbouring a SCA28 patient mutation in AFG3L2 develop late-onset ataxia associated with enhanced mitochondrial proteotoxicity', *Neurobiol Dis*, 124: 14-28.
Manolaras, I., A. Del Bondio, O. Griso, L. Reutenauer, A. Eisenmann, B. H. Habermann, and H. Puccio. 2023. 'Mitochondrial dysfunction and calcium dysregulation in COQ8A-ataxia Purkinje neurons are rescued by CoQ10 treatment', *Brain*, 146: 3836-50.
Mark, M. D., M. Krause, H. J. Boele, W. Kruse, S. Pollok, T. Kuner, D. Dalkara, S. Koekkoek, C. I. De Zeeuw, and S. Herlitze. 2015. 'Spinocerebellar ataxia type 6 protein aggregates cause deficits in motor learning and cerebellar plasticity', *J Neurosci*, 35: 8882-95.
Markaki, M., and N. Tavernarakis. 2020. 'Mitochondrial turnover and homeostasis in ageing and neurodegeneration', *FEBS Lett*, 594: 2370-79.
Marquez, B. T., T. C. S. Leung, J. Hui, F. Charron, R. A. McKinney, and A. J. Watt. 2023. 'A mitochondrial-targeted antioxidant (MitoQ) improves motor coordination and reduces Purkinje cell death in a mouse model of ARSACS', *Neurobiol Dis*, 183: 106157.
Martin, K. B., I. M. Williams, C. V. Cluzeau, A. Cougnoux, R. K. Dale, J. R. Iben, N. X. Cawley, C. A. Wassif, and F. D. Porter. 2019. 'Identification of Novel Pathways Associated with Patterned Cerebellar Purkinje Neuron Degeneration in Niemann-Pick Disease, Type C1', *Int J Mol Sci*, 21.
Massudi, H., R. Grant, N. Braidy, J. Guest, B. Farnsworth, and G. J. Guillemin. 2012. 'Age-associated changes in oxidative stress and NAD+ metabolism in human tissue', *PLoS One*, 7: e42357.
Matsuyama, Z., M. Wakamori, Y. Mori, H. Kawakami, S. Nakamura, and K. Imoto. 1999. 'Direct alteration of the P/Q-type Ca2+ channel property by polyglutamine expansion in spinocerebellar ataxia 6', *J Neurosci*, 19: RC14.
Minakawa, E. N., and Y. Nagai. 2021. 'Protein Aggregation Inhibitors as Disease-Modifying Therapies for Polyglutamine Diseases', *Front Neurosci*, 15: 621996.
Mishra, E., and M. K. Thakur. 2023. 'Mitophagy: A promising therapeutic target for neuroprotection during ageing and age-related diseases', *Br J Pharmacol*, 180: 1542-61.

Miyai, I., M. Ito, N. Hattori, M. Mihara, M. Hatakenaka, H. Yagura, G. Sobue, M. Nishizawa, and Collaboration Cerebellar Ataxia Rehabilitation Trialists. 2012. 'Cerebellar ataxia rehabilitation trial in degenerative cerebellar diseases', *Neurorehabil Neural Repair*, 26: 515-22.

Moriarty, A., A. Cook, H. Hunt, M. E. Adams, L. Cipolotti, and P. Giunti. 2016. 'A longitudinal investigation into cognition and disease progression in spinocerebellar ataxia types 1, 2, 3, 6, and 7', *Orphanet J Rare Dis*, 11: 82.

Murphy, M. P. 2013. 'Mitochondrial dysfunction indirectly elevates ROS production by the endoplasmic reticulum', *Cell Metab*, 18: 145-6.

Murphy, M. P., and R. C. Hartley. 2018. 'Mitochondria as a therapeutic target for common pathologies', *Nat Rev Drug Discov*, 17: 865-86.

Nakamura, K., K. Yoshida, D. Miyazaki, H. Morita, and S. Ikeda. 2009. 'Spinocerebellar ataxia type 6 (SCA6): clinical pilot trial with gabapentin', *J Neurol Sci*, 278: 107-11.

Niewiadomska-Cimicka, A., F. Doussau, J. B. Perot, M. J. Roux, C. Keime, A. Hache, F. Piguet, A. Novati, C. Weber, B. Yalcin, H. Meziane, M. F. Champy, E. Grandgirard, A. Karam, N. Messaddeq, A. Eisenmann, E. Brouillet, H. H. P. Nguyen, J. Flament, P. Isope, and Y. Trottier. 2021. 'SCA7 Mouse Cerebellar Pathology Reveals Preferential Downregulation of Key Purkinje Cell-Identity Genes and Shared Disease Signature with SCA1 and SCA2', *J Neurosci*, 41: 4910-36.

Nigri, A., L. Sarro, A. Mongelli, A. Castaldo, L. Porcu, C. Pinardi, M. Grisoli, S. Ferraro, L. Canafoglia, E. Visani, M. G. Bruzzone, L. Nanetti, F. Taroni, and C. Mariotti. 2022. 'Spinocerebellar Ataxia Type 1: One-Year Longitudinal Study to Identify Clinical and MRI Measures of Disease Progression in Patients and Presymptomatic Carriers', *Cerebellum*, 21: 133-44.

Nishizawa, M., O. Onodera, A. Hirakawa, Y. Shimizu, M. Yamada, and Group Rovatirelin Study. 2020. 'Effect of rovatirelin in patients with cerebellar ataxia: two randomised double-blind placebo-controlled phase 3 trials', *J Neurol Neurosurg Psychiatry*, 91: 254-62.

Pandya, V. A., and R. Patani. 2021. 'Region-specific vulnerability in neurodegeneration: lessons from normal ageing', *Ageing Res Rev*, 67: 101311.

Pastor, P. D. H., X. Du, S. Fazal, A. N. Davies, and C. M. Gomez. 2018. 'Targeting the CACNA1A IRES as a Treatment for Spinocerebellar Ataxia Type 6', *Cerebellum*, 17: 72-77.

Paukert, M., Y. H. Huang, K. Tanaka, J. D. Rothstein, and D. E. Bergles. 2010. 'Zones of enhanced glutamate release from climbing fibers in the mammalian cerebellum', *J Neurosci*, 30: 7290-9.

Penner, I. K., and F. Paul. 2017. 'Fatigue as a symptom or comorbidity of neurological diseases', *Nat Rev Neurol*, 13: 662-75.

Perkins, E. M., Y. L. Clarkson, N. Sabatier, D. M. Longhurst, C. P. Millward, J. Jack, J. Toraiwa, M. Watanabe, J. D. Rothstein, A. R. Lyndon, D. J. Wyllie, M. B. Dutia, and M. Jackson. 2010. 'Loss of beta-III spectrin leads to Purkinje cell dysfunction recapitulating the behavior and neuropathology of spinocerebellar ataxia type 5 in humans', *J Neurosci*, 30: 4857-67.

Perkins, E. M., Y. L. Clarkson, D. Suminaite, A. R. Lyndon, K. Tanaka, J. D. Rothstein, P. A. Skehel, D. J. A. Wyllie, and M. Jackson. 2018. 'Loss of cerebellar glutamate transporters EAAT4 and GLAST differentially affects the spontaneous firing pattern and survival of Purkinje cells', *Hum Mol Genet*, 27: 2614-27.

Perkins, E. M., D. Suminaite, Y. L. Clarkson, S. K. Lee, A. R. Lyndon, J. D. Rothstein, D. J. Wyllie, K. Tanaka, and M. Jackson. 2016. 'Posterior cerebellar Purkinje cells in an SCA5/SPARCA1 mouse model are especially vulnerable to the synergistic effect of loss of beta-III spectrin and GLAST', *Hum Mol Genet*, 25: 4448-61.

Perlman, S. 1993. 'Hereditary Ataxia Overview.' in M. P. Adam, J. Feldman, G. M. Mirzaa, R. A. Pagon, S. E. Wallace, L. J. H. Bean, K. W. Gripp and A. Amemiya (eds.), *GeneReviews((R))* (Seattle (WA)).

Person, A. L., and I. M. Raman. 2011. 'Purkinje neuron synchrony elicits time-locked spiking in the cerebellar nuclei', *Nature*, 481: 502-5.

Piedras-Renteria, E. S., K. Watase, N. Harata, O. Zhuchenko, H. Y. Zoghbi, C. C. Lee, and R. W. Tsien. 2001. 'Increased expression of alpha 1A Ca2+ channel currents arising from expanded trinucleotide repeats in spinocerebellar ataxia type 6', *J Neurosci*, 21: 9185-93.

Pilotto, F., C. Douthwaite, R. Diab, X. Ye, Z. Al Qassab, C. Tietje, M. Mounassir, A. Odriozola, A. Thapa, R. A. M. Buijsen, S. Lagache, A. C. Uldry, M. Heller, S. Muller, W. M. C. van Roon-Mom, B. Zuber, S. Liebscher, and S. Saxena. 2023. 'Early molecular layer interneuron hyperactivity triggers Purkinje neuron degeneration in SCA1', *Neuron*, 111: 2523-43 e10.

Poetschke, C., E. Dragicevic, J. Duda, J. Benkert, A. Dougalis, R. DeZio, T. P. Snutch, J. Striessnig, and B. Liss. 2015. 'Compensatory T-type Ca2+ channel activity alters D2-autoreceptor responses of Substantia nigra dopamine neurons from Cav1.3 L-type Ca2+ channel KO mice', *Sci Rep*, 5: 13688.

Raman, I. M., and B. P. Bean. 1999. 'Ionic currents underlying spontaneous action potentials in isolated cerebellar Purkinje neurons', *J Neurosci*, 19: 1663-74.

Raudvere, U., L. Kolberg, I. Kuzmin, T. Arak, P. Adler, H. Peterson, and J. Vilo. 2019. 'g:Profiler: a web server for functional enrichment analysis and conversions of gene lists (2019 update)', *Nucleic Acids Res*, 47: W191-W98.

Reeber, S. L., J. J. White, N. A. George-Jones, and R. V. Sillitoe. 2012. 'Architecture and development of olivocerebellar circuit topography', *Front Neural Circuits*, 6: 115.

Reeg, S., and T. Grune. 2015. 'Protein Oxidation in Aging: Does It Play a Role in Aging Progression?', *Antioxid Redox Signal*, 23: 239-55.

Robinson, K. J., M. Watchon, and A. S. Laird. 2020. 'Aberrant Cerebellar Circuitry in the Spinocerebellar Ataxias', *Front Neurosci*, 14: 707.

Robitaille, Y., L. Schut, and S. J. Kish. 1995. 'Structural and immunocytochemical features of olivopontocerebellar atrophy caused by the spinocerebellar ataxia type 1 (SCA-1) mutation define a unique phenotype', *Acta Neuropathol*, 90: 572-81.

Rodriques, S. G., R. R. Stickels, A. Goeva, C. A. Martin, E. Murray, C. R. Vanderburg, J. Welch, L. M. Chen, F. Chen, and E. Z. Macosko. 2019. 'Slide-seq: A scalable technology for measuring genome-wide expression at high spatial resolution', *Science*, 363: 1463-67.

Rueden, C. T., J. Schindelin, M. C. Hiner, B. E. DeZonia, A. E. Walter, E. T. Arena, and K. W. Eliceiri. 2017. 'ImageJ2: ImageJ for the next generation of scientific image data', *BMC Bioinformatics*, 18: 529.

Ruggiero, A., M. Katsenelson, and I. Slutsky. 2021. 'Mitochondria: new players in homeostatic regulation of firing rate set points', *Trends Neurosci*, 44: 605-18.

Russo, M. S. T., A. Napylov, A. Paquet, and D. Vuckovic. 2020. 'Comparison of N-ethyl maleimide and N-(1-phenylethyl) maleimide for derivatization of biological thiols using liquid chromatography-mass spectrometry', *Anal Bioanal Chem*, 412: 1639-52.

Ryan, K. C., Z. Ashkavand, and K. R. Norman. 2020. 'The Role of Mitochondrial Calcium Homeostasis in Alzheimer's and Related Diseases', *Int J Mol Sci*, 21.

Saegusa, H., M. Wakamori, Y. Matsuda, J. Wang, Y. Mori, S. Zong, and T. Tanabe. 2007. 'Properties of human Cav2.1 channel with a spinocerebellar ataxia type 6 mutation expressed in Purkinje cells', *Mol Cell Neurosci*, 34: 261-70.

Sarna, J., S. R. Miranda, E. H. Schuchman, and R. Hawkes. 2001. 'Patterned cerebellar Purkinje cell death in a transgenic mouse model of Niemann Pick type A/B disease', *Eur J Neurosci*, 13: 1873-80.

Sarna, J. R., and R. Hawkes. 2003. 'Patterned Purkinje cell death in the cerebellum', *Prog Neurobiol*, 70: 473-507.

Sasaki, H., H. Kojima, I. Yabe, K. Tashiro, T. Hamada, H. Sawa, H. Hiraga, and K. Nagashima. 1998. 'Neuropathological and molecular studies of spinocerebellar ataxia type 6 (SCA6)', *Acta Neuropathol*, 95: 199-204.

Sawada, K., Y. Fukui, and R. Hawkes. 2008. 'Spatial distribution of corticotropin-releasing factor immunopositive climbing fibers in the mouse cerebellum: analysis by whole mount immunohistochemistry', *Brain Res*, 1222: 106-17.

Scherz-Shouval, R., H. Weidberg, C. Gonen, S. Wilder, Z. Elazar, and M. Oren. 2010. 'p53-dependent regulation of autophagy protein LC3 supports cancer cell survival under prolonged starvation', *Proc Natl Acad Sci U S A*, 107: 18511-6.

Schindelin, J., I. Arganda-Carreras, E. Frise, V. Kaynig, M. Longair, T. Pietzsch, S. Preibisch, C. Rueden, S. Saalfeld, B. Schmid, J. Y. Tinevez, D. J. White, V. Hartenstein, K. Eliceiri, P. Tomancak, and A. Cardona. 2012. 'Fiji: an open-source platform for biological-image analysis', *Nat Methods*, 9: 676-82.

Scholefield, M., S. J. Church, J. Xu, A. C. Robinson, N. J. Gardiner, F. Roncaroli, N. M. Hooper, R. D. Unwin, and G. J. S. Cooper. 2020. 'Effects of Alterations of Post-Mortem Delay and Other Tissue-Collection Variables on Metabolite Levels in Human and Rat Brain', *Metabolites*, 10.

Schols, L., R. Kruger, G. Amoiridis, H. Przuntek, J. T. Epplen, and O. Riess. 1998. 'Spinocerebellar ataxia type 6: genotype and phenotype in German kindreds', *J Neurol Neurosurg Psychiatry*, 64: 67-73.

Shao, J., and M. I. Diamond. 2007. 'Polyglutamine diseases: emerging concepts in pathogenesis and therapy', *Hum Mol Genet*, 16 Spec No. 2: R115-23.

Shuvaev, A. N., N. Hosoi, Y. Sato, D. Yanagihara, and H. Hirai. 2017. 'Progressive impairment of cerebellar mGluR signalling and its therapeutic potential for cerebellar ataxia in spinocerebellar ataxia type 1 model mice', *J Physiol*, 595: 141-64.

Sillitoe, R. V., and R. Hawkes. 2002. 'Whole-mount immunohistochemistry: a high-throughput screen for patterning defects in the mouse cerebellum', *J Histochem Cytochem*, 50: 235-44.

Sinke, R. J., E. F. Ippel, C. M. Diepstraten, F. A. Beemer, J. H. Wokke, B. J. van Hilten, N. V. Knoers, H. K. van Amstel, and H. P. Kremer. 2001. 'Clinical and molecular correlations in spinocerebellar ataxia type 6: a study of 24 Dutch families', *Arch Neurol*, 58: 1839-44.

Slemmer, J. E., E. D. Haasdijk, D. C. Engel, N. Plesnila, and J. T. Weber. 2007. 'Aldolase C-positive cerebellar Purkinje cells are resistant to delayed death after cerebral trauma and AMPA-mediated excitotoxicity', *Eur J Neurosci*, 26: 649-56.

Solesio, M. E., T. A. Prime, A. Logan, M. P. Murphy, M. Del Mar Arroyo-Jimenez, J. Jordan, and M. F. Galindo. 2013. 'The mitochondria-targeted anti-oxidant MitoQ reduces aspects of mitochondrial fission in the 6-OHDA cell model of Parkinson's disease', *Biochim Biophys Acta*, 1832: 174-82.

Solodkin, A., and C. M. Gomez. 2012. 'Spinocerebellar ataxia type 6', *Handb Clin Neurol*, 103: 461-73.

Srivastava, S. 2016. 'Emerging therapeutic roles for NAD(+) metabolism in mitochondrial and age-related disorders', *Clin Transl Med*, 5: 25.

Statsenko, Y., N. V. Kuznetsov, D. Morozova, K. Liaonchyk, G. L. Simiyu, D. Smetanina, A. Kashapov, S. Meribout, K. N. Gorkom, R. Hamoudi, F. Ismail, S. A. Ansari, B. S. Emerald, and M. Ljubisavljevic. 2023. 'Reappraisal of the Concept of Accelerated Aging in Neurodegeneration and Beyond', *Cells*, 12.

Stoyas, C. A., D. D. Bushart, P. M. Switonski, J. M. Ward, A. Alaghatta, M. B. Tang, C. Niu, M. Wadhwa, H. Huang, A. Savchenko, K. Gariani, F. Xie, J. R. Delaney, T. Gaasterland, J. Auwerx, V. G. Shakkottai, and A. R. La Spada. 2020. 'Nicotinamide Pathway-Dependent Sirt1 Activation Restores Calcium Homeostasis to Achieve Neuroprotection in Spinocerebellar Ataxia Type 7', *Neuron*, 105: 630-44 e9.

Stromme, P., K. Dobrenis, R. V. Sillitoe, M. Gulinello, N. F. Ali, C. Davidson, M. C. Micsenyi, G. Stephney, L. Ellevog, A. Klungland, and S. U. Walkley. 2011. 'X-linked Angelman-like syndrome caused by Slc9a6 knockout in mice exhibits evidence of endosomal-lysosomal dysfunction', *Brain*, 134: 3369-83.

Stucki, D. M., C. Ruegsegger, S. Steiner, J. Radecke, M. P. Murphy, B. Zuber, and S. Saxena. 2016. 'Mitochondrial impairments contribute to Spinocerebellar ataxia type 1 progression and can be ameliorated by the mitochondria-targeted antioxidant MitoQ', *Free Radic Biol Med*, 97: 427-40.

Styr, B., N. Gonen, D. Zarhin, A. Ruggiero, R. Atsmon, N. Gazit, G. Braun, S. Frere, I. Vertkin, I. Shapira, M. Harel, L. R. Heim, M. Katsenelson, O. Rechnitz, S. Fadila, D. Derdikman, M. Rubinstein, T. Geiger, E. Ruppin, and I. Slutsky. 2019. 'Mitochondrial Regulation of the Hippocampal Firing Rate Set Point and Seizure Susceptibility', *Neuron*, 102: 1009-24 e8.

Sucha, M., S. Benediktova, F. Tichanek, J. Jedlicka, S. Kapl, D. Jelinkova, Z. Purkartova, J. Tuma, J. Kuncova, and J. Cendelin. 2023. 'Experimental Treatment with Edaravone in a Mouse Model of Spinocerebellar Ataxia 1', *Int J Mol Sci*, 24.

Sulzer, D., E. Mosharov, Z. Talloczy, F. A. Zucca, J. D. Simon, and L. Zecca. 2008. 'Neuronal pigmented autophagic vacuoles: lipofuscin, neuromelanin, and ceroid as macroautophagic responses during aging and disease', *J Neurochem*, 106: 24-36.

Suski, J. M., M. Lebiedzinska, M. Bonora, P. Pinton, J. Duszynski, and M. R. Wieckowski. 2012. 'Relation between mitochondrial membrane potential and ROS formation', *Methods Mol Biol*, 810: 183-205.

Takahashi, H., T. Ikeuchi, Y. Honma, S. Hayashi, and S. Tsuji. 1998. 'Autosomal dominant cerebellar ataxia (SCA6): clinical, genetic and neuropathological study in a family', *Acta Neuropathol*, 95: 333-7.

Takahashi, H., K. Ishikawa, T. Tsutsumi, H. Fujigasaki, A. Kawata, R. Okiyama, T. Fujita, K. Yoshizawa, S. Yamaguchi, H. Tomiyasu, F. Yoshii, K. Mitani, N. Shimizu, M. Yamazaki, T. Miyamoto, T. Orimo, S. Shoji, K. Kitamura, and H. Mizusawa. 2004. 'A clinical and genetic study in a large cohort of patients with spinocerebellar ataxia type 6', *J Hum Genet*, 49: 256-64.

Takei, A., S. Hamada, S. Homma, K. Hamada, K. Tashiro, and T. Hamada. 2010. 'Difference in the effects of tandospirone on ataxia in various types of spinocerebellar degeneration: an open-label study', *Cerebellum*, 9: 567-70.

Tao-Cheng, J. H. 2018. 'Stimulation-induced structural changes at the nucleus, endoplasmic reticulum and mitochondria of hippocampal neurons', *Mol Brain*, 11: 44.

Tezenas du Montcel, S., A. Durr, M. Rakowicz, L. Nanetti, P. Charles, A. Sulek, C. Mariotti, R. Rola, L. Schols, P. Bauer, I. Dufaure-Gare, H. Jacobi, S. Forlani, T. Schmitz-Hubsch, A. Filla, D. Timmann, B. P. van de Warrenburg, C. Marelli, J. S. Kang, P. Giunti, A. Cook, L. Baliko, B. Melegh, S. Boesch, S. Szymanski, J. Berciano, J. Infante, K. Buerk, M. Masciullo, R. Di Fabio, C. Depondt, S. Ratka, G. Stevanin, T. Klockgether, A. Brice, and J. L. Golmard. 2014. 'Prediction of the age at onset in spinocerebellar ataxia type 1, 2, 3 and 6', *J Med Genet*, 51: 479-86.

Thier, P., P. W. Dicke, R. Haas, and S. Barash. 2000. 'Encoding of movement time by populations of cerebellar Purkinje cells', *Nature*, 405: 72-6.

Thompson Legault, J., L. Strittmatter, J. Tardif, R. Sharma, V. Tremblay-Vaillancourt, C. Aubut, G. Boucher, C. B. Clish, D. Cyr, C. Daneault, P. J. Waters, Lsfc Consortium, L. Vachon, C. Morin, C. Laprise, J. D. Rioux, V. K. Mootha, and C. Des Rosiers. 2015. 'A Metabolic Signature of Mitochondrial Dysfunction Revealed through a Monogenic Form of Leigh Syndrome', *Cell Rep*, 13: 981-9.

Todorov, B., L. Kros, R. Shyti, P. Plak, E. D. Haasdijk, R. S. Raike, R. R. Frants, E. J. Hess, F. E. Hoebeek, C. I. De Zeeuw, and A. M. van den Maagdenberg. 2012. 'Purkinje cell-specific ablation of Cav2.1 channels is sufficient to cause cerebellar ataxia in mice', *Cerebellum*, 11: 246-58.

Toru, S., T. Murakoshi, K. Ishikawa, H. Saegusa, H. Fujigasaki, T. Uchihara, S. Nagayama, M. Osanai, H. Mizusawa, and T. Tanabe. 2000. 'Spinocerebellar ataxia type 6 mutation alters P-type calcium channel function', *J Biol Chem*, 275: 10893-8.

Toscano Marquez, B., A. A. Cook, M. Rice, A. Smileski, K. Vieira-Lomasney, F. Charron, R. A. McKinney, and A. J. Watt. 2021. 'Molecular Identity and Location Influence Purkinje Cell Vulnerability in

Autosomal-Recessive Spastic Ataxia of Charlevoix-Saguenay Mice', *Front Cell Neurosci*, 15: 707857.
Tretter, L., and V. Adam-Vizi. 2000. 'Inhibition of Krebs cycle enzymes by hydrogen peroxide: A key role of [alpha]-ketoglutarate dehydrogenase in limiting NADH production under oxidative stress', *J Neurosci*, 20: 8972-9.
Tsou, W. L., B. W. Soong, H. L. Paulson, and E. Rodriguez-Lebron. 2011. 'Splice isoform-specific suppression of the Cav2.1 variant underlying spinocerebellar ataxia type 6', *Neurobiol Dis*, 43: 533-42.
Tsuchiya, K., T. Oda, M. Yoshida, H. Sasaki, C. Haga, H. Okino, I. Tominaga, K. Matsui, H. Akiyama, and Y. Hashizume. 2005. 'Degeneration of the inferior olive in spinocerebellar ataxia 6 may depend on disease duration: report of two autopsy cases and statistical analysis of autopsy cases reported to date', *Neuropathology*, 25: 125-35.
Ueno, T., H. Nishizawa, C. Suzuki, J. I. Nunomura, and M. Tomiyama. 2017. 'Downbeat nystagmus as an initial clinical sign in spinocerebellar ataxia type 6', *Neurol Sci*, 38: 1543-45.
Uittenbogaard, M., and A. Chiaramello. 2014. 'Mitochondrial biogenesis: a therapeutic target for neurodevelopmental disorders and neurodegenerative diseases', *Curr Pharm Des*, 20: 5574-93.
Unno, T., M. Wakamori, M. Koike, Y. Uchiyama, K. Ishikawa, H. Kubota, T. Yoshida, H. Sasakawa, C. Peters, H. Mizusawa, and K. Watase. 2012. 'Development of Purkinje cell degeneration in a knockin mouse model reveals lysosomal involvement in the pathogenesis of SCA6', *Proc Natl Acad Sci U S A*, 109: 17693-8.
Valavanidis, A., T. Vlachogianni, and C. Fiotakis. 2009. '8-hydroxy-2' -deoxyguanosine (8-OHdG): A critical biomarker of oxidative stress and carcinogenesis', *J Environ Sci Health C Environ Carcinog Ecotoxicol Rev*, 27: 120-39.
Virmani, M. A., and M. Cirulli. 2022. 'The Role of l-Carnitine in Mitochondria, Prevention of Metabolic Inflexibility and Disease Initiation', *Int J Mol Sci*, 23.
Vos, M., E. Lauwers, and P. Verstreken. 2010. 'Synaptic mitochondria in synaptic transmission and organization of vesicle pools in health and disease', *Front Synaptic Neurosci*, 2: 139.
Wang, D., S. Honda, M. K. Shin, K. Watase, H. Mizusawa, K. Ishikawa, and S. Shimizu. 2024. 'Subcellular localization and ER-mediated cytotoxic function of alpha1A and alpha1ACT in spinocerebellar ataxia type 6', *Biochem Biophys Res Commun*, 695: 149481.
Wang, X., G. Chen, W. Gao, and T. J. Ebner. 2011. 'Parasagittally aligned, mGluR1-dependent patches are evoked at long latencies by parallel fiber stimulation in the mouse cerebellar cortex in vivo', *J Neurophysiol*, 105: 1732-46.
Wang, X., and E. K. Michaelis. 2010. 'Selective neuronal vulnerability to oxidative stress in the brain', *Front Aging Neurosci*, 2: 12.
Ward, J. M., C. A. Stoyas, P. M. Switonski, F. Ichou, W. Fan, B. Collins, C. E. Wall, I. Adanyeguh, C. Niu, B. L. Sopher, C. Kinoshita, R. S. Morrison, A. Durr, A. R. Muotri, R. M. Evans, F. Mochel, and A. R. La Spada. 2019. 'Metabolic and Organelle Morphology Defects in Mice and Human Patients Define Spinocerebellar Ataxia Type 7 as a Mitochondrial Disease', *Cell Rep*, 26: 1189-202 e6.
Watase, K., C. F. Barrett, T. Miyazaki, T. Ishiguro, K. Ishikawa, Y. Hu, T. Unno, Y. Sun, S. Kasai, M. Watanabe, C. M. Gomez, H. Mizusawa, R. W. Tsien, and H. Y. Zoghbi. 2008. 'Spinocerebellar ataxia type 6 knockin mice develop a progressive neuronal dysfunction with age-dependent accumulation of mutant CaV2.1 channels', *Proc Natl Acad Sci U S A*, 105: 11987-92.
Westenbroek, R. E., T. Sakurai, E. M. Elliott, J. W. Hell, T. V. Starr, T. P. Snutch, and W. A. Catterall. 1995. 'Immunochemical identification and subcellular distribution of the alpha 1A subunits of brain calcium channels', *J Neurosci*, 15: 6403-18.
White, J. J., L. W. J. Bosman, F. G. C. Blot, C. Osorio, B. W. Kuppens, Whjj Krijnen, C. Andriessen, C. I. De Zeeuw, D. Jaarsma, and M. Schonewille. 2021. 'Region-specific preservation of Purkinje cell

morphology and motor behavior in the ATXN1[82Q] mouse model of spinocerebellar ataxia 1', *Brain Pathol*: e12946.

Xie, N., L. Zhang, W. Gao, C. Huang, P. E. Huber, X. Zhou, C. Li, G. Shen, and B. Zou. 2020. 'NAD(+) metabolism: pathophysiologic mechanisms and therapeutic potential', *Signal Transduct Target Ther*, 5: 227.

Xu, J., W. Du, Y. Zhao, K. Lim, L. Lu, C. Zhang, and L. Li. 2022. 'Mitochondria targeting drugs for neurodegenerative diseases-Design, mechanism and application', *Acta Pharm Sin B*, 12: 2778-89.

Xu, M., Q. Ouyang, J. Gong, M. F. Pescosolido, B. S. Pruett, S. Mishra, M. Schmidt, R. N. Jones, E. D. Gamsiz Uzun, S. B. Lizarraga, and E. M. Morrow. 2017. 'Mixed Neurodevelopmental and Neurodegenerative Pathology in Nhe6-Null Mouse Model of Christianson Syndrome', *eNeuro*, 4.

Yabe, I., H. Sasaki, I. Yamashita, A. Takei, and K. Tashiro. 2001. 'Clinical trial of acetazolamide in SCA6, with assessment using the Ataxia Rating Scale and body stabilometry', *Acta Neurol Scand*, 104: 44-7.

Yang, B., X. Dan, Y. Hou, J. H. Lee, N. Wechter, S. Krishnamurthy, R. Kimura, M. Babbar, T. Demarest, R. McDevitt, S. Zhang, Y. Zhang, M. P. Mattson, D. L. Croteau, and V. A. Bohr. 2021. 'NAD(+) supplementation prevents STING-induced senescence in ataxia telangiectasia by improving mitophagy', *Aging Cell*, 20: e13329.

Yang, Q., Y. Hashizume, M. Yoshida, Y. Wang, Y. Goto, N. Mitsuma, K. Ishikawa, and H. Mizusawa. 2000. 'Morphological Purkinje cell changes in spinocerebellar ataxia type 6', *Acta Neuropathol*, 100: 371-6.

Zeviani, M., A. Simonati, and L. A. Bindoff. 2012. 'Ataxia in mitochondrial disorders', *Handb Clin Neurol*, 103: 359-72.

Zhang, Y., M. Zhang, W. Zhu, J. Yu, Q. Wang, J. Zhang, Y. Cui, X. Pan, X. Gao, and H. Sun. 2020. 'Succinate accumulation induces mitochondrial reactive oxygen species generation and promotes status epilepticus in the kainic acid rat model', *Redox Biol*, 28: 101365.

Zhou, H., Z. Lin, K. Voges, C. Ju, Z. Gao, L. W. Bosman, T. J. Ruigrok, F. E. Hoebeek, C. I. De Zeeuw, and M. Schonewille. 2014. 'Cerebellar modules operate at different frequencies', *Elife*, 3: e02536.

Zhuchenko, O., J. Bailey, P. Bonnen, T. Ashizawa, D. W. Stockton, C. Amos, W. B. Dobyns, S. H. Subramony, H. Y. Zoghbi, and C. C. Lee. 1997. 'Autosomal dominant cerebellar ataxia (SCA6) associated with small polyglutamine expansions in the alpha 1A-voltage-dependent calcium channel', *Nat Genet*, 15: 62-9.

Zoghbi, H. Y. 1997. 'CAG repeats in SCA6. Anticipating new clues', *Neurology*, 49: 1196-9.

Zorova, L. D., V. A. Popkov, E. Y. Plotnikov, D. N. Silachev, I. B. Pevzner, S. S. Jankauskas, V. A. Babenko, S. D. Zorov, A. V. Balakireva, M. Juhaszova, S. J. Sollott, and D. B. Zorov. 2018. 'Mitochondrial membrane potential', *Anal Biochem*, 552: 50-59.